HRVATSKO DRUŠTVO
ZA STROJARSKE TEHNOLOGIJE

CROATIAN SOCIETY
FOR MECHANICAL TECHNOLOGIES

In association with:

University of Split
Faculty of Electrical Engineering,
Mechanical Engineering and
Naval Architecture

Slovak Academy of Science
Institute of Materials and
Machine Mechanics

Sveučilište u Splitu
Sveučilišni
odjel za stručne studije

Croatian Society for
Materials and Tribology

Dublin Institute
of Technology

Rogante Engineering
Office

ISSN 1847-7917

6th International Conference

Mechanical Technologies and Structural Materials 2016

General sponsors:

University of Split - Faculty of Electrical Engineering, Mechanical Engineering and Naval Architecture
Split - Dalmatia County
EVN Croatia Plin d.o.o.


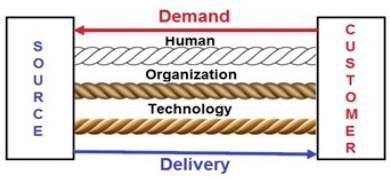

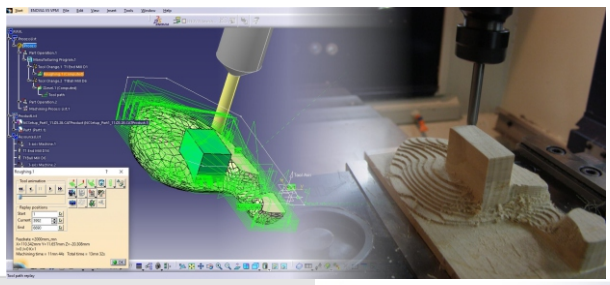
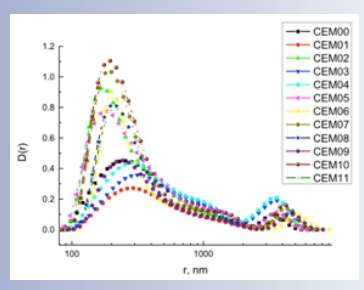

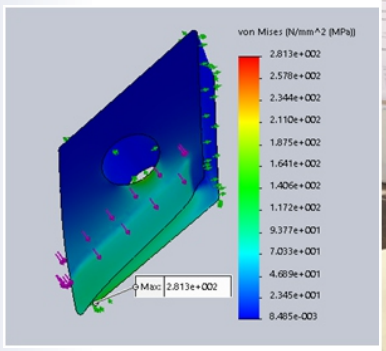


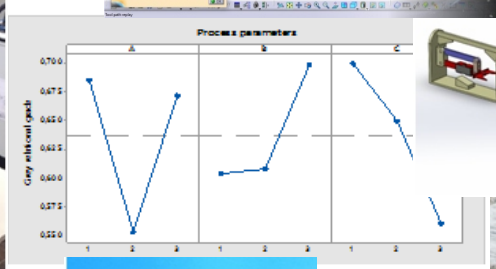

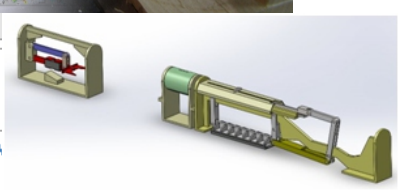
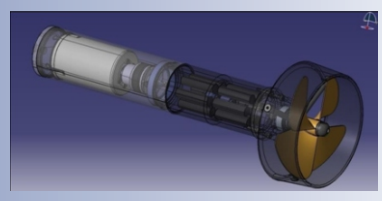
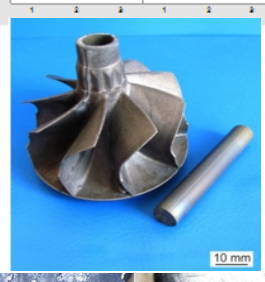
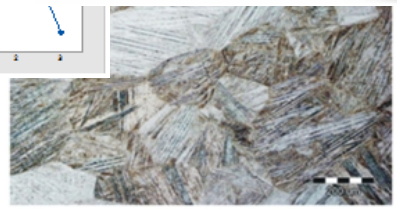
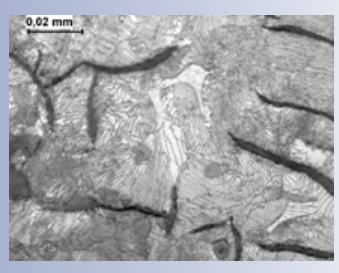

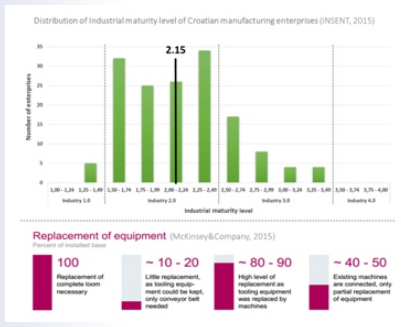

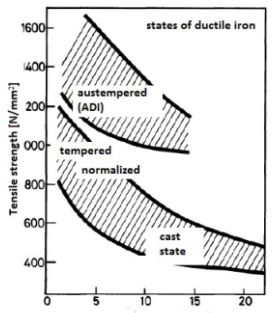

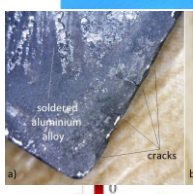

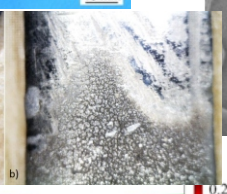

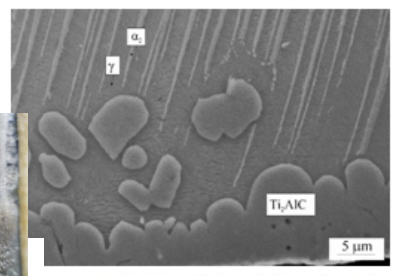

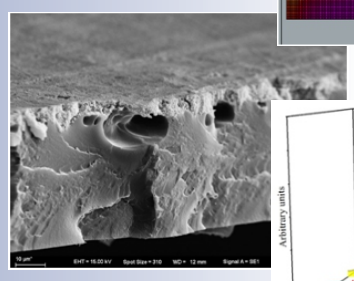
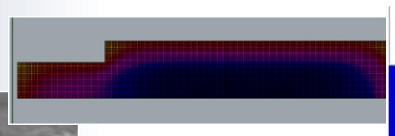
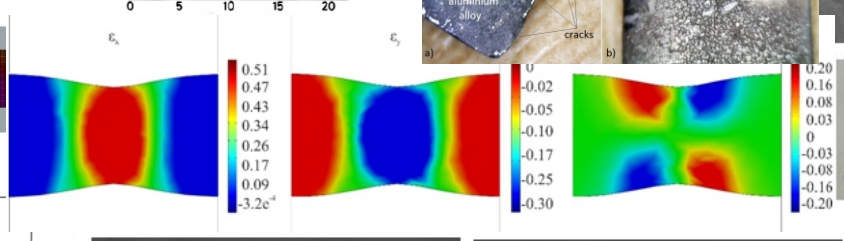

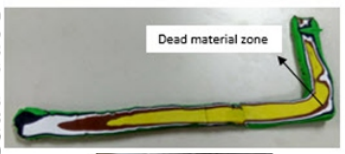

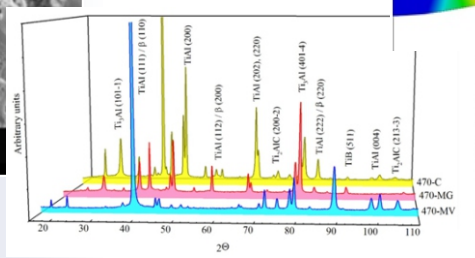

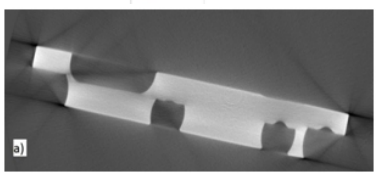

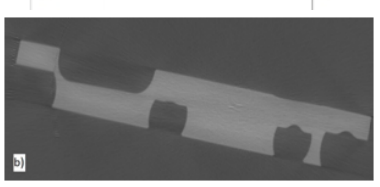

http://www.strojarska-tehnologija.hr

September, 22nd - 23rd, 2016.
FESB, Ruđera Boškovića 32, Split

CONFERENCE PROCEEDINGS

ZBORNIK RADOVA

MECHANICAL TECHNOLOGIES AND STRUCTURAL MATERIALS

STROJARSKE TEHNOLOGIJE I KONSTRUKCIJSKI MATERIJALI

Split

Croatia / Hrvatska

22. - 23. September / rujan 2016.

ORGANIZED BY / ORGANIZATOR:

CROATIAN SOCIETY FOR MECHANICAL TECHNOLOGIES, Croatia

HRVATSKO DRUŠTVO ZA STROJARSKE TEHNOLOGIJE, Hrvatska

CO-ORGANIZERS / SURGANIZATORI:

UNIVERSITY OF SPLIT
FACULTY OF ELECTRICAL ENGINEERING, MECHANICAL ENGINEERING AND NAVAL ARCHITECTURE

CROATIAN SOCIETY FOR MATERIALS AND TRIBOLOGY

DUBLIN INSTITUTE OF TECHNOLOGY

SLOVAK ACADEMY OF SCIENCE INSTITUTE OF MATERIALS AND MACHINE MECHANICS

ROGANTE ENGINEERING OFFICE

UNIVERSITY OF SPLIT
UNIVERSITY DEPARTMENT OF PROFESSIONAL STUDIES

SPONSORS / SPONZORI:

UNIVERSITY OF SPLIT

SPLIT – DALMATIA COUNTY

MINISTRY OF SCIENCE, EDUCATION AND SPORTS OF THE REPUBLIC OF CROATIA

EVN CROATIA PLIN d.o.o.

PUBLISHER / IZDAVAČ:

CROATIAN SOCIETY FOR MECHANICAL TECHNOLOGIES, Croatia

HRVATSKO DRUŠTVO ZA STROJARSKE TEHNOLOGIJE, Hrvatska

c/o FESB, Ruđera Boškovića 32, 21000 SPLIT

tel.: +385 21 305 910; fax.: +385 21 463 877

e-mail: info@strojarska-tehnologija.hr

http://www.strojarska-tehnologija.hr

EDITORS / UREDNICI:

dr. sc. Sonja Jozić
dr .sc. Branimir Lela

ISSN 1847-7917

ISSUE / NAKLADA: 70

ORGANIZING COMMITTEE:
ORGANIZACIJSKI ODBOR

- Sonja JOZIĆ (Croatia) - Chairman
- Branimir LELA (Croatia) – Vice Chairman

- Ante ALUJEVIĆ (Croatia)
- Ante BAROVIĆ (Croatia)
- Nikša ČATIPOVIĆ (Croatia)
- Zvonimir DADIĆ (Croatia)
- Igor GABRIĆ (Croatia)
- Nikola GJELDUM (Croatia)
- Dario ILJKIĆ (Croatia)
- Neven KUZMANIĆ (Croatia)
- Zvonimir MRDULJAŠ (Croatia)
- Petar LJUMOVIĆ (Croatia)
- Slaven ŠITIĆ (Croatia)

PROGRAMME AND REVIEW COMMITTEE:
PROGRAMSKI I RECENZENTSKI ODBOR

- Dražen ŽIVKOVIĆ (Croatia) – President
- Dražen BAJIĆ (Croatia) – Vice President

- Boris ANZULOVIĆ (Croatia)
- Frane BARBIR (Croatia)
- Franjo CAJNER (Croatia)
- Goran CUKOR (Croatia)
- Vinko IVUŠIĆ (Croatia)
- Zlatko JANKOSKI (Croatia)
- Jaroslav JERZ (Slovakia)
- David KENNEDY (Ireland)
- John LAWLOR (Ireland)
- Zoran PANDILOV (Macedonia)
- Massimo ROGANTE (Italy)
- Zdravko SCHAUPERL (Croatia)
- Wilfried SIHN (Austria)
- František SIMANČIK (Bratislava)
- Božo SMOLJAN (Croatia)
- Goran ŠIMUNOVIĆ (Croatia)
- Katica ŠIMUNOVIĆ (Croatia)
- Matej VESENJAK (Slovenia)
- Ivica VEŽA (Croatia)

CONTENT

ISSN 1847-7917

Supply chain model based on management principles of supply chain key elements and on Lean principles

***Nikola BANDUKA*[1, 2], *Ivica VEŽA*[1], *Nikola GJELDUM*[1]**

1) University of Split, Faculty of Electrical Engineering, Mechanical Engineering and Naval Architecture
Sveučilište u Splitu, Fakultet elektrotehnike, strojarstva i brodogradnje
R. Boskovica 32, 21 000 Split, **Croatia**
2) University of Kargujevac, Faculty of Engineering
Univerzitet u Kragujevacu, Fakultet inženjerskih nauka
Sestre Janjić 6, 34 000 Kragujevac, Srbija

nbanduka@fesb.hr
iveza@fesb.hr
ngjeldum@fesb.hr

Keywords
Dobavljački lanac
Lean
Ključni elementi
Osoblje
Organizacija
Tehnologija

Ključne riječi
Supply Chain
Lean
Key elements
Personal
Organization
Technology

Preliminary communication

Abstract: Due to financial crisis and rapid development of technology was created high level of turbolency at market, which making big problems everyday in business, to companies. Losing of control of any of this type of problems should lead to sudden fall of companies business preformances or even to sudden downfall, while on the other side good control and management of this problems made by market turbolency, would result with sudden increase of company preformances and with holding on dominant position on market. One of potential problems of this type or possibiliy, it depends of point of view is supply chian. Every try for pecisly and comprehensive defining or describing of supply chain is fall from start, because it's an complex, inter and multi disciplinary process, which in todays conditions demands maximal flexibility. According to this, to understanding of Supply chian should be accessed essentially through key, indispensable elements from which are supply chian is made of in basic. And this are: human as basic element, then organization and technology. Similar approach is noticed at Lean supply chian (LSC), so in this paper will be also overviewed Lean approach to supply chains and to business, and it will be made comparation between LSC approach and Key elements approach to supply chains. Also through eaxmple will be shown model of supply chain based on identification of problems of supply chain through key elements.

Prethodno priopćenje

Sažetak: Uslijed financijske krize i ubrzanog razvoja tehnologije stvoren je visok stupanj turbulencije na tržištu, što kompanijama stvara probleme pri poslovanju s kojima se svakodnevno suočavaju. Izmicanje kontroli ovog tipa problema moglo bi dovesti do naglog pada preformansi poslovanja kompanija ili čak do iznenadne propasti, dok bi s druge strane dobra kontrola i upravljanje problemima koje izaziva turbulentno tržište moglo rezultirati naglim porastom preformansi kompanija i držanjem dominantne pozicije na tržištu. Jedan od potencijalnih problema ovog tipa ili mogućnosti, u zavisnosti od pozicije gledišta je dobavljački lanac. Svi pokušaji da se precizno i sveobuhvatno definira ili opiše dobavljački lanac su unaprijed osuđeni na neuspeh jer se radi o jednom složenom, inter i multi disciplinarnom procesu koji u uvjetima današnjice zahtijeva maksimalnu fleksibilnost. Prema tome bi se razumijevanju dobavljačkog lanca trebalo pristupiti esencijalno kroz ključne, neizostavne elemente koji u osnovi sačinjavaju dobavljački lanac. A to su: čovijek kao osnovni element, zatim organizacija i tehnologija. Sličan pristup je primjećen kod Lean dobavljačkih lanaca (LSC) te će u ovom radu biti pregledan i Lean pristup dobavljačkim lancima i poslovanja i bit će napravljena usporedba između LSC pristupa i pristupa dobavljačkim lancima preko ključnih elemenata. Također će kroz primjer biti prikazan model dobavljačkog lanca zasnovan na upravljanju ključnim elementima.

1. Introduction

During financial crisis and rapid technology development market become very turbolent, which initiated business problems to many companies. Losing of control by any of this problems would lead to rapid fall of company business preformances or to the totally company fall, while to the other side good management and control of problems indicated by turbolent market would result with rapid increase of company preformanses and lead to dominant position on market. One of potential problems or possibilies, according to point of view is supply chain, which is proven with study realized by Bozarth, C. C. et all [17] conducted on 209 companies in 7 different countries.

Rapid techology development and increase of competiotion on market lead to "spoiled" of customers. Customers wants procured goods fast (or at the moment), with appropriate quality and with lower as it is possible

price. In this case term "spoiled" is best explaned on example with increased number of competition and possibility of customers to change vendor even for a small trifle.

Term supply chain is used to metaforicly explan serie of relations from source of repro-material need for production of goods to the delivery of same goods to a end customer. Today supply chains more look like network then chain, because of various industries. Harrison, A., & Van Hoek, R. I. [1] approved that many authors uses term supply network rather than supply chain. Many various authors defined what supply chain is and here will be overviewed some of them:

- Harrison, A., & Van Hoek, R. I. [1] sees supply chain as a range from basic commodities (which are in ground, sea or air) to selling of final product to customer, and also recycling of the used product.
- Supply chain is alignment of complanies which marketing products or service at market [2].
- Supply chain is made of whole phases directly or indirectly involved in fullfilment of customer demand. Supply chain doesn't include only manufacturing and supply, but also stransport, warehousing, retailing, even a customers, etc. [3].
- Supply chain is company and distribution network option which doing function of material procurement, transformation of this materils in subproducts or final products, and distribution of this products to customer [4].
- Supply chain is integral production process where raw material is being transformed into final product, and then delivered to customer [21].
- Supply chain is defined by author Christopher, M. [24] as a network organization included in different process and activities which making value in form of product or service in hands of final customer.
- Supply chain is a network of material, information's and process service links with characteristics of supply, transformation and demand [30].
- Supply chain represents all activities related with flow and transformation of goods, from raw material phase, to end customer [32].

According to Hugos, M. H. [5] supply chain capabilities curtains from special demands of market and operational challenges, currently form customer demand which is served. On some markets customer demands higher quality of products/services and they are ready to pay even more for that, but on the others is demanded lower level of quality, so customers are ready to pay lower price for that. But regardless to market there are five basic fields according to companies could define supply chain capabilities: Production, inventory, location, transport and information's.

All tryouts by authors and companies to precisely define supply chain or to define some framework are in advance convicted to fall, because supply chain is a very complex, inter and multi-disciplinary system and it's impossible to frame all elements which influencing on supply chain process. According to that to understanding of supply chain should be accessed essentially cross key, indispensable elements which constitute supply chain in basic. This key elements are: Human as an initiative element, then organization and technology.

2. Literature review

According to importance of supply chains for business process of various industries, number of books and scientific, expert and review papers exceeds 2 000 000. So only relevant review papers and state-of-the-art papers from period of last two decades will be reviewed. On example of advancement of company Hewlett-Packard (HP) supply chain, presented by Davis, T. [18] are visible four key factors:

- Including more instances in multiposition production, with aditional independent entities included in production and dilivery process
- Increased number of marketing channels, like independent computer dealer
- Increase for need of local products
- Pressure of competiotion for providing of quality service to customer, including rapid and reliable dilivery

Thomas, D. J., & Griffin, P. M. [19] made literature review of coordinated supply chains with focus on: operational models (different types of coordinated planning and scheduling), strategic issues (based on programing - IT) and third is consciously supply chain environment. Vidal, C. J., & Goetschalckx, M. [20] were focused on identification of relevant factors at defining specific, characteristic methods and computer experiences on example of global supply chain. Beside good literature review of use of simulations and software for improvement of supply chain performances Swaminathan, J. M. et all. [22] represented model of supply chain library in which key elements are structure (production and transport) and control (flow, inventory, demands, supply, information) elements, and part of presented concept was used by IBM company. Vrijhoef, R., & Koskela, L. [23] presented three supply chain key factors in construction industry and that: convergent management of supply chains, change of production and typical production supply chain according to order. Also are allocated four roles of supply chain management: improvement of site activities interface and supply chain, supply chain improvement, transfer of activities from site to supply chain and, site integration and supply chain. Lambert, D. M., & Cooper, M. C. [25] also allocated three interrelated key elements: network structure of supply chain, busyness process of supply chain and management of supply chain components. Tan, K. C. [26] in his paper presents development and evaluation of supply chain management with good literature review

from field of purchasing and transport in supply chain. Morash, E. A. [27] was focused on strategies, capabilities and performances of supply chains. Lee, H. L. [28] sees today main goals of supply chain in rapid delivery with less time as it possible, and for that goals represents model "The triple A" based on three dominant characteristics which every supply chain should have: agility, alignment and adaptability. Power, D. [29] in his review paper is focused on integration and implementation of supply chains. Chen, I. J., & Paulraj, A. [30] made literature review almost of 400 papers related to field of supply chain, and papers are mostly related to relations, relationships, purchasing, structure, strategies, etc. And also should be mentoned that this authors recommends essential look on supply chains with review of wider sense, rather then robustness approach. Authors Giannakis, M., & Croom, S. R. [31] presented "3S conceptual frame" based on synthesis, synergy and synchronization. Authors Seuring, S., & Müller, M. [32] presented sustainable conceptual model based on comprehensive literature review. Also is important to mention supply chains actual in last decades, and which are showed as very efficient and effective: Lean [1,8,12,33,35,36], agile [1,33,35,36], and off course state-of-the-art Green supply chains [34]. According to this comprehensive literature review is notable that no one of this authors used human, organization and technology all together as a three key elements as approach.

3. Key elements for functionality of supply chains

Three key elements before listed are chosen, becouse with them supply chain starting and finishing. If it's taken look esentialy on supply chain, basics and start point of every system and process, even this one is made by human. Then organization which presents way of doing and possibility to human, and at the end techology which is made by humans for easy way to goals or psysical result. Group of 3 key elements is shown on figure 1.

3.1. Key elements for functionality of supply chians

3.1.1 Role of human factor in systems

Humans were allways key element during a creation of something physical because of intelectual possibilities, which helps them to transfer ide in something real. Intelectual possibilities are not same at all people, moreover it could be even totally diferent, which with time lead to social desintegration and creation of hierarchial management system. This social deintegration lead to totally inhuman treatment of employed in industry, especially of shoop flor workers.

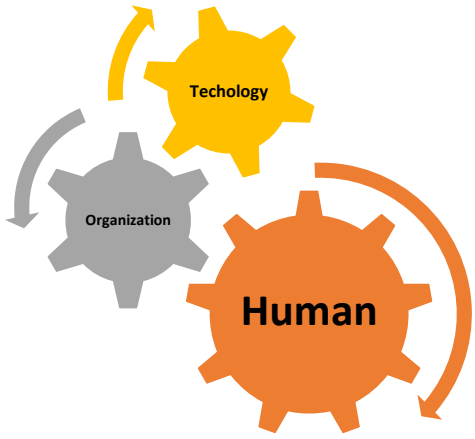

Figure 1. Group of 3 key elemnts

People were treated as robots which first was documented on start of 18. century by Fredric Taylor. Teylor discovered that is possible to make triple more quantity and weight of coal in shovel. Later Frenk and Lilian Gilbert made an extension of this method with development of study of "time and movement", which had for a goal increase of efficiency with elimination of unnecessary activities and movements. With this new method brother Gilbert reduce number of movements in masonry from 18 to 4.5 with aditional increase of productivity from 120 to 350 briks per hour This approaches lead to scenario of converting people to working machines and they are rejected in 1921 [6,7].

With progress of modern society people started to get more and more rights, which allowed them freedom and possibility of choice. During time while industry were developing parallel with technology development, scientist realized that influence of human factor in industry could be considerably reduced, but not replaced. Today in modern companies which functioning on principles of Just in time (JIT) delivery and total quality management, human error can led to lateness of delivery or delivery with scraps and defects, which can bring to lose of customer. It's also important for employer to have a continuity of employed. According to that, it is very important that people are treated as integral part of company. Japanese discovered this among the first, precisely founder of company Toyota Kiichiro Toyoda, which he explained with one sentence, from source [8]:

"My father wasn't educated man. Only strength he had is one thing he believed: that Japanese have latent possibilities. An automatic loom was product of his conviction."

There's also one sentence which greatly describes relation of Toyota company with their employees, and that is [8]: purpose of Lean leadership is in investing in people and making scientist of every man. Recognition of people as main potential for advancment of any system led Toyota company to the place number one on world list of car producers.

3.1.2 Human factor in supply chain

When is said role of human factor in supply chain, first association is are supply chain managers which siting in offices and planning deliveries, communicating with suppliers, purchase materials, etc. But human factor in supply chain have far more important role and influence. This influence is related to worker who works in shop floor at production line (he can work bad and casually and make batch of defects), to maintenance manager (who can make an mistake during maintenance of equipment which could lead to halt), to truck driver who transporting delivery from supplier to company (because he could led to lateness during car accident or wrong turn), etc. So every human who doing influence directly or indirectly on supply chain of a company, presents supply chain key element (basis) or initiator, as it's shown on figure 1.

- People who directly influencing on supply chain of an enterprise are all employees at all enterprises of whole supply chain.
- People who influencing indirectly on supply chain are people who works in companies or state institutions with which is made busyness deal according to before agreed frameworks. For example (if its halt on border during increased control).

According to this division of influence it could be concluded that is almost impossible to control this key element with high level of accuracy and efficiency. But with influence and better control could be increased efficiency of supply chain. Opposite of people with indirect control, to people with direct control is possible to affect. This group could be divided in three sub-groups: controllable, partially-controllable and, uncontrollable

- Controllable are people who are employed in enterprise of observed supply chain and on them could be influenced positively and negatively. For example positively could be influenced with increase of working conditions, with stimulation in sight of higher wages, with additional education and specialization, with increase of sense of belonging in enterprise, etc. While negative influence could be opposite to this.
- Partially-controllable are people who influencing on supply chain of enterprise and they are not under direct control of enterprise. For example that could be first suppliers workers or management (if referent enterprise delivering semi-product or raw material). On them is possible to make partially control if there's close cooperation between two enterprises. A control would be like increase of education, increase of cooperation between employees in enterprises, sending of workers or managers to work in another enterprise, etc.
- And third group are uncontrollable, it's people who are not indirectly team with referent enterprise or doesn't belong to first suppliers or customers, but to next in the chain or network of suppliers. For example: The worker in the mine who mining an ore.

According to this divisions it could be defined common model of improvement of human as one of basic supply chain elements. So, with increase of performances of people who have a directly influence on supply chain, it could be increased efficiency of supply chain. The problem is that respectively looking, largest group is uncontrollable, then partially-controllable and at the end as a smallest group controllable. Also during improvement of this groups firstly should be improved controllable group and then the others.

Gowen Iii, C. R., & Tallon, W. J. [9] are also noticed that influence of improvement of human performances as a aditional training, support, etc. Influencing on supply chain management, which approving before mentioned approach. In this paper is also provided good literature review of authors who shawn relations of human resurse improvement with supply chain progress.

- Authors Bubshait, A. A., & Farooq, G. [10] thinks that effectivnes of supply chain becoming limited with involment of organizationl barriers, but also could be improved with human resourse improvement. Also they are mentioning that supply chain service users who were included in research, reported that they in courtein with succesfull system of introdution of stuff training, which resulted with increase of number of coorporative universities..
- Goldstein, I. L., & Ford, J. K. [11] shows that improvement of human performances influance on competition in supply chain practise.
- Bowersox, D. J. [12] implemented study on state University of Michigen and shown that human resourse development directly influancing on supply chain.

Besides authors before mentoned, users of Lean approach highlights importance of human factor for whole system, and especially for supply chain. So for example: Liker, J. K. [8] highlighted importance of human factor and cooperation across one whole part of his book. Also, on example for development of company TESCO could be seen that development of this company is related for periodes and people who influented on development. Company TESCO is widely famous by her effective and efficient supply chain and human factor is very important by their experiences.

3.2 Organization as key element of supply chain

Organization is a second key element of supply chain and it's really hard to define it by essential point of view for supply chain. On micro level (for example, production inside an enterprise) it could be said that is set of activities which people realize in goal of getting better results. On macro level (Enterprise) it could be said that it's set of activities in interaction. While sense of organization for an supply chain could be defined as a set of all units (enterprises or service companies) which are in interaction and joint in common goal – busyness (or goal to deliver finished goods to end user). So complexity of model of organization influence as a key element on a supply chain is almost a same as in case of human influence as a key element, but it's just a bit more complex. It best could be seen on an example: partially-controllable organization is far less controllable then partially-controllable human, because with influence on organization of first supplier is made direct influence on politics of a company, on what owners are not ready because of sharing confidential information and busyness strategies of company. This problematics is directly related for trust between two companies and with their level of cooperation.

Examples of this kind of cooperation are evident mostly at companies with Lean approach. For example [8]: Toyota company have education programs for helping their partners in supply chain. This programs helping also with approaching of philosophies of each company to Toyota way.

Based on before mentioned text, organization presents ways and possibilities according to which people in supply chain would made product and deliver it to end user. The most important thing for customer is to get product on right time, with right quality with as less as it possible price.

So basic things on which organization should affect are reduction of lead time and increase of quality (both directly influencing on costs), with additional organizational activities which supporting basic.

About relevance of organization speaks many authors who were working on this topics.

For example Miles, R. E., & Snow, C. C. [15] spliting organization on three periods according to focus on which organization was directed. Mason, R., & Evans, B. [12] shows accross example of TESCO supply chain pheriods of company related by people who contributed to organization. Some of authors as for example Barney, J. B. [14] sees organization as key factor of competition. Also should be mentioned that organization have direct influence on performances of humen, as for example is Ergonomy.

According to this organization is recognized in literature also as one of key elements of supply chain and with control of organization performances of supply chain could be improved.

3.3 Technology as key element of supply chain

Opposite to organization, technology could be defined very easy. In essential look technology for supply chain presents instrumentality which people in supply chain using to made products more easily and deliver them to customer. So technology in supply chain could be equipment in shop floor, computer in office, vehicle which transporting finished goods to distributer or customer, etc., and presents all technology and technique at a supply chain. Essentially looked according to needs of supply chain it could be divided in two groups: Technological trends and technology for intern needs of an enterprise.

- Technological trends presents technology and techniques imposed by rapid development of technology and technological revolutions. That is unavoidable technology without modern systems could not be competitive on market: RFID, CNC, internet, PLM, software's, robots, computers, IT, vehicles, etc.
- In second group is whole technology made by measures and needs of an enterprise or unites in supply chain: Software's by need, tools, special machines, construction profiles, etc.

Second group mostly depends of R&D sector in an enterprise and of innovative people, so is more controllable then first group. First group could be advantage or risk for enterprise and for her an enterprise need to be always ready. Best example of technology trends from relatively new period is advent of concurrent engineering. If it's used fact that 85% of cost occurs is design of product phase [16], it can be concluded that dynamics of turbulent market led to movement of enterprises from traditional to digital way of manufacturing, and simple projection techniques are changed for information technologies and digital software's.

3.4 Interaction of supply chain key elements

Supply chain key element interaction is functional system which is directly dependent of elements. Every interaction firstly depends of human, because of that human is defined as basic key element of supply chain. If every of key element is observed independently it could be concluded that functionality of system is impossible. For example, if technology is observed as key element of a supply chain, she doesn't have sense without adequate use by human, no matter if it's the latest technology. Even a robot which can do operations by itself, indirectly is depended by human who programing it and organization in which working. Or it could be seen on example of Ford and Toyota [8] with implementing of organizationl system it could be concluded that even perfect organizacion isn't enaugh, if people doesn't now how to use it adequatly. After successful implementing of JIT sistem in Toyota company from which Toyota had

a lot of benefites, Ford hired special company to implement JIT for them too, and they tried to implement same thing with their supliers, but they resulted in failure because people in system doesn't understuded a principle, or philosophy of that organizacional technique.
Interaction possibilities are in direct dependence with key elements of supply chain and they are divided on: human – organization, human – technology, human – organization – technology, and human – technology – organization.

- Human – organization is interaction of human with way of acting in system. For example: If organization element is 5S – Lean technique, interaction would be based on human ability to use this technique efficiently.
- Human – technology is direct interaction of man with technology with which he achieving goals. For example: Concreate work on computer.
- Human – organization – technology is interaction based on human abilities to organize technology with organization skills. For example: Projecting of company layout with skills and knowledge.
- Human – technology – organization is interaction opposite to before one and is based on human ability to project organization with using of technology. For example: Using of software for process simulation.

So conclusion is that progress of supply chain key elements also depends of interactive factor of key elements.

4. Development and alignment of supply chain key elements with Lean approach

Words of famous president of Toyota corporation Fujio Cho explaining key of Toyota success, and they are perfectly fit's in progress and alignment of supply chain key elements [8]: „ Key of Toyota way and thing which sustaining Toyota aren't individual elements, but set of all elements which all togeder making entairety. "
According to Liker, J. K. [8] Toyota way is based on four key elements: philosophy, process, People and partners, and continuesly solving of problems. As it could be noticed Toyota mostly investing in people and partners, after these in organization, and at last in technology if it's needed and checked.
Advent of Lean philosophy and Toyota production system (TPS) is related for period after II world war in which Japan lose. After big destructions by atomic bombs and big losses of human population, Japanese industry collapsed, and that wawe also get to Toyota company where workers already were in the strike. State of Japan prohibited dissmmisial of workers and Toyota had it 1600 more then is enaugh. With some of them is made deal for early retirement, to some one are reduced wages for 10%, but that wasn't a solution. Toyota needed solution which will turn on company and make it competitive on market. TPS in founded as this soulution. Mass production which was widely used in that time in the world, and esspetialy in USA, is changed by „pull system", or with production of only what and how much is needed by customer, and company focus was directed to continous improvement and totaly quality control in every step. Lean concept wasn't famouns besides a company untill 1973. when first oil impact hited a world and made a first global crissis. Lean managed world popularity yet at 1990s [8]. The most inportant fact is that Lean philosophy or TPS led Toyota company to the number one of world list of car manufacturers. Also should be mentioned that in that time main opponent was Ford motors with founder Henry Ford who was recognized engineer with wealth experience with all abailable technology, while Kiischiro Toyoda first mold of engine made in earth. The most important thing is that Toyota used all available resourses they had, and that mostly was people. They realized that they can not folow rapid development of technology, but they realized that they could invent many of organizational techniques which could save them energy, time, and money. As for example: JIT, Kaizen, 5S, SMED, poka yoke, etc.
So, primarly Lean is focused on human and organization as supply chain key elements.

4.1 Lean supply chain

Defining of Lean supply chains isn't so easy job, and best it could be explaned true examples. But it could be said that it's supply chain constructed according to long term philosophy of Lean concept, with elements of integrated cooperation between units in chain, in sight of helping each others, progressing, and jonit education.
Examples on which Lean supply chain will be described are based on literatures [8] and [12] and they are about Toyota company where Lean is advented and another one is TESCO company, world wide known food manufacturer, for which Harrison, A., & Van Hoek, R. I. [1] said that it's a company where logistics starts and ends.

4.1.1 Toyota supply chain

Toyota produce 70% of parts outside its own company, but they take care very much what it what will be produced is. So conclusion is that they have big supplier network. Relations between Toyota and its suppliers are based on strong cooperation, and what Toyota demand from them is shown on figure 2. in shape of hierarchical pyramid. Thing that makes Toyota very different from the other companies, are cooperation principles with suppliers. Usual practice at car companies and their suppliers is that supplier could be very easy changed because another one is cheaper, but that's not Toyota way. This company understands that costs could be reduced only if their suppliers reduce their costs, so they rather practice investment and improvement of suppliers

system, then often changes of suppliers. Their suppliers are categorized from 1 (supplier which can make line stop) to 5 (Supplier which perfectly using Lean) and practice is that they have always two suppliers for same part, and they are in competition with each other.

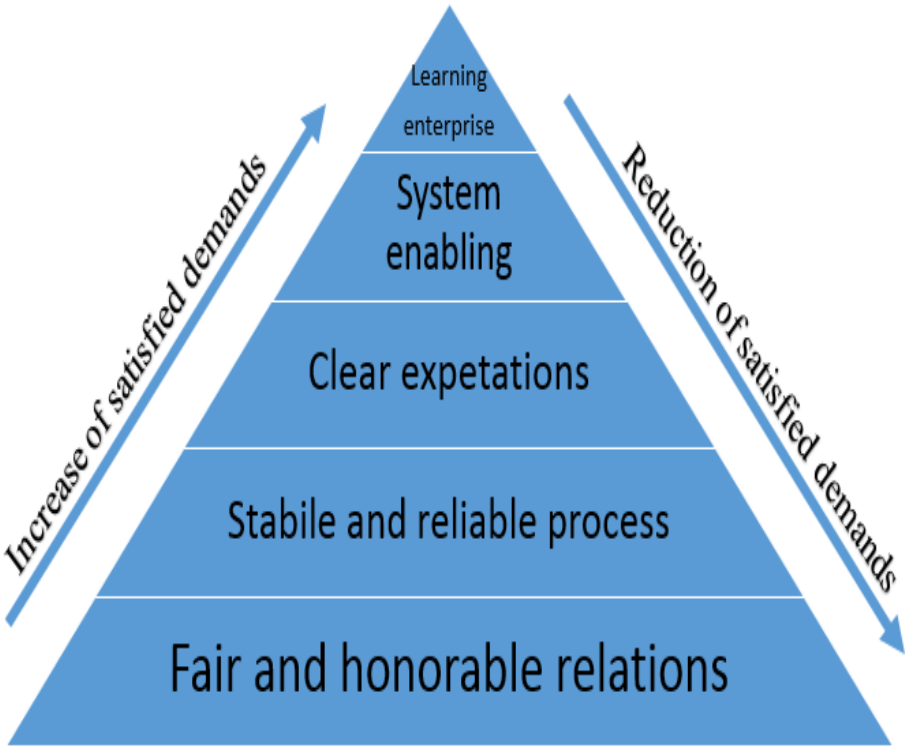

Figure 2. Hierarchical demand of supply chain [8].

Toyota have special society for all key suppliers and special center for helping and educating suppliers – Toyota supplier support center (TSSC) which helping to "sick suppliers", as they call them, and that are usually suppliers which have interior problems. But also it doesn't mean that they will keep a supplier at all costs. On DENSO example it could be concluded in which framework is tolerant relation with suppliers. DENSO was one of Toyotas key suppliers for electronics. But during the time electronics became one of most important things in Automotive industry and that was almost 30% of most important car components (in that time). As DENSO became much stronger, and increased cooperation with competition, and reduced cooperation with Toyota, Toyota decided to open their own company for producing of electronic components.

One of basic busyness principles with suppliers is that production system which supplier using need to be TPS or to fit with TPS, but that's not absolutely strictly. For example: When is worked on development of Prius[1]. One of key elements for this vehicle is hybrid battery, which were produced at supplier outside a company. Cultures of this two companies were totally different and even Prius general manager one time said that suppliers are too "relaxed", but at the end they managed to made battery successful.

Suppliers understands role of strong cooperation with Toyota company, because they see that it helps them to develop and improve their production systems. And about that also testifies data from 2003, where Toyota was estimated as best company for cooperation, by suppliers. This also could be seen on example when one of Toyota suppliers for breaking vehicle system was burned in fire, even 63 Toyota suppliers engage to replace production of that parts, to avoid line stop at Toyota's. So Toyota power isn't in modern technology and IT systems, but in people and strong partner relationships.

4.1.2 TESCO supply chain

For TESCO as a company it could be said that it is supplier, but also and customer. TESCO doesn't produce their products, but get them from suppliers and just put its label, and on that way provides to customers big diversity of products on one place. So TESCO's key of

[1] **Prius** is Toyota's hybrid vehicle first time presented at 1995.

competitiveness on market depends of effectiveness, and then by efficiency of supply chain.
In period from 1997 to 2014 TESCO identified four ways for supply chain key improvements, from which one was use of Lean thinking and principles. Opposite to Toyota company which cover both human and organization as a key factors of improvement, TESCO is mostly oriented to organization (because 95% of problems was made by bad organization). This best could be seen on example from table 1, using of Lean approach on 5 key TESCO principles (customer oriented, responsibility, planning, discipline, and refill on touch). Improvement of this TESCO's supply chain key elements among which is Lean also, influenced to move TESCO from position of second food retailer to first on world.

Table 1. Connection of TESCO operation principles with Lean principles

TESCO operational principles	**Lean principles**	**Sequence**
Customer oriented	Value	/
Responsibility	Flow and "pull"	Effectivity at first
Planning	Value stream	/
Discipline	Perfection	Efficiency at second
Refill on touch	Waste elimination	/

5. Future research

According to before all literature review it could be concluded that enterprises which using Lean approach for supply chain improvements, managing big success with control and management of supply chain key elements. According to fact that market conditions are now more turbulent then ever and that competition is largest then ever, companies will align among them self's in future and they will make more and more stronger and better cooperation to stay competitive or to survive on market. Modern studies shows how much time could be saved in nanoseconds by speeding up internet software's, which is not a solution, because that studies are possible only when stabile and ideal systems are considered, while supply chain is in opposite with it. So supply chain in which every enterprise presents individual link will be changed with supply rope where all enterprises will be linked together as one, with all information allowed among them (figure 3).

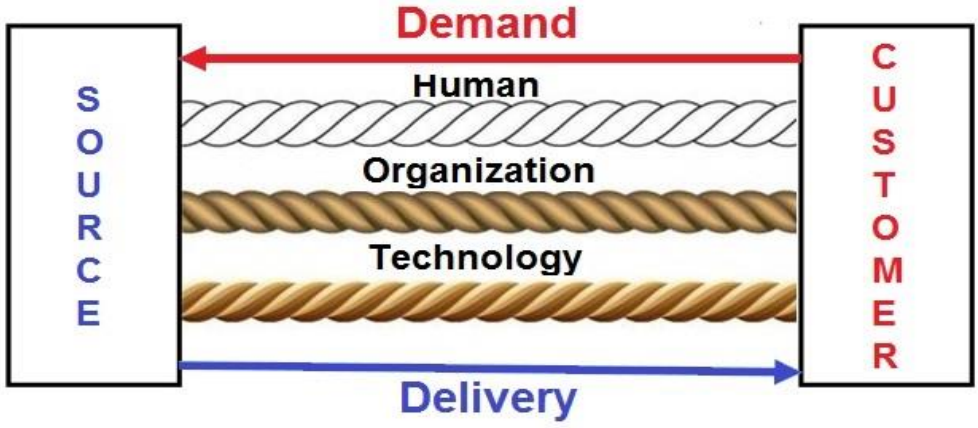

Figure 3. Supply rope model.

6. Conclusion

Today when technology is in very rapid progress, it's very hard to invent something revolutionary which could change market dynamics. During last 100 years the world passed across different periods form mechanization, automatization, IT, Leadership, etc., until today when key of success is in cooperation. This is especially important for supply chain, because many factors depends from many units or links in chain.
Companies are still "skeptical" in term of sharing information and about so close cooperation which leads almost to one big enterprise made by many little enterprises, but market dynamics and competition which is in rise from day to day will lead to this way of busyness.

With management model of supply chain key elements is shown how can be improved whole supply system with performance improvement of any unit in row. Influence possibilities are reduced to improvement of performances of three supply chain key factors (human, organization, and technology) and their four possible interactions (human – organization, human – technology, human – organization – technology, and human – technology - organization). Also is noticed that on this way is easier to control and follow whole supply chain just with mapping of process flow manually or with software.

Acknowledgements

This work has been fully supported by Croatian Science Foundation under the project Innovative Smart Enterprise – INSENT (1353).

REFERENCES

[1] Harrison, A., & Van Hoek, R. I. (2008). *Logistics management and strategy: competing through the supply chain*. Pearson Education.

[2] Lambert, D. M., Stock, J. R., & Ellram, L. M. (1998). *Fundamentals of logistics management*. McGraw-Hill/Irwin.

[3] Chopra, S., & Meindl, P. (2003). Supply chain

[4] Ganeshan, R., & Harrison, T. P. (1995). An introduction to supply chain management. *Department of management sciences and information systems*, *303*.

[5] Hugos, M. H. (2011). *Essentials of supply chain management* (Vol. 62). John Wiley & Sons.

[6] Jamil, M. G., Saxena, A., & Mr Vivek Agnihotri, M. (2013). Optimization of Productivity by Work Force Management through Ergonomics and Standardization of Process Activities using MOST Analysis-A Case Study. *Global Journal of Researches in Engineering*, *13*(6).

[7] Moray, N. (Ed.). (2005). *Ergonomics: The history and scope of human factors* (Vol. 1). Taylor & Francis.

[8] Liker, J. K. (2005). *The Toyota way*. Esensi.

[9] Gowen Iii, C. R., & Tallon, W. J. (2003). Enhancing supply chain practices through human resource management. *Journal of Management Development*, *22*(1), 32-44.

[10] Bubshait, A. A., & Farooq, G. (1999). Team building and project success. *Cost engineering*, *41*(7), 34-38.

[11] Goldstein, I. L., & Ford, J. K. (2002). Training in organizations Belmont. *CA: Wadsworth*.

[12] Mason, R., & Evans, B. (2015). *The Lean Supply Chain: Managing the Challenge at Tesco*. Kogan Page Publishers.

[13] Salvendy, G. (2012). *Handbook of human factors and ergonomics*. John Wiley & Sons.

[14] Barney, J. B. (2002). Gaining and sustaining competitive advantage.

[15] Miles, R. E., & Snow, C. C. (2007). Organization theory and supply chain management: An evolving research perspective. *Journal of operations management*, *25*(2), 459-463.

[16] Ayadi, M., Affonso, R. C., Cheutet, V., Masmoudi, F., Riviere, A., & Haddar, M. (2013). Conceptual model for management of digital factory simulation information. *International Journal of Simulation Modelling*, *12*(2), 107-119.

[17] Bozarth, C. C., Warsing, D. P., Flynn, B. B., & Flynn, E. J. (2009). The impact of supply chain complexity on manufacturing plant performance. *Journal of Operations Management*, *27*(1), 78-93.

[18] Davis, T. (1993). Effective supply chain management. *Sloan management review*, *34*(4), 35.

[19] Thomas, D. J., & Griffin, P. M. (1996). Coordinated supply chain management. *European journal of operational research*, *94*(1), 1-15.

[20] Vidal, C. J., & Goetschalckx, M. (1997). Strategic production-distribution models: A critical review with emphasis on global supply chain models. *European Journal of Operational Research*, *98*(1), 1-18.

[21] Beamon, B. M. (1998). Supply chain design and analysis:: Models and methods. *International journal of production economics*, *55*(3), 281-294.

[22] Swaminathan, J. M., Smith, S. F., & Sadeh, N. M. (1998). Modelling supply chain dynamics: A multiagent approach*. *Decision sciences*, *29*(3), 607-632.

[23] Vrijhoef, R., & Koskela, L. (2000). The four roles of supply chain management in construction. *European journal of purchasing & supply management*, *6*(3), 169-178.

[24] Christopher, M. (1998). Logistics and supply chain management: Strategies for reducing cost and improving service.

[25] Lambert, D. M., & Cooper, M. C. (2000). Issues in supply chain management. *Industrial marketing management*, *29*(1), 65-83.

[26] Tan, K. C. (2001). A framework of supply chain management literature. *European Journal of Purchasing & Supply Management*, *7*(1), 39-48.

[27] Morash, E. A. (2001). Supply chain strategies, capabilities, and performance. *Transportation journal*, 37-54.

[28] Lee, H. L. (2004). The triple-A supply chain. *Harvard business review*, *82*(10), 102-113.

[29] Power, D. (2005). Supply chain management integration and implementation: a literature review. *Supply chain management: an International journal*, *10*(4), 252-263.

[30] Chen, I. J., & Paulraj, A. (2004). Towards a theory of supply chain management: the constructs and measurements. *Journal of operations management*, *22*(2), 119-150.
[31] Giannakis, M., & Croom, S. R. (2004). Toward the development of a supply chain management paradigm: a conceptual framework. *Journal of Supply Chain Management*, *40*(1), 27-37.
[32] Seuring, S., & Müller, M. (2008). From a literature review to a conceptual framework for sustainable supply chain management. *Journal of cleaner production*, *16*(15), 1699-1710.
[33] Naylor, J. B., Naim, M. M., & Berry, D. (1999). Legality: integrating the lean and agile manufacturing paradigms in the total supply chain. *International Journal of production economics*, *62*(1), 107-118.
[34] Srivastava, S. K. (2007). Green supply-chain management: a state-of-the-art literature review. *International journal of management reviews*, *9*(1), 53-80.
[35] Christopher, M., & Towill, D. R. (2000). Supply chain migration from lean and functional to agile and customised. *Supply Chain Management: An International Journal*, *5*(4), 206-213.
[36] Stratton, R., & Warburton, R. D. (2003). The strategic integration of agile and lean supply. *International Journal of Production Economics*, *85*(2),

ISSN 1847-7917

The Model of Stress Distribution in the Cutting Tool During Turning Process Obtained by SolidWorks

Andrej BORIĆ[1)]***, Goran CUKOR***[1)]
Duško PAVLETIĆ[1)]
1) Sveučilište u Rijeci, Tehnički fakultet/ University of Rijeka, Faculty of Engineering, Vukovarska 58, 51000 Rijeka, **Hrvatska/Croatia**
aboric@riteh.hr, goranc@riteh.hr

Keywords
Turning
Stress
FEM
SolidWorks Simulation
Taguchi experimental design
S/N ratio

Ključne riječi
Obrada rezanjem
Naprezanje
Metoda konačnih elemenata
SolidWorks simulacija
Taguchijev plan eksperimenta
Omjer signal/šum

Original scientific article
Abstract: During the turning process, stresses appear within the tool. Knowing these stresses is crucial for selection of optimum cutting tool and avoidance of its fracture. This work reveals how various shapes, angles and radii of the cutting tool insert made of tungsten carbide affect the distribution of stresses in the cutting insert. Finite element method was used to obtain stress distribution using the SolidWorks Simulations software. Taguchi experimental design with three parameters was used to create model of nine different inserts. Using statistical analysis, i.e. S/N (Signal/Noise) ratio output parameters were analyzed. Based on the aforementioned, optimum shape, clearance angle and nose radius of the insert have been obtained. Simulation of stress distribution on the cutting insert was also obtained.

Model raspodjele naprezanja u alatu pri obradi rezanjem primjenom SolidWorks-a

Izvorni znanstveni rad
Sažetak**:** Prilikom obrade rezanjem unutar alata dolazi do pojave naprezanja, čije je poznavanje od presudne važnosti prilikom odabira optimalnog reznog alata i izbjegavanja njegovog loma. Ovaj rad otkriva kako razni oblici, slobodni kutovi i polumjeri vrha pločice alata, izrađene od volframovog karbida utječu na raspodjelu naprezanja u reznoj pločici. Primjenom metode konačnih elemenata dobivena je raspodjela naprezanja pomoću softvera SolidWorks Simulations. Potom je primijenjen Taguchijev plan eksperimenta s tri parametra, na temelju čega je izvršeno modeliranje devet različitih pločica. Statističkom analizom, tj. S/N (signal/šum) omjerom analizirani su izlazni parametri. Na temelju navedenog dobiven je optimalni oblik, stražnji kut i polumjer vrha pločice alata te je izvršena simulacija raspodjela naprezanja na reznoj pločici.

1. Introduction

Previous research was based on complexed, conventional software for FEM analysis (Abaqus, Ansys etc.) which are being used since 1970s. This paper is based on use of simpler and more user-friendly software. For that reason, SolidWorks Simulations was chosen, by help of which model of stressed tools distribution was made during cutting.

By using the input data related with material and input data dependent on the geometry of tools and parameters of orthogonal cutting is possible to calculate the force of cutting and to determine the contact length of chip and a tool. After modelling the geometry of insert in appropriate computer software the plan of experiment can be made.

With minimal number of testing, the Taguchi plan method of experiment can be used to determine the optimal shape of tool insert based on minimal stress and minimal S/N ratio.

2. FEM Analysis

Determination of input data for orthogonal turning model is the first step of FEM analysis. Input data for workpiece material Ti6A14V were taken from Johnson-Cook constitutive model for this material [1, 2, 3, 4]. Remaining input data: γ =8°, Φ = 15°, v_c = 0,5 m/s, $h = 2{,}5 \cdot 10^{-3}$ m, $a_p = 2{,}5 \cdot 10^{-3}$ m, $b = 2{,}5 \cdot 10^{-3}$ m, ρ = 47 °. Based on these data, calculation of cutting data has been made for orthogonal cutting model. The results are presented in Table 1.

Table 1. Data obtained with orthogonal cutting model calculation

Tablica 1. Podaci dobiveni proračunom za model ortogonalnog rezanja

Tool-chip contact length/ Duljina kontakta strugotine i alata, l_c:	0,011458 m
Resultant cutting force/ Rezultantna sila rezanja, R:	2532,425 N

Symbols/Oznake

a_p	- depth of cut, m - dubina rezanja
b	- width of cut, m - širina rezanja
C	- insert shape - oblik pločice
D	- insert shape - oblik pločice
h	- uncut chip thickness, m - debljina neodrezane strugotine
L	- number of levels - broj razina
l_c	- tool-chip contact length, m - duljina kontakta strugotine i alata
n	- number of tests - broj testova
P	- number of parameters - broj parametara
R	- resultant cutting force, N - rezultantna sila rezanja, N
S	- insert shape - oblik pločice
S/N	- signal to noise ratio - signal šum omjer
v_c	- cutting speed, m/s brzina rezanja
y_i	- value of maximum stress for i-th test - iznos max. naprezanja za i-ti test

Greek letters/Grčka slova

γ	- rake angle, ° - prednji kut alata
Φ	- shear angle, ° - kut smicanja
ρ	- friction angle, ° - kut vanjskog kliznog trenja

Following the calculation in SolidWorks, nine different models of insert tools based on Taguchi method were made, Figure 1.

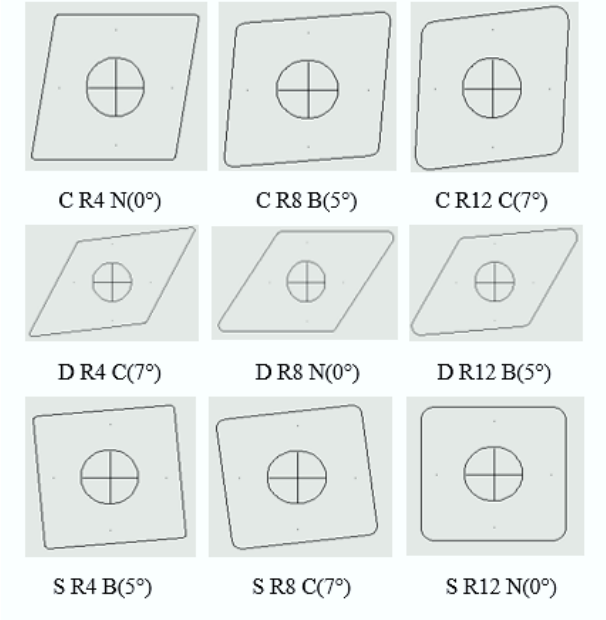

Figure 1. Nine different models of insert tools
Slika 1. Devet različitih modela pločice alata

Also the material of insert tool has been defined. Characteristics of material of tool insert are listed in Table 2.

Table 2. Insert material characteristics [5]
Tablica 2. Karakteristike materijala pločice [5]

Material/ Materijal	Density/ Gustoća, kg/m^3	Hardness/ Tvrdoća, HV	Flexural strength/ Savojna čvrstoća, N/mm^2	Tensile strength/ Vlačna čvrstoća, N/mm^2
Tungsten Carbide/ Volfram karbid (WC)	14800	1650	1900	5700

The next step represents production simulation of finite element method executed by SolidWorks Simulation software which generates three dimensional structure of mesh for every single insert. Figure 2 presents discretization of the finite elements by triangular finite elements mesh.
Figure 3 presents information about size of elements, total number of nodes and the number of finite elements for one of the nine inserts – insert CNMG 120404.

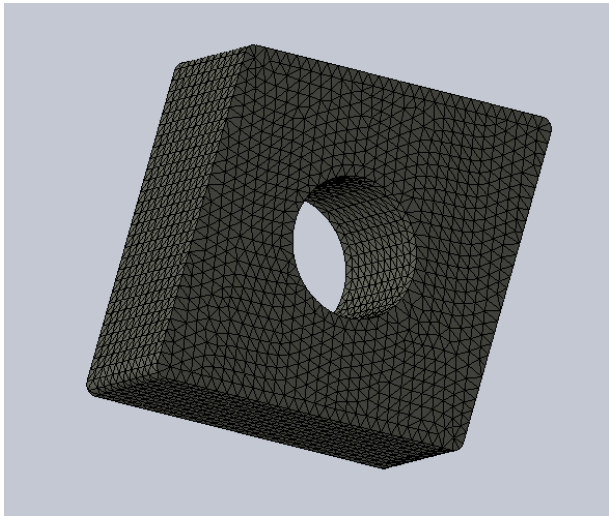

Figure 2. Finite element discretization of insert CNMG 120404

Slika 2. Diskretizacija konačnih elemenata pločice alata CNMG 120404

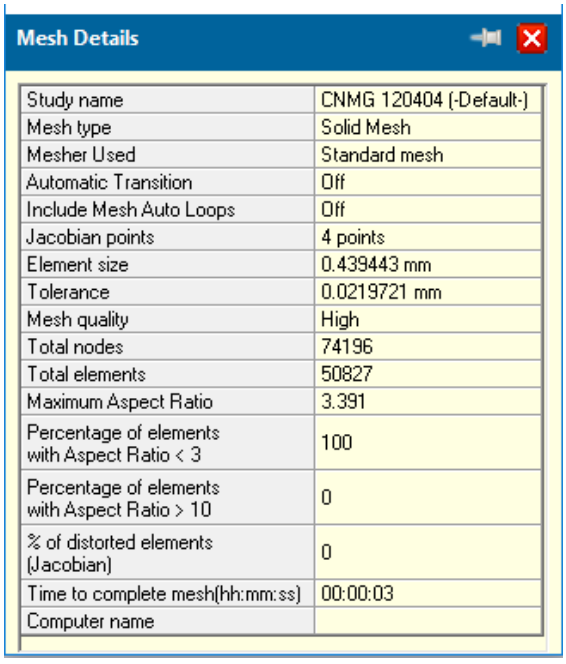

Mesh Details

Study name	CNMG 120404 (-Default-)
Mesh type	Solid Mesh
Mesher Used	Standard mesh
Automatic Transition	Off
Include Mesh Auto Loops	Off
Jacobian points	4 points
Element size	0.439443 mm
Tolerance	0.0219721 mm
Mesh quality	High
Total nodes	74196
Total elements	50827
Maximum Aspect Ratio	3.391
Percentage of elements with Aspect Ratio < 3	100
Percentage of elements with Aspect Ratio > 10	0
% of distorted elements (Jacobian)	0
Time to complete mesh(hh:mm:ss)	00:00:03
Computer name	

Figure 3. Mesh details for tool insert CNMG 120404

Slika 3. Pregled podataka mreže pločice CNMG 120404

3. Taguchi Experimental Design

In order to optimize the number of experiments, a method developed by Genichi Taguchi was applied, for the need of finding the high quality production products regardless on the variation of process parameters. This method represents a powerful tool while optimizing the quality. It also recommends the use of orthogonal plan experiment matrix to investigate characteristics of quality through minimum number of experiments.

Experimental results are based on orthogonal matrix which converts in S/N ratio for characteristics evaluation. In this paper, Taguchi experimental design is applied during production of orthogonal matrix with three parameters (insert shape, clearance angle and nose radius). Three different values were taken for every parameter, level 1, 2 and 3 (Table 3).

Table 3. Three parameters-three levels

Tablica 3. Tri parametra-tri razine

Parameters/ Parametri	Level 1/ Razina 1	Level 2/ Razina 2	Level 3/ Razina 3
Insert shape/ Oblik pločice	C (80°)	D (55°)	S (90°)
Clearance angle/ Stražnji kut pločice	N (0°)	B (5°)	C (7°)
Nose radius/ Polumjer vrha pločice	0,4 mm	0,8 mm	1,2 mm

Minimum number of experiments that are carried out in order to get optimal parameters calculates as:

Minimum number of experiments =

$$P(L-1)+1=3\cdot(3-1)+1=7\approx L_9 . \quad (1)$$

Different combinations of insert shapes, clearance angles and nose radii according to which simulation is implemented, based on Taguchi design of experiments L_9 are presented in Table 4.

Table 4. Taguchi Experimental Design

Tablica 4. Taguchi-jev plan eksperimenta

Exp. No./ Br. pokusa	Insert shape/ Oblik pločice	Clearance angle/ Stražnji kut	Nose radius/ Polumjer vrha pločice	Insert/ Pločica
1.	C	0°	0,4	CNMG 120404
2.	C	5°	0,8	CBMG 120408
3.	C	7°	1,2	CCMG 120412
4.	D	0°	0,8	DNMG 150408
5.	D	5°	1,2	DBMG 150412
6.	D	7°	0,4	DCMG 150404
7.	S	0°	1,2	SNMG 120412
8.	S	5°	0,4	SBMG 120404
9.	S	7°	0,8	SCMG 120408

Before the simulation it is necessary to determine the fixtures and external loads. By placing fixtures, degrees of freedom are deducted from the tool insert; that way its position within the tool holder is simulated. External loads are placed along the length of the contact chip and tool and are distributed on the front surface of the tool insert. Presentation of set external loads and fixtures on insert DNMG 150408 is shown in Figure 4.

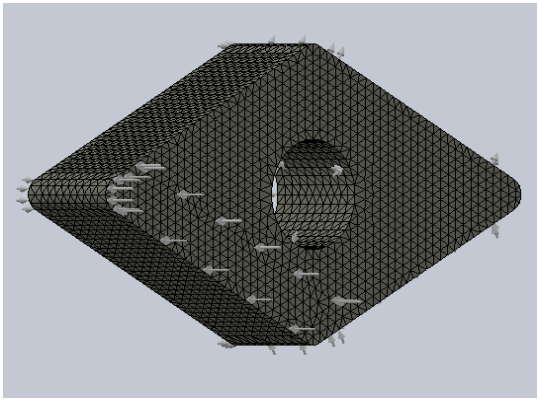

Figure 4. Presentation of external loads and fixtures on insert DNMG 150408

Slika 4. Prikaz postavljenih opterećenja i učvršćenja na pločici alata DNMG 150408

4. Simulation Results

Based on the L_9 orthogonal matrix simulation was conducted in order to test the influence of various parameters on the distribution of stress on the total surface of the tool blade considering the effect of the external load which effects along the length of contact of chip and tool insert.

In order to define optimal results of insert shape, clearance angle and nose radius, it is necessary to take into consideration maximum stress for every single insert (Table 5).

The experimental results are then transformed into a signal to noise (S/N) ratio. Taguchi recommends the use of the S/N ratio to measure the quality characteristics deviating from the desired values. Usually, there are three categories of quality characteristics in the analysis of the S/N ratio, i.e. the-lower-the-better, the-higher-the-better, and nominal-the-better. The S/N ratio for each level of process parameters is computed based on the S/N analysis [6].

Thereby statistical analysis of S/N ratio is applied, calculated according to the formula (the-lower-the-better quality characteristics):

$$S/N = -10\log\left(\frac{1}{n}\sum_{i=1}^{n} y_i^2\right) \qquad (2)$$

Table 5 presents the calculated S/N ratio for every single stress.

Table 5. Maximum stress and S/N ratio

Tablica 5. Maksimalno naprezanje i S/N omjer

Insert/ Pločica	Max. stress/ Max. naprezanje, MPa	S/N ratio/ S/N omjer
CNMG 120404	159,246	-44,0414
CBMG 120408	230,8	-47,2647
CCMG 120412	242,2	-47,6835
DNMG 150408	156,6	-43,8958
DBMG 150412	188,4	-45,5016
DCMG 150404	281,3	-48,9834
SNMG 120412	151,7	-43,6197
SBMG 120404	194,1	-45,7605
SCMG 120408	234,7	-47,4103

Based on S/N ratio the calculation was made for all three input parameter levels, Table 6.

Table 6. S/N ratio for three input parameter levels

Tablica 6. S/N omjer za tri razine ulaznih parametara

Lev./Par./ Raz./Par.	Insert shape/ Oblik pločice	Clearance angle/ Stražnji kut	Nose radius/ Polumjer vrha pločice
1	-46,3299	-43,8523	-46,2618
2	-46,1269	-46,1756	-46,1903
3	-45,5968	-48,0257	-45,6016

Based on the data in table 6 the main effects of S/N ratio considering insert shape, clearance angle and nose radius were obtained (Figures 5-7).

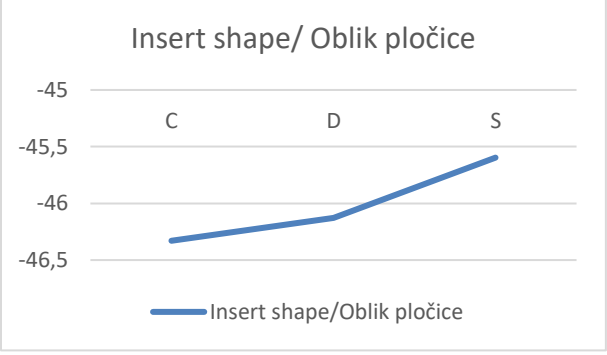

Figure 5. Main effect of S/N ratio for insert shape case

Slika 5. Glavni učinak S/N omjera za slučaj oblika pločice

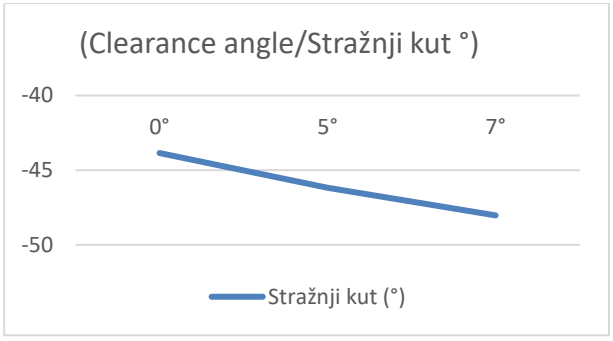

Figure 6. Main effect of S/N ratio for insert clearance angle
Slika 6. Glavni učinak S/N omjera za slučaj stražnjeg kuta

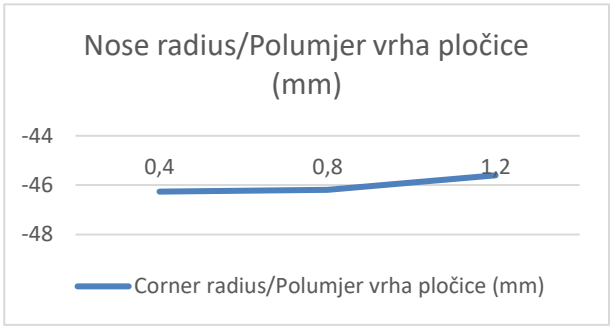

Figure 7. Main effect of S/N ratio for nose radius case
Slika 7. Glavni učinak S/N omjera za slučaj polumjera vrha

It has been determined that the optimal parameters are: insert shape S (90°), clearance angle N (0°) and insert nose radius 1,2 mm. Optimal insert tool is SNMG 120412, at which by evaluation of simulation minimum of maximum stress was given, 151,7 MPa (Figure 8).

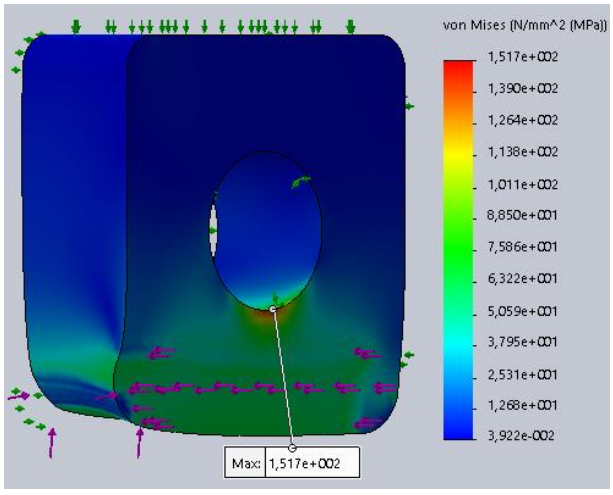

Figure 8. Optimal insert with minimum amount of stress (von Mises 151,7 MPa)
Slika 8. Optimalna pločica alata, pločica s najmanjim iznosom naprezanja (von Mises 151,7 MPa)

However, highest maximum stress of 281,3 MPa was obtained at the smallest nose radius, 0,4 mm, and clearance angle C (7°), i.e., at insert DCMG 150404 (Figure 9).

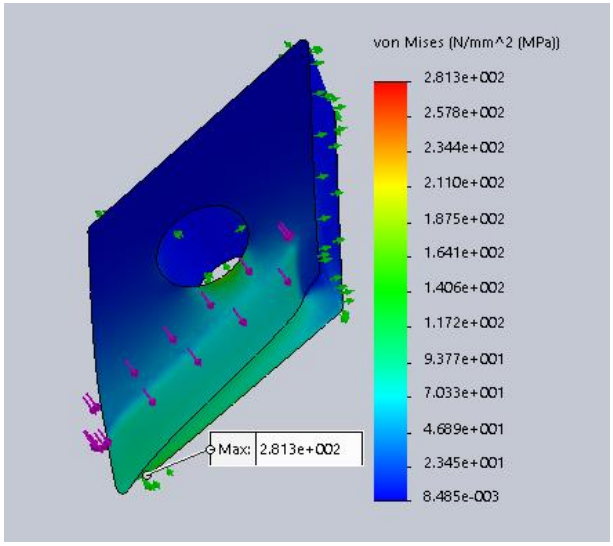

Figure 9. Insert with maximal amount of stress (von Mises 281,3 MPa)
Slika 9. Pločica alata s najvećim iznosom naprezanja (von Mises 281,3 MPa)

5. Conclusion

In this paper the authors have established that, with the help of Taguchi experiment plan, the optimal parameters are: insert shape S (90°), clearance angle N (0°) and nose radius 1,2 mm. Accordingly, optimal insert tool is SNMG 120412, at which by evaluation of simulation is also obtained minimum of maximal stress, 151,7 MPa.
It is possible to conclude that stress distribution model in the cutting tool during turning process can be made with simpler and more user-friendly FEM software such as SolidWorks Simulations.

Acknowledgements

This work was financially supported by the University of Rijeka, Croatia, contract number 13.09.1.2.10.

REFERENCES

[1] Johnson, G. R., Cook, W. H.: A constitutive model and data for metals subjected to large strains, high strain rates and high temperatures, Seventh International Symposium on Ballistics, Hague, Netherlands, 1983, 541-547.
[2] Lee, W.-S., Lin, C.-F.: High-temperature deformation behaviour of Ti6Al4V alloy evaluated by high strain-rate compression tests, Journal of

Materials Processing Technology, 75(1998)1-3, 127-136.
[3] Tounsi, N., Vincenti, J., Otho, A., Elbestavi, M. A.: From the basic mechanics of orthogonal metal cutting toward the identification of the constitutive equation, International Journal of Machine Tools and Manufacture, 42 2002, 1373-1383.
[4] Cukor, G.: Obrada metala rezanjem, Sveučilište u Rijeci, Tehnički fakultet, Rijeka, 2014., 54-57.
[5] Filetin, T., Kovačićek, F., Indof, J.: Svojstva i primjena materijala, Sveučilište u Zagrebu, Fakultet strojarstva i brodogradnje, Zagreb, 2002., 206-208.
[6] Yang, W. H., Tarng, Y.S.: Design optimization of cutting parameters for turning operations based on the Taguchi method, Journal of Materials Processing Technology, 84(1998), 122-129.

ISSN 1847-7917

Reverse engineering process application in single item production

***Luka CELENT*[1)], *Dražen BAJIĆ*[1)], *and Sonja JOZIĆ*[1)]**

1) University of Split
Faculty of Electrical Engineering, Mechanical Engineering and Naval Architecture, R. Boškovića 32, Split, Croatia
Sveučilište u Splitu
Fakultet elektrotehnike, strojarstva i brodogradnje, R. Boškovića 32, Split, Hrvatska

luka.celent@fesb.hr; drazen.bajic@fesb.hr; sonja.jozic@fesb.hr

Keywords

Reverse engineering
Single item production
3D scanning
CAD
Surface creation
CAM

Ključne riječi

Reverzibilno inženjerstvo
Jednokomadna proizvodnja
3D skeniranje
CAD
Kreiranje površine
CAM

Review paper

Abstract: This paper presents reverse engineering approach in single item production. Conventional forward engineering for single item production is often too expensive and does not complete the time requirements. Therefore this approach has a negative effect on the economy of production. In order to solve this problem, manufacturing industry is forced to implement a reverse engineering approach due to its significant advances and practical application in this field.
Reverse engineering process in single item production, presented in this paper, involves the use of 3D scanner as a device to capture and digitize the data from the existing object. Measurement data are acquired by 3D stereo-photogrammetric scanning. Processing the measurement data by CATIA V5 software a CAD model was created. The analysis and modifications of design are preformed on that CAD model. A physical prototype is then made using 3D printing technology, according to the CAD model for validation of the same. Due to the improvement of design specific customer requirements are met, and efficient single item production is achieved.

Pregledni rad

Sažetak: Ovaj rad predstavlja novi pristup u jednokomadnoj proizvodnji korištenjem Reverznog Inženjerstva. Konvencionalno, antegradno inženjerstvo u jednokomadnoj proizvodnji, je vrlo često preskupo i ne ispunjava vremenske uvjete isporuke. Ovaj pristup time negativno utječe na profitabilnost proizvodnje. U svrhu rješavanja ovog problema, proizvodna inustrija je prisiljena uvesti novi reverzno inženjerski pristup u proizvodnji, zahvaljujući njegovim značajnim prednostima i praktičnoj primjeni u ovom području. Proces reverznog inženjerstva u jednokomadnoj proizvodnji predstavljen u ovom radu, obuhvaća korištenje 3D skenera kao uređaja za dobivanje podataka od već postojećeg objekta i njihovu digitizaciju. 3D fotogramatskim skeniranjem su prikupljeni parametri na temelju kojih je u programu CATIA V5 kreiran CAD model. Analize i izmjene dizajna su izvršene na tom CAD modelu. Fizički prototip je izrađen korištenjem tehnologije 3D tiskanja, prema Cad modelu u svrhu validacije istog. Poboljšanim dizajnom u potpunosti su ispunjeni specifični zahtjevi kupca i ostvareni uvjeti za efikasnu jednokomadnu proizvodnju.

1. Introduction

Reverse engineering (RE) in manufacturing and engineering is used for a wide variety of reasons. It can be used to take apart engineering equipment or a manufactured product for discover the materials it is made from and how it works. In that case RE can help a business to determine and improve production processes and enhance product effectiveness. Also, it can be used as a process of taking the existing physical model and reproducing its surface geometry in three-dimensional (3D) data file on a computer-aided-design (CAD) system. With the easy availability of CAD packages, reverse engineering technology has become a practical tool to create a three-dimensional virtual model of an existing physical part. That, in turn, has made the use of 3-D CAD, computer-aided manufacturing, or other computer-aided engineering applications easier [1].

RE process is now accepted as a necessary phase in manufacturing for it provides the achievement of prescribed quality with significant cost reduction as compared to conventional forward approach. The main difference between conventional forward engineering and RE is that the former is an explicit physical implementation process from high-lever abstract concept to design, whilst the latter is an inferential process that is obtained by adjusting and modifying the feature parameters to approach an object model [2].
Single item production sometimes known as one-off or custom production is when only one product is made at a particular time. There is a clear difference between single item and mass production based upon the purpose of the production, the costs involved, the business model and lead times.

There is an increasing pressure on manufacturing industry especially in single item production, to develop new ways to make their production more cost effective.
Introduction of RE approach was very successful and resulted in giving maximal benefit of invested money. In RE process, a physical object is translated in mathematical model allowing the adjustments and modifications in order to optimize the product concept before manufacturing. Methods of RE have different application areas for extracting data from the existing object for which the documentation doesn´t exist, recovery of a damaged part, modification of model, inspection and analyses of model etc [3]. With application of RE the product development times are rapidly compressing. For the existing parts RE approach can speed up research and development of products, shorten the cycle from design to manufacturing and allows realization of some modern design concepts.
Most firms now make use of CAD programs for solid modelling and shape optimization. Creating a 3D model of the part is a time-taking task. For existing parts, the solid modelling time can be minimized by reverse engineering: scanning the part geometry using a contact or non-contact (laser) scanner and using software programs for improvement of product design [4].

2. Chinrest model as a custom product

A chinrest is a shaped piece of wood (or plastic) attached to the body of a violin or a viola to aid in the positioning of the player's jaw or chin on the instrument (Figure 1). Many instruments are sold or rented with chin rest models that fit relatively few people. But, by playing with a generic chin rest that "works for someone else" or "came with the instrument," a player may miss an opportunity to improve technically or to prevent physical problems. Well-fitted chin rest can help to facilitate better posture and support of the instrument which ultimately contributes to the playing excellence. In this paper chin rest for viola is taken as a single item or custom product.

Figure 1. Chinrest model for viola as a custom product

Slika 1. Podbradak za violu kao prilagođeni proizvod

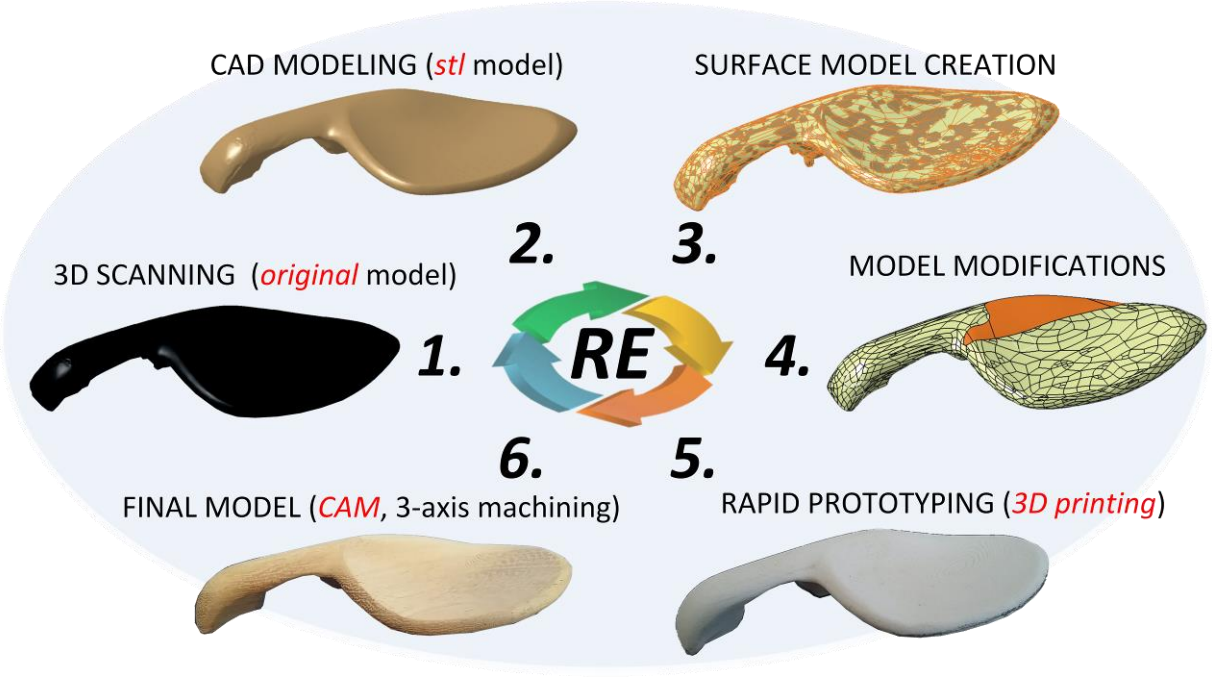

Figure 2. General steps of RE on chinrest model

Slika 2. Faze procesa reverzibilnog inženjerstva na modelu naslona za bradu

3. Reverse Engineering process phases on chinrest model

RE process was performed on the original model of chinrest model that came as a part of the instrument (Figure 2). The request for modification of the original chinrest model came as a result of specific order for a young viola player. The variation of design depended on customer requirements considering specifications that should be met, and in this case they are: jaw shape, neck length, right height, flexibility and placement.
The objective of the process is to be able to generate model-to-CAD and CAD-to-model reconstruction of the original model for future usage.

3.1. Original model digitization

The first phase of RE consist of capturing or recreating the geometry of the object by digitization. Strategy for digitization of the object depends on complexity of the surfaces [5]. As the original chinrest has a relatively complex shape and small dimensions, the RE of chinrest model digitization was performed by 3D stereo-photogrammetric scanning using measurement volume of 65mm. During this process, the system records information about the surface in the form of numerical data-generates a point's cloud matrix (3D-coordinates). This approach can provide high-quality overall geometry as well as increased resolution and accuracy of selected details.
The obtained point cloud data is then imported to CATIA V5 software to develop the 3D model.

3.2. Surface model creation in CATIA V5

CATIA V5 makes possible quickly capture and enhance physical prototype shapes, making the 3D virtual model the design reference. It also provides powerful technologies embedded within CATIA that allow the easy manipulation of points cloud or meshes, while quickly transforming them into 3D surface shapes.

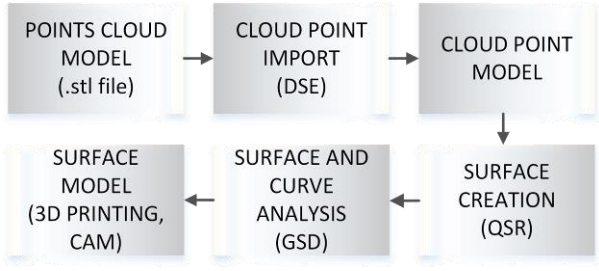

Figure 3. The surface creation process in CATIA V5 software

Slika 3. Proces reverzibilnog inženjerstva u programskom paketu CATIA V5

In CATIA V5 CAD three modules were used: Digitized Shape Editor (DSE), Quick Surface Reconstruction (QSR), Part design (PD) and Generative Shape Design (GSD). The process of RE in CATIA used in this article is shown in Figure 3. In order to create surface a points cloud acquired by 3D stereo-photogrammetric scanner was tessellated by CATIA software into a STL mesh [6]. Building a surface from the STL mesh requires an extensive analysis and a good quality of STL file [7].
Rough and noisy parts on the surface of the mesh were avoided and twisted or in any other way corrupted triangles were prevented and quality of the layout was ensured by closing all small holes. Mean surface deviation was checked and the Surface detail was set to 4000 (Figure 4). Due to a rough edge of the mesh free edge tolerance was set to higher value of 1mm, also the full internal tangency was checked. Satisfying layout of the sub-surface was gained.

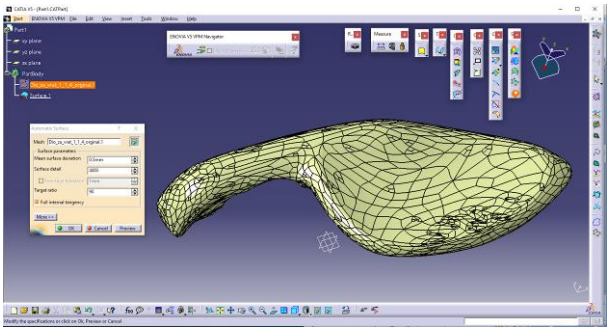

Figure 4. The surface creation process in CATIA V5

Slika 4. Formiranje površinskog modela u CATIA V5

3.3. CAD model improvements

The modification of the original chinrest model came as a result of specific order for a young viola player wit some specifications that should be met like jaws shape and neck length. Improved CAD model was analyzed in order to make certain adjustments based on the requirements of function.

3.4. Rapid prototyping using 3D printer technology

For 3D printing, first step is to import an STL format, 3D data file into ZPrint® software. By executing the command to start printing a 3D model is emerging from the bottom up one cross-section at a time (Figure5). A thin layer of ceramic powder is spread and then an ink jet print head deposits a silicate binder onto the powder in the shape of the part. When printing is complete, using vacuum cleaner a 90% of loose powder should be removed and recycled for future use.

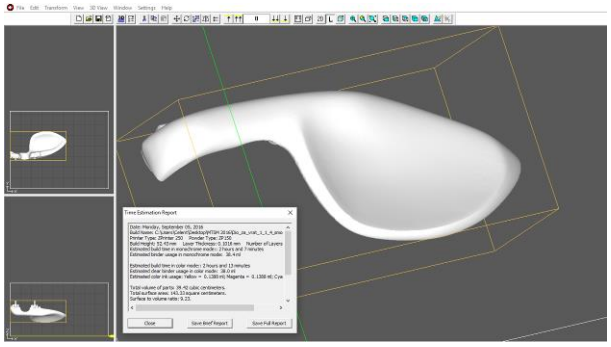

Figure 5. ZPrint interface for 3D printing

Slika 5. Sučelje ZPrint paketa za 3D printanje

Final analyses are carried out mostly on physical prototype which was made on 3D printer. Analyzing the CAD model a certain disproportions involving possible poor performance and reduce of the functionality were visible. However, disadvantages of chinrest design are not clearly reflected in the CAD model therefore a physical prototype was important.

3.5. CAM supported by CATIA V5

Once when the CAD model was repaired and improved as a result of detailed analysis of physical prototype, the final chinrest model was ready for production on 3-axis CNC machining centre.

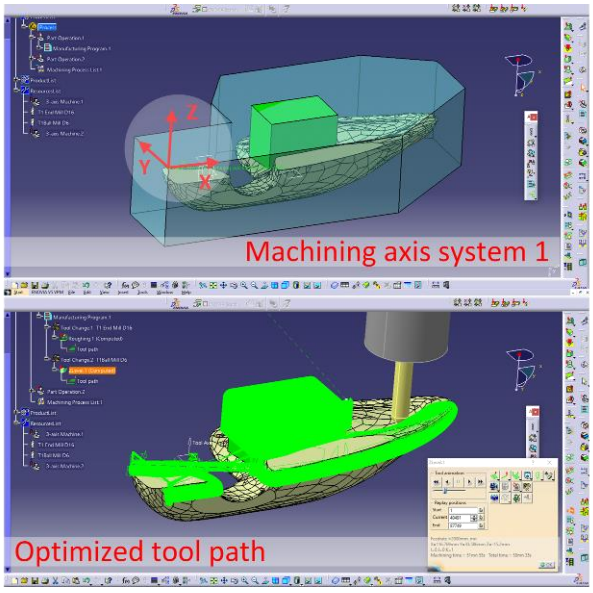

Figure 6. Machining axis system for part operation 1

Slika 6. Nul točka strojne obrade za operaciju 1

The complexity of chinrest design would normally require 5-axis machining centre. In that case the special CAM program was made using 2 different axis systems in 2 part operations (Figure 6 and 7). CATIA module Surface Machining was used to generate NC code for machining of wooden model of chinrest. The type of machine used for the milling of chinrest was machining centre VC560 manufactured by Spinner (Figure 8.)

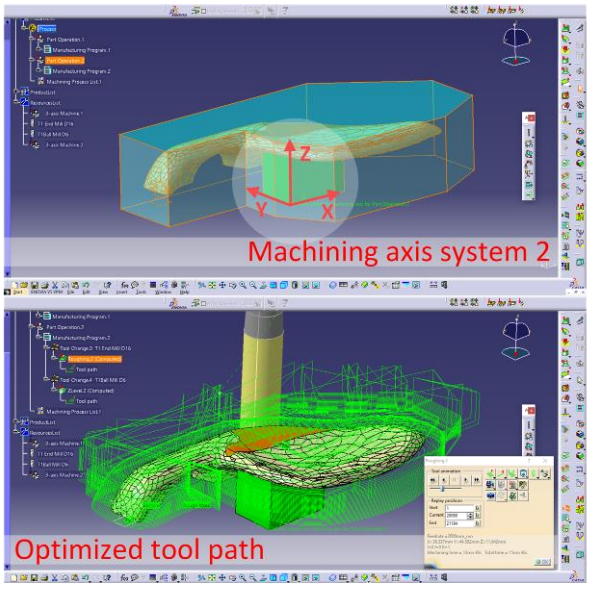

Figure 7. Machining axis system for part operation 2

Slika 7. Nul točka strojne obrade za operaciju 2

Viola chinrest was made of maple. Considering the specifics of that same material, special attention was paid to the selection of cutting parameters.

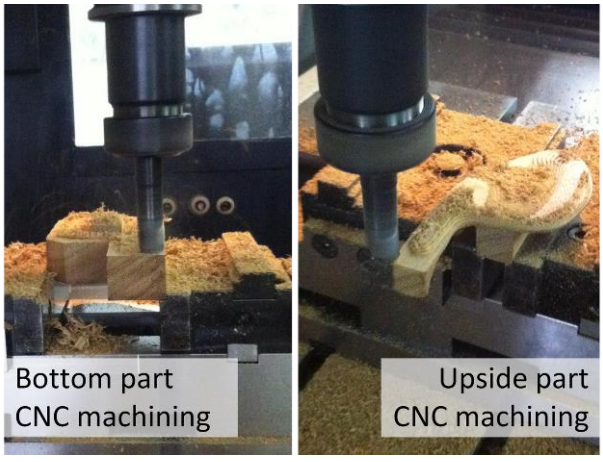

Figure 8. CNC machining of final chinrest model

Slika 8. Strojna obrada konačnog modela podbratka

4. Conclusion

The integration of RE approach compresses the product development times compared to conventional method, and enables for faster manufacturing of any custom or single item product. Any changes in design can be easily updated in the backup 3D CAD model considering customer requirements, quality specifications and manufacturing facilities. Due to the improvement of design specific customer requirements are met, and efficient single item production is achieved.

REFERENCES

[1] BRYDEN, D.: CAD and Rapid Prototyping for Product Design, Laurence King Publishing Ltd (2014),

[2] GUPENG, Z.; JIANNGHUA, Z.: The effects of forward and reverse engineering on firm innovation performance in stages of technology catch-up: an empirical study of China, Technological Forecasting and Social Change (2016), Vol. 104, 212-222

[3] NABIL, A.; MATHIEU, L.: From reverse engineering to shape engineering in mechanical design, CIRP Annals – Manufacturing Technology. (2015) Vol. 65, 165-168

[4] HERRAEZ, J.; MARTINEZ, J.C.; COLL, E.; MARTIN, M.T.; RODRIGUEZ, J.: 3D modeling by means of videogrammetry and laser scanners for reverse engineering, Measurement (2016), Vol. 87, 216-227

[5] HONG-TZONG, Y..: Reverse Engineering of the engine intake ports by digitization and surface approximation, International Journal of Machine Tools and Manufacture (1997), Vol. 37, 855-971

[6] SZILVASI-NAGY, M.; MATYASI, GY.: *Analysis of STL Files, Mathematical and Computer Modeling,* (2003), Vol. 38, 945-960

[7] BITTNAR, Z.; RYPL, D.: *Generation of computational surface meshes of STL models*, Journal of Computational and Applied Mathematics (2006), Vol. 192, 148-151

ISSN 1847-7917

Effects of copper and heat treatment parameters on mechanical properties of austempered ductile iron

***Nikša ČATIPOVIĆ*[1)], *Dražen ŽIVKOVIĆ*[1)], *Zvonimir DADIĆ*[1)]**
1) Fakultet Elektrotehnike, Strojarstva i Brodogradnje, Sveučičišta u Splitu (Faculty of Electrical Engineering, Mechanical Engineering and Naval Architecture, University of Split) Ruđera Boškovića 32, 21000 Split, **Republic of Croatia**

niksa.catipovic@fesb.hr
drazen.zivkovic@fesb.hr
zvonimir.dadic@fesb.hr

Keywords
ductile iron
austempered ductile iron
austempering
microstructure
copper
mechanical properties

Ključne riječi
žilavi lijev
izotermički žilavi lijev
izotermičko poboljšavanje
mikrostruktura
bakar
mehanička svojstva

Review papper

Abstract: In this review papper insight is given how both copper and heat treatment parameters affect mechanical properties of austempered ductile iron (ADI). It has been shown that both copper and other alloying elements such asNi and Mo affect the mechanical properties of ADI. Also, it has been shown that the strenght, hardness, elongation and fracture toughnes strongly depend on amount of ausferritic ferrite and stable, high carbon enriched retained austenite. The results shown confirm that alloying with Co + Ni produce ductile grades of ADI, while alloying with Cu produce grades of higher strength. The standard processing window depends on the austempering parameters and alloying elements, as well as standard used to produce ADI.

Utjecaj bakra i parametara toplinske obrade na mehanička svojstva izotermički poboljšanog žilavog lijeva

Pregledni rad

Sažetak: U ovom preglednom radu dan je uvid u utjecaj bakra i parametara toplinske obrade na mehanička svojstva izotermički poboljšanog žilavog lijeva. Pokazano je da i bakar i drugi legirni elementi poput Ni i Mo imaju utjecaja na mehanička svojstva ADI-ja. Također je pokazano da čvrstoća, tvrdoća, produljenje i udarna radnja loma mnogo ovise on količini ausferitnog ferita te stabilnog, ugljikom bogatog zaostalog austenite. Prikazani rezultati potvrđuju da legiranje sa Cu + Ni dovodi do žilavih vrsta ADI-ja, dok legiranje sa Cu dovodi do čvršćih vrsta ADI-ja. Standardni vremenski okvir ovisi o parametrima izotermičke obrade i legirnim elementima, te o korištenom standardu toplinske obrade.

1. Introduction

In recent years, there has been great demand for light weight, durable and cost effective materials. Ductile iron is one such material. A lot of research has been done on this material and focus has been set on possible improvements of mechanical properties by appropriate heat treatment processes and also by alloying, which can enhance its properties. Ductile iron when subjected to an isothermal heat treatment process known as "austempering" produces Austempered Ductile Iron (ADI), [1]. It has better properties than ductile iron.

ADI materials possess a unique microstructure of ausferrite, produced by austempering of ductile irons. The ausferrite is a mixture of fine acicular ferrite and carbon enriched stabilized austenite, [2, 3]. This new microstructure results with capability superior to many ferrous and aluminium alloys. As compared with pearlitic, ferritic or martensitic structures, ausferrite exhibits twice the strength for a given level of ductility formed by conventional heat treatment processes, [1].

The mechanical properties of the austempered ductile iron depand on the ausferrite microstructure. The austempered matrix offers better tensile strength to ductility ratio than is possible with any other grade of ductile iron. Various combinations of properties can be obtained from austempered ductile iron because of the ausferrite microstructure which depends on heat treatment conditions and alloyingelements, [4].

The heat treatment of the austempering process consists of austenitising ductile iron, quenching to the austempering temperature for controlled time, and then cooling to room temperature, Fig. 1.

Several authors [2, 3, 6] have well established that during the austempering, ADI undergoes a two stage transformation process.

In the first stage, the austenite (γ) decomposes into bainitic ferrite (α) and a carbon enriched retained austenite (γ_{hc}), a product known as ausferrite.

$$\boldsymbol{\gamma \rightarrow \alpha + \gamma_{hc}} \qquad (1)$$

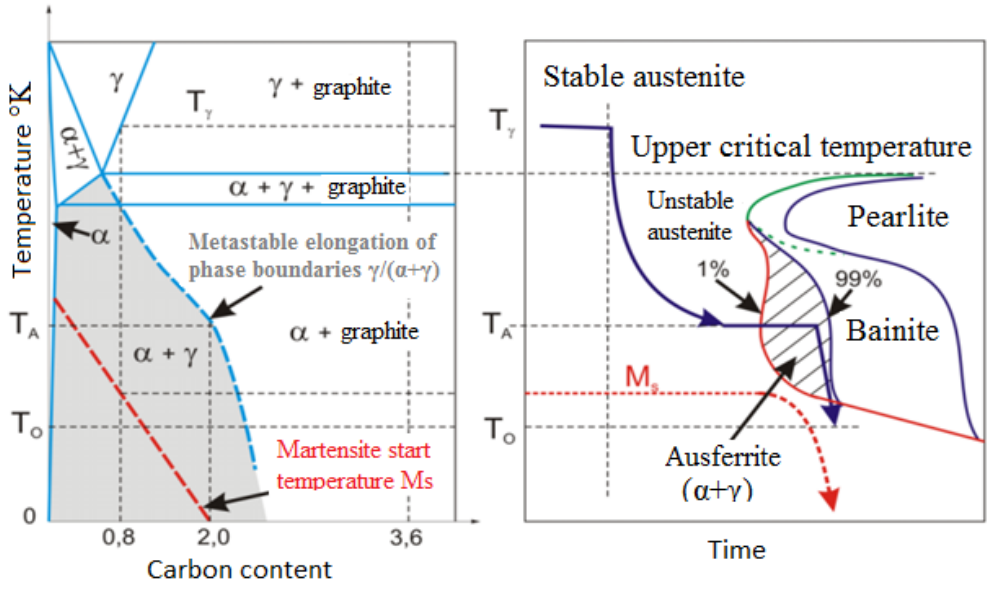

Figure 1: Principle phase and isothermal transformation diagrams illustrating the M_S temperature change with respect to austempering time and the metastable α + γ region [5]

Carbon enriched retained austenite (γ_{hc}) further decomposes into ferrite (α) and carbides if the casting is held at the austempering temperature for too long, [2].

$$\gamma_{hc} \rightarrow \alpha + carbide \quad (2)$$

The occurrence of carbides in the microstructure makes the material brittle and therefore, that reaction should be avoided. Hence, the optimum mechanical properties of ADI material can be achived upon completion of the first reaction, but before the second reaction starts, i. e. inside processing window, [7, 8].

The investigation and determination of a processing window has attracted great interest in previous years, [3, 6, 11-15]. Processing window can be defined as "microstructure" or "standard" processing window. "Microstructure" processing window is defined by microstructural features and it is best determined with criterion proposed by Elliott and Bayati, [3, 15]. The beginning of the processing window represents a point when the unreacted austenite volume decreases to 3% (value obtained using quantitative metallography), while the end of window is correlated to a decrease of reacted (carbon enriched) retained austenite volume ($V\gamma$) to 90% of its maximum (where $V\gamma$ was determined by X-ray diffraction), [8]. On the other hand, "standard" processing window is defined regarding mechanical properties of ADI material produced in microstructure processing window, which have to satisfy ASTM A897M:1990 standard. However, there are three ADI standards used currently worldwide: ASTM A897M-06 (first edition from 1990), EN 1564:1997 and ISO 17804:2005, [16]. As those standards vary in some details regarding the number of grades and minimal requirements of ultimate tensile strength and elongation for different grades, so the processing window will differ and depend on the standard used, [8].

Alloying elements have influence on the isothermal temperature, nitiation time and completion of the austempering reaction, and thereby affording a larger processing window and ease off control of the reaction. The influence of copper and nickel is of interest in this respect. Copper delays nucleation of ferrite plates around graphite nodules and favours formation of plate-like morphology. Furthermore, Cu suppresses the formation of carbides in the microstructure. Presence of nickel reduces the transformation speed and lowers the temperature of the isothermal reaction. The synergetic effect of Cu and Ni on suppressing the nucleation and early growth of ferrite plates and thus expanding the time for isothermal reaction is especially important, [8, 9, 10].

2. Literature review on copper effect

Cast irons are alloys of iron and carbon, such as steels, that have greater amount of carbon, between 2 and 6,67%. Most commercially manufactured cast irons have carbon content from 2,5 to 4% and are very brittle and have very low ductility. However, as cast irons melted very easily and as they are very brittle in nature, casting is the only process for the manufacture of complicated shapes. Controlling the alloying addition, good foundry practice and appropriate heat treatment, the properties vary over a wide range. The shape and distribution of free carbon particles gratly influencthe physical properties of cast irons. There are different types of cast irons in use:

malleable cast iron, gray cast iron, wite cast iron, nodular (ductile) cast iron and alloyed cast iron, [1].

2.1. Ductile Iron

Ductile iron or nodular cast iron or spheroidal graphite cast iron is a type of a cast iron where graphite is present in the form of nodules, tiny balls or spheroids, [1]. It derives its name from the fact that in the as-cast structure it exhibits measurable ductility, which other types of cast irons do not exhibit. Based on the matrix, spheroidical graphite iron may be classified into different types, namely: ferritic, pearlitic, martensitic and austenitic. Depending on the cooling rate, the matrix may vary from a soft ductile ferritic structure through a hard and higher strength pearlitic structure to and austenitic structure. One of the most fascinating features of ductile iron is that the tensile elongation is as high as 17% which is not comparable to other types of cast iron, [1].

The amount of graphite or Fe_3C depends on the carbon content and increases as the carbon content increases. The graphitization potential of iron and castability depends on high carbon and silicon content. Typically, the Mg varies from 0.03% for ferritic irons to as high as 0.06% for pearlitic irons. Phosphorous and sulphur are also present in the composition. They can be as high as 0.15% for low-quality iron and are considerably less for high-quality iron, [17].

Depending on the grade of spheroidal gray cast (SG) iron its properties can vary, Fig. 2. The tensile strength can vary from 400 MPa for ferritic grades to as high as 1300 MPa for austempered ductile irons. The yield strength can also vary over range of 250 MPa to 800 MPa. The elongation can sometimes be as high as 25%, only for ferritic grades. High fluidity enables the castability of SG iron. Also, they have good machinability because of the graphite present which makes chip formation easier. And also ductile iron is higly corrosion resistant, [18, 19].

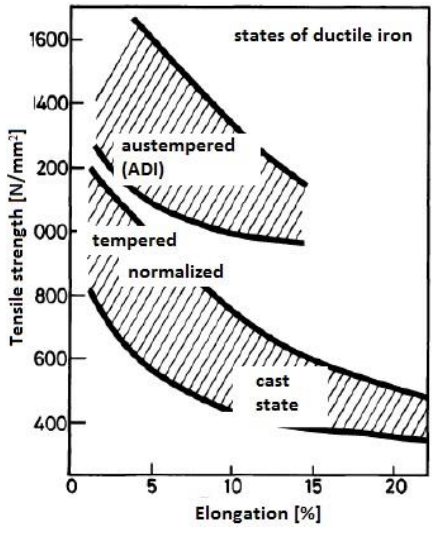

Figure 2: Different states of ductile iron [20]

2.2. Austempered Ductile Iron (ADI)

ADI is the most recent one added to the ductile iron family produced by austempering of the conventional ductile iron. ADI is nearly twice as strong as pearlitic ductile iron along with high elongation and toughness. This combination of properties provides a material with superior wear resistance and fatigue strength, [1].

In the early 1930's, the work of Bain, et al, on the isothermal transformation of steel developed the heat treatment process known as austempering process. In the early 1940's Flinn applied this process of austempering to cast iron, namely gray iron. In 1950's, both the austempering process and ductile iron had been developed.

In austempering austenite transforms isothermally to lower bainite and as a result it reduces distortion and cracking, [21]. In this heat treatment process the steel is heated to a temperature up to austenitizing temperature and then the steel is quenched by holding the steel in a molten salt bath at a temperature above Ms and the austenite is led to transform to lower bainite at this temperature, Fig 3.

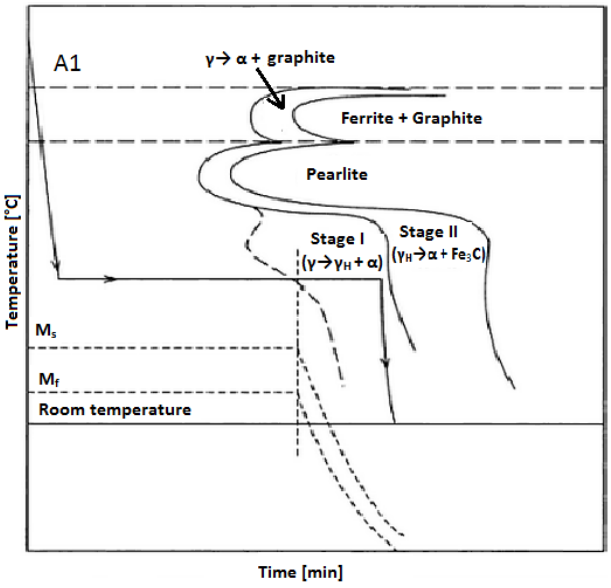

Figure 3: Austempering process [22]

When the steel is quenched from A1 temperature to the molten salth bath above Ms temperature, for proper austempering adequate hardenability of the steel is required to avoid pearlitic transformation. The process of austempering results in enhanced ductility, increased toughness, higher hardness, lesser distortion and quench cracks as compared with tempered specimen.

ADI gives a combination of properties such as high strength with good ductility, good fatigue strength and wear resistance along with fracture toughness. Great combination of properties can be obtained by varying the

austempering variables i.e. austempering temperature and holding time, [23].

As mentioned in introduction, the microstructure of ADI is different from the austempered steels where the microstructure consists of ferrite and carbide. In ADI the product of austempering reaction iron is often referred to as "ausferrite" rather than bainite, [23]. The addition of alloying element, silicon, suppresses the carbide precipitation during austempering reaction and retains high carbon austenite (γ_{hc}). In austempering of steel the bainitic ferrite forms by the rejection of carbon into the residual austenite. As the process proceeds more bainitic transformation takes place and more carbon is rejected into the surrounding austenite. In earlier stages, the austenite transform to martensite as the carbon content of austenite is insufficient to make it stable, but at longer times it becomes thermally stable, [23, 24, 25].

Austempered ductile iron produced by the austempering of the ductile iron undergoes the following steps:

1. Austenitising: The ductile cast iron is heated to the austenitising temperature i.e. above A1 temperature (850°C to 950°C) so that the casting gets converted to austenite.
2. Austempering: The austenitised part is rapidly quenched in a molten salt bath to avoid pearlitic transformation. Quenching is done from austenitising temperature 850°C – 950°C in a salt bath maintained at a temperature of 200°C – 450°C.
3. Holding time: the casting is hold at the desired temperature for sufficient time to allow bainitic transformation to be complete.
4. Air cooling: After holding the sample for sufficient time it is air cooled to the room temperature.

The applications of ADI are very vast based on the properties coupled with cost and flexibility benefits in different sectors:

I. Agriculture: excellent resistance to soil wear.
II. Digger/grab teeth: high strength and wear resistance.
III. Industrial: wear components, pumps etc.
IV. Gears: for wear resistance and better vibration damping than steel.
V. Construction: crushing, grading and wear components etc.
VI. Food and feeding milling: grinding, mixing, palletisation etc.

Austempered ductile iron has found successful application in many industries including construction and mining, automotive, heavy trucks and rail road.

The mayor disadvantage of ADI is that welding is not recommended for this type of material.

Effect of copper

Copper generally suppresses the carbide formation in lower bainite but do not alter the diffusion of carbon in austenite or its stability, [25]. It increases both the transformation rate and the carbon content in the matrix during austenitising process and widens the austenite zone of the phase diagram. Due to Cu addition stage II reaction is delayed and results in prevention from deterioration of properties, [26].

3. Experimental work

Many attemps were made to understand and predict the behaviour of austempered ductile iron that considers the study of ausferrite matrix structure and the response of the matrix structure to heat treatment, structure and properties correlation, and its mechanical properties with different variables and applications. A brief description of some of the literatures in these areas is presented here below.

1) Behera G. and Sohala S. R. have in their bachelor thesis experimented on two grades of SG irons which have been subjected to austempering process. One sample had 0.003% Cu and other 0.48% Cu. Other alloying elements were almost the same. 12 numbers of SG iron specimens of each melt were taken for carrying out austempering at four different temperatures (250°C, 300°C, 350°C and 400°C) for duration of 0.5 hour, 1 hour and 1.5 hour. Samples were heated to 900°C for one hour (austenitising) and then transferred quickly to a salt bath containing 50 wt% $NaNO_3$ + 50 wt% KNO_3 maintained at four austempering temperatures as mentioned for 0.5, 1 and 1.5 hours. Hardness is increasing from half an hour to one hour and then decreasing, Fig. 4. The alloyed ductile iron (alloyed with copper) has increased hardness as compared to specimens without copper as shown in the figure 4. After completion of bainitic transformation, if austempering is continued for still longer duration, stage II reaction sets in and retained austenite decomposes to bainitic ferrite and carbide. Stage II reaction is undesirable since it causes the embrittlement of structures and degrades the mechanical properties. This results in decrease of hardness, tensile strength and yield strength after achieving a peak value. Figure 5 shows variation of tensile strength values with different austempering times and figure 6 shows variation of yield strength. Also elongation has been measured and results have been shown in figure 7. Low ductility of ADI is achieved at lower austempering temperature. This is attributed to brittle fracture which

occurred in the matrix due to the presence of martensite, [1].

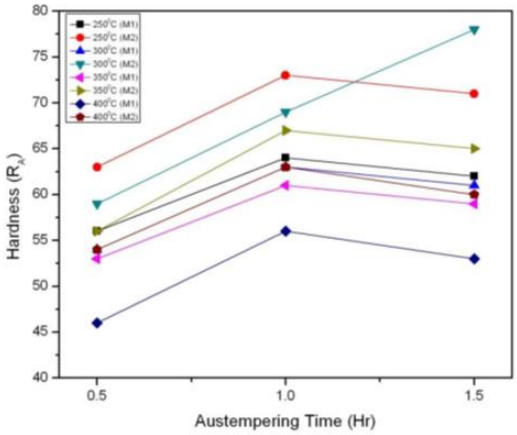

Figure 4: Influence of austempering time on hardness of different samples [1].

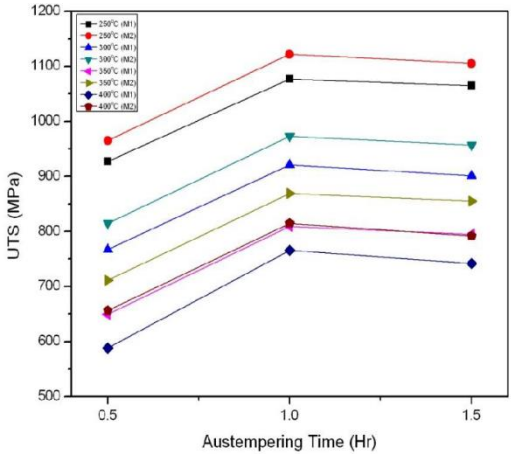

Figure 5: Influence of austempering time on tensile strength of different samples [1].

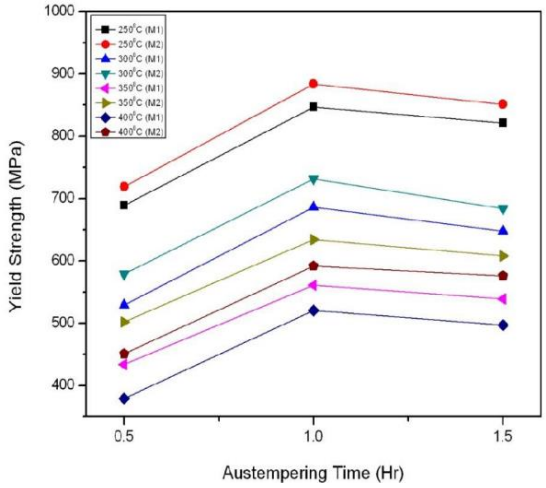

Figure 6: Influence of austempering time on yield strength of different samples [1].

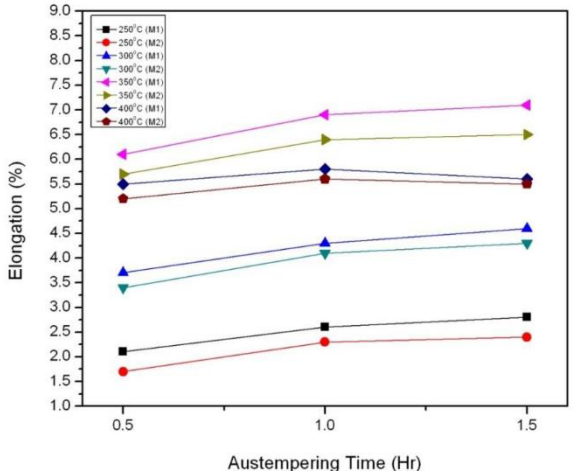

Figure 7: Influence of austempering time on elongation of different samples [1].

2) Olivera Eric, Dragan Rajnovic, Slavica Leposlava, Sidjanin T. Jovanovic observed and studied the microstructure and fracture of two types of austempered ductile irons, one is alloyed with copper and another is alloyed with copper and nickel. They also observed the effect of copper and copper plus nickel on the microstructure and impact properties of both austempered ductile irons. According to them there is dealy in the transformation kinetics of the residual austenite, Fig. 8. by the addition of copper plus nickel which results in a shift of the maximum of volume fraction of retained austenite to 3 hours of austempering, compared to 2 hours in austempered ductile iron alloyed with copper. In this way they could demonstrate that the volume fraction of the retained austenite strongly effects the fracture toughness of both the irons, i.e., with retained austenite content up to maximum value fracture tougness increases, then a decrease occurs with the decrease of the retained austenite, Fig. 9, [26].

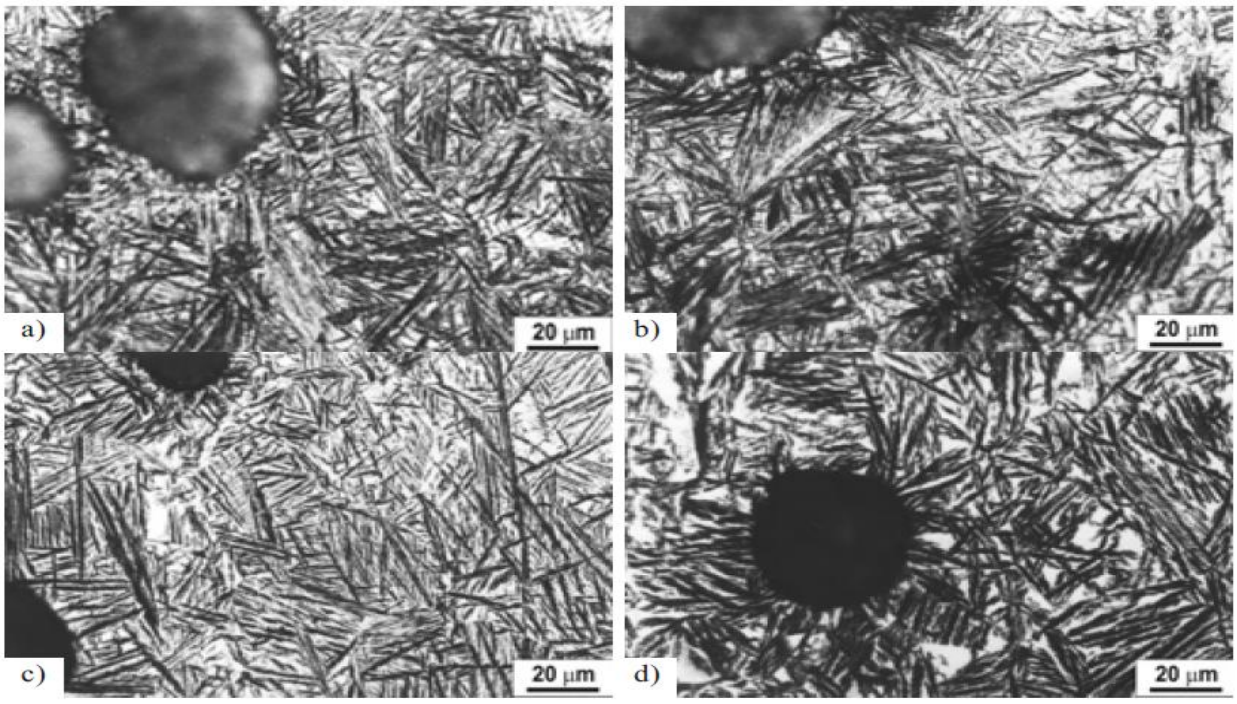

Figure 8: LM. Microstructure after austempering for 1 h at (a) 300 ºC and for 2 h at: (b) 300 ºC: (c) 350 ºC and (d) 400 ºC. M-martensite, [26].

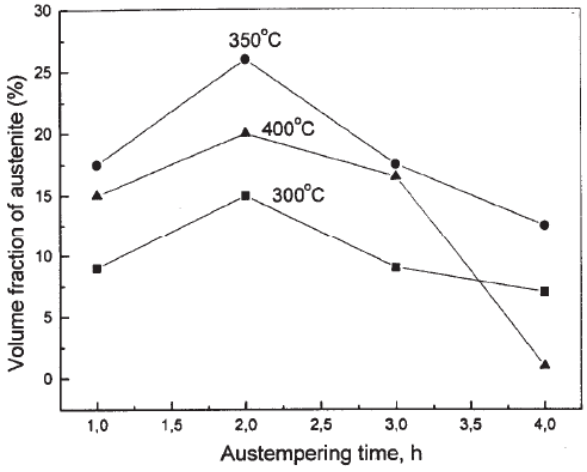

Figure 9: The effect of austempering time on the volume fraction of retained austenite at different austempering temperatures, [26].

3) Studies of J. Zimba, D. J. Simbi and E. Navara have shown the abrasive, wear and mechanical properties of the austempered ductile iron in comparison of these properties with that of the quenched and tempered steel. They found that as austempering temperature increases, the ferrite lath spacing and volume fraction of retained austenite increases. The tensile strength and hardness decreases with austempering temperatures while there is a significant increase in elongation and impact toughness as the austempering temperature is raised. The wear resistance of austempered ductile iron is good enough despite of the low initial hardness because during abrasion there is a surface transformation of retained austenite to martensite. Consequently, the surface hardness and wear resistance of the iron is increased, [27].

4) Studies of Uma Batra, S. Ray and S. R. Prabhakar show the variation in the austempered microstructure, the volume fraction of retained austenite, the average carbon content of retained austenite, their product and the size of bainitic ferrite needles with austempering temperature for 0.6% Cu alloyed ductile iron. For this, copper alloyed ductile iron specimens were taken and austempered at different temperatures and times. They observed that the bainite morphology changes from lower bainite to upper bainite with increasing austempering temperature. Also, with increasing austempering temperature, the average volume fraction of austenite, its carbon content, and the size of bainitic ferrite increases. Increasing the

austempering time initially increases the amount of retained austenite and its carbon content, and then both reach a plateau. The plateau extends over a period of stability of retained austenite, after which there is a decrease of both, [28].

Further they studied the effect of alloying elements on the austempering process, microstructure and structural parameters of both the austempered ductile iron containing 0.6% Cu and 0.6% Cu + 1.0% Ni as the main alloying elements. Optical metallography and x-ray diffraction are used to study the changes of the structure. Effect of alloying additions on the austempering kinetics was studied using Avrami equation. The austempering kinetics is slowed down by addition of Ni, [29].

5) O. Eric, M. Jovanovic, L. Sidnjanin and D. Rajnovic studied the microstructure and mechanical properties of the austempered ductile iron which is alloyed with Cu, Ni and Mo. When the austempering is done at 320°C in the range of 2 to 5 hours, a special type of austempered ductile iron microstructure is produced containing free bainitic ferrite and a stable higly carbon enriched retained austenite. During austempering of this iron at 400°C, yield strength, tensile strength and ductility obtained are twice lower that at 320°C. The appearance of martensite in the microstructure pertains to the lower values of tensile properties, [30].

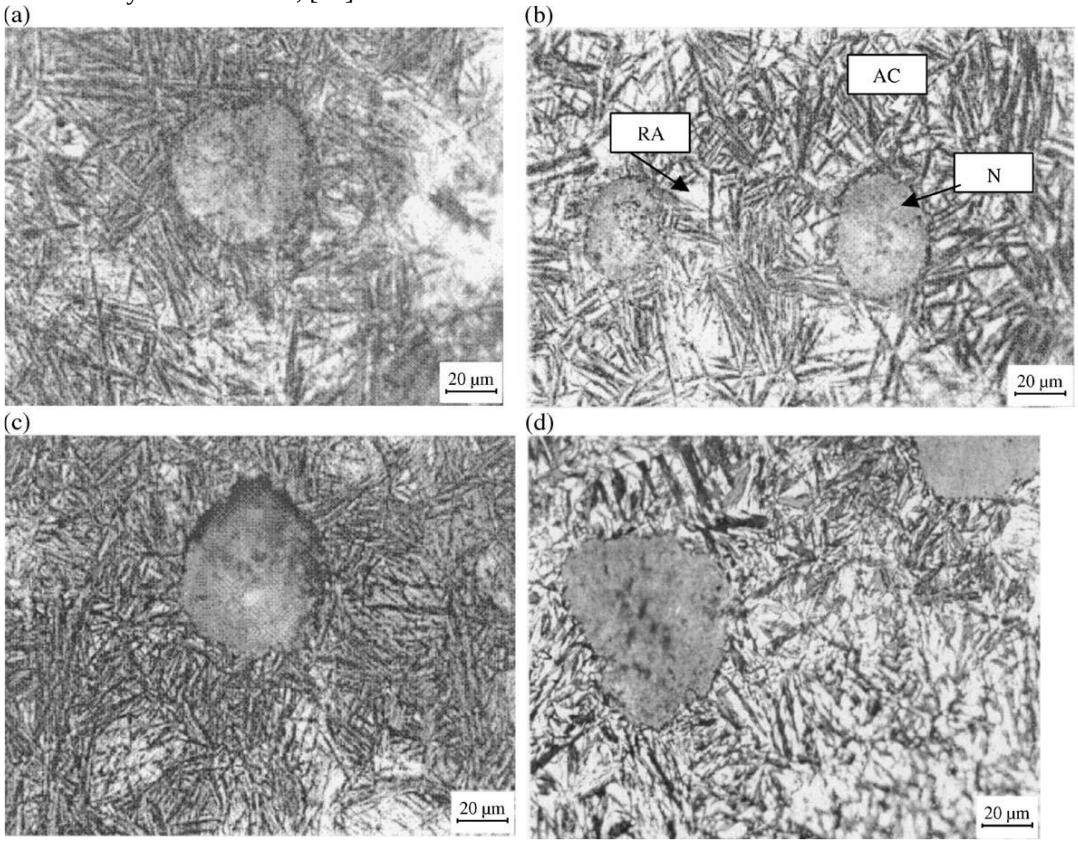

Figure 10: Light microscopy, etched. Microstructure after austempering at 320 jC for 1 h (a), 2.5 h (b), and 5 h (c); at 400 jC for 1 h (d). AC—acicular ferrite; RA—retained austenite; N—graphite nodule.

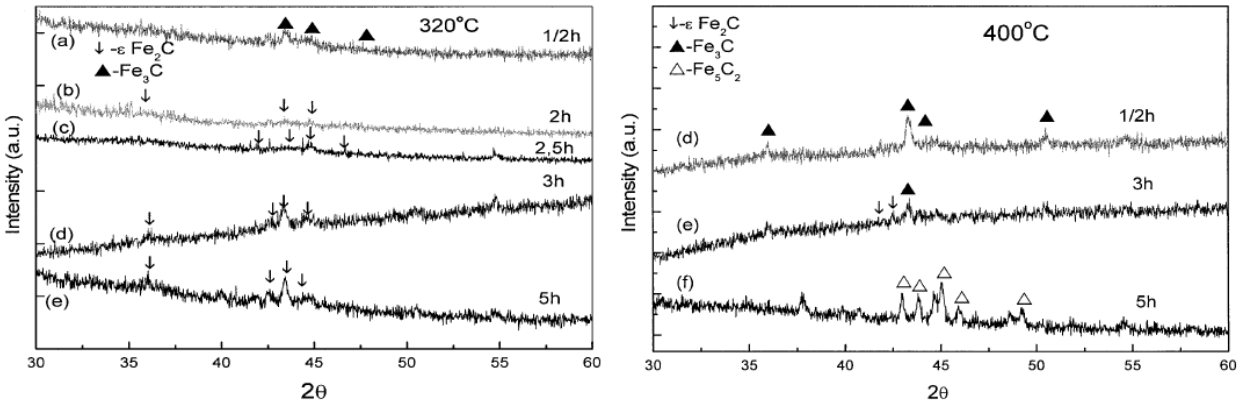

Figure 11: X-ray diffraction patterns of electrolytically extracted carbide residues of specimens austempered at 320C for 1/2h (a), 2h (b), 2,5h (c), 3h (d), 5h (e) and at 400 jC for 1/2h (d), 3h (e) and 5h (f).

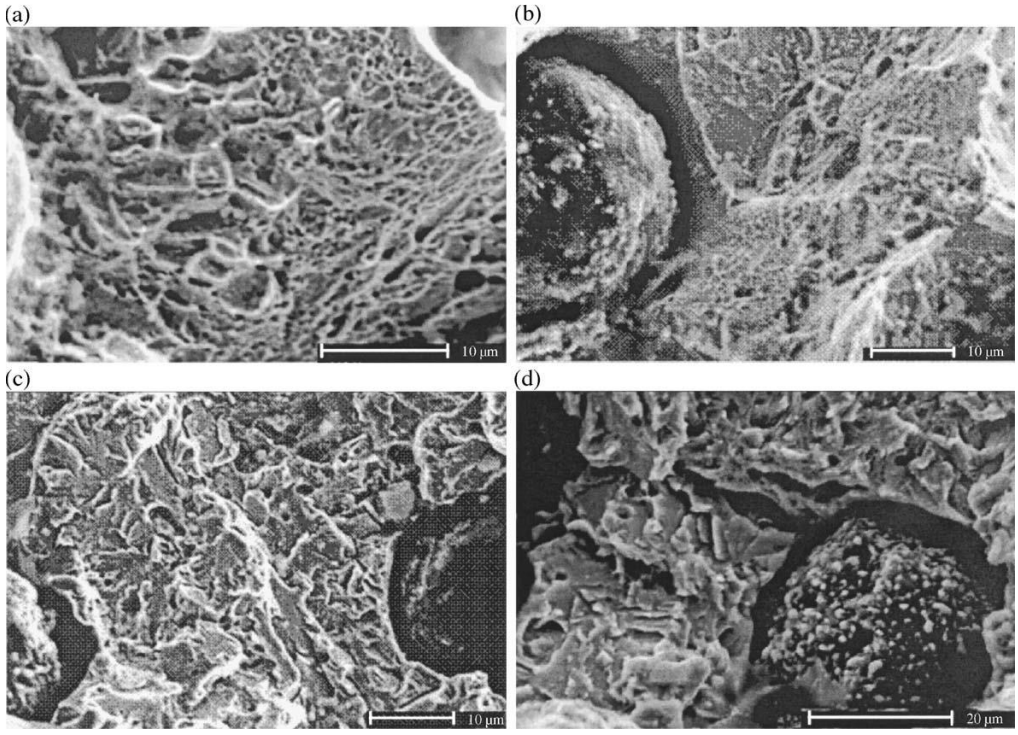

Figure 12: SEM. Fracture morphology after austempering at 320 jC for 2 h (a), 3 h (b), and 5 h (c); at 400 jC for 1 h (d). RA—retained austenite, q-carbide.

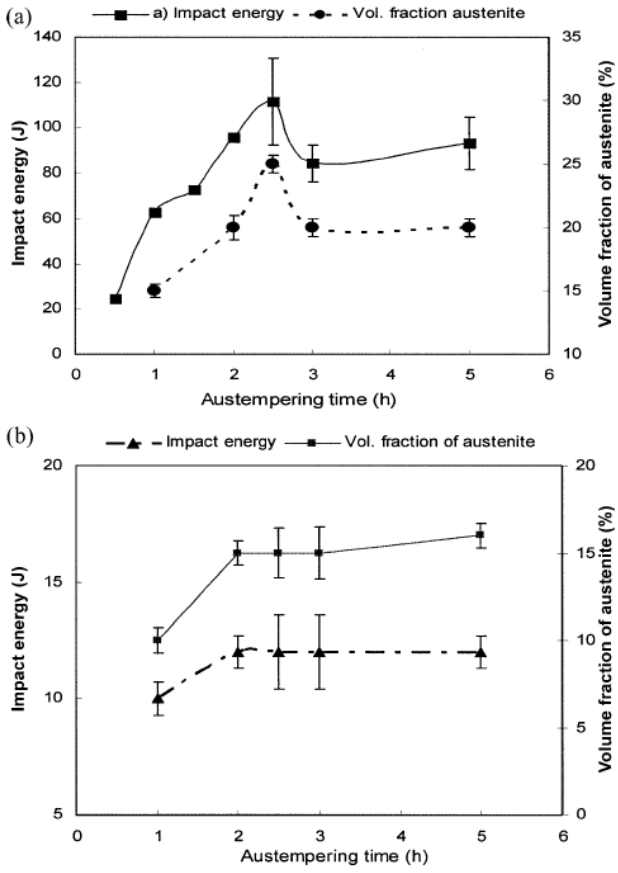

Figure 13: The effect of time of austempering on impact energy and volume fraction of retained austenite at 320 jC (a) and 400 jC (b).

6) M. Nili Ahmadabi, H. M. Ghasemi and M. Osia have studied the effect of austempering process on the wear behaviour of the austempered ductile iron. They considered a 0.75 wt. %Mn ductile iron with different nodule count and was austempered by conventional and successive austempering process at 315°C and 375°C for different time periods. They concluded from sliding wear tests on specimens with optimum mechanical properties austempered by different processes were delaminated which has a moninant wear mechanism. Thus the results from the mechanical and wear tests show that successive austempering processes improve both mechanical properties and wear resistance of ADI in comparison with conventional austempering process, [31].

4. Conclusions

The effect of copper as alloying element on the mechanical properties of SG iron austempered at different temperatures with varying austempering time has been investigated by different authors and the following conclusion have been made:

1. Alloying element copper improves the mechanical properties of spheroidal graphite iron after austempering. The properties are enhanced with austempering time but with increasing austempering temperature it initially increases and then gradually becomes constant.
2. The ductility of ADI also initially increases with austempering time up to a certain value and then it starts decreasing with further increase in time. Hardness, tensile strength and yield strength of ADI decreases continuously with austempering temperature.
3. The ductility of ADI initially increases with austempering temperature and then after reaching some maximum value at around 350°C, it starts decreasing with further rise of temperature.

Many works may be required to properly characterize both mechanical properties as well as graphite morphology of austempered ductile iron. Austempering times and temperatures should be further extended to observe changes in mechanical behaviour. Also, different wt% of copper should be studied to further understand its influence on mechanical properties of ADI and to find maximum limit of copper that enhances mechanical properties. Furthermore, it would be wise to come up with mathematical model which would incorporate copper adition, austenitising and austempering parameters with mechanical properties of ADI.

Acknowledgements

This work has been fully supported by Croatian Science Foundation under the project 5371.

REFERENCES

[1] Behera G., Sohala S. R., Effect of copper on the properties of austempered ductile iron castings. Bachelor thesis. Department of Metallurgical and Materials Engineering, National Institute of Technology, Rourkela, India, (2012).
[2] Sidjanin L., Smallman R. E., Mater. Sci. Tech. – Lond., 8, pp. 1095, (1992).
[3] Elliot R., Heat Treatments of Metals. 3, pp. 55, (1997).
[4] Chandler H., Heat treaters guide: practices and procedures for irons and steels. ASTM International, 2 Sub edition (December 1995).

[5] Živković D., Gabrić I., Dadić Z., Čatipović N., Vrljičak I., Analysis of austempering treatment parameters on properties of ductile iron EN-GJS-400. Zbornik radova Proceedings, Hrvatsko društvo za strojarske tehnologije, MTSM 2015, Split, pp. , (2015)
[6] Harding R. A., Kovove Mater., 45, p. 1, (2007).
[7] Sidjanin L., Smallman R. E., Young J. M., Acta Mater., 42, pp. 3149, (1994). doi:10.1016/0956-7151(94)90412-X
[8] Rajnovic D., Eric O., Sidjanin L., The standard processing window of alloyed ADI materials. Kovove Mater., 50, pp. 199-208, (2012).
[9] Bartra U., Ray S., Prabhakar S. R., J. Mater. Eng. Perform., 13, pp. 64, (2004). doi:10.1361/10599490417515
[10] Chang C. H., Shih T. S., Trans. Jpn. Foundrymen Soc., 13, pp. 56, (1994).
[11] Thomson R. C., Mater. Sci. Tech. – Lond., 16, pp. 1412, (2000).
[12] Bayati H., Elliott R., Mater. Sci. Forum, 329, pp. 73, doi:10.4028/www.scientidic.net/MSF.329-30.73 (2000)
[13] Zahiri S. H., Davies C. H. J., Pereloma E. V., Mater. Sci. Tech. – Lond., pp. 1761, (2003).
[14] Eric O., Rajnovic D., Zec S., Sidjanin L., Jovanovic M. T., Mater. Charact., 57, pp. 211, (2006). doi: 10.1016/j.matchar.2006.01.014
[15] Bayati H., Elliott R., Int. J. Cast Metal Res., 11, pp. 413, (1999).
[16] Dorn T., Keough J. R., Schroeder T., Thoma T., In: Proceedings of the Keith D. Millis Symposium. Ed.: Wood J. N., Hilton Head, South Carolina, USA, Ductile Iron Society and AFS, pp 1. (2003). doi: 10.1016/j.msea.2004.04.076
[17] Ductile iron, http://www.rastgar.com/rec/papers/paper-2.pdf
[18] Ductile iron, http://www.ductile.org/didata/Section3/3part1.htm
[19] Ductile iron, http://www.ductile.org/didata/Section3/3part2.htm
[20] Sučić, A. "Utjecaj izotermičke temperature i vremena držanja na strukturu i tvrdoću izotermičkog žilavog lijeva", diplomski rad, FESB, veljača 2015, Split.
[21] V. Singh, Physical Metallurgy, First Edition (1999), Reprint 2007, Standard Publishers Distributers, 1705-B, NaiSarak, New Delhi-110006.
[22] Čatipović, N., Živković, D., Dadić, Z., Sučić, A., Ljumović, P., "Utjecaj izotermičke temperature i vremena držanja na mikrostrukturu i tvrdoću izotermičkog žilavog lijeva", MTSM 2015, Split, rujan 2015.
[23] J. Yang, S. K. Putatunda, "Improvement in strength and toughness of austempered ductile cast iron by a novel two-step austempering process", Mater. Des. 25 (2004) 219 to 230.
[24] O. Eric, L. Sidjanin, Z. Miskovic, S. Zec, M. T. Jovanovic, "Microstructure and toughness of Cu, Ni Mo austempered ductile iron", Mater. Lett. 58 (2004) 2707 to 2711.
[25] U. Batra, S. Ray and S. R. Prabhar, "The influence of nickel and copper on austempering of ductile iron", JMEPEG (2004) 13:64-68.
[26] O. Eric, L. Sidjanin, Z. Miskovic, S. Zec, M. Jovanovic, "An Austempering study of ductile iron alloyed with copper", J. Serb. Chem. Soc. 70 (7) (2005) 1015-1022.
[27] J. Zimba, D. J. Simbi, E. Navara, "Austempered ductile iron: An alternative material for earth moving components", Cement & Concrete Composites, vol. 25 (2003) pp. 643-649.
[28] U. Batra, S. Ray, S. R. Prabhakar, "Austempering and austempered ductile iron microstructure in copper ductile iron", JMEPEG, vol. 12 (2003) pp. 426 – 429
[29] U. Batra, S. Ray, S. R. Prabhakar, "Impact properties of copper alloyed and nickel copper alloyed ADI", JMEPEG, vol. 13 (2004) pp. 64 – 68.
[30] O. Eric, M. Jovanovic, L. Sidnjanin, D. Rajnovic, "Microstructure and mechanical properties of CuNiMo austempered ductile iron", Journel of Mining and Metallurgy, vol 40b (1) (2004), pp. 11 – 19.
[31] M. Nili Ahmadabi, H. M. Ghasemi, M. Osia, "Effects of successive austempering on the tribological behaviour of ductile cast iron", Wear, vol. 231 (1999), pp. 293 – 300.

ISSN 1847-7917

Manufacturing and testing of underwater remotely operated vehicle propulsion unit

***Ante ČORIĆ*[1)], *Slaven ŠITIĆ*[2)], *Ivan MADUNIĆ*[3)]**

1) Plovput d.o.o. Tvrtka za sigurnost plovidbe i svjetioničarsku službu/ Croatian Maritime Safety and Lighthouse Authority, Obala Lazareta 1, 21000 Split, Hrvatska/Croatia
2) Sveučilište u Splitu, Sveučilišni odjel za stručne studije/ University of Split, University Department of Professional Studies, Kopilica 5, 21000 Split, Hrvatska/Croatia
3) Sveučilište u Splitu, Sveučilišni odjel za stručne studije/ University of Split, University Department of Professional Studies, Kopilica 5, 21000 Split, Hrvatska/Croatia

antecoric89@gmail.com

Keywords

Propulsion
Underwater robotics
Design
Manufacturing
Testing

Ključne riječi

Propulzija
Podvodna robotika
Projektiranje
Izrada
Ispitivanje

Professional paper

Abstract: The aim of this paper is to describe the process of manufacturing and testing the propulsion unit for an underwater remotely operated vehicle. The basis for the development of the propulsion unit is the previously designed remotely operated vehicle model and the use for which the submersible was designed; that is recording and documentation of all objects which are under water, with the possibility of greater autonomy and depth opposed to diver capability. Through the design stage of this project, all aspects relevant to the proper functioning of the propulsion system were reviewed, and basic calculations were carried out. The paper also describes constructive solutions in design such as the use of magnetic coupling for torque transmission. Particular emphasis is placed on the application of newer technologies such as CAD/CAM software, 3D printing and the use of CNC machining in the manufacturing process. In the end the propulsion unit was manufactured. The testing procedure and results were described as a part of this report.

Izrada i testiranje propulzijske jedinice daljinski upravljane ronilice

Stručni članak

Sažetak: Cilj ovog rada je opisati postupak izrade i ispitivanja propulzijske jedinice za daljinski upravljanu ronilicu. Osnova za razvoj propulzora je prethodno koncipirani model daljinski upravljane ronilice, te primjena za koju se ronilica projektira, a to je snimanje i dokumentiranje svih objekata koji se nalaze pod vodom, s mogućnošću veće autonomije i dubine u odnosu na mogućnosti ronioca. Kroz fazu projektiranja obrađeni su svi aspekti važni za pravilno funkcioniranje propulzora, te su izvršeni temeljni proračuni. U radu su opisana konstrukcijska rješenja, kao što je primjena magnetske spojke za prijenos okretnog momenta. Poseban naglasak stavljen je na primjenu novijih tehnologija kao što su CAD/CAM računalni programi, 3D printanje i upotreba CNC obradnih centara za izradu dijelova propulzora. U konačnici je izvršena i izrada projektiranog propulzora, te opisan postupak i rezultati.

1. Uvod

Daljinski upravljana bespilotna ronilica, u svijetu poznata kao ROV (eng. remotely operated vehicle), je vozilo kojim ROV pilot preko površinske jedinice upravlja i izvršava mnogobrojne podvodne zadatke. Ovisno o namjeni koju ronilica treba obaviti, dodaju se razni alati poput mehaničke ruke, senzora za toplinu, bioloških senzora, sonara za mapiranje podmorja i raznih drugih alata koji omogućuju izvršavanje zadataka.

S obzirom na različitosti u primjeni podvodnih robota, postoje i razne izvedbe propulzorskih jedinica: propeler pogonjen elektromotorom, propeler pogonjen hidrauličnim motorom, mlazni (Jet) propulzor pogonjen električnim ili hidrauličnim motorom. U novije vrijeme izrađuju se i prototipovi ronilica s propulzijom koja simulira životinjska kretanja, npr. kretanje sipe, kornjače i sl.

Kao neizostavan dio mobilne podvodne robotike, propulzijski sustav predstavlja kritičnu komponentu daljinski upravljanih ronilica. Bez adekvatne propulzije, podvodno vozilo bilo bi podložno vanjskim utjecajima kao što su morske struje i bilo bi onemogućeno obavljanje radnog zadatka, [1].

U ovom radu opisan je postupak izrade i ispitivanja propulzijske jedinice sa elektromotornim pogonom propelera. Odabir ove vrste propulzije u potpunosti je izvršen temeljem pravila metodičkog razvoja proizvoda, na osnovu prethodno koncipiranog modela daljinski upravljane ronilice, slika 1.

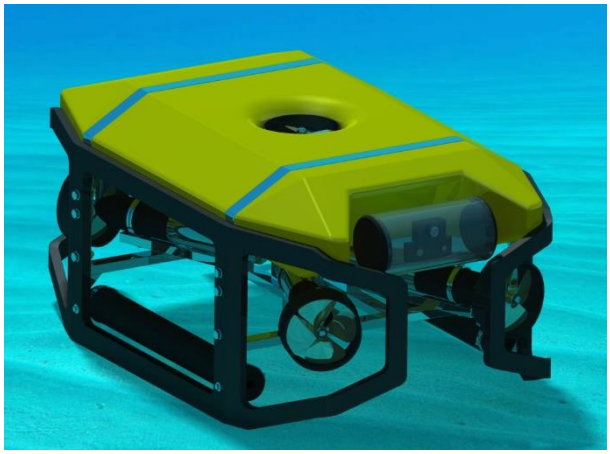

Figure 1. 3D model of the designed underwater remotely operated vehicle

Slika 1. 3D model projektirane daljinski upravljane ronilice

2. Opis faze projektiranja

Da bi se na kvalitetan način pristupilo fazi projektiranja, potrebno je definirati kakav se zadatak postavlja, [2].

Za potrebe izrade propulzora, izvršeno je prikupljanje informacija u obliku istraživanja, na temelju kojeg je izrađena lista zahtjeva. Ona uključuje niz čimbenika koji mogu utjecati na kvalitetu i ispravnost konačnog proizvoda. Neki od njih su: geometrija, kinematika, sile, energija, materijali, sigurnost, proizvodnja, montaža, upotreba, održavanje i troškovi.

Pri projektiranju i planiranju izrade, postavljaju se zahtjevi vezani za materijale. Neki od tih zahtjeva su: otpornost na koroziju, međusobna kompatibilnost kako bi se spriječilo stvaranje galvanskih članaka, čvrstoća s obzirom na opterećenja pojedinih dijelova, dostupnost materijala i obradivost s obzirom na dostupne proizvodne metode.

Važan aspekt projektiranja je planiranje i koncipiranje propulzora u skladu sa proizvodnim mogućnostima. Propulzor daljinski upravljane ronilice, odnosno njegove dijelove potrebno je oblikovati da budu jednostavni za strojnu i ručnu obradu. Osim same izradivosti pojedinih dijelova, veliku ulogu imaju i dodatni troškovi koji proizlaze iz skupih proizvodnih postupaka. Proizvodni postupci također su usko vezani za odabir materijala, pa je potrebno i o tome voditi računa.

Veliki dio zahtjeva, koji se odnose na propulzor iz ovog rada, uvjetovan je ronilicom za koju je predviđen, a najvažniji su: izdržljivost na vanjski tlak maksimalne radne dubine od 150 m, a koji iznosi 16,25 bar-a (1,625 N/mm^2) i proračunska snaga jednog propulzora (od ukupno 4) potrebna za pogon ronilice sa kabelom iznosi ~225 W.

2.1. Osnovna konstrukcijska rješenja

2.1.1. Pogonski elektromotor

Odabrani pogonski elektromotor je „Turnigy XK4074-B-1400kv Brushless Inrunner". Brushless elektromotori su sinkroni motori, koji se napajaju istosmjernom strujom putem integriranog pretvarača „switching napajanja". On proizvodi električni signal izmjenične AC struje koja pokreće motor. U ovom slučaju izmjenična struja ne podrazumijeva sinusoidalni valni oblik, nego bi-direkcionalnu struju kojoj valni oblik nije ograničen. Dodatni senzori i elektronika kontroliraju izlaze pretvarača amplitude i valnog oblika. Snaga motora na 12V je 900 W. Razlog velikog odstupanja snage u odnosu na proračunsku je rezultat istraživanja, a može se opravdati i gubicima na propeleru, smanjenoj učinkovitosti elektromotora (zagrijavanje i sl.) i trenju.

Figure 2. Driving motor of the designed thruster

Slika 2. Pogonski elektromotor projektiranog propulzora

2.1.2. Propeler s "Kort Nozzle" mlaznicom

Temeljem provedenog istraživanja, pronađeno je nekoliko potencijalnih propelera za ugradnju na projektirani propulzor. Model tvrtke Robbe, s promjerom od 95 mm i 4 elise, odabran je kao najprikladnije rješenje. Osobita prednost ovog propelera je prilagođenost za ugradnju unutar mlaznice.

„Kort Nozzle" je kratka mlaznica cilindričnog oblika koja obavija propeler. U određenim okolnostima značajno poboljšava učinkovitost propelera, čak i do 40 %. Kanal mlaznice je usko priljubljen uz vrhove propelera, a rubovi mlaznice su hidrodinamičkog oblika. Osim poboljšanja učinkovitosti, mlaznica služi i kao zaštita propelera od stranih tijela.

2.1.3. Princip brtvljenja

Kako bi se osigurala nepropusnost tlačno opretećenog kućišta propulzora, potrebno je projektirati principe brtvljenja. Na koncipiranom propulzoru postoje 3 spojna mjesta, koja je potrebno zabrtviti:

- spoj poklopca pogonskog dijela i kućišta pogonskog dijela
- spoj kućišta pogonskog dijela i srednjeg pregradnog kućišta
- brtvljenje osovine propelera uz osiguranje prijenosa okretnog momenta od motora do propelera

Za prva dva navedena spojna mjesta brtvljenjenje je izvedeno sa gumenim O-ringovima. Brtvljenje osovine propelera, uz osiguranje prijenosa okretnog momenta od motora do propelera, izvedeno je magnetskom spojkom, odnosno vodonepropusnom pregradom.

2.1.4. Ležaji

Zbog potrebnog svojstva potpune nemagnetičnosti i dielektričnosti, kao najbolji izbor odabrani su keramički ležaji. Osim što udovoljavaju svim postavljenim zahtjevima, imaju i izvrsna antifrikcijska svojstva, malu ili nikakvu potrebu podmazivanja, dobru postojanost na habanje i mogućnost postizanja velikih brzina zbog male mase valjnih tijela, a time i malih centrifugalnih sila.

2.1.5. Magnetska spojka

Magnetske spojke omogućuju brtvljenje vratila bez uporebe brtvenih elemenata, koji se s vremenom troše zbog trenja o površinu vratila. Dodatna prednost je što omogućuju pomake u osima vratila, te manje radijalne i aksijalne pomake, [3].

Projektirana magnetska spojka propulzijske jedinice je aksijalnog tipa. Geometrija spojke i sile magneta prikazane su slikom 3.

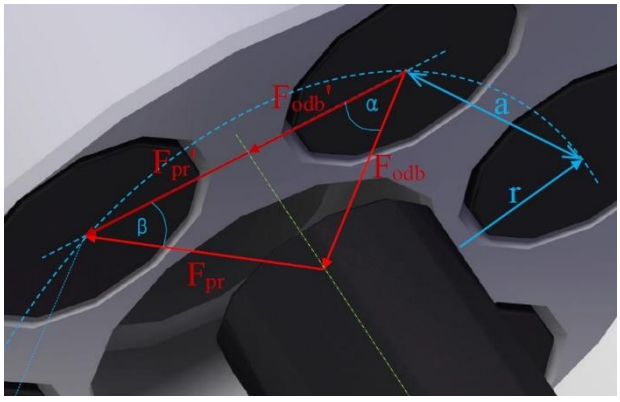

Figure 3. The forces in the axial magnetic coupling

Slika 3. Sile u aksijalnoj magnetskoj spojki

2.1.6. Materijali

Način na koji se odabire pogodan materijal ponajprije ovisi o broju i važnosti zahtjeva i kriterija koji su postavljeni. Obzirom da je projektirani propulzor prototip, kriteriji odabira materijala ne uključuju ekonomske i kvantitativne faktore. Glavni kriteriji pri odabiru materijala propulzora su: uvjet čvrstoće i maksimalno dozvoljene deformacije, otpornost na atmosferske uvjete i koroziju, te dostupnost na tržištu.

2.2. Izrada 3D modela propulzora

Propulzor projektne daljinski upravljane ronilice, kao i cijela ronilica, izrađen je u obliku trodimenzionalnog modela koristeći programski paket CATIA V5 r20. CATIA omogućava izradu 3D modela koristeći 2D skice presjeka i kontura, koje se izvlače, rotiraju, ukopavaju i sl., kako bi se stvorio trodimenzionalni model.

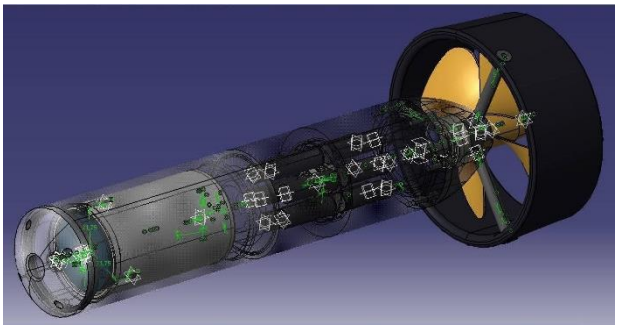

Figure 4. 3D model of the designed thruster

Slika 4. 3D model projektiranog propulzora

Proizvodni procesi koji su planirani za izradu pojedinih dijelova propulzora uključuju CNC (eng. Computer Numerical Control) obradu, za koju je zbog kompleksnosti pojedinih dijelova, neophodno izraditi 3D modele. CAD/CAM (eng. computer-aided design and computer-aided manufacturing), računalno potpomognuti način dizajniranja i proizvodnje, omogućava vrlo jednostavno generiranje numeričkog programa za CNC obradu. U skladu s navedenim, neizostavan dio projektiranja i pripreme za predviđeni postupak proizvodnje je i izrada 3D modela.

2.3. Simulacija opterećenja metodom konačnih elemenata

Kako bi projektirani model propulzora bilo primjenjiv i u stvarnim uvjetima, potrebno je izdvojiti kritično opterećene dijelove te izvršiti provjeru njihove čvrstoće s obzirom na uvjete definirane u zahtjevima za izradu. U slučaju projektne daljinski upravljane ronilice, koja se projektira za zarone i do 150m dubine gdje vlada vanjski tlak od 16 bara, kritični dijelovi propulzora su zabrtvljeni elementi, koji su podvrgnuti najvećim razlikama u tlaku. Na slici 5 moguće je vidjeti naprezanje koje se javlja na jednom od kritičnih dijelova propulzora, a različite veličine naprezanja prikazane su u različitim bojama - plava predstavlja područje najnižeg opterećenja, dok crvena predstavlja ona najveća. Točne vrijednosti opterećenja, koje su predstavljene bojama, vidljive su u donjem desnom uglu. Analizom rezultata simulacije i

poznatih karakteristika odabranog materijala, utvrđeno je da svi elementi zadovoljavaju.

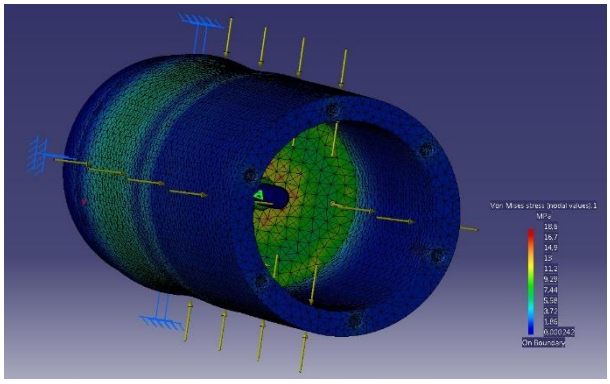

Figure 5. Load simulation in Catia
Slika 5. Simulacija opterećenja u Catia-i

2.4. Tehnička dokumentacija

Sklopni i radionički crteži propulzora projektne daljinski upravljane ronilice izrađeni su na temelju koncepcijskih skica, uvažavajući proračune, proizvodne mogućnosti s obzirom na materijale, računalne strukturne analize i maksimalno iskorištavanje standardnih dijelova. Upotrebom računalnih programa za 3D modeliranje kao što je CATIA, moguće je automatsko generiranje 2D nacrta pogleda, presjeka, detalja, kota, sastavnica, popisa dijelova itd.

3. Izrada prototipa propulzora

Za izradu propulzora korištene su razne metode proizvodnih postupaka. Otežavajuća okolnost pri izradi, bila su ograničena financijska sredstva, ali i nedostupnost obradnih centara neophodnih za izradu pojedinih dijelova propulzora. Rješenje ovih okolnosti došlo je u obliku tvrtki – partnera projekta izrade daljinski upravljane ronilice. Samoj izradi prethodila je nabava materijala i sirovina.

3.1. Priprema i simulacija CNC obrade

Kao dio postupka izrade, programskim paketom CATIA izvršene su simulacije obrade CNC obradnim centrom. Simulacije obrade jednog od dijelova propulzora su prikazane na slici 6. Postupak CNC obrade komponente propulzora, prikazanog na slici, moguće je podijeliti na 3 faze:

- tokarenje sa stražnje strane izratka (širi dio gotovog elementa)
- tokarenje s prednje strane izratka (uži dio gotovog elementa)
- glodanje s prednje strane izratka

Temeljem simulacija generiran je numerički program, koji sadrži sve naredbe neophodne za izradu dijelova propulzora. Naime, moderni CNC sustavi su u potpunosti automatizirani i koriste CAD (eng. Computer Aided Design) i CAM (eng. Computer Aided Manufacturing) programe.

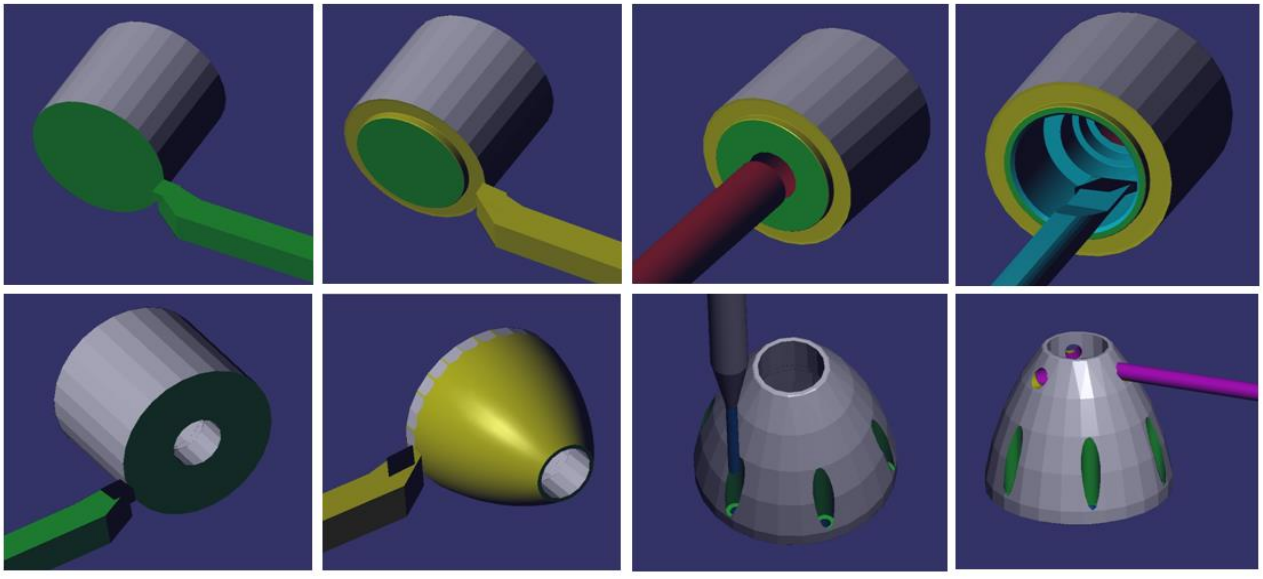

Slika 6. CNC simulacija obrade jednog od dijelova ropulzora
Figure 6. CNC processing simulation of one thruster part

Uz pomoć ovih programa izrađuju se računalne datoteke, koje interpretira pos-procesor određenog stroja, te stvara naredbe potrebne za izradu obratka. Obzirom da većina izradaka zahtjeva korištenje brojnih alata pri obradi, noviji uređaji često kombiniraju razne alate, [4].

3.2. Postupci izrade

Veći dio komponenti propulzora, izrađen je postupkom klasničnog tokarenja. Naime, poznato je kako cilindrični oblik predstavlja najbolje rješenje za strojne elemente opterećene hidrostatskim tlakom. Veliki udio upravo cilindričnih dijelova na propulzoru, rezultat je navedenog.

Složena geometrija nekoliko dijelova propulzora, uvjetovala je korištenje CNC obradnih centara. Partner tvrtka projekta Banko d.o.o. ustupila je svoj strojni park obradnih centara marke "OKUMA".

Uz numerički upravljane obradne centre, za izradu propulzora, korišten je i 3D printer. Dio propulzora koji je izrađen ovom metodom je zaštita, odnosno mlaznica propelera, a printanje je prikazano na slici 7. Sama izrada mlaznice 3D printanjem, vrlo je slična postupku CNC obrade. Naime, potrebno je izraditi 3D model željenog dijela i na temelju njega, posebnim programskim paketom generirati numerički kod, kojeg je printer u stanju interpretirati.

Za razliku od CNC glodalice koja uklanja materijal sa obratka, 3D printer ga dodaje u slojevima.

Osim navedenih proizvodnih postupaka izrade, korišteni su i oni konvencionalni, kao što su tokarenje i razne ručne obrade. Izrađeni prototip propulzora prikazan je slikom 8.

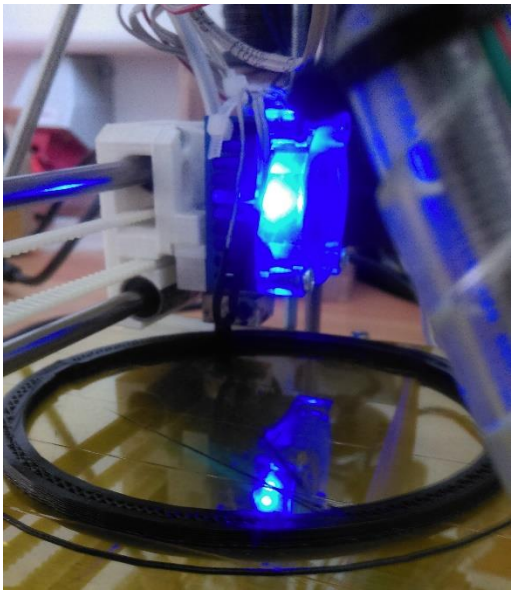

Figure 7. 3D printing of the kort nozzle
Slika 7. 3D printanje "kort nozzle" mlaznice

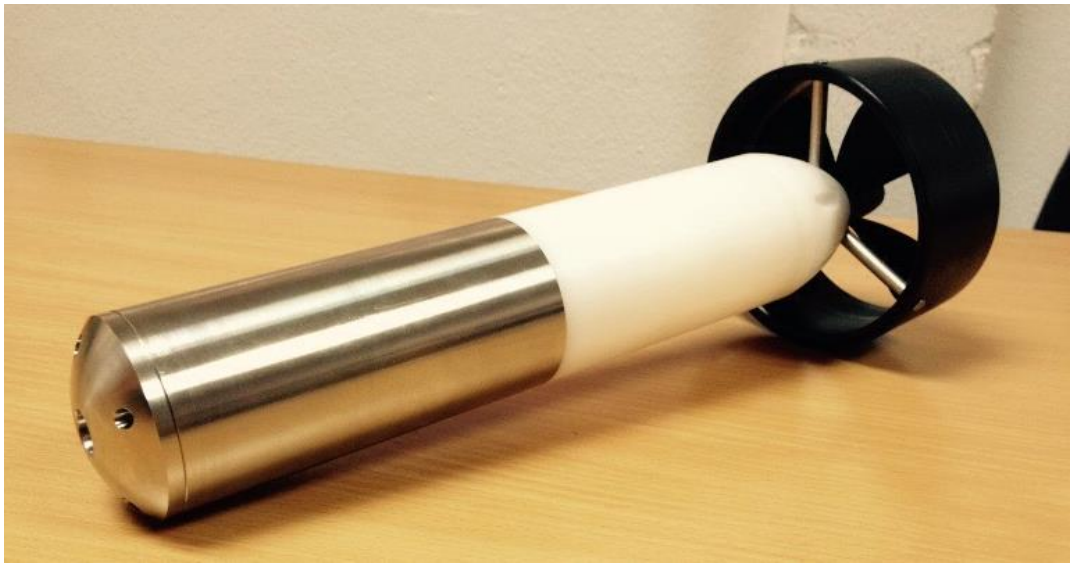

Figure 8. Produced thruster
Slika 8. Izrađeni propulzor

4. Ispitivanje propulzora

Kako bi se izvršilo ispitivanje prototipa propulzora, potrebno je definirati zahtjeve te sukladno njima izraditi plan ispitivanja.

4.1. Ispitivanje dimenzionalne i geometrijske točnosti izrade

Već pri samoj izradi dijelova propulzora, vrši se sistematično testiranje svih dimenzija izradaka. Sve dimenzije su definirane u radioničkim crtežima, te se prema njima utvrđuje da li izradak zadovoljava propisane tolerancije dimenzija, oblika i položaja. Odstupanje od propisanih tolerancija može ozbiljno ugroziti tehnološku i funkcionalnu ispravnost propulzora.

4.2. Ispitivanje električnih spojeva i upravljanja

Kvalitetan pristup ovoj vrsti ispitivanja je da se prvo pojedinačno testira svaki element elektronike i upravljačkog programa, kako bi se utvrdio njihov ispravan rad. Tek nakon što su pojedinačno ispitani, mogu se implementirati u cijeli sustav. U fazi testiranja propulzora potrebno je izraditi pouzdan upravljački program, i planirati ugradnju mjernih instrumenata kako bi se vršilo mjerenje električnih karakteristika.

4.3. Ispitivanje kućišta na tlak i propusnost

Iako su izvedena ispitivanja svih dijelova metodom konačnih elemenata u programskom paketu CATIA, potrebno je izvesti i testiranje u stvarnim uvjetima opterećenja. Tlačno ispitivanje kućišta uz provjeru uvjeta nepropusnosti vode, moguće je izvesti na dva načina:

- testiranje propulzora u tlačnoj komori ispunjenom vodom uz povećanje tlaka na ispitnu vrijednost (radni tlak uvećan za 30 do 40%)
- testiranje propulzora kontroliranim uranjanjem na dubinu koja odgovara ispitnom tlaku

Zbog nedostupnosti tlačne komore, izvršeno je uranjanje propulzora na dubinu od 200 m, što je za 50 m više od predviđene radne dubine. Naknadnim pregledom i mjerenjem potvrđena je nepropusnost i dimenzionalna stabilnost propulzora.

4.4. Ispitivanje pogonskih karakteristika propulzora u kontroliranim uvjetima

Ispitivanje pogonskih karakteristika propulzora vrši se kako bi se utvrdili podatci o stvarnoj porivnoj sili propulzora, potrošnji električne energije u radnim uvjetima/opterećenjima, odnosu porivne sile i potrošnje električne energije, učinkovitosti propulzora, i sl. Za potrebe ispitivanja projektiranog propulzora, izrađena je naprava za ispitivanje, a ista je prikazana slikom 9.

Propulzor je pričvršćen na donji dio njihala koji je skupa sa njim postavljen u bazen s vodom. Na suprotnom dijelu se nalazi dinamometar, koji prikazuje silu koju generira propulzor. Točan iznos sile se jednostavno izračunava jer su poznate duljine krakova njihala s obzirom na os rotacije njihala. Osim dinamometra, postavljaju se i električni mjerni uređaji (multimetri), kako bi se mjerili parametri vezani za potrošnju električne energije, jakost struje i pad napona na elektromotoru.

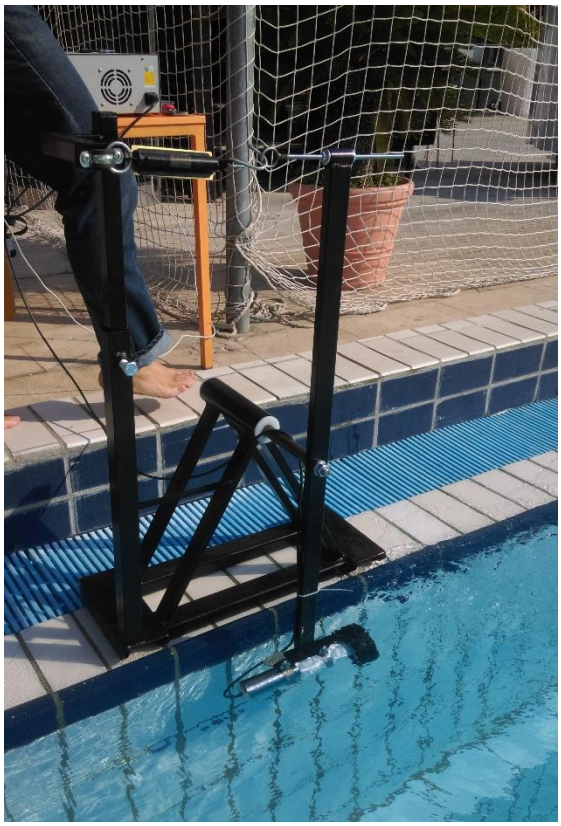

Figure 9. The testing device for the thruster
Slika 9. Naprava za ispitivanje propulzora

Figure 10. The device for measuring force (dynamometer)
Slika 10. Naprava za mjerenje sile (dinamometar)

Kako bi rezultati ispitivanja bili jasno prikazani, izrađeni su grafovi koji prikazuju međusobne odnose pojedinih rezultata dobivenih testiranjem.
Na slici 11, prikazan je graf odnosa snage i porivne sile (potiska). Desnom stranom grafa prikazan je pozitivan smjer vrtnje, a lijevom negativan. Testiranjem je utvrđeno da propulzor pri snazi utroška električne energije od 500 W na 12V, stvara potisak od 3,9 kg ili 38,3 N. U suprotnom smjeru vrtnje, za isti utrošak el. energije, ostvaren je potisak od 3 kg, odnosno 29,4 N.

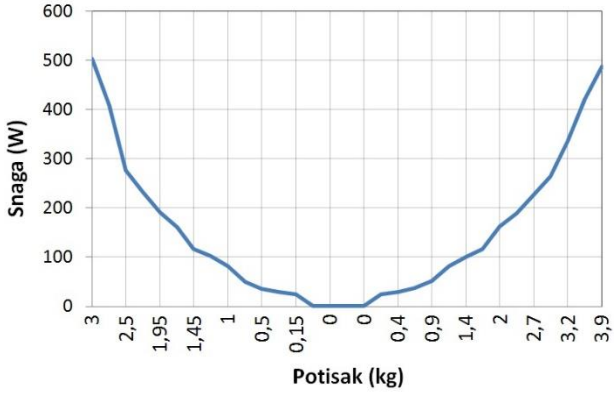

Figure 11. Power vs. thrust chart
Slika 11. Graf odnosa snage i porivne sile

Kontrola broja okretaja "Brushless" motora vrši se posebnim elektroničkim sklopom, koji se zove ESC (eng. electronic speed controller). Kontrola ESC-a se vrši PWM (eng. pulse width modulation) signalom, kojeg u slučaju propulzora generira mikrokontroler.
Učinkovitost propulzora možemo promatrati kao odnos potiska izraženog u gramima po jednom vatu snage. Kada taj odnos prikažemo u zavisnosti o dodijeljenom gasu (PWM) signalu dobivamo graf prikazan na slici 12.

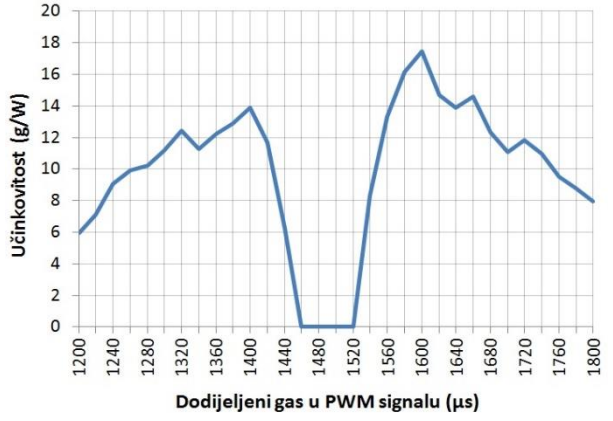

Figure 12. Efficiency vs. assigned throttle chart
Slika 12. Graf odnosa učinkovitosti po dodjeljenom gasu

Iz grafa je vidljivo kako maksimalna postignuta učinkovitost projektiranog propulzora iznosi 17,5 g/W pri PWM signalu od 1600 µm (25% dodijeljenog gasa).
U suprotnom smjeru rotacije, vidljiv je pad učinkovitosti kojeg uzrokuje oblik propelera. Naime, svi propeleri su projektirani da u jednom smjeru rotacije imaju maksimalnu učinkovitost, što u konačnici smanjuje učinkovitost pri suprotnom smjeru rotacije. Daljnje opadanje učinkovitosti, nakon što je postignut maksimum, rezultat je eksponencijalnog porasta hidrodinamičnog otpora koji se javlja povećanjem brzine rotacije propelera.

5. Zaključak

U ovom radu, obrađen je postupak izrade i ispitivanja sustava propulzora za daljinski upravljanu ronilicu. Opsežnost cijelog projekta, pa i ovog rada, nije ostavila dovoljno vremena i prostora kako bi se detaljno opisala svaka faza projektiranja, izrade i ispitivanja propulzora. Korištenje CAD/CAM programa pri projektiranju i izradi, pokazalo se vrlo uspješno. Naime simulacije opterećenja, simulacije CNC obrade, te generiranje tehničke dokumentacije programskim paketom CATIA značajno je podiglo kvalitetu projektiranog propulzora. Osnovna prednost spomenutih programa je mogućnost da se naknadne izmjene na modelu odražavaju kroz sve module programa.
Kritična komponenta propulzijske jedinice, bila je magnetska spojka, odnosno osiguranje prijenosa okretnog momenta preko fiksne barijere. Glavna mana ove vrste osiguravanja nepropusnosti i prijenosa je povećanje ukupnih dimenzija propulzora, no pravilnim projektiranjem predstavlja idealno rješenje.
Ispitivanjem propulzora utvrđen je njegov ispravan rad i većim dijelom su zadovoljeni ulazni zahtjevi.
Rezultati konačnog ispitivanja projektirane propulzijske jedinice, mogu se usporediti s komercijalnim propulzorima slične namjene.
Osim navedenog, ispitivanjem su utvrđena i moguća unaprjeđenja koja bi se odrazila na samu učinkovitost propulzora. Neka od njih su smanjenje zračnosti između propelera i mlaznice, hidrodinamičniji oblik mlaznice, implementacija planetarnog prijenosnika radi smanjenja broja okretaja propelera.
Obzirom da projektirani propulzor predstavlja prototip, prilikom projektiranja ostavljena je mogućnost jednostavne izmjene pogonskog elektromotora sa nekim drugim, što je ostvareno adaptacijskim elementom. Izmjenom pogonskog motora, moguća su dodatna optimiziranja propulzora u odnosu na odabrani propeler.

LITERATURA

[1] Robert D Christ, Robert L. Wernli, Sr. (2014): A User Guide for Remotely Operated Vehicles, Elsevier Ltd.
[2] Prof. dr. sc. Božidar Križan (2007), Metodičko Konstruiranje, Tehnički fakultet, Sveučilište u Rijeci
[3] Magnetic cupling https://en.wikipedia.org/wiki/Magnetic_coupling,
[4] Web stranica: https://en.wikipedia.org/wiki/Numerical_control

ISSN 1847-7917

Surface wear of steel X38CrMoV5-1 in conditions of die casting

Zvonimir DADIĆ[1)]***, Dražen ŽIVKOVIĆ***[2)]
Nikša Čatipović[1)]
1) Fakultet elektrotehnike, strojarstva i brodogradnje, Sveučilišta u Splitu (Faculty of Electrical Engineering, Mechanical Engineering and Naval Architecture, University of Split) Ruđera Boškovića 32, 21000 Split, **Republic of Croatia**

zdadic@fesb.hr;
Drazen.Zivkovic@fesb.hr;
ncatipov@fesb.hr.

Keywords

Mold wear
Thermal fatigue
Erosion
Aluminium alloy
Tool steel

Ključne riječi

Trošenje kalupa
Toplinski umor
Erozija
Aluminijska legura
Alatni čelik

Original scientific paper

Abstract: Previous research in area of high-pressure die casting mould surface wear has led to conclusions shown in this paper. Most significant wear parameters are defined according to previous research. Led by these conclusions, a machine was designed which is capable of simulating similar work conditions of the mould material surface. This paper presents four differently treated samples. All samples were manufactured from steel X38CrMoV5-1 which is commonly used for high-pressure die casting moulds. Two samples were heat treated by spheroidize annealing. One was quenched and tempered at high temperature. The other one was also treated by quenching and high temperature tempering and then nitrided. Quenching, tempering and then nitriding are common heat treatment procedures of mould material used for high-pressure die casting. The results, after 10000 and 32000 testing cycles, are presented in this paper.

Izvorni znanstveni rad

Sažetak: Dosadašnje istraživanje u području trošenja površine materijala kalupa za visokotlačno lijevanje aluminijskih legura dovelo je do zaključaka o najutjecajnijim parametrima ovakvog procesa lijevanja na trošenje površine kalupa. Vodeći se ovim zaključcima dizajniran je uređaj za ispitivanje koji je sposoban simulirati uvjete rada površine materijala kalupa. U ovom radu ispitana su 4 uzorka u različitim početnim stanjima. Svi uzorci izrađeni su od čelika X38CrMoV5-1 često korištenog za izradu kalupa za visokotlačno lijevanje aluminijskih legura. Dva uzorka su u omekšanom stanju, jedan je obrađen toplinskom obradom poboljšavanja a jedan je poboljšan i zatim nitriran, kao što se često izvodi sa materijalom stvarnog kalupa. Prikazani su rezultati ispitivanja nakon 10000 i 32000 ciklusa ispitivanja.

1. Introduction

This paper presents the preliminary research of mould surface wear as a part of project "Optimisation and modelling of thermal processes of materials". The project is funded by Croatian Science Foundation. Most influential wear mechanism of mould surface of high-pressure die casting process is thermal fatigue. Erosion and adhesive wear or soldering have a high impact on surface wear [1, 2]. When the molten casting alloy is in contact with the mould surface, the surface material is heated and expands. The heat is conducted through the massive mould and the surface is cooled, which leads to contraction of the material on the surface. The greater the difference between the mould temperature and the molten alloy, the larger is the expansion and contraction of the surface which causes cracks to occur sooner [2]. When the yield strength of the material was exceeded near the surface, local accumulation of plastic deformation occurs, that leads to initial cracks. Propagation of initial crack leads to detachment of material from the surface [3, 4, 5]. Difference between mould temperature and molten aluminium temperature will be reduced by increasing moulds preheating temperature. Therefore, mould preheating temperature directly affects the occurrence and propagation of thermal fatigue cracks.
While filling the mould, molten alloy reaches speed up to 60 *m/s* [6, 7]. Erosion wear is additional increased by presence of hard particles in molten alloy. For example, Al_2O_3 particles have high hardness (2000 *HV*) and high melting temperature (2072 °*C*). Erosion wear is most intense on surfaces where molten alloy firstly reaches mould surface [8]. Previous scientific research has shown that erosion wear with hard particles has the greatest effect with smaller angles of impact (around 30°) [9]. Therefore, when considering erosion wear of mould surface for high-pressure die casting, the most influential wear mechanism is abrasion. It was shown that increasing the mould temperature, erosion wear increases but thermal fatigue wear decreases [9]. Application of hard coatings with metal carbides or nitrides can significantly increase resistance to erosion wear [7].
Because aluminium has high affinity toward iron from the mould steel, soldering of the casting alloy with the surface of the mould may occur. Soldering occurs in the case the lubricating agent was washed out by the molten alloy. At increased temperatures, intermetallic bonds form between aluminium from the casting alloy and iron from the steel mould [10, 11]. Therefore, aluminium corrodes the mould material on the surface by reacting with iron. Combined with erosion, it can cause significant loss of material on the mould surface. Erosion aggravates soldering of the casting alloy on the mould surface, which enhances adhesion wear [8, 12]. According to other research, aluminium alloy temperature had a significant effect on mould wear. Increasing the molten aluminium alloy temperature, results in increased adhesion wear but reduced erosion wear [13]. Formation of intermetallic bonds can be significantly

reduced by applying various types of coatings and surface modifications [7, 14]. High-pressure die casting mould surface wear examples are shown on figure 1.

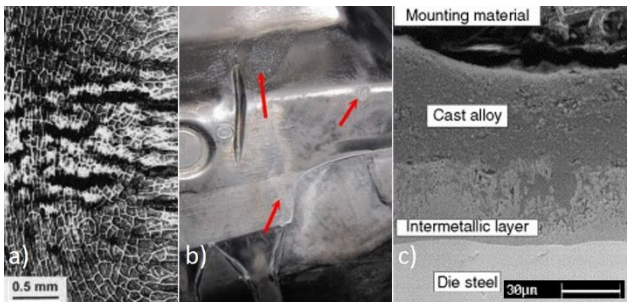

Figure 1. Wear mechanisms examples: thermal fatigue (a), erosion (b) and adhesion (c) [15, 16, 17]

Slika 1. Primjer trošenja površine toplinskim umorom (a), erozijom (b) i adhezijom (c) [15, 16, 17]

2. Development of laboratory equipment

Ideally, the experiment would be done on the high-pressure die casting machine but this kind of experiment would be very expensive. Review of previous research led to conclusion that there is an interaction between wear mechanisms that influence the total mould surface wear [2, 13, 18]. Testing of wear should be done on a testing device which takes in consideration most of the influential parameters, so the conditions of testing would be as similar as possible as real conditions. It is desirable to use casting aluminium alloy that is used in real processes to simulate the heat transfer as real as possible, and to achieve the ability to test erosion and adhesion wear. To reduce soldering of aluminium alloy on mould surface and to make the testing more relevant, it is necessary to use a lubricant. Lubricants that are usually used in these processes are based on molybdenum disulphide, graphite and hexagonal boron nitride.

Thermal fatigue wear mechanism is not evident in most of previous research because it does not occur at small number of testing cycles [19]. For corresponding test effects of all wear mechanisms, testing device must have a capability to execute a large amount of testing cycles. It is also necessary to have the possibility to test the effects of different impact angles of molten aluminium, considering previous research showed that angle of impact has a significant effect on wear [9]. For testing material, a hot work steel which is commonly used for high-pressure casting should be used (H10, H11, H13). Except this, it should be possible to vary the mould preheat temperature, relative speed between the sample and molten aluminium during contact, molten aluminium alloy temperature, lubricant, casting alloy, sample material, sample material heat treatment, coating and surface modification. These parameters influence the total amount of wear and should be tested.

Under these conditions, a testing device is designed. When designing the device, goal was to simplify testing, reduce testing costs, speed up the testing process and enable a high number of testing cycles. Testing was done by immersing the sample, made from mould material, in molten aluminium casting alloy. After leaving the molten alloy, sample is immersed in the lubricant. Mould temperatures are simulated and adjusted by holding times in molten aluminium alloy and lubricant. Wear is measured by weighing the samples on a Mettler B5 scale with accuracy of ±0,0001 *g*. Erosion was tested by varying the sample speed on impact with molten aluminium alloy. Motions are achieved by servo motor Kollmorgen AKM54K-ACDNCA-00. Arm which holds the sample is 200 *mm* long so a high circumferential speed can be achieved using a relatively small angle for acceleration. Motion of the servo motor was programmed in BASIC computer language. Motor is controlled by Kollmorgen AKD-T01207-NBAN-E000 servo drive. Aluminium alloy is melted by 650 *W* heaters. Temperature of the molten aluminium alloy is controlled by a type K theromelement (NiCr-Ni). Regulation of the temperature was done by Novus N480D controller. Sample temperature after exiting the molten aluminium alloy and lubricant was controlled by ScanTemp 480 infrared thermometer. Testing device is shown on figure 2.

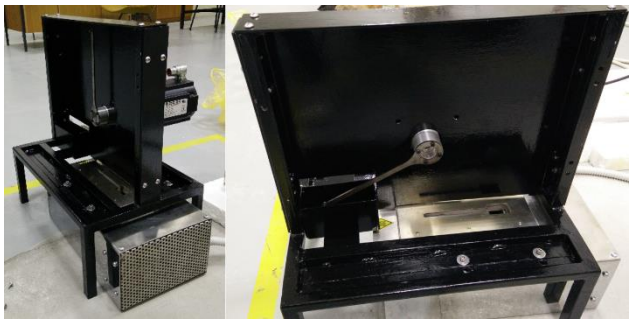

Figure 2. Testing device

Slika 2. Uređaj za ispitivanje

3. Laboratory experiment

This preliminary testing was done on samples made from X38CrMoV5-1 material. This is a hot work tool steel (H11). Chemical composition of the material is given in table 1. Samples were made on a five-axis CNC machining center MAHO. Cross section shape is a symmetrical NACA 0012 profile (National Advisory Committee for Aeronautics). This profile was chosen because of its low drag coefficient. The goal is to reduce resistance on impact and when moving through molten aluminium. Dimensions of the sample are 10x58x4 *mm*. Part of the sample used for testing is 40 *mm* in height and 2,5 *mm* thick. Samples after machining and nitriding are shown in figure 3.

Table 2. Chemical composition of testing steel X38CrMoV5-1

Tablica 2. Kemijski sastav korištenog čelika X38CrMoV5-1

C, %	*Si, %*	*Mn, %*	*Cr, %*	*Mo, %*	*Ni, %*	*V, %*
0,39	0,97	0,43	5,01	1,14	0,21	0,45

All samples have the same shape and were made from the same material. Two samples (69 and 70) are heat treated by spheroidize annealing. Their hardness is 221 *HV*. One was quenched in oil from 1050 °*C*. Hardness after quenching of the sample was 564 *HV*. Then it was tempered three times on high temperatures (sample 15).

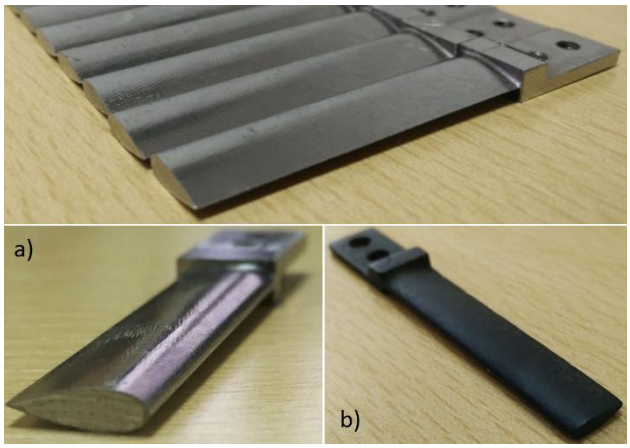

Figure 3. Samples for testing after machining (a) and nitriding (b)

Slika 3. Uzorci za ispitivanje nakon strojne obrade (a) i nitriranja (b)

Hardness after tempering was 480 *HV*. Second sample was treated the same way, but also nitrited in salt bath with holding time of 4 *h* on temperature 580 °*C* (sample 14). Hardness of nitrided sample was 1100 *HV*.

One testing cycle is consisted of heating the sample in molten aluminium alloy, then cooling in the lubricant. Aluminium alloy AlSi9Cu3(Fe) was used in molten state at constant temperature of 675 °*C*. Lubricant used for testing was molybdenum disulphide (MoS_2). MoS_2 particles are transferred in oil that is dispersed in water (1:80 ratio). Circumferential impact speed of the sample was set to 10 *m/s*. After holding the sample in molten aluminium alloy for 0.5 *s*, the sample heated up to 220 °*C*. Immersing the sample in the lubricant and holding it for 0,2 *s* cools the sample to 50 °*C*. One test cycle time is 4 *s*.

4. Results and analysis

On samples 14, 15 and 69 testing was done for 10000 cycles according to the previous parameters. After removing from the testing device the samples were cleaned by immersion in a NaOH solution (20%). The goal is to remove soldered aluminium alloy and other impurities from the surface to have accurate weight loss wear results. Then the samples were weighted. The results are shown in figure 4. Unexpectedly, most weight loss was on the nitrided sample. Wear of quenched and tempered sample was less than wear of sample treated by spheroidize annealing. Samples are shown on figure 5, after testing, before immersion in NaOH solution.

Figure 5 shows that nitrided sample (14) was significantly damaged on the sharp edge of the sample. This indicated the problem of the brittle nitrided layer when nitriding areas of small radius of curvature. There is no soldered aluminium alloy on this sample because the nitrided layer prevents reaction between iron from the mould steel and aluminium from the casting alloy. Therefore, there are no intermetallic bonds and adhesion wear [20].

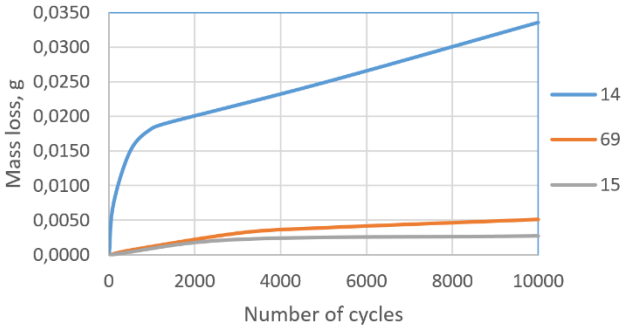

Figure 4. Mass loss of samples

Slika 4. Gubitak mase uzoraka

Figure 5. Samples 14, 15 and 69 after testing

Slika 5. Uzorci 14, 15 i 69 nakon ispitivanja

Heat treated sample (15) was worn significantly less because of the high initial hardness. As it was not nitrided, the sharp edge of the sample was minimally damaged. There was no protective layer that could prevent formation of intermetallic bonds. Soldered aluminium alloy can be seen on the sample.

Sample treated by spheroidize annealing (69) was damaged more than the quenched and tempered sample (15) because of the significantly less initial hardness. There was a significant amount of soldered aluminium alloy on the sample also.

Thermal fatigue did not manifest using these testing parameters and 10000 test cycles. Therefore, testing of the final sample treated by spheroidize annealing (70) was done by different parameters to achieve thermal fatigue. Maximum temperature was increased to 350 °*C* by holding the sample in molten aluminium alloy for 6 *s*. Then the sample was cooled in the lubricant (MoS_2) for 2 *s* which lowered the temperature to 70 °*C*. After 32000 test cycles, a characteristic thermal fatigue network of cracks appeared on the surface. Some cracks caused by thermal fatigue could be seen on the edges of the sample too. The sample also had a significant amount of soldered aluminium alloy. Surface of the sample after 32000 test cycles is shown on figure 6.

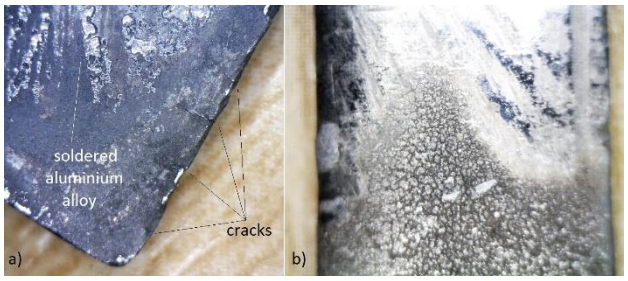

Figure 6. Sample 70 after testing, before (a) and after cleaning (b)

Slika 6. Uzorak 70 nakon ispitivanja, prije (a) i poslije čišćenja (b)

5. Conclusion

There was less wear for quenched and tempered sample (15) than for sample treated with spheroidize annealing (14) because higher initial hardness lowers accumulation of plastic deformation on the surface layer [21]. Therefore, high initial hardness improves resistance to thermal fatigue wear of the material.

Most significant wear was in the case of nitrided sample. It was mostly at the sharp edge of the sample. On the edges, during the nitriding process, nitrogen diffuses from all angles and causes oversaturation of nitrogen [22]. If this is not controlled, a network of iron nitrides will form at the edges. This network forms at the grain boundaries. The result is a very brittle surface and premature cracks or removal of material from the surface.

Thermal fatigue was not noticeable before 32000 test cycles. Therefore, further testing has to be done with high number of test cycles, to correctly determine the effect of thermal fatigue wear mechanism. Most influential parameters for thermal fatigue wear are the preheating temperature of the mould and relative speed between the mould and casting alloy. These parameters will be varied in further experiments to determine their effect and interaction.

Acknowledgements

This work has been fully supported by Croatian Science Foundation under the project 5371.

REFERENCES

[1] M. Muhič, J. Tušek, F. Kosel, D. Klobučar, M. Pleterski: „Thermal fatigue cracking of die-casting dies", Metalurgija 9 (1), 9-12, 2010.

[2] B. Kosec: „Failures of dies for die-casting aluminium alloys", Metalurgija 47 (1), 51-55, 2008.

[3] B. Kosec, G. Kosec, M. Soković: „Case of temperature field and failure analysis of die-casting die", Journal of Achievements in Materials and Manufacturing Engineering 20 (1-2), 2007.

[4] E. Lugscheider, K. Bobzin, T. Hornig, M. Maes: „Increasing the lifetime of aluminium and magnesium pressure die casting moulds by arc ion plating pvd coatings", 6th international tooling conference, 980-990, 2002.

[5] M. Muhič, J. Tušek, F. Kosel, D. Klobčar: „Analysis of Die Casting Tool Material", Journal of Mechanical Engineering 56(6), 351-356, 2010.

[6] E. J. Vinarcik: "High integrity die casting processes", John Wiley Press, New Jersey, 2002.

[7] C. Mitterer, F. Holler, F. Ustel, D. Heim: „Application of hard coatings in aluminium die casting — soldering, erosion and thermal fatigue behaviour", Surface and Coatings Technology 125, 233–239, 2000.

[8] A. Persson, S. Hogmark, J. Bergström: „Failure modes in field-tested brass die casting dies", Journal of Materials Processing Technology 148, 108–118, 2004.

[9] A.H. Mohammed: „Experimental Simulation of Reduction of Erosion Damage in Dies Used in Aluminium Casting", Doktorski rad, 2013.

[10] Q. Han, S. Viswanathan: „Analysis of the mechanism of die soldering in aluminum die casting", Metalurgical and material transactions 34(A), 139-142, 2003.

[11] V. Joshi, A. Srivastava and R. Shivpuri: „Investigating tribochemical behavior of nitrided die casting die surfaces", 6th international tooling conference, 961-977, 2002.

[12] M. Yan, Z. Fan: „Durability of materials in molten aluminum alloys", Journal of materials science 36, 285-295, 2001.

[13] R. Shivpuri, M. Yu, K. Venkatesan, Y-L. Chu: "A Study of Erosion in Die Casting Dies by a Multiple Pin Accelerated Erosion Test", Journal of Materials Engineering and Performance 4, 145-153, 1995.

[14] A. Persson: „On Tool Failure in Die Casting", ACTA Universitatis Upsaliensis, Uppsala 2003.

[15] C.M.D Starling, J.R.T Branco, Thermal fatigue of hot work tool steel with hard coatings, Thin Solid Films, Volumes 308–309, 31 October 1997, Pages 436–442

[16] N. N.: „Mould erosion", http://www.giessereilexikon.com/en/foundry-lexicon/?tx_contagged%5Bsource%5D=default&tx_contagged%5Buid%5D=4594&tx_contagged%5BbackPid%5D=3&cHash=5127b12a9da411d323d4f20959e0dfab , april 2014.

[17] Z.W. Chen: „Formation and progression of die soldering during high-pressure die casting", Volume 397, Issues 1–2, 25 April 2005, Pages 356–369

[18] Z.W. Chen, M.Z. Jahedi: "Die erosion and its effect on soldering formation in high-pressure die casting of aluminium alloys", Materials and Design 20, 303-309, 1999.

[19] G.M. Ludtka, V.K. Sika: „Aluminum Soldering Performance Testing of H13 Steel as Boron Coated by the Cathodic Arc Technique", 47th Annual Technical Conference Proceedings, 168-173, Dallas, Texas, 2004.

[20] I. Duplančić: "Materijali 2 – Aluminij i njegove legure", FESB Split, 2009.

[21] V. Velay, A. Persson, G. Bernhart, J. Bergström, L. Penazzi, "Thermal fatigue of a tool steel: Experiment and numerical simulation", Proceedings of the 6th International Tooling Conference, Karlstad, , 667-685. 2002.

[22] Santosh Hosmani, P. Kuppusami, Rajendra Kumar: „An Introduction to Surface Alloying of Metals", Springer, 2014.

ISSN 1847-7917

Optimization of cutting parameters during the dry and near dry turning of steel 30CrNiMo8

Sabahudin EKINOVIĆ[1)]***, Edin BEGOVIĆ***[1)]***, Alma KUNDALIĆ***[1)]
1) University of Zenica,
Faculty of Mechanical Engineering
Fakultetska 1, 72000 Zenica,
Bosna i Hercegovina
sekinovic@mf.unze.ba; ebegovic@mf.unze.ba;
alma.kundalic@gmail.com

Keywords
Grey relational analysis
Taguchi orthogonal array
Parameters optimization

Ključne riječi
GRA analiza
Taguchi ortogonalni niz
Optimizacija parametara

Original scientific paper
Abstract: This paper applies Taguchi's design of experiment methodology and Grey relational analysis for multi – response optimization of process parameters. Experiments were performed using two cutting techniques: dry machining and minimum quantity lubrication machining (MQL). These environment – friendly cutting techniques are considered to be two practical ways to the clear manufacturing in the context of the sustainable production since the reduction of environmental harmful impact is an important topic in sustainable production. Experiments have been performed based on L9 Taguchi orthogonal array design by three input process parameters, namely cutting speed, feed rate and depth of cut. The objective of process parameters optimization is to achieve at the same time the maximum material removal rate and minimum surface roughness and minimum cutting force components. Based on Grey relation analysis, the optimal settings of process parameters were identified.

Izvorni znanstveni rad
Sažetak: Ovaj rad opisuje Taguchijev dizajn eksperimentalne metodologije kao i Grey relational analysis (GRA analizu) za višeparametarsku optimizaciju režima obrade. Eksperimenti su izvedeni sa dvije tehnike obrade: suha obrada i obrada sa minimalnom količinom sredstva za hlađenje i podmazivanje (MQL). Ove ekološki prihvatljive tehnike obrade se smatraju praktičnim načinima za čišću proizvodnju u kontekstu održive proizvodnje, uzimajući u obzir da je smanjenje ekološki štetnih uticaja važna tema održive proizvodnje. Eksperimenti se baziraju na L9 Taguchijevom ortogonalnom nizu sa tri ulazna parametra obrade: brzina, posmak i dubina obrade. Cilj procesa optimizacije parametara je istovremeno postizanje maksimalne količine skinutog materijala, minimalne površinske hrapavosti, te minimalnih komponenti sile rezanja. Izbor optimalnih parametara procesa se bazira na GRA analizi.

1. Introduction

Machining processes are complex in nature and require often optimizing various different and conflicting objectives. Optimization of machining parameters is continuous engineering task which goals are to reduce the product cost and to achieve the desired product quality. Correct choice of cutting environment as well as appropriate machining technique are determining factors for obtaining better performance characteristics [6].

In this paper two cutting environments: dry machining and near dry machining (MQL) were optimized by using Grey – based Taguchi method. Grey – based Taguchi method, which is a combination of Grey relational analysis and the Taguchi method, that is very often used in multi-response optimization process [1][2][3][4][5]. The same methodology was employed in this case in order to determine the optimal cutting conditions (cutting speed, feed rate and depth of cut) to fulfill different technological request at the same time (goals of optimization) i.e. obtain minimal surface roughness, minimal cutting force and maximal material removal rate.

2. Experimental procedure

Experimental research was performed on universal lathe Potisje ADA 501M. Material of workpieces is steel 30CrNiMo8. Cutting tool has the following tag CNMG 102408 – WG.

For each cut the new cutting insert was used to eliminate the effect of tool wear. Software used for cutting force generating, analysis and representation is KISTLER DynoWare type 2825A – 02. Surface roughness measurements were performed with MarSurf TS 50. The material removal rate is calculated as follows:

$$MRR = v \cdot f \cdot d \quad (1)$$

Symbols/Oznake

MRR	- material removal rate, cm^3/min - količina skinutog materijala	*Ra*	- surface roughness, μm - površinska hrapavost
v	- speed, m/min - brzina		
f	- feed rate, mm/rev - posmak		**Subscripts/Indeksi**
d	- depth of cut, mm - dubina obrade	n	- number of measurements - broj mjerenja
γ	- Grey relational grade, - GRA ocjena	m	- number of responses (parameters) - broj analiziranih parametara
x	- normalized values of responses - normalizovana obrada podataka	i	- number of experimental run - broj eksperimenta
S/N	- signal-to-noise ratio - S/N odnos	k	- number of optimization parameter - broj parametara optimizacije
F	- cutting force, N - sila rezanja		

3. Results and discussions

3. 1. Taguchi method

The Taguchi method was developed by Dr. Genichi Taguchi from Japan. The experimental design proposed by Taguchi involves using orthogonal arrays to organize the parameters affecting the process and the levels at which they should be varied. In this case there are three levels and three parameters (*m=3*, number of responses) given in Table 1 and analysed by using Taguchi L9 orthogonal array (Table 2). To determine the effect of the each variable on the output value, the signal-to-noise ratio, or the S/N number, needs to be calculated for each experiment conducted. For the case of maximizing the performance characteristic, the following definition of the S/N ratio should be calculated:

$$S/N = -10\log\left[\frac{1}{n}\sum_{i=1}^{n}\frac{1}{y_i^2}\right] \quad (2)$$

Where: n=9, number of measurements,
i=1,…, n – experimental run number,
y_i – Grey relational grade (γ_i).

Table 1. Cutting parameters and their levels

Tablica 1. Parametri i nivoi obrade

Level/ Nivo	Speed/ Brzina ***v*** *(m/min)*	Feed rate/ Posmak ***f*** *(mm/rev)*	Depth of cut/ Dubina obrade ***d*** *(mm)*
1	69	0,049	0,2
2	125,7	0,124	0,4
3	180	0,196	0,6

3. 2. Grey Relational Analysis

Data normalization is performed in order to transform original sequence to a comparable sequence. Data are normalized between zero and one. In this study, normalized value of original sequence for surface roughness and cutting force which are smaller – the – better performance characteristics can be expressed as:

$$x_i(k) = \frac{\max y_i(k) - y_i(k)}{\max y_i(k) - \min y_i(k)} \quad (3)$$

The normalised value of original sequence for material removal rate which is larger – the – better performance characteristic can be expressed as:

$$x_i(k) = \frac{y_i(k) - \min y_i(k)}{\max y_i(k) - \min y_i(k)} \quad (4)$$

Where: *i=1, ...,n* (orthogonal array), and
k=1, ..., m (Ra, F and MRR).

The second step is to calculate the grey relational coefficient based on the normalised experimental data to represent the correlation between the desired and actual experimental data by using the following equation:

$$\xi_i(k) = \frac{\Delta_{\min} + \varsigma \cdot \Delta_{\max}}{\Delta_{ik} + \varsigma \cdot \Delta_{\max}} \quad (5)$$

Table 2. Experimental layout using L9 orthogonal array and performance results for dry and near dry machining
Tablica 2. Eksperimentalna podešavanja upotrebom L9 ortogonalnog niza i rezultati performansi za suhu i polusuhu obradu

Exp.No/ Br. eks.	Level of *v* / Nivo faktora *v*	Level of *f* / Nivo faktora *f*	Level of *d* / Nivo faktora *d*	Dry machining/Suha obrada			Near dry machining/ Polusuha obrada		
				F (N)	Ra (μm)	MRR (cm^3/min)	F (N)	Ra (μm)	MRR (cm^3/min)
1	1	1	1	139	1.3	0.6762	126	1.2	0.6762
2	1	2	2	246	1.7	3.4224	250	1.2	3.4224
3	1	3	3	538	1.6	8.1144	469	1.2	8.1144
4	2	1	2	235	1.7	2.4637	182	1.8	2.4637
5	2	2	3	457	1.2	9.3521	439	1.4	9.3521
6	2	3	1	272	1.3	4.9274	257	1.2	4.9274
7	3	1	3	337	1.5	5.2920	322	1.3	5.2920
8	3	2	1	223	1.4	4.4640	264	1.2	4.4640
9	3	3	2	447	1.4	14.112	356	1.2	14.112

Table 3. Grey relational coefficients and grey relational grade for dry machining
Tablica 3. GRA koeficijenti i GRA ocjena za suhu obradu

Exp.No/ Br. Eks.	Normalized values of responses/ Normalizovana vrijednost odziva			Grey relational coefficient/ GRA koeficijent			Grey relational grade/ GRA ocjena	Rank/ Rang
	F	Ra	MRR	F	Ra	MRR		
1	**1.0000**	0.8000	0.0000	1.0000	0.7143	0.3333	0.6825	1
2	0.7318	0.0000	0.2044	0.6509	0.3333	0.3859	0.4567	8
3	0.0000	0.2000	0.5536	0.3333	0.3846	0.5283	0.4154	9
4	0.7594	0.0000	0.1330	0.6751	0.3333	0.3658	0.4581	7
5	0.2030	**1.0000**	0.6457	0.3855	1.0000	0.5853	0.6569	2
6	0.6667	0.8000	0.3164	0.6000	0.7143	0.4224	0.5789	4
7	0.5038	0.4000	0.3435	0.5019	0.4545	0.4324	0.4629	6
8	0.7895	0.6000	0.2819	0.7037	0.5556	0.4105	0.5566	5
9	0.2281	0.6000	**1.0000**	0.3931	0.5556	1.0000	0.6496	3

T**able 4.** Grey relational coefficients and grey relational grade for near dry machining
Tablica 4. GRA koeficijenti i GRA ocjena za polusuhu obradu

Exp.No/ Br. exp.	Normalized values of responses/ Normalizovana vrijednost odziva			Grey relational coefficient/ GRA koeficijent			Grey relational grade/ GRA ocjena	Rank/ Rang
	F	Ra	MRR	F	Ra	MRR		
1	**1.0000**	1.0000	0.0000	1.0000	1.0000	0.3333	0.7778	2
2	0.6385	1.0000	0.2044	0.5804	1.0000	0.3859	0.6554	4
3	0.0000	1.0000	0.5536	0.3333	1.0000	0.5283	0.6206	6
4	0.8367	0.0000	0.1330	0.7538	0.3333	0.3658	0.4843	9
5	0.0875	0.6667	0.6457	0.3540	0.6000	0.5853	0.5131	8
6	0.6181	**1.0000**	0.3164	0.5669	1.0000	0.4224	0.6631	3
7	0.4286	0.8333	0.3435	0.4667	0.7500	0.4324	0.5497	7
8	0.5977	1.0000	0.2819	0.5541	1.0000	0.4105	0.6549	5
9	0.3294	1.0000	**1.0000**	0.4271	1.0000	1.0000	0.8090	1

Where $\Delta_{ik}=\left|x_{ok}-x_i(k)\right|$, Δ_{min} and Δ_{max} are min and max [Δ_{ik}, i=1,2,...n; k=1,2,...m], ς is distinguishing coefficient 0<ς<1, ς=0,5. After averaging the grey relational coefficients, the grey relational grade γ_i can be obtained as follows:

$$\gamma_i=\frac{1}{m}\sum_{k=1}^{m}\xi_i(k) \tag{6}$$

Where *i=1,..., n* (L9 orthogonal array), $\xi_i(k)$ is the grey relational coefficient. The optimal level of the process parameters is the level with the highest grey relational grade. The highest grey relational grade is the rank of 1.

3.3. Analysis of grey relational grades

Optimal process condition for dry and near dry machining can be evaluated from Table 5 and Figure 1.

Table 5. Average grey relational grades for the levels of factors

Tablica 5. Prosječne vrijednosti GR ocjena za nivoe faktora

Level /Nivo	Dry machining/ Suha obrada			Near dry machining/ Polusuha obrada		
	v (A)	f (B)	d (C)	v (A)	f (B)	d (C)
1	0.518	0.535	**0.606**	**0.685**	0.604	**0.699**
2	**0.565**	**0.557**	0.521	0.554	0.608	0.650
3	0.556	0.548	0.512	0.671	**0.698**	0.561
Delta	0.047	0.022	0.094	0.131	0.094	0.138
Rank	2	3	1	2	3	1

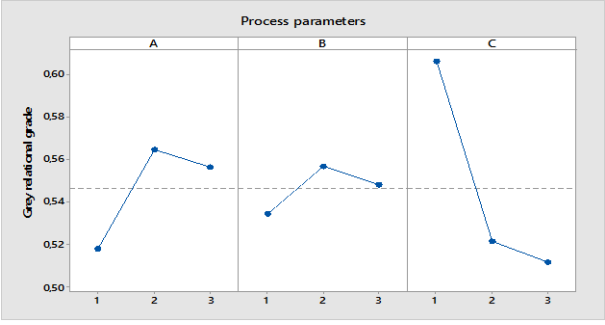

Figure 1. Impact of cutting parameters on dry machining
Slika 1. Uticaj parametara obrade na suhu obradu

The optimal parameters for dry machining are as follows: cutting speed v=125,7 [m/min] (level 2), feed rate f=0,124 [mm/rev] (level 2), depth of cut d=0,2 [mm] (level 1). In Figure 1 we can see that the greatest impact on multi response parameter characteristics for dry machining has the depth of cut. Second influential factor is the speed. On the third place is the feed rate.

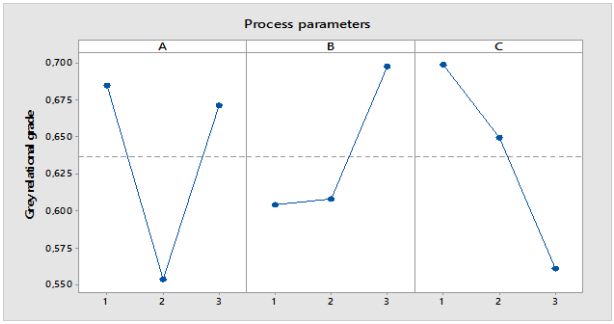

Figure 2. Impact of cutting parameters on near dry machining

Slika 2. Uticaj parametara obrade na polusuhu obradu

The optimal parameters for near dry machining are as follows: cutting speed v=69 [m/min] (level 1), feed rate f=0,196 [mm/rev] (level 3), depth of cut d=0,2 [mm] (level 1). In Figure 2 the greatest impact on multi response parameter characteristics for near dry machining has the depth of cut. Second influential factor is the speed. On the third place is the feed rate.

3.4. Verification test

Verification test consists of three experiments and we have three measurements of which we take the mean value.

Table 6. Results of verification test for dry machining

Tablica 6. Rezultati verifikacijskog testa

	Ra	F	MRR	GRA. grade/ GRA ocjena	Change of GRA grade/ Promjena GRA ocjene
Dry mach./ Suha obrada: ***v1f1d1***	1.3	139	0.676	0.6825	
Optimal dry m./ Optimalna suha obrada: ***v2f2d1***	1.1	298	3.117	0.8675	0.185
Near dry mach./ Polusuha obrada: ***v3f3d2***	1.2	356	14.112	0.809	
Optimal near dry m./ Optimalna polusuha obrada ***v1f3d1***	1.3	293	2.705	0.5424	-0.2666

Table 6 shows the comparison of the estimated grey relational grade with the actual grey relational grade obtained in verification experiment using the optimal cutting parameters v2f2d1. Namely, surface roughness Ra was improved from 1.3 [μm] to 1.1 [μm] and material

removal rate was improved from 0.6762 [cm^3/min] to 3.1174 [cm^3/min].

In conclusion, it is clearly shown that multiple performance characteristics in turning 30CrNiMo8 steel were significantly improved by increase in grey relational grade of 0,1850. Also Table 6 shows the comparison of the estimated grey relational grade with the actual grey relational grade obtained in verification experiment using the optimal cutting parameters v1f3d1. Surface roughness Ra wasn't improved and material removal rate wasn't improved. Also, multiple performance characteristics were not improved due to gray relational grade being lowered. It is obvious that in this case (near dry machining) some important influential factors are not included in the experimental investigations.

4. Conclusion

The optimum turning parameters were determined for better multiple performance characteristics (minimal surface roughness and cutting force, maximal material removal rate). The application of grey relational analysis based on the Taguchi method directly integrates the multiple quality characteristics into single performance characteristic called grey relational grade. A L9 Taguchi orthogonal array, signal to noise (S/N) ratio were used for optimization of cutting parameters considering grey relational grade. The optimal levels of dry machining parameters for the desired performance characteristics is the combination v2f2d1. The Grey relational grade can be significantly improved by 0,1850 through this method. The optimal levels of near dry machining parameters for desired performance characteristics is the combination labelled as v1f3d1, but multiple performance characteristics were not improved due to Grey relational grade being lowered. This result might indicate that some important factor(s) in near dry machining process analysis are missing. Therefore, the integration of grey relational analysis and the Taguchi method can be applicable for the optimization of process parameters and help to improve process efficiency, but also to indicate some mistakes in experimental design.

REFERENCES

[1] Franko Puh, Miran Brezocnik, Zoran Jurković, Goran Cukor, Mladen Perinić, Milenko Sekulić, (2015), *Multi – response optimization of turning parameters using the Grey – based Taguchi method*, TMT 2015, Barcelona, Spain

[2] Dragičević, Mario; Jozić, Sonja; Bajić, Dražen. *Optimization of cutting parameters in end-milling of 42CrMo4 steel by applying Taguchi method and the Grey relational analysis* MTSM 2015,/ Jozić, Sonja ; Lela, Branimir (ur.). Split : Croatian society for mechanical technologies, 2015. 41-46

[3] Arun Kumar Parida, Rajesh Kumar Bhuyan, Bharat Chandra Routara, (2014), *Multiple characteristics optimization in machining of GFRP composites using Grey relational analysis*, School of Mechanical Engineering Odisha, Odisha, India

[4] Md. Israr Equbal, Randhir Kumar, Mohammad Shamim, R. K. Ohdar, (2014), *A Grey – based Taguchi Method to Optimize Hot Forging Process*, Procedia Materials Science 6, India

[5] Stephanie Fraley, Mike Oom, Ben Terrien, John Zalewski, (2007), *Design of experiments via Taguchi methods: orthogonal arrays*, University of Michigan Chemical Engineering Process Dynamics and Controls Open Textbook, USA

[6] Dr. Sabahudin Ekinović, Dr. Edin Begović, (2012), *Napredne proizvodne tehnologije*, Mašinski fakultet Univerziteta u Zenici, Zenica, B&H

ISSN 1847-7917

Dimensional measurements with usage of computed tomography method

Amalija HORVATIĆ NOVAK[1)]***, Biserka RUNJE***[1)]

1) Faculty of mechanical engineering and naval architecture
Fakultet strojarstva i brodogradnje
Ivana Lučića 5, 10 000 Zagreb, **Croatia**

amalija.horvatic@fsb.hr
biserka.runje@fsb.hr

Keywords

Computed tomography
Dimensional measurements
Measurement uncertainty
Influence parameters
Number of projections

Ključne riječi

Računalna tomografija
Dimenzionalna mjerenja
Mjerna nesigurnost
Utjecajni parametri
Broj projekcija

Original scientific article

Abstract: Application of Computed Tomography (CT) in dimensional metrology is a new and relatively unexplored field. Metrological CT devices enable measurement of both external and internal geometry and structure of measurement objects with use of non-contact and non-destructive scanning method. It is a method with more advantages than disadvantages which makes it very desirable in the field of dimensional measurements and its wide use in different industries. The paper explains computed tomography measurement process and presents example of coordinate measurement of aluminium plate.

Izvorni znanstveni rad

Sažetak: Primjena računalne tomografije (CT) u dimenzionalnom mjeriteljstvu novo je i relativno neistraženo područje. Mjeriteljski CT uređaji omogućuju mjerenje kako vanjske tako i unutarnje geometrije i strukture predmeta mjerenja beskontaktnom i nerazornom tehnikom skeniranja. Riječ je o metodi s više prednosti nego nedostatka, što je čini veoma poželjnom metodom u području dimnezionalnih mjerenja kao i u njezinom primjeni u različitim granama industrije. U radu je objašnjen princip procesa mjerenja primjenom računalne tomografije te je dan primjer koordinatnog mjerenja aluminijske pločice.

1. Introduction to computed tomography

Computed tomography is a method that uses nature of X-ray to obtain information about inspected object. The history of computed tomography goes back to begin of 20th century when X-radiation was discovered. In the 1970s scientist Godfrey Hounsfield proposed the idea for determination internal structure of objects with usage of 2D images obtained with X-ray scanning. At the same, independent of Hounsfield work, Allan Cormack was also working on developments of computed tomography. They both were awarded with Nobel prize in Psychology or Medicine in 1979 for their achievements [1, 2]. Method was first used in Medicine where first CT scanning of human brain in 1971 was done. Later, at the beginning of 1980s, CT began to apply in a field of material analysis, and it is from 2005 used for dimensional measurements [1].

Computed tomography (CT) is a non-contact and non-destructive method that uses X-ray to obtain information about inner and outer structure and characteristics of the object under examination. Its biggest advantage is possibility of measurement and analysis conduction of both inner and outer structures with no need for object destruction. It is a method widely used in different industries, such as aerospace, automotive and electronic industry, security systems at airports, also in food industry for detection of contaminants in packages. It provides an opportunity of analysis and measurement of single part in assembled state and is of substantial importance in the application in reverse engineering [3]. However, apart from the lot of advantages, this method has also some disadvantages. The main problem in CT usage in dimensional metrology is a big number of influencing parameters on the whole system which introduce many measurement uncertainties and make determination of total measurement uncertainty extremely complicated [1,3-6]. Because of the fact that total measurement uncertainty is still not evaluated, measurement result obtained with CT are not traceable to SI unit, metre. Traceability is property of a measurement result whereby the result can be related to a reference through a documented unbroken chain of calibrations, each contributing to the measurement uncertainty [7]. Following aforementioned, assessment of measurement uncertainty will increase the usage of CT system in industries and make obtained results comparable.

Symbols/Oznake

l	- aluminum plate length, mm - duljina aluminijske pločice	U*	- voltage, kV - napon
w_1	- aluminum plate width, mm - širina aluminijske pločice	I	- current, µA - jakost struje
w_2	- distance between two pockets, mm - udaljenost između dva utora	N	- number of projections - broj projekcija
d_1	- distance between two holes, mm - udaljenost između dva provrta	U	- expanded measurement uncertainty,µm - proširena mjerna nesigurnost, µm
d_2	- distance between plane and hole, mm - udaljenost između ravnine i otvora, mm	k	- coverage factor - faktor pokrivanja
D	- hole diameter, mm - promjer provrta	P	- probability, % - vjerojatnost, %

2. Working principle

CT measurement is conducted in CT systems and can be divided into three separate parts. Each process of CT measurement consists of scanning the object under investigation, generating a 3D model from 2D images and measuring which is carried out on the model of actual state (Figure 1).

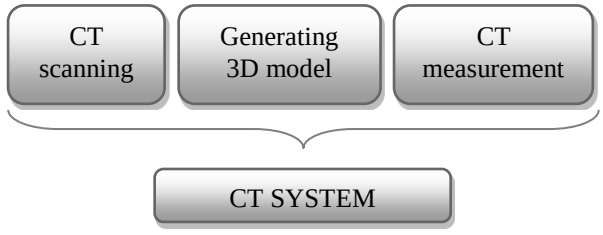

Figure 1. Structure of CT system

2.1. CT scanning

CT scanning is a first part of the whole CT measurement process and it is held in the CT scanner. There are many types of CT scanners, but still each of them consists of an X-ray source where X-ray are produced, rotational table where object under investigation is placed and rotated during the scanning process, and detector which collects projection images of the object from different angles. Scanning process can last up to several hours, but once the object is scanned and the model is generated, all information about object is available from the same model e.g. geometrical characteristics, dimensional measurements, material analysis. Figure 2 shows the configuration of cone beam scanner, which is the most frequent configuration of industrial CT systems used for metrological purposes. Scanning process is probably the most difficult one, because there are no standards that explain how the scanning should be done.

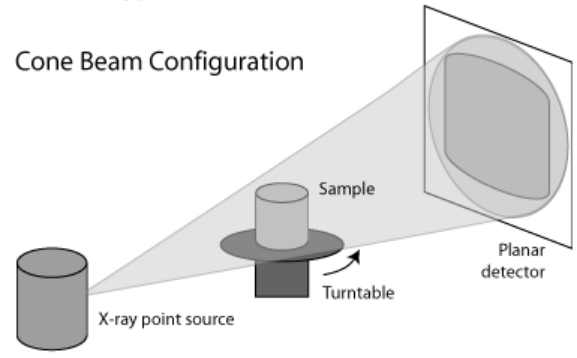

Figure 2. Cone beam scanner configuration [8]

It this part of CT measurement process, operator has the biggest role, and because of the lack of standard, scanning setups are based on operator experience. These setups include selection of current, voltage, number of projections, object positioning, geometrical magnification, etc. All these parameters depend on object size and material.

2.2. 3D Modelling

After scanning process, where huge number of 2D projections is collected and where each projection stands for different angle of object, generating the model follows. First step is to find the centre of rotation of slices. Second step can include software beam hardening correction and noise reduction. It is optional but certainly recommended to use this option. It lowers the possibility of systematic errors such as, appearance of streaks, circles and noises on the model which make the measurement difficult. Figure 3a displays one slice of the scanned object before beam hardening correction, and figure 3b shows the same slice after beam hardening correction. 3D model of actual state is generated from projection that covers 360 degrees of the object.

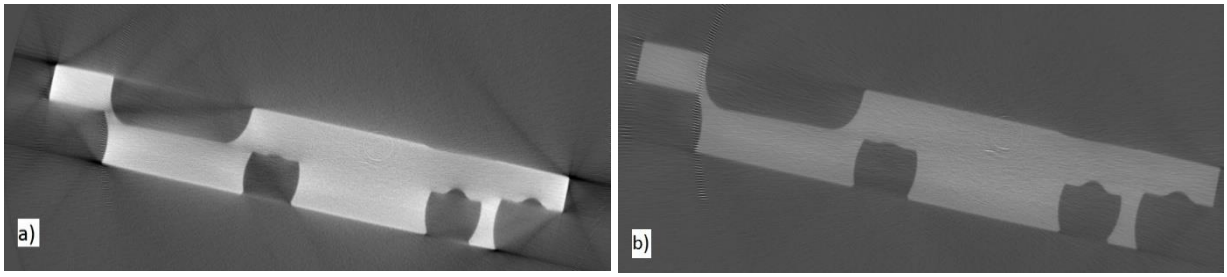

Figure 3. Slice of the scanned object (a) before beam hardening correction; (b) after beam hardening correction

2.3. Measurements

Implementation of measurement process is held in software which enables conduction of measurement on 3D model. It is a coordinate measurement process and several approaches are possible to carry out the measurement. One way implies fitting reference objects with simple geometry to polygon data and then measure relations between those reference objects, second approach is nominal/actual comparison where model of the real part is compared to CAD model and third is the usage of instrument tools. The first approach is most used and covers many measurement requests; second approach is the fastest because it easily overlaps two models and indicates measures out of tolerance with colour coding approach. Third one is mostly used for special demands like measurement of complex lines.

3. Example of CT dimensional measurement

Dimensional measurements of aluminium plate (Figure 4) were conducted on both tactile coordinate machine and on CT measurement system and comparison of obtained results was made. Both methods enable coordinate measurements and use same approach for carrying the measurement process – method of fitting the simple geometry objects, with selected Gaussian approach.

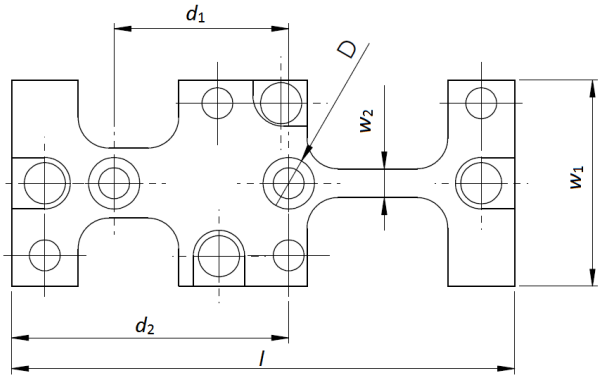

Figure 4. Aluminium plate

Measured were only dimensional characteristics: length, diameter, distances between pockets and holes. Table 1 contains measured characteristics, their symbols and measurement approach used in CMM and CT measurements.

Table 1. Display of measured characteristics and measurement approach

Symbol / Simbol	Measured characteristic / Mjerena značajka	Measurement approach / Mjerni pristup
l	Al plate length	Plane -plane
w_1	Al plate width	Plane -plane
w_2	Distance between two pockets	Plane -plane
d_1	Distance between two holes	Cylinder-cylinder
d_2	Distance between plane and hole	Plane - Cylinder
D	Diameter	Cylinder

First measurements of aluminium plate were performed on coordinate measuring machine Ferranti Merlin using software MODUS. Measured were only dimensional characteristics given in Table 1 according to above mentioned measurement strategy, and results are given in Table 2. Expanded measurement uncertainty of all results obtained with usage of CMM equals $U = 4$ μm, where coverage factor is $k = 2$ and probability $P = 95$ %.

Table 2. Results from CMM measurements, mm

Measurand / Mjerena veličina	CMM results / CMM Rezultati	CT results/ CT rezultati
l	48,357	48,36
w_1	19,261	19,31
w_2	2,870	2,92
d_1	17,006	16,99
d_2	26,873	26,95
D	5,045	5,06

The same aluminium plate was also measured by using computed tomography method at CT device, model Nikon XT H 225; 3D modelling was performed in software CT Pro; and measurements were conducted in

VolumeGraphics Studio Max 2.2. The same measurement approach was used as the one used for CMM measurements, described in Table 1. Results obtained from CT measurements are given in Table 2. Setups for CT scanning are given in Table 3, voltage, current and numbers of projections were chosen by operator, while others are determined by CT configuration.

Table 3. Setups for CT scanning process

Parameter / Parametar	**Amount / Iznos**
*U**, kV	74
I, µA	45
N	720
Detector size, pixels	3192 x 2296
Pixel size, µm	127 x 127
X-ray spot size, µm	3,33

4. Results and discussion

Two coordinate measurements were provided on aluminium plate, on CMM and with usage of computed tomography method. Because of the fact that metrological traceability is achieved for CMM systems, results from CMM will be considered as reference values and results obtained with usage of CT system will be compared and analyzed according to reference values. Figure 5 displays deviations of CT results from reference values and their amounts.

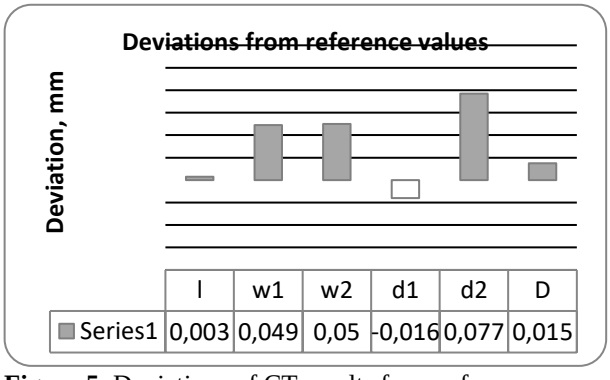

Figure 5. Deviations of CT results from reference values

The best agreement between results is seen for case where plate length was measured, while the biggest deviation occurs in case where length between plane and hole was measured. In first case, measurement approach that implies distance measurement between two planes was used, while in second case, distance measurement between plane and circle was used. Relatively small deviations are observed in measurements of diameter and distance between two holes. Here, fit objects were cylinders. With analyzing results depending on chosen measurement approach, exclusive conclusion about behaviour of results cannot be made. Second observed from results is fact that results do not behave in one way, either plus or minus deviation, meaning that possible systematic error cannot be easily determined and excluded. Obtained results behave in accordance with previous researches.

5. Conclusion

Because of the fact that CT method allows insight into internal structure without destroying parts, and because of possibility of caring out many different analyses with only one CT scanning process, CT method is desirable in field of dimensional measurements. Absence of metrological traceability and evaluated measurement uncertainty of results prevents its wider usage in the field of dimensional measurements. Results obtained by usage of computed tomography, compared with reference values, are close to each other, but deviations in results from reference measurements do not behave in a predictable way. Further researches with aim of measurement uncertainty assessment are the certain need in CT metrology and are the base for its wider application in industries.

REFERENCES

[1] Kruth J. P. et al. (2011), *Computed tomography for dimensional metrology*, CIRP Annals – Manufacturing Technology 60, pp. 821-842

[2] Kalender W. A., (2011), *Computed Tomography – Fundamentals, System Technology, Image Quality, Application*, Publicis Publishing, Germany

[3] Sun W., Brown S.B. and Leach, R.K., (2012), *An overview of industrial X-ray computed tomography*, NPL Report

[4] Müller P. et al., (2013), *Computed tomography as a tool for tolerance verification of industrial parts*, Procedia CIRP 10, pp. 125-132

[5] Welkenhuyzen et al. (2009), *Industrial Computer Tomography for Dimensional Metrology: Overview of Influence Factors and Improvement Strategies*, OPTIMESS2009, Antwerp, Belgium

[6] Müller P. et al., (2011), *Investigation of measuring strategies in computed tomography*, NEWTECH 2011, Brno, Czech Republic

[7] JCGM 200:2008, *International vocabulary of metrology – Basic and general concepts and associated terms* (VIM)

[8] http://d32ogoqmya1dw8.cloudfront.net/images/research_education/geochemsheets/techniques/_1172960774.png, Assesed on 02 June 2016

ISSN 1847-7917

XRD analysis of CuAlNi shape memory alloy before and after heat treatment

Ivana IVANIĆ[1)], Stjepan KOŽUH[1)], Stanislav KURAJICA[2)], Borut KOSEC[3)], Ivan ANŽEL[4)], Mirko GOJIĆ[1)]

1) University of Zagreb, Faculty of Metallurgy, Aleja narodnih heroja 3, 44103 Sisak, Croatia
2) University of Zagreb, Faculty of Chemical Engineering and Technology, Marulićev trg 19, Zagreb, Croatia
3) University of Ljubljana, Faculty of Natural Sciences and Engineering, Aškerčeva cesta 12, 1000 Ljubljana, Slovenia
4) University of Maribor, Faculty of Mechanical Engineering, Smetanova 17, 2000 Maribor, Slovenia

iivanic@simet.hr,
kozuh@simet.hr
stankok@fkit.hr,
borut.kosec@omm.ntf.uni-lj.si
ivan.anzel@um.si,
gojic@simet.hr

Keywords

Shape memory alloys
Heat treatment
Microstructure
Martensite
XRD analysis

Ključne riječi

Slitine s prisjetljivošću oblika
Toplinska obrada
Mikrostruktura
Martenzit
XRD analiza

Original scientific article

Abstract: Shape memory alloys (SMAs) belong to a class of shape memory materials which have the ability to 'memorise' or retain their previous shape when subjected to certain thermal or mechanical loading. SMAs have drawn significant attention due to their unique properties. The Cu-based SMAs are low costing SMAs comparing to the NiTi-based alloys. Among the Cu-based SMAs, the CuAlNi alloys show good shape memory properties and the possibility of high temperature application (up to 200 °C). In this work the CuAlNi alloy was produced by vertical continuous casting method in form of a cylinder rod of 8 mm in diameter. After the casting the heat treatment was performed, i.e. solution annealing and tempering. The microstructure characterization of SMAs was carried out by X-ray diffraction analysis, optical microscopy (OM) and scanning electron microscopy (SEM) equipped by device for energy dispersive spectroscopy (EDS). The peaks of different types of martensite (β_1' and γ_1') were observed at XRD diffractograms. The homogenous martensite microstructure was confirmed by OM and SEM micrographs.

Izvorni znanstveni rad

Sažetak: Slitine s prisjetljivošću oblika (SMA) pripadaju skupini materijala s prisjetljivošću oblika koji posjeduju sposobnost „pamćenja" ili zadržavanja prethodnog oblika kada su izložene toplinskom ili mehaničkom opterećenju. SMA slitine privlače značajnu pažnju zbog njihovih jedinstvenih svojstava. SMA slitine na bazi bakra su jeftinije u odnosu na slitine na bazi NiTi. Među slitinama na bazi bakra, CuAlNi slitine imaju dobra svojstva prisjetljivosti oblika i mogućnost primjene na visokim temperaturama (do 200 °C). U ovom radu CuAlNi slitina je proizvedena metodom vertikalnog kontinuiranog lijevanja u obliku štapa promjera 8 mm. Nakon lijevanja provedena je toplinska obrada, tj. žarenje i popuštanje. Mikrostrukturna karakterizacija provedena je rendgenskom faznom analizom (XRD), optičkom mikroskopijom (OM) i pretražnom elektronskom mikroskopijom (SEM) opremljenom s energetsko disperzijskim spektrometrom (EDS). Na XRD difraktogramima zamijećeni su pikovi različitih tipova martenzita (β_1' and γ_1'). Homogena martenzitna mikrostruktura potvrđena je na OM i SEM mikrografijama.

1. Introduction

Cooper based shape memory alloys (SMAs) have attracted more attention in past few decades owning to their low price, easy fabrication and good thermal and electrical conductivity. SMAs possess remarkable properties such as pseudoelasticity, one-way shape memory effect and two-way shape memory effect. The shape memory effect makes them suitable for innovative application in various fields [1].

Cu-based alloys exhibit a shape memory properties within a certain range of composition, having the disordered bcc structure, called β – phase. The β – phase is stable at higher temperatures and has two successive ordering transitions during quenching from 1173 K to room temperature [2,3].

The functional behavior of SMAs is related to the first-order displacive and diffusionless martensite transformation between high temperature β – phase and low temperature martensite phase [3].

CuAlNi shape memory alloys undergo a single transformation (β→β_1' or β→γ_1') or a mixed transformation (β→β_1' + γ_1') depending on alloys chemical composition [3-5]. At aluminium contents above 11 wt.%, the parent phase transforms to ordered β_1 phase, having a DO3-type superlattice, prior to martensitic transformation. In this case, the martensite "inherits" the ordered structure. At aluminium contents between 11 and 13 wt.%, β_1' martensite, having a monoclinic 18R1 structure prevails. At aluminium contents over 13 wt.%, orthorhombic 2H-type γ_1'

martensite prevails. Which of them will appear depends on the temperature and the stress condition [4,6].
In this work, the CuAlNi shape memory alloy microstructural properties has been studied depending on heat treatment procedure which is applied to the samples in order to obtain the stabile structure.

Symbols/Oznake

Cu	- cooper - bakar
Al	- aluminium - aluminij
Ni	- nickel - nikal
DO_3	- type of lattice - tip kristalne rešetke
18R1	- monoclinic lattice type - monoklinski tip rešetke
2H	- orthorhombic lattice type - ortorompski tip rešetke

Greek letters/Grčka slova

β	- body centered cubic phase - volumno centrirana kubična faza
β_1'	- martensite - martenzit
γ_1'	- martensite - martenzit

2. Experiment

Cu-12.8%Al-4.1%Ni (wt.%) shape memory alloy was produced by vertical continuous casting procedure by melting pure elements (99.9 %). The device for vertical continuous casting was connected to a vacuum induction furnace, Fig. 1. A bar of 8 mm in diameter solidifies in the crystallizer and comes out passing between two rolls which rotate in opposite directions with pull-pause sequence withdrawal. The casting speed was 320 mm min^{-1} and casting temperature 1240°C.
The alloy in as-cast state (sample A) was heat treated at different temperatures. The heat treatment was carried out by solution annealing at 850 °C held for 60 minutes and water quenched (WQ) immediately after heating (sample C), and afterwards the sample was tempered at 300 °C holding for 60 minutes and WQ (sample C-300). The samples investigated in this work are presented in Table 1 showing the marks of the samples and the heat treatment regime.
After heat treatment the samples were prepared adequately for microstructural examination. Metallographic preparation was obtained by grinding with different grade paper (240-1000), polishing in alumina suspension and etching in a solution composed from 2.5 g $FeCl_3$, 48 ml methanol and 10 ml HCl.
The microstructural characterization was carried out by optical microscopy (OM) and scanning electron microscopy (SEM) and X-ray diffraction analysis (XRD). The samples for XRD measurement were adequately prepared in the form of thin plates of 8 mm in diameter and were subjected to a XRD analysis. XRD analysis was performed on Shimadzu XRD-6000 difractometer with CuK_α source of radiation with X-ray tube voltage of 40 kV and current of 30 mA. Scan range was from 3 to 83 ° (in 2θ° range) and the scan speed was 2.0 deg/min.

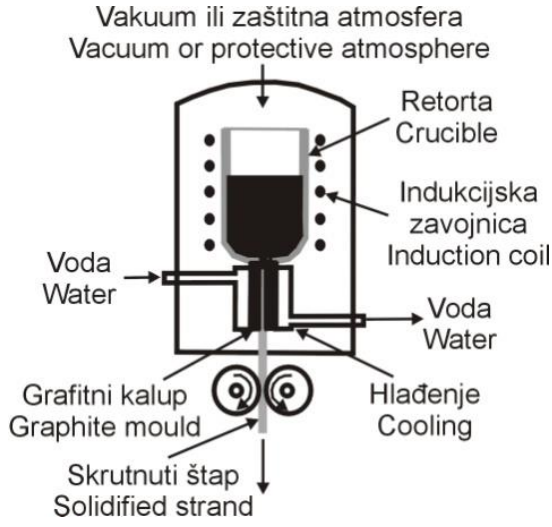

Figure 1. Schematic illustration of casting the CuAlNi alloy by vertical casting technology [7]

Slika 1. Shematski prikaz lijevanja CuAlNi slitine tehnologijom vertikalnog lijevanja [7]

Table 1. List of investigated CuAlNi SMA samples
Table 1. Popis ispitivanih uzoraka CuAlNi SMA

Sample/Uzorak	Heat treated state/Toplinska obrada
A	As – cast state/Lijevano stanje
C	900 °C/60'/WQ
C-300	900 °C/60'/WQ + 300 °C760'/WQ

3. Results and discussion

3.1. Optical microscopy

Optical micrographs of investigated samples were presented on Figure 2. As can be seen in all three samples are visible martensite microstructure with cleary visible characteristic self-accommodating zig-zag morphology of martensite plates in particular grain.

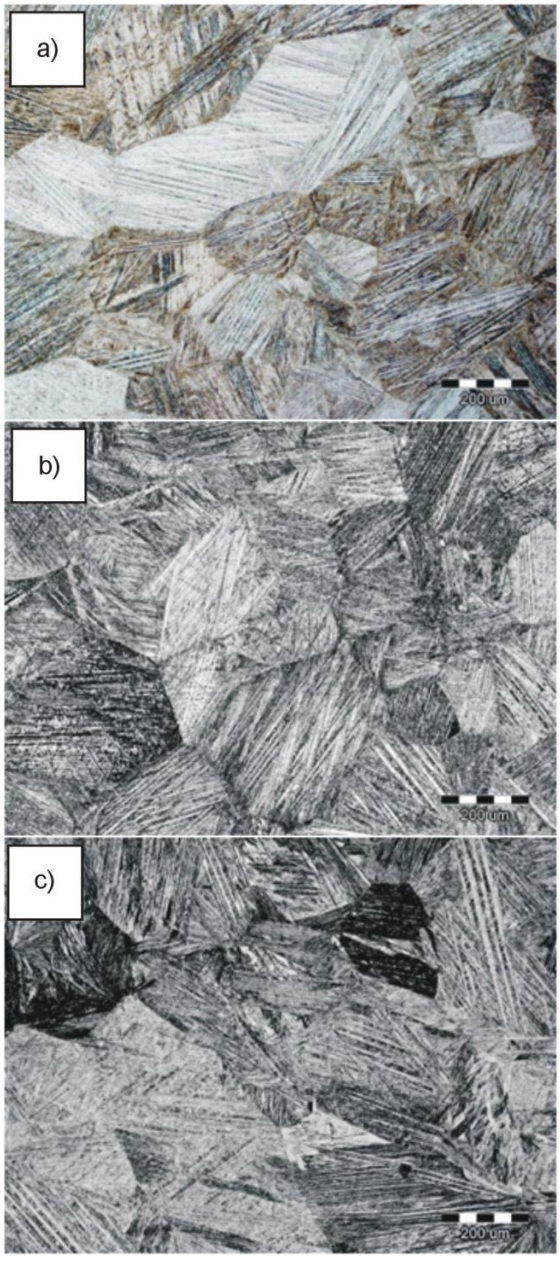

Figure 2. Optical micrographs of CuAlNi SMA in as-cast state (a), solution annealed at 850 °C/60'/WQ (b) and tempered at 300 °C/60'/WQ (c)

Slika 2. Optičke mikrografije CuAlNi slitine s prisjetljivošću oblika u lijevanom stanju (a), kaljeno kod 900 °C/60'/voda (b) i popušteno kod 300 °C/60'/voda (c)

3.2. Scanning electron microscopy

To obtain more detail information of the microstructures and the crystal structures of the self-accommodating martensites we carried out SEM and XRD measurements of the alloy in as-cast state, and alloy in quenched and tempered state. Fig. 3 shows the SEM micrographs of the self-accommodating martensites in all three investigated samples. Here it is obviously seen that the microstructure of martensite consists of self-accommodating plate groups.

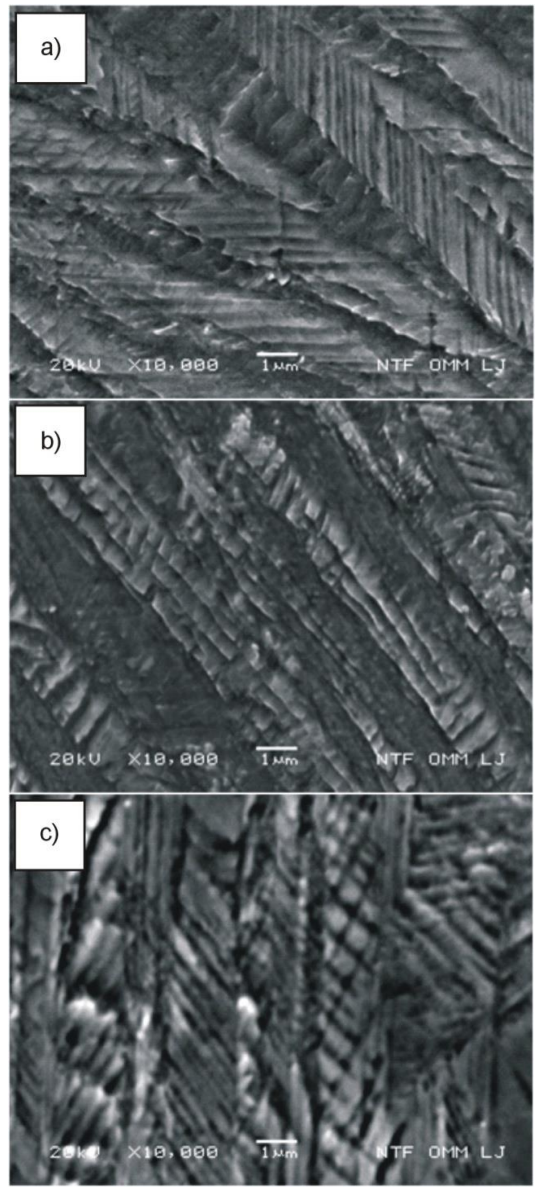

Figure 3. SEM micrographs of CuAlNi SMA in as-cast state (a), solution annealed at 850 °C/60'/WQ (b) and tempered at 300 °C/60'/WQ (c)

Slika 3. SEM mikrografije CuAlNi slitine s prisjetljivošću oblika u lijevanom stanju (a), kaljenom kod 900 °C/60'/voda (b) i popuštenom kod 300 °C/60'/voda (c)

According to the literature [8], martensite plate groups nucleate at numerous sites in the grain and the martensite growth process involves accommodation of local stress fields which require the formation of other plate groups. Thus, the different plate groups form in the same parent phase grain.

The SEM/EDS analysis was obtained to examine the chemical composition on surface of the samples. The examination reveals some difference between brighter and darker fields, Fig. 4.

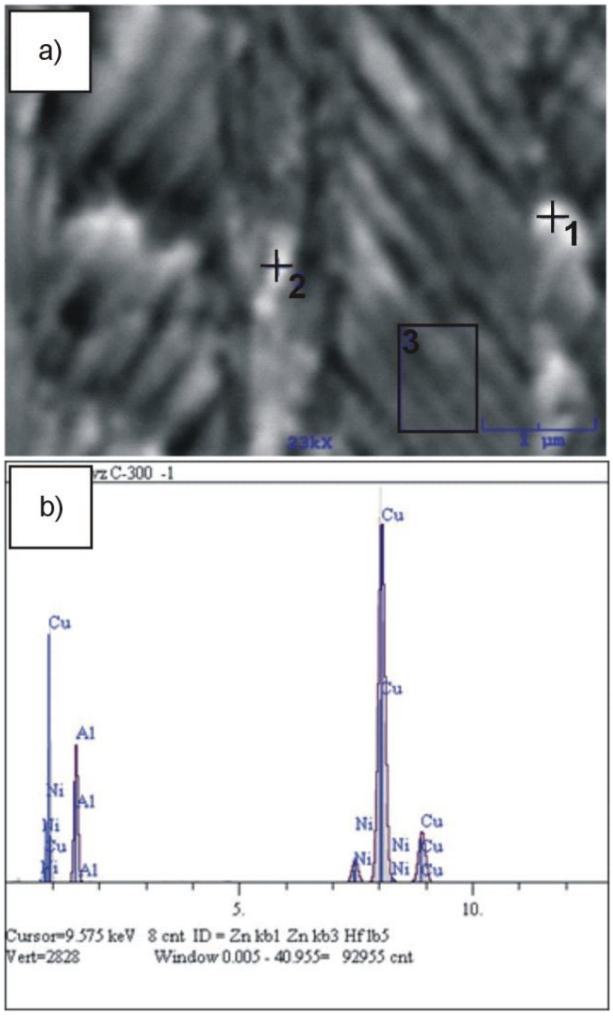

Figure 4. SEM micrograph of CuAlNi SMA in tempered state at 300 °C/60'/WQ (a) and EDS spectrum of position 1 (b)

Slika 4. SEM mikrografija CuAlNi slitine s prisjetljivošću oblika u popuštenom stanju na 300 °C/60'/voda (a) i EDS spektar pozicije 1 (b)

The chemical composition of marked position was given in Table 2. The brighter fields (position 1 and position 2) have the lower amount of cooper (86.46% and 86.00%) and higher amount of aluminium (9.79% and 9.88%) than the darker field (position 3) with the amount of cooper 88.30% and aluminium 7.51%. The difference in the amount of nickel in all three positions is very small (< 0.50 wt.%).

Table 2. Chemical composition of positions marked at Fig. 4a, wt. %

Table 2. Kemijski sastav pozicija označenih na slici 4a, mas. %

Sample C-300/Uzorak C-300	Cu	Al	Ni
	wt.%		
Position 1	86.46	9.79	3.75
Position 2	86.00	9.88	4.12
Position 3	88.30	7.51	4.19

3.3. XRD analysis

The results of XRD analysis on CuAlNi samples before and after heat treatment are shown graphically as a function of intensity of the diffraction maximum and diffraction angle, Fig. 5. XRD analysis in all samples shows the diffraction maximum that respond to the CuAlNi shape memory alloys.

According to microscopic observations, the XRD confirms the presence of monoclinic β_1' martensite (18R1) in all three samples. The X-ray diagrams of all samples looked quite similar. In all three samples β_1' martensite was represented with more than three peaks with the highest intensity. Between 40° and 45° in the area of 2θ, both types of martensite have their peaks only a few hundredths of a degree apart, so at these three positions β_1' and γ_1'-peaks could be overlapping.

Due to the relatively high detection limit by XRD, the absence of γ_1' martensite in the as-cast state sample can be explained [4].

It is well established that CuAlNi alloy can transform from one type of martensite to another type depending on alloy composition, change of stress state, thermal history (e.g. heat treatment) etc. [4,5,9].

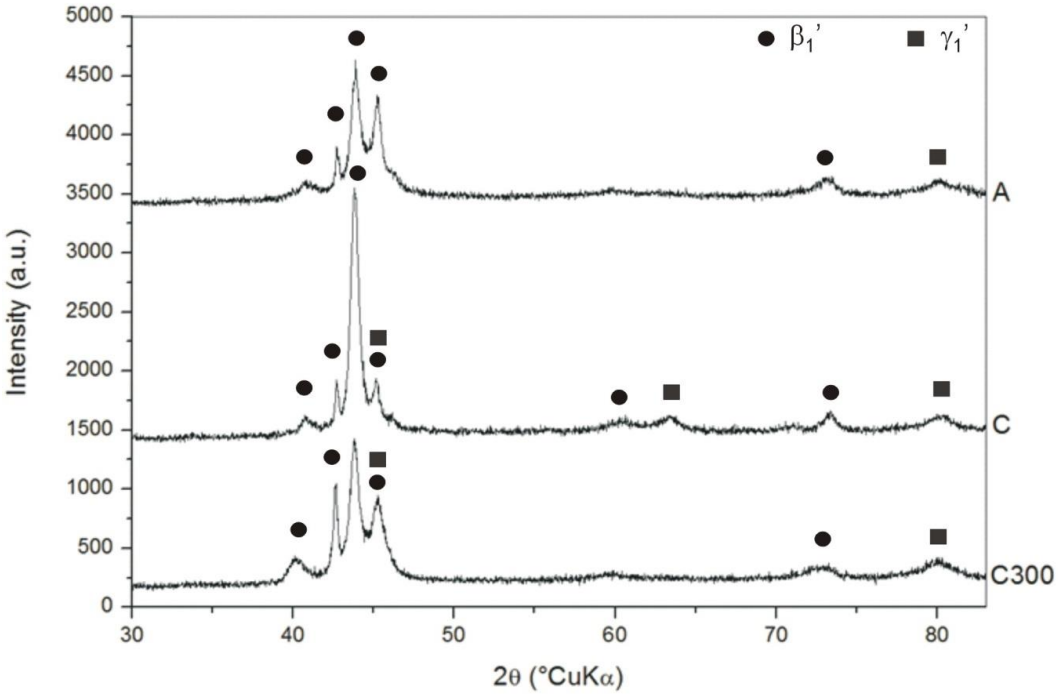

Figure 5. XRD difractograms of CuAlNi shape memory alloys

Slika 5. XRD difraktogrami CuAlNi slitina s prisjetljivošću oblika

4. Conclusion

The vertical continuously casted Cu-12.8%Al-4.1%Ni (wt.%) shape memory alloy samples were produced and the certain heat treatment procedure (solution annealing and tempering) was carried out. The microstructural investigation by optical microscopy, scanning electron microscopy equipped with EDS analysis and XRD analysis was performed, and on the basis of obtained results can be withdrawn following conclusions:

- Optical microscopy reveals the martensite microstructure in all three samples. The martensite self-accommodating lattice in particular grains and the grain boundaries are clearly visible.
- Scanning electron microscopy confirms martensite microstructure in CuAlNi shape memory alloy samples. The self-accommodating plate group of martensites appears in all three samples.
- EDS analysis reveals a small difference in chemical composition in the dark field and bright field area. The bright field has a lower amount of cooper between 1.84 and 2.30 wt.%, and the higher amount of aluminium in the range of 2.28 to 2.37 wt.% than the dark field. The difference in the amount of nickel between all three positions is negligible.
- The β_1' and γ_1' martensites can be noticed on X-ray diffractograms. Due to the fact that the between 40° and 45° peaks of both types of martensites could be overlapping, the actual confirmation of the existence of the γ_1' martensite, especially in as-cast state sample, can't be assured. On the other hand, this doesn't mean that the no γ_1' martensite was present.

Acknowledgements

This work has been fully supported by Croatian Science Foundation under the project IP-2014-09-3405.

REFERENCES

[1] Nevin Balo Ş., Sel N., (2012), *Effects of thermal aging on transformation temperature and some physical parameters of Cu-13.5 wt.%Al-4 wt.%Ni shape memory alloy*, Thermochimica Acta 536, p 1-5 Germany

[2] Aydogdu A., Aydogdu Y., Adigüzel O., (1997), *Improvement of Hardness and Microstructure by Ageing in Shape Memory CuAlNi Alloys*, Journal de Physique IV France 7, p 311-316 France

[3] Recarte V., Pérez-Landazábal J.I., Rodríguez P.P., Bocanegra E.H., Nó M.L., San Juan J., (2004), *Thermodynamics of thermally induced martensitic transformations in Cu-Al-Ni shape memroy alloys*, Acta Materialia 52, p 3941-3948 USA

[4] Lojen G., Anžel I., Kneissl A., Križman A., Unterweger E., Kosec B., Bizjak M., (2005),

Microstructure of rapidly solified Cu-Al-Ni shape memory alloy ribbons, Journal of Materials Processing Technology 162-163, p 220-229 Germany

[5] Sari U., Aksoy I., (2006), *Electron microscopy study of 2H and 18R martensites in Cu-11.92 wt% Al-3.78 wt% Ni shape memory alloy*, Journal of Alloys and Compounds 417, p 138-142 Germany

[6] Chang S. H., (2011), *Influence of chemical composition on the damping characteristics of Cu-Al-Ni shape memory alloys*, Materials Chemistry and Physics 125, p 358-363 Australia

[7] Ivanić I., Gojić M, Kožuh S., (2014), *Slitine s prisjetljivosti oblika (II. dio): podjela, proizvodnja i primjena*, Kemija u industriji 63 No. 9-10, p 331-344 Croatia

[8] Sari U., Aksoy I., (2008), *Micro-structural analysis of self-accommodating martensites in Cu–11.92 wt%Al–3.78 wt%Ni shape memory alloy*, Journal of Materials Processing Technology 195, p 72-76 Germany

[9] Suresh N., Ramamurty U., (2008), *Aging response and its effect on the functioal properties of Cu-Al-Ni shape memory alloys*, Journal of Alloys and Compounds 449, p 113-118 Germany

ISSN 1847-7917

Application of aluminium foam for heat exchangers on building facades and interior ceilings

Jaroslav JERZ, František SIMANČÍK, Jozef ŠEBEK, Jaroslav KOVÁČIK and Ján ŠPANIELKA

Institute of Materials & Machine Mechanics, Slovak Academy of Sciences, Dúbravská cesta 9, 84513 Bratislava, **Slovakia**

ummsjerz@savba.sk

Keywords

aluminium foam
heat exchanger
heat storage
phase-change materials

Ključne riječi

aluminijske pjene
izmjenjivač topline
skladištenje topline
faze promjena materijali

Professional article

Abstract: The high energy efficiency of buildings can be achieved if energy needs are almost entirely covered by the supply of renewable energy sources obtained directly on the building or in its immediate vicinity. This contribution addresses on advanced solutions for reduction of thermal losses with the aim to improve the energy efficiency of future zero-energy buildings by reduction of energy consumption in such a way, that the vast majority of energy needs is covered by heat obtained from solar energy directly at the building roof and facade.

The concept presented in this contribution is based on the storage of energy obtained through the aluminum foam roof and facade cladding, which is capable to absorb the desired, or even take away the excess energy to the surroundings if necessary. The energy effectively generated by this way is by means of piping system distributed by heating liquid medium/coolant to interior ceiling heat exchangers made of aluminum foam enabling due to filling by Phase-Change Materials (PCMs) to store the energy required for heating/cooling for a period of at least several hours.

This progressive technology therefore contributes significantly to reducing of energy demand and thus the prices of future not only large buildings but also small family houses that are able to achieve the optimal thermal comfort by extremely low costs.

1. Introduction

The development of efficient materials for energy storage has become a popular research topic recently as the amount of energy gained from solar power depends significantly on day and night cycle. That's why the right choice of material for energy storage directly affects the utilization efficiency of solar energy.

The different forms of energy that can be stored include mechanical (e.g., gravitational energy storage or pumped hydropower storage, compressed air energy storage, flywheels etc.), electrical (batteries, supercapacitors, etc.) and thermal energy – heat.

The heat can be stored as a change in internal energy of a material as sensible heat, latent heat, thermo-chemical energy storage or a combination of these. In the case of sensible heat storage system, thermal energy is stored by raising the temperature of a solid or liquid. The amount of repeatedly stored and later released energy depends on the specific heat of the medium, the temperature change during the process of charging and discharging and the amount of storage medium. The water appears to be thanks to extremely high specific heat (4 190 J/(kg·K)) the best available sensible heat storage liquid, however above 100°C, oils, molten salts, etc. are used. For air heating applications rock bed type sensible heat storage solids (unconsolidated, such as sand, clay, or mud, or consolidated, such as granite, limestone, etc.), but also stones, bricks, and concrete are successfully used. The thermochemical energy storage systems rely on the energy absorbed and released by breaking and reforming molecular bonds in a completely reversible chemical reaction.

However, the research on heat storage materials nowadays focuses on PCMs enabling repeatedly utilize the latent heat of the phase-change between the solid and liquid phase. In comparison with two above mentioned thermal energy storage systems, the latent heat storage is based on the heat absorption and release when a storage material undergoes a phase-change from solid to liquid or vice versa. In addition to the change from solid to liquid, the phase transition can be also in following forms: solid-solid, solid-gas, liquid-gas, and vice versa. In solid-solid transition, heat is stored as the material is transformed from one crystalline stage to another, but these transitions generally have significantly smaller amount of latent heat than the most solid-liquid transitions.

The regular alternation of day and night cycle resulting in continuously changing amount of sunshine falling on the building roof, causes even though a small but very well usable potential.

The PCMs impregnated in ceiling heat exchangers is capable to capture a large proportion of the energy from solar radiation falling on the roofing and facade cladding in the case that interior heat exchangers are interconnected with building jacketing system

via circulating heating liquid medium. On the other hand during hot summer days is this same system of interior ceiling heat exchangers impregnated by PCMs capable to remove excess heat from interior during whole day long and during nights to dissipate the undesirable heat through preferably the north facade to surroundings of the building. Because of high thermal mass of PCMs impregnated in the ceiling heat exchangers, they are also capable to minimize the effect of large fluctuations in the ambient temperature on the inside temperature of the building. That is why this system can very effectively to shift the heating and cooling load to off-peak energy periods.

2. Latent heat storage in zero-energy buildings

Amongst all above mentioned heat storage techniques, latent heat storage is particularly attractive due to its ability to provide extremely high energy storage density and its characteristics to store heat at a constant temperature corresponding to the phase transition temperature of PCM. Moreover, solid-liquid transitions have proven to be economically the most attractive for the use of heat storage systems. PCMs, of course, themselves cannot be used as heat transfer medium. A separate heat transfer medium must be therefore employed with a heat exchanger in between to transfer energy from the source to the PCM and from PCM to the load. The heat exchanger to be used has to be designed specially, in view of the low thermal diffusivity of PCMs in general. The volume changes of PCMs on melting would also necessitate special design of voluminous containers for PCM. It should be able to absorb these volume changes and should also be compatible with the PCM used.

This implies that the development of a latent heat storage system involves an understanding of heat flows through PCMs, the material of the container walls and the heat exchanger. A wide range of technical options with regard to the development of systems for latent heat storage at low temperature is shown in **Fig. 1** [4].

The main disadvantage of light building structures, which are currently built mainly due to savings of the energy costs for the production of concrete, is their very low thermal mass. That is why they tend to have high temperature fluctuations, which result in high heating and cooling loads. Using PCMs in such buildings can smooth out the temperature variations. Ceiling heat exchangers can very effectively to shift the heating and cooling load to off-peak energy periods. However, the main obstacle is the low thermal conductivity of both the PCMs and the conventional porous building materials (e.g., gypsum wall boards, aerated concretes, etc.). The best technical solution to avoid this lack is to use the advanced heating/cooling aluminium foam ceiling panels (**Fig. 2**) able to distribute homogenously heat to/from interior via heating/cooling liquid medium. The main benefit of using these panels is that the porous structure created by thermal conductive aluminium pore walls is characterized by pores interlinked by microcracks in pore walls. These open cell structure of aluminium foam with extremely low permeability allows to impregnate porous structure by PCMs and thus to achieve significantly improved thermal conductivity of resulting composite material. As can be seen from **Fig. 3**, filling 80% of free volume with PCM can significantly reduce the temperature fluctuations during cooling and heating by these panels, which results in considerable energy savings necessary for compliance with optimal thermal comfort in the rooms.

3. Solar heating system with latent heat storage materials

Integrating solar energy collection system into the building shell and mechanical systems providing pumping of the heat transfer fluid from the surface of building roof and facade to the indoor heat exchangers may significantly reduce the cost of the solar energy systems as well as improve the efficiency of the thermal energy collection and storage. The PCMs used in the design of any heat storage systems should have high latent heat of fusion, high heat conductivity (at least more than 0.5 W/(m·K)), phase transition temperature should be in the functional interval if it stores solar energy, congruent melting, minimal sub-cooling, chemical stability, economic efficiency and aspects of environmental protection [13].

PCMs can be broadly classified into two types: organic PCMs, e.g. paraffin wax and inorganic PCMs, e.g. salt hydrates. Early efforts in the development of materials for latent heat storage used inorganic PCMs like salt hydrates, including Glauber's salt (sodium sulphate decahydrate).

However, their unsuitable characteristics, e.g. corrosiveness, instability, improper re-solidification, suffer from decomposition and sub-cooling, etc. have led to the investigation of organic PCMs for heat storage [13]. Various nucleating and thickening agents can be easily added to inorganic PCMs to minimize sub-cooling and decomposition. That is why they can currently provide not only much higher energy storage densities but the heat can be stored and released at an almost constant temperature. Organic PCMs (**Table 1**) have a number of characteristics which render them useful for latent heat storage in building elements.

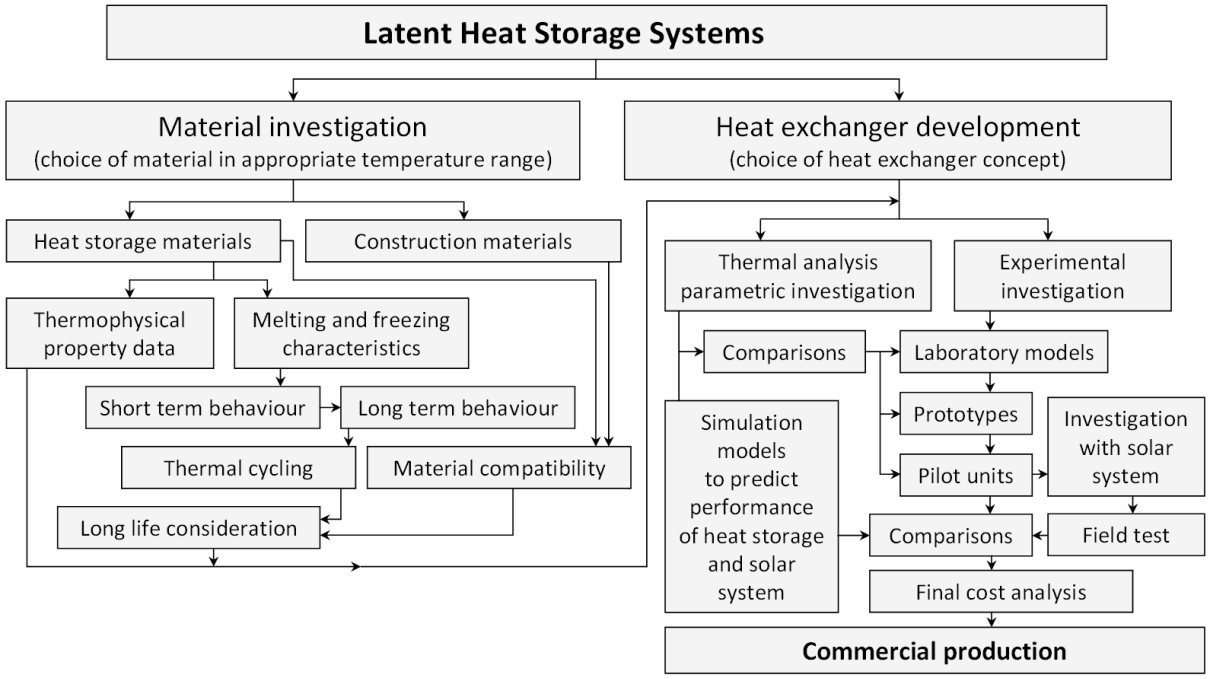

Figure 1. Flow chart showing different stages involved in the development of a latent heat storage system

Figure 2. Aluminium foam ceiling panels for heating/cooling of building interiors installed in the open space office area 260 m^2 of company Sapa Profily a.s. in Ziar nad Hronom, Slovakia

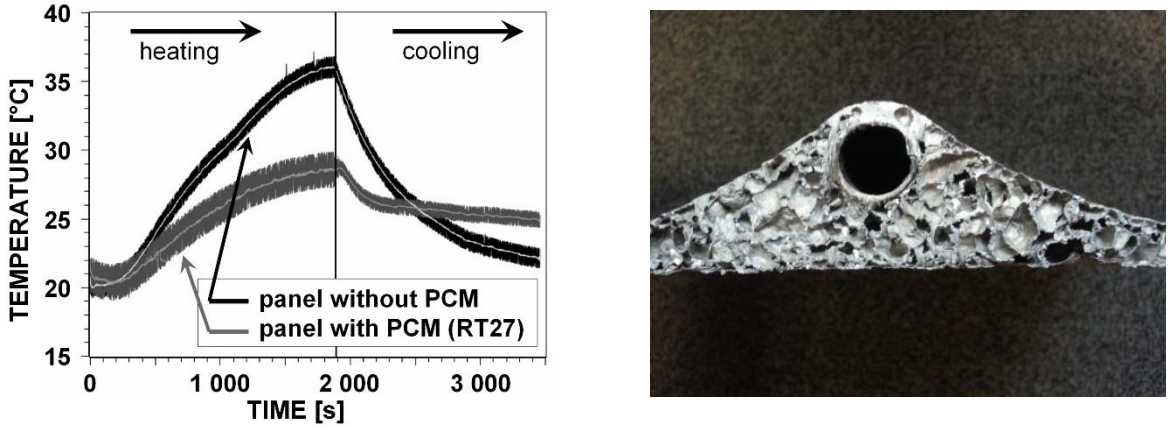

Figure 3. Comparison of thermal behaviour during heating and cooling of empty aluminium foam ceiling panel and a panel filled with PCM RUBITHERM® RT27 having a phase transition temperature of 27°C

Table 1. Organic PCMs (thermal properties) [13]

PCM Name		Melting Temperature [°C]	Heat of Fusion [kJ/kg]
$CH_3(CH_2)_{16}COO(CH_2)_3CH_3$	Butyl stearate	19	140
$CH_3(CH_2)_{11}OH$	1-dodecanol	26	200
$CH_3(CH_2)_{12}OH$	1-tetradecanol	38	205
$CH_3(CH_2)_nCH_3$…	Paraffin	20 - 60	200
45% $CH_3(CH_2)_8COOH$ 55% $CH_3(CH_2)_{10}COOH$	45/55 capric-lauric acid	21	143
$CH_3(CH_2)_{12}COOC_3H_7$	Propyl palminate	19	186

Table 2. Advantages and disadvantages of PCMs [12, 13]

	Organic PCMs (Paraffins)	Inorganic PCMs (Salt Hydrates)
Advantages	✓ non-corrosive, non-toxic ✓ chemical and thermal stability ✓ no or little sub-cooling ✓ high heat of fusion ✓ low vapor pressure	✓ high phase-change enthalphy ✓ high heat of fusion ✓ high thermal conductivity ✓ high density ✓ non-flammability ✓ low price
Disadvantages	✓ low phase-change enthalphy ✓ low thermal conductivity ✓ low density ✓ high volume changes on phase-change ✓ inflammability	✓ sub-cooling ✓ high corrosivity ✓ phase decomposition, ✓ lack of thermal stability

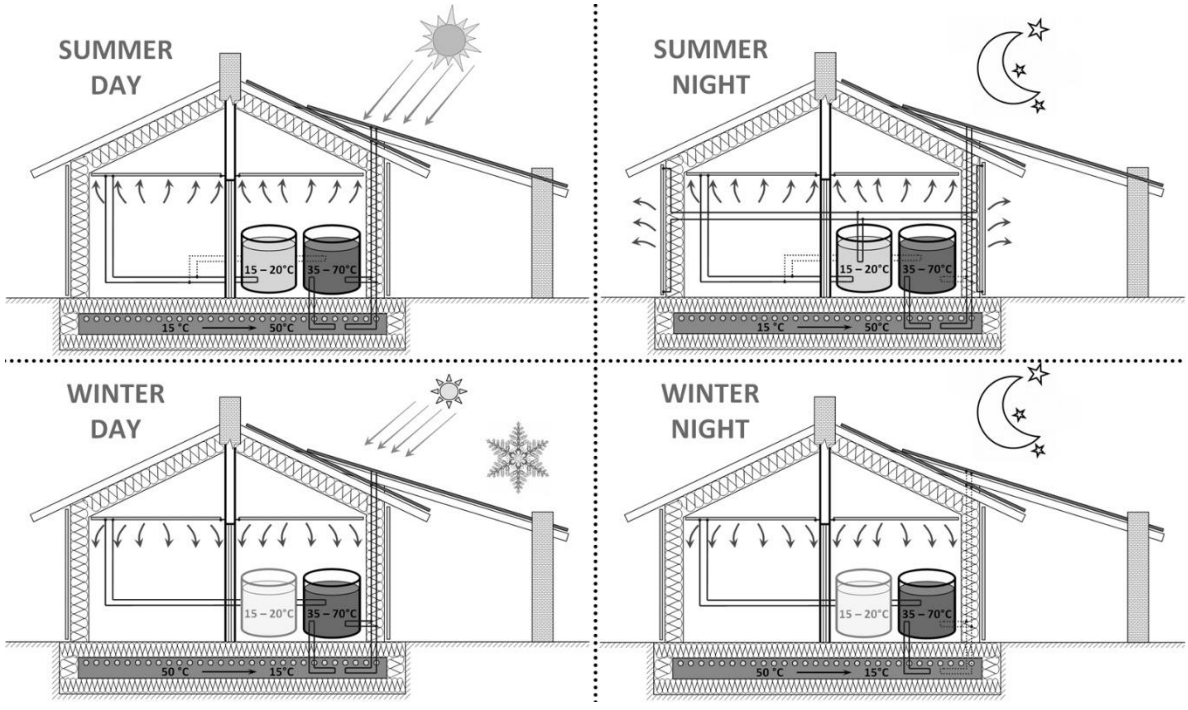

Figure 4. Schematic illustration of zero-energy house with interior ceiling panels impregnated with PCM, exterior aluminium foam cladding for removing of excess heat during the cold summer nights and system of seasonal heat storage into the base plate.

They are more chemically stable than inorganic substances, they are non-corrosive, they have a high latent heat per unit weight, they are recyclable, they melt congruently and they exhibit little or no sub-cooling, i.e. they do not need to be cooled below their transition temperature to initiate solidification.

PCMs have not always re-solidified properly, because some PCMs get separated and stratify in the liquid state. They did not completely solidify when temperature is dropped and their capacity to store latent heat is in this case reduced. These problems are overcome by packaging PCM in containers and by adding thickening agents. To solve some of the problems inherent in organic PCMs, an interest has turned towards a new class of materials: low volatility, anhydrous organic substances such as paraffins, fatty acids and polyethylene glycol. Those materials are more expensive than common salt hydrates and they have slightly lower heat storage capacity per unit volume. It has now been realized that some of these materials have good physical and chemical stability, good thermal behaviour and adjustable transition temperature [13].

The main advantages and disadvantages of organic and inorganic PCMs are described in **Table 2**.

In general it can be summarized that PCM is suitable for the purpose of heat storage in the case that it is characterized by desirable thermo-physical, kinetic, chemical and economic features described in **Table 3**.

4. Efficient utilization of solar gains

The direct solar gain hitting the surface of building roof and facade cladding is the heat retained by the thermal mass of building construction. It can be, as contemporary builders nowadays often do, also avoided with reflective materials. However, the direct solar gain is important for any site that needs heating, because it is the simplest and least costly way of passively heating a building with solar heat gain. Avoiding direct solar gain is also important in hot sunny climates.

In many climates, much more heat gain is desired in the winter, when the sun is low, while less or none is desired in the summer. Likewise, it is usually desired more in the morning, but less or none in the late afternoon. Sunlight can heat a space through the solid walls or roofs of the envelope. Sunlight also enters the space through windows and heats interior surfaces. Part of solar energy is long-wavelength radiation, which is called the heat. Moreover, the light of any wavelength absorbed by surfaces turns into heat in those materials. These materials then warm interiors by conducting heat to them directly, by warming air, or more effectively warming water, which carries heat by convection as well as by radiating of accumulated heat.

In this regard, the use of the active surface heat exchangers made from aluminium foam forming the inclined roofs and vertical facades seems to be highly beneficial. The significant cost savings for optimal maintenance of thermal comfort inside buildings during winter as well as summer operation can be achieved primarily if the facade system is interlinked with interior panels by an appropriate heating/cooling liquid medium and if the heat can be stored also in the form of latent heat of phase transition of PCMs impregnated in the aluminium foam structure of interior panels. The seasonal storage of excess heat from the periods of hot summer days can be ensured by its accumulation to thermally active isolated base plate of the building or by its dissipating during night hours by active innovative facade system made of aluminium foam panels as shown in **Fig. 4**. It is important to manage this system properly by an intelligent control software during winter as well as summer operation mode. The advanced control system ensures that the heat accumulated during summer will be efficiently utilized primarily to cover large energy needs for heating and generating of hot domestic water especially during the cold winter season.

5. Conclusions

The aluminium foam panels provide an excellent alternative for large built-in ceiling radiators for efficient winter heating and summer cooling of building interiors using low potential energy sources. The porous structure of aluminium foam allows to absorb or dissipate latent heat very homogeneously at almost constant temperature if PCMs with phase transition temperature in the range between 23°C and 28°C are used for storage of the heat obtained from renewable energy sources. These features of aluminium foam panels in combination with smart temperature control systems allow reducing significantly the energy consumption of heating/air conditioning systems of future zero-energy buildings characterized by very low investment as well as operating costs. The heat storage systems based on PCMs with enhanced thermal conductivity seem to be unavoidable in order to have return-on-investment period below ten years especially in the case of energy efficient small family houses.

Table 3. Main desirable properties of PCMs [12, 13]

Thermal
✓ suitable phase-change temperature,
✓ high latent heat of phase-change,
✓ high thermal conductivity (in both liquid and solid),
✓ high heat transfer coefficient (measured in W/(m^2·K), i.e., the amount of heat transferred per unit area divided by temperature difference between the solid surface and surrounding fluid area), etc.
Physical
✓ favourable phase equilibrium (occurs when the transfer of heat from one phase to another is equal to the rate of transfer of heat in the reverse direction),
✓ high density,
✓ small volume change during phase-change,
✓ low vapour pressure, etc.
Kinetic
✓ no sub-cooling (i.e., solidification without cooling to a temperature below that at which phase-change should occur),
✓ sufficient solidification rate (the velocity at which solidification occurs), etc.
Chemical
✓ long-term chemical stability,
✓ chemical compatibility with materials of the heat exchanger as well as container walls (optionally),
✓ non-toxic, non-poisonous, non-flammability, etc.
Economic
✓ abundant, available, simply producible, cost effective (in order to make the system economically feasible)

Acknowledgements

The financial support from the Slovak R&D Agency (project: Heating/cooling panel based on aluminum foam filled by PCM, APVV-0692-12) is gratefully acknowledged.

REFERENCES

[1] Jerz, J. – Simančík, F. and Orovčík, Ľ. Advanced solution for energy storage in net zero-energy buildings. In: *Mechanical Technologies and Structural Materials 2014*. – Split: Croatian Society for Mechanical Technologies, 2014, pp. 47-54. ISSN 1847-7917.

[2] Jerz, J. – Tobolka, P. – Michenka, V. and Dvorák, T. Heat storage in future zero-energy buildings. In: *International Journal of Innovative Research in Science, Engineering and Technology, 2015*, vol. 4, iss. 8, pp. 6722-6728. ISSN 2319-8753 (http://www.ijirset.com/upload/2015/august/3_Heat.pdf)

[3] Teng, T. P. and Yu, C. C. Characteristics of phase-change materials containing oxide nano-additives for thermal storage, In: *Nanoscale Research Letters 2012*, 7:611. (http://wwwnanoscalereslett.com/content/7/1/611)

[4] Sharma, A. – Tyagi, V. V. – Chen, C. R. and Buddhi, D. Review on thermal energy storage with phase change materials and applications. In: *Renewable and Sustainable Energy Reviews 13 (2009)*, pp. 318-345 (doi: 10.1016/j.rser.2007.10.005)

[5] Bruno, F. Using phase change materials (PCMs) for space heating and cooling in buildings, In: *Proceedings of AIRAH 2004 – Conference of enhanced buildings environmentally sustainable design*, pp. 26-31 (http://citeseerx.ist.psu.edu/viewdoc/download?doi=10.1.1.466.6725&rep=rep1&type=pdf)

[6] Kenisarin, M. and Mahkamov, K. Solar energy storage using phase change materials. In: *Renewable and Sustainable Energy Reviews 11 (2007)*, pp. 1913-1965 (doi: 10.1016/j.rser.2006.05.005)

[7] Himran, S. – Suwono, A. and Ali Mansoori, G. Characterization of alkanes and paraffin waxes for application phase change energy storage medium. In: *Energy Sources*, vol. 16, no. 1, pp. 117-128, 1994 (doi: 10.1080/00908319408909065)

[8] Inaba, H and Tu, P. Evaluation of thermophysical characteristics on shape-stabilized paraffin as a solid-liquid phase change material. In: *Heat and Mass Transfer 32 (1997)*, pp. 307-312 (http://link.springer.com/article/10.1007%2Fs002310050126)

[9] Dotsenko, S. P. – Martsinkovskii A. B. and Danilin V. N. Thermal storage properties of n-paraffins, fatty acids and multicomponent systems on their basis. In: *e-Journal: Fiziko-khimicheskii analiz svoistv mnogokomponentnykh system, 2004*, vol. 1 (in Russian)

[10] Velraj, R. – Seeniraj, R. V. – Hafner, B. – Faber, C. and Schwarzer, K. Experimental analysis and numerical modeling of inward solidification on a finned vertical tube a latent heat storage unit. In: *Solar Energy 60 (5), 1997*, pp. 281-290 (doi: 10.1016/S0038-092X(96)00167-3)

[11] RUBITHERM® RT28HC Data sheet, Rubitherm Technologies GmbH, Berlin, 2013

[12] Sharma, A. and Chen, C. R. Solar water heating system with phase change materials. In: *International review of chemical engineering*, Vol. 1, N. 4, 2009, pp. 297-307

[13] L. G. Socaciu Thermal Energy Storage with Phase Change Material. In: *Leonardo Electronic Journal of Practices and Technologies*, Issue 20, January-June 2012, pp. 75-98, ISSN 1583-1078 (http://lejpt.academicdirect.org/A20/075_098.

ISSN 1847-7917

Induction melting and centrifugal casting of intermetallic TiAl alloy

***Kateryna KAMYSHNYKOVA*[1,2], *Juraj LAPIN*[1)]**

1) Institute of Materials and Machine Mechanics, Slovak Academy of Sciences, Dúbravská cesta 9, 845 13 Bratislava, **Slovak Republic**

2) Faculty of Materials Science and Technology Slovak university of technology in Bratislava, Paulinska 16, 917 24 Trnava, **Slovak Republic**

kateryna.kamyshnykova@savba.sk

Keywords

Titanium aluminides, based on TiAl
Melting
Casting
Microstructure

Original scientific article

Abstract: Induction melting of intermetallic alloy with nominal composition Ti-47Al-5Nb-0.2B-0.2C (at.%) was studied in graphite crucibles. The melted alloy was solidified either directly in the graphite crucibles or centrifugally cast into graphite mould. Chemical composition of the castings was measured by energy dispersive spectroscopy (EDS), carbon content was determined by combustion infrared detection technique and nitrogen, oxygen and hydrogen contents were measured by infrared and thermal conductivity detection technique. The microstructure analysis show that the samples solidified directly in the graphite crucibles contain columar grains composed of γ(TiAl) and α_2(Ti_3Al) lamellae. The columnar grain size and interlamellar α_2-α_2 spacing depend on cooling conditions. Centrifugally cast samples contain equiaxed lamellar grains and numerous homogenously distributed Ti_2AlC particles formed as the primary solidification phase. In addition, TiB and TiB_2 particles and β phase were identified by EDS and X-ray diffraction analysis (XRD). The induction melting in graphite crucible and centrifugal casting into graphite mould increase carbon content and affect the solidification path of the studied alloy.

1. Introduction

The development of aircraft engines with improved energy efficiency is connected with reducing the weight of components using advanced new materials. TiAl alloys are the most promising candidates to replace Ni-based superalloys in low pressure stage of aircraft engines due to their low density, high melting temperature, good elevated-temperature strength and modulus retention, low diffusion coefficient, good structural stability, high resistance to oxidation and excellent creep properties [1-3]. The main factors limiting mass application of TiAl components are their intrinsic characteristics such as microstructure, chemical heterogeneity, brittleness, low room temperature ductility, poor hot workability and the high production costs [4]. Nowadays, the most useful routes for production of TiAl components are forging, powder metallurgy and casting. Forging can be limited by chemical and microstructure heterogeneity and powder metallurgy is highly expensive [5]. On the other hand, casting processes allow mass production of TiAl components at a cost-effective way.

Different melting methods have been applied for TiAl alloys such as vacuum arc melting, plasma arc melting, induction skull melting and electron beam melting. Investment casting, centrifugal casting, metal mould casting and countergravity low-pressure casting have been used for processing of TiAl components [6].

Various ceramic materials have been evaluated for processing crucibles and moulds for TiAl alloys. Until now no refractory material has been found to be absolutely inert against the TiAl melts and some interactions between the melt and the crucible material leading to metal contamination always occur [7-9]. Among various refractory materials, only several can be successfully used for melting and casting of TiAl alloys, such as Y_2O_3, ZrO_2, CaO and graphite [10]. The use of Y_2O_3 and ZrO_2 has been limited by their high cost, and CaO is unstable because absorbs moisture. The graphite is relatively cheap to reduce production costs and has a good formability. It can be used for processing melting crucibles and casting moulds for some TiAl alloys in which an increase of carbon content can be beneficial to improve their properties [11]. The additions of C can improve strength and creep resistance of TiAl alloys through solid-solution strengthening and/or precipitation hardening. From the point of view of microstructure formation during solidification and solid state transformations, carbon changes primary solidification phase from β (Ti-based solid solution with cubic crystal structure) to α (Ti-based solid solution with hexagonal crystal structure) phase, stabilizes the α_2(Ti_3Al) phase and has only little influence on solid phase transformation of the type γ(TiAl)→α [12-14].

The aim of this work is to study the effect of induction melting in graphite crucibles followed either solidification directly in the graphite crucibles or by centrifugal casting into graphite mould on chemical composition and microstructure of intermetallic TiAl alloy. In addition, the increase of carbon content on phase composition and solidification behaviour of the studied alloy is discussed.

Symbols

α_2	- Ti_3Al intermetallic phase	*P*	- Porosity
γ	- TiAl intermetallic phase	*SEM*	- Scanning electron microscopy
α *or* β	- Ti-based solid solution with hexagonal or cubic crystal structure, respectively	*BSEM*	- Backscattered electron microscopy
λ	- interlamellar α_2-α_2 spacing	*XRD*	- X-ray diffraction
C	- Columnar grains	*OM*	- Optical microscopy
E	- Equiaxed grains	*EDS*	- Energy-dispersive spectroscopy

2 Experimental procedure

2.1 Melting and casting

The studied alloy with nominal composition of Ti-47Al-5Nb-0.2B-0.2C (at.%) was provided in the form of cylindrical ingot with a diameter of 200 mm. The ingot was cut by spark machining to smaller samples for induction melting and casting with a diameter of 38 mm and length of 26 mm. Each sample was put into a graphite crucible with a diameter of 45/49 mm (inside/outside diameter) and length of 75 mm. The graphite crucible was placed into protective Al_2O_3 based crucible equipped with a sprue allowing pouring the melt during centrifugal casting, as seen in Figure 1. The ceramic crucible was connected to the graphite mould through pouring cup and sprue allowing filling mould cavity with a diameter of 15 mm and length of 120 mm. Before melting and casting, the vacuum chamber of the induction melting furnace of Titancast 700 apparatus was evacuated to a pressure of 5.9 Pa and flushed with argon (purity 99.9995%) three times, as seen in Figure 2. The melting process was carry out under the both protective argon atmosphere and vacuum. The alloy was induction heated to a melt pouring temperature of 1640°C and held constant at this temperature for 60 s before casting.

The solidification of the alloy was carried out directly inside the melting crucible under the vacuum or protective argon atmosphere by switching off the induction heating. The centrifugal casting was performed under vacuum by pouring the melt into the cold cylindrical graphite mould at a rotation speed of 250 rpm, which was achieved within 2 s.

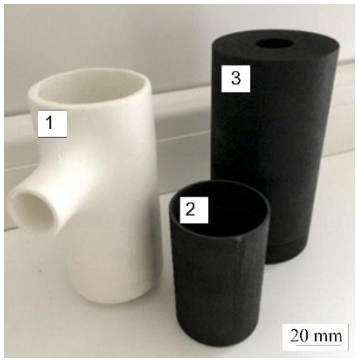

Figure 1. 1 - Al_2O_3 based ceramic crucible, 2 - graphite insert crucible and 3 - graphite mould for centrifugal casting.

2.2 Characterization of microstructure and chemical composition

The cast samples were cut to smaller pieces using wire spark cutting and diamond saw machines. Standard metallographic techniques such as grinding on SiC papers with grain sizes ranging from 80 to 2000 μm, polishing on diamond pastes with various grain sizes ranging from 10 to 0.25 μm and etching in a solution of 100 ml H_2O, 6 ml HNO_3 and 3 ml HF were applied. Macrostructure characterization was carried out by optical microscopy (OM), scanning electron microscopy (SEM) and backscattered electron microscopy (BSEM). Chemical composition of coexisting phases was measured by energy dispersive spectroscopy (EDS). Content of gases (N, O, H) and carbon content were measured with LECO ONH836 and LECO CS844 elemental analysers, respectively. X-ray diffraction analysis (XRD) was performed by diffractometer Bruker D8 using the database PDF-2 2004. Grain size and interlamellar spacing were measured by computerized image analysis and the achieved experimental data were treated statistically.

Figure 2. Titancast 700 apparatus for induction melting and centrifugal casting.

3. Results

3.1 Melting and solidification in graphite crucibles

Figure 3 shows the typical macrostructure of the samples solidified directly in the graphite crucibles under protective argon atmosphere or vacuum. The macrostructure of the samples consists of surface layer composed of fine grains nucleated at the mould walls, which is followed by columnar grains (C) growing to the central part of the samples and few equiaxed grains (E) formed in the central part. Large shrinkage porosity (P) is formed in the central region of the samples. While the grain structure of the sample solidified under argon can be characterised by an average diameter of columnar grains of (616 ± 14) μm and length of (2957 ± 118) μm (Figure 3a), the sample solidified under vacuum shows two types of the columnar grains (Figure 3b). The large columnar grains in the upper part of the sample have an average diameter of (2600 ± 460) μm and length of (6644 ± 920) μm and the bottom part contains columnar grains with an average diameter of (560 ± 20) μm and length of (5133 ± 703) μm. Figures 4a and 4b show the typical dendritic structure of the samples solidified under argon atmosphere and vacuum, respectively. The cubic symmetry of the dendrites representing by the typical Maltese cross indicates that the β is the primary solidification phase. The microstructure within the columnar dendritic grains is lamellar, as shown in Figures 4d and 4e. Some ribbon and needle like particles are observed within the lamellar and interdendritic regions of the samples. Table 1 summarizes the chemical composition of different regions of the samples indicated by the positions 1 to 5 in Figures 4a, 4b, 4d and 4e. Chemically, 5 different regions can be identified in the as-solidified microstructures. Figure 5 shows XRD patterns for the samples solidified in the crucibles under argon and vacuum. Based on the chemical composition (Table 1) and XRD analysis, the microstructure of these samples contains lamellar regions composed of γ(TiAl) and $\alpha_2(Ti_3Al)$ lamellae (position 1), γ phase solidified in the interdendritic region (position 2), TiB and TiB_2 particles formed within the dendrites and interdendendritic region (position 3), β phase (position 4) and Ti_2AlC particles (position 5). Table 2 summarizes the results of the measurements of N, O, H and C in the samples.

While the amount of N, O and H increases only slightly when compared to the initial composition of the alloy, the carbon content increases significantly. The sample prepared under protective argon atmosphere has lower content of carbon by about 0.06 wt.% than the sample solidified under vacuum. This difference can be related mainly to different heat transfer conditions from the melt into the protective ceramic crucible connected with a water cooled part of the furnace and surrounding atmosphere in the vacuum chamber of the furnace when argon atmosphere or vacuum are applied. The pressurized argon atmosphere leads to higher cooling rates during solidification and shorter interaction time between the melt and crucible.

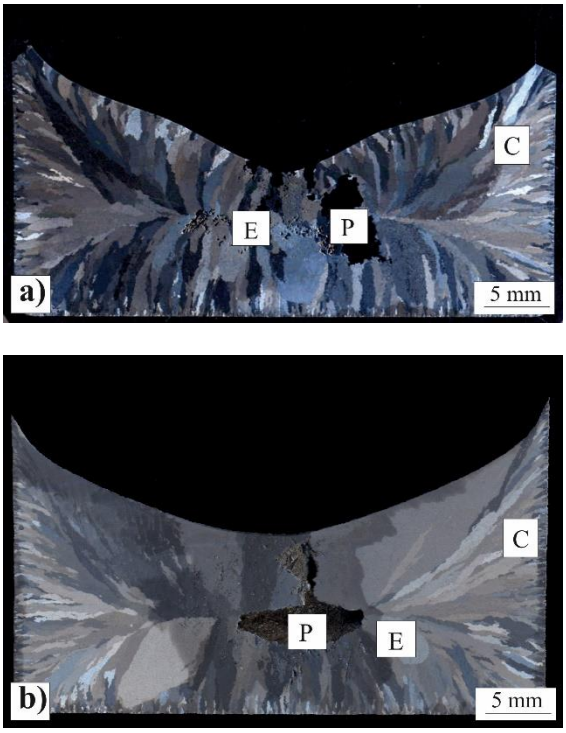

Figure 3. Macrostructure of samples solidified directly in graphite crucibles under: (a) argon protective atmosphere and (b) vacuum.

3.2 Melting in graphite crucible and centrifugal casting into graphite mould

Figure 6 shows the typical example of the centrifugally cast samples. The centrifugal casting into the cold graphite mould leads to formation of closed cast porosity in the central region of the samples, which is connected with a premature closure of the sprue by the solidified melt. The microstructure of the sample consists of equiaxed lamellar grains, as shown in Figure 4c. Statistical data of the measured grain size (minimum 2000 measurements) can be very well fitted log-normal distribution function with a mean grain size of (53.2 ± 1.2) μm. As shown in Figure 4e and indicated by the XRD pattern in Figure 5, the microstructure of the centrifugally cast sample consists of lamellar grains composed of the γ and α_2 phases. While TiB and TiB_2 particles are formed preferentially in the interdendritic region, the Ti_2AlC particles are relatively homogenously distributed within the whole volume of the sample.

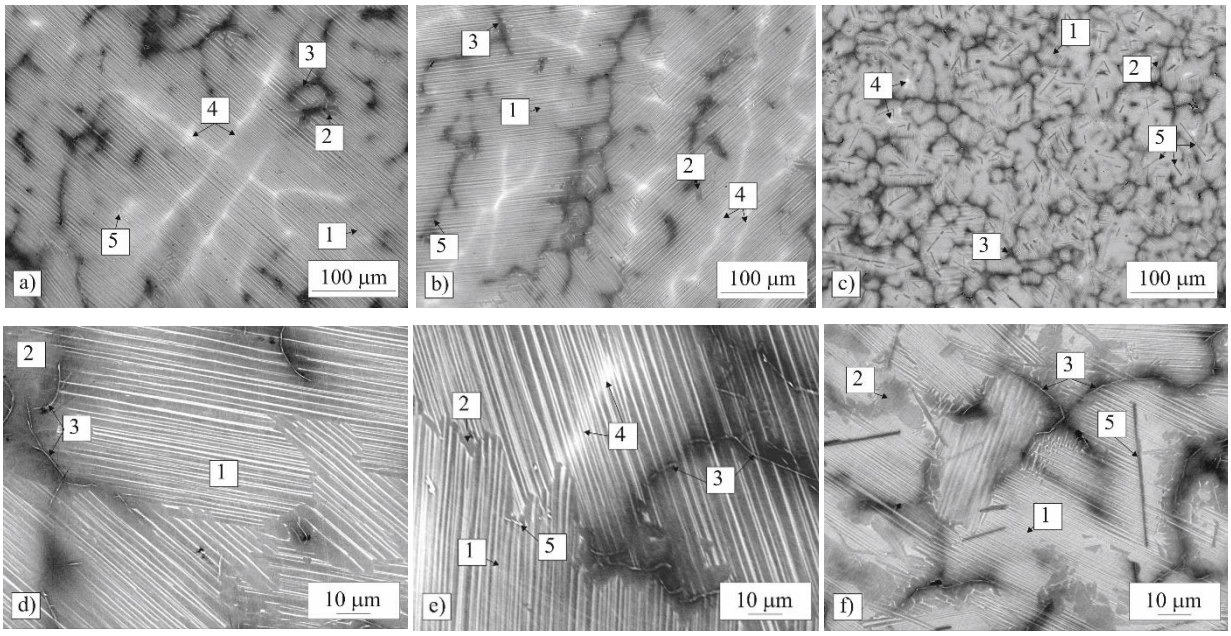

Figure 4. BSEM micrographs showing the typical microstructure of samples: (a) and (d) solidified under protective argon atmosphere; (b) and (e) solidified under vacuum; (c) and (f) centrifugally cast.

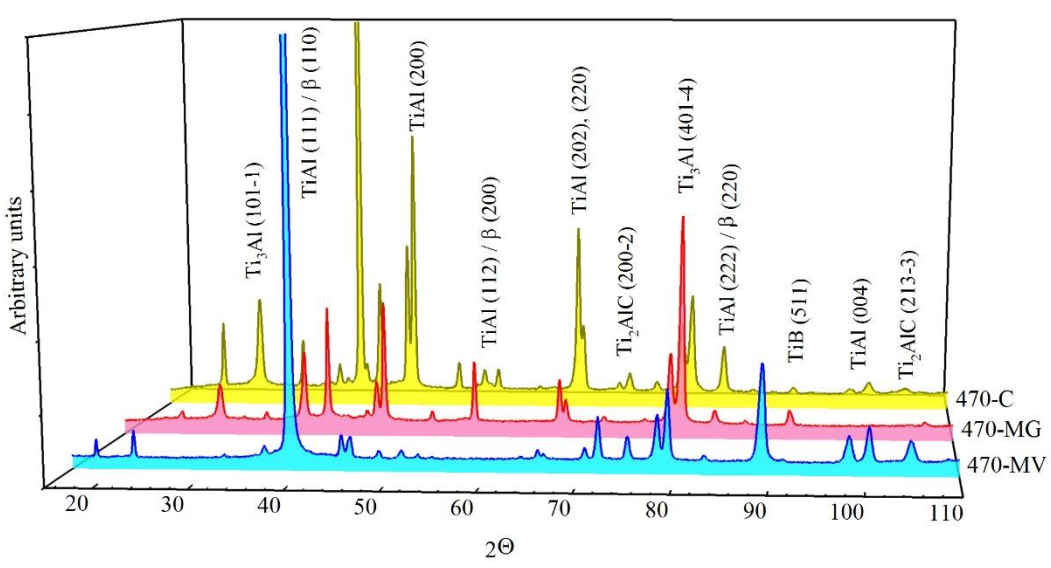

Figure 5. XRD patterns for the samples: 470-MV - solidified under vacuum; 470-MG - solidified under protective argon atmosphere; 470-C - centrifugally cast.

Table 1. Chemical composition of coexisting phases (at.%)

Position	Ti	Al	Nb	C	B
1	47.65±0.18	46.93±0.25	5.01±0.07	0.28±0.01	0.13±0.05
2	46.62±0.28	48.83±0.42	4.17±0.24	0.29±0.03	0.09±0.05
3	49.29±1.27	39.08±1.88	4.60±0.23	0.41±0.03	6.64±0.84
4	54.78±0.83	38.30±1.17	6.92±0.47	-	-
5	41.95±0.95	16.56±0.73	2.61±0.06	38.78±0.89	0.27±0.17

The amount of the Ti_2AlC particles in the centrifugally cast samples are significantly higher than that observed in the samples solidified under argon or vacuum. The mean length of these particles is measured to be (8.73 ± 0.12) μm. Table 2 shows that the carbon content increases nearly four times in the centrifugally cast samples when compared to that of the initial alloy and is higher than those measured in the samples solidified under argon or vacuum. Figure 4f shows details of the dendrites, interdendritic region and grain boundaries. The gray colour layer separating lamellar microstructure of the dendrites from the interdendritic γ phase (black colour phase) indicates that the studied alloy solidifies through a peritectic reaction/transformation as follows: liquid → β + liquid → $\alpha_{peritectic}$, which is similar to solidification of Ti-44Al-5Nb-0.2B-0.2C (at.%) alloy reported by Klimová et al. [15].

Table 2. Measurements of N, O, H and C (wt.%)

Sample	O	N	H	C
Initial ingot	0.0539	0.0055	0.0036	0.0542
Sample melted under argon	0.0859	0.0063	0.0010	0.1420
Sample melted under vacuum	0.0404	0.0054	0.0001	0.2040
Centrifugally cast sample	0.0592	0.0369	0.0014	0.2840

Figure 6. Centrifugally cast sample.

4. Discussion

4.1. Interactions between the melt and graphite during melting and casting

During the melting the TiAl alloy reacts with the surface of the graphite crucible. Since the wettability between molten aluminium and graphite is bad at the melting temperature of the TiAl alloy, the carburization process of the melt is mainly caused by the reaction of high-active titanium and carbon. The reaction between titanium and graphite is represented by an equation

$$Ti_{(l)} + C_{(s)} \rightarrow TiC_{(s)} \quad (1)$$

The induction stirring of the melt can significantly affect the stability of the TiC interface reaction layer and following reaction might also occur

$$TiAl_{(l)} + TiC_{(s)} \rightarrow Ti_2AlC \quad (2)$$

Depending on the melt temperature and stirring intensity, TiC and Ti_2AlC particles or even some graphite grains released from the mould by melt erosion can be well redistributed from the melt/crucible interface into the whole volume of the melt, where they are dissolved and enrich the melt by carbon. These process of carbon increase in the alloy is controlled by the melt temperature, interaction time between the melt and graphite crucible and intensity of stirring.

Centrifugal casting is associated with turbulent mould filling which causes that the interface TiC layer formed by the reaction between the melt and the cold graphite crucible reacts with the melt and transforms to Ti_2AlC phase, as shown in Figure 7. Table 2 clearly indicates that the induction melting in graphite crucibles followed by centrifugal casting into graphite moulds significantly increase carbon content of the studied alloy. In the present study, carbon content is increased by 0.08 wt.% in centrifugally cast samples when compared to that of the sample solidified directly in the graphite crucible under vacuum, which can be fully related to the melt/graphite mould interactions during the casting.

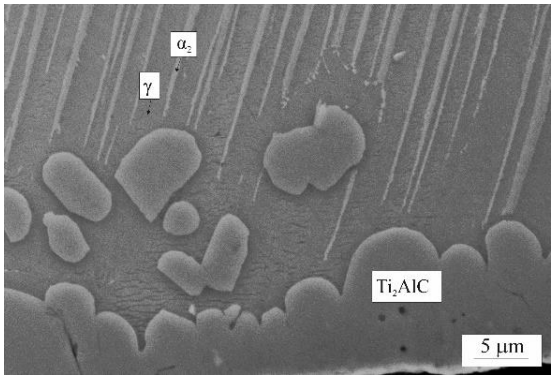

Figure 7. Ti_2AlC layer formed on the surface of the centrifugally cast samples.

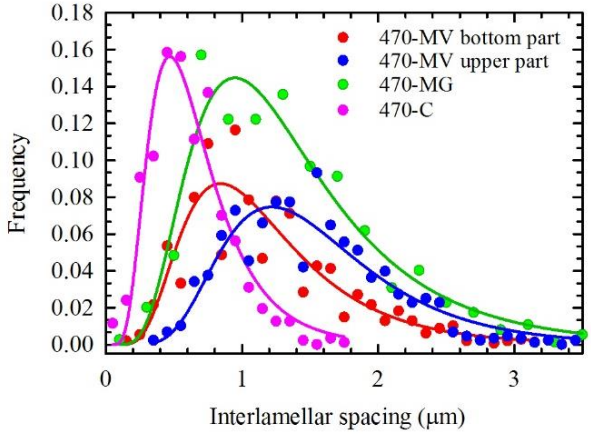

Figure 8. Log-normal distribution function of interlamellar spacing.

4.2 Effect of carbon content on solidification behaviour

The content of carbon affects significantly solidification behaviour of the studied alloy. The sample solidified under argon atmosphere shows the lowest content of carbon of 0.142 wt.%. Such amount of carbon is still soluble in the solid solution and practically no primary carbide particles have been identified in the microstructure. The Ti_2AlC particles were only identified within the surface layer which was in contact with the graphite crucible during solidification. Increase of the carbon content to 0.204 wt.% in the sample solidified under vacuum resulted in formation of small amount of Ti_2AlC particles which solidified as primary phase directly from the melt. Increase of the carbon content to 0.284 wt.% in the centrifugally cast samples affects significantly the solidification path, leads to the change of the β primary solidification phase to Ti_2AlC phase and formation of numerous Ti_2AlC particles.

4.3 Effect of solidification conditions on microstructure

The solidification conditions, namely cooling rate significantly affect the final microstructure of TiAl alloys. The local temperature gradients in liquid are sufficiently high and solidification rates are sufficiently low to promote the growth of columnar grains in the samples solidified under argon or vacuum. As shown by Lapin [16], the local cooling rates in solid state can be well related to interlamellar α_2-α_2 spacing λ. Figure 8 shows statistical distribution of measured interlamellar spacing (minimum 1000 measurements) in the form of probability plot. The measured data can be well fitted by log-normal distribution function and characterised by mean interlamellar α_2-α_2 spacing values. It is clear, that the cooling rates were the slowest ones in the sample solidified under vacuum (470-MV), which resulted in $\lambda = (1218 \pm 35)$ μm in the upper part of the sample. The transformation of the α phase to lamellar $\alpha_2 + \gamma$ microstructure occurs at higher cooling rate in the sample solidified under argon (470-MG), which results in $\lambda = (947 \pm 32)$ μm. The highest cooling rates are achieved in centrifugally cast samples (470-C) casting, which leads to $\lambda = (598 \pm 23)$ μm.

From the point of view of the effect of carbon on mechanical properties, it should be noted that carbon contributes to solid solution strengthening of the both α_2 and γ phases and formation of carbide particles can contribute to precipitation strengthening of the lamellar $\alpha_2 + \gamma$ matrix. The Ti_2AlC particles are considered to improve high temperature strength and creep properties of TiAl alloys. Further study will be carried out to evaluated the effect of such carbon increase on mechanical properties of the studied alloy.

5. Conclusions

Induction melting of intermetallic alloy with nominal composition Ti-47Al-5Nb-0.2B-0.2C (at.%) was carried out in the graphite crucibles under vacuum or argon. The samples solidified directly in the graphite crucibles contain columnar grains composed of γ and α_2 lamellae. The diameter of columnar grains and interlamellar α_2-α_2 spacing depend on cooling conditions which are significantly affected by the applied vacuum or argon atmosphere. The centrifugally cast samples contain equiaxed lamellar grains and numerous homogenously distributed Ti_2AlC particles formed as the primary solidification phase. In addition, the boride particles and β phase are identified by EDS and XRD analysis. The induction melting in the graphite crucibles and centrifugal casting into cold graphite mould increase carbon content of the alloy and affect the solidification path by changing the β primary solidification phase to the Ti_2AlC phase.

Acknowledgment

This work was financially supported by the Slovak Research and Development Agency under the contract APVV-15-0660, the Slovak Grant Agency for Science under the contract VEGA 2/0125/16 and the Slovak Academy of Sciences under the contract of MVTS funding of the project GRADECET.

REFERENCES

[1] Zollinger, J., Lapin, J., Daloz, D., Combeau, H., (2007), *Influence of oxygen on solidification behaviour of cast TiAl-based alloys*, Intermetallics 15, p 1343–1350.

[2] Qu, H.P., Wang, H.M., (2007), *Microstructure and mechanical properties of laser melting deposited - TiAl intermetallic alloys*, Mater. Sci. Eng. A 466, p 187–194.

[3] Cao, R., Lei, M.X., Chen, J.H., Zhang, J., (2007), *Effects of loading rate on damage and fracture behavior of TiAl alloys*, Mater. Sci. Eng. A465, p 183–193.

[4] Imayev RM, Imayev VM, Oehring M, Appel F. (2007), *Alloy design concepts for refined gamma titanium aluminide based alloys*, Intermetallics 15, p 451–460.

[5] Gomes, F., Barbosa, J., Ribeiro, C.S., (2008), *Induction melting of γ-TiAl in CaO crucibles*, Intermetallics 16, p 1292-1297.

[6] Shouren, W., Peiquan, G., Liying, Y., (2008), *Centrifugal precision cast TiAl turbocharger wheel using ceramic mold*, J. Mater. Process. Technol. 204, p 492-497.

[7] Sung S.Y., Kim Y.J. (2006), *Economic net-shape forming of TiAl alloys for automotive parts*, Intermetallics 14, p 1163–1167.
[8] Barbosa J., Ribeiro C.S., Monteiro C., (2007), *Influence of superheating on casting of γ-TiAl*, Intermetallics 15, p 945–955.
[9] Barbosa J, Silva Ribeiro C, Monteiro C., (2005), *Process for obtaining γ-TiAl pieces by casting*, Patent Pending WO2005/025778 A1.
[10] Liu, X., Liu, F., Du, H., Zhang, Z., Cai, Q., Fan, Z., (2014), *Effect of hydrogen on interfacial reaction between TiAl alloy melt and graphite mold*, Intermetallics 53, p 107-111.
[11] Xie C., (2004), *Cast of titanium and its alloys*. China Machine Press, Beijing, China.
[12] Nemoto, M., Tian, W. H., Harada, K., Han, C. S., Sano, T., (1992), *Microstructure of precipitation strengthened Ni_3Al and TiAl*, Materials Science and Engineering: A 152(1–2), p 247-252.
[13] Noda, T., Okabe, M., Isobe, S., Sayashi, M., (1995), *Silicide precipitation strengthened TiAl*, Materials Science and Engineering: A 192–193, Part 2(0), p 774-779.
[14] Worth, B., Jones, J., Allison, J., (1995), *Creep deformation in near-γ TiAl: II. influence of carbon on creep deformation in Ti-48Al-1V-0.3C*, Metallurgical and materials transactions A 26, p 2961-2972.
[15] Klimová, A., Lapin, J., Pelachová, T., Nosko, M., (2013), *Effect of solidification parameters on microsegregation behaviour of main alloying elements in a peritectic TiAl based alloy*, Kovove Mater. 51, p 2013 89–99.
[16] Lapin J., (2003), *Effect of lamellar structure on microhardness and yield stress of directionally solidified intermetallic Ti-46Al-2W-0.5Si alloy*, J. Mater. Sci. Lett. 22, p 747– 749.

ISSN 1847-7917

Influence of normalizing heat treatment on gray iron properties

Štefanija KLARIĆ[1)]***, Vladimir PECIĆ***[2)] ***and Marko NOVOSELOVIĆ***[3)]
1) School Of Engineering & Information Technology, Charles Darwin University, Darwin, Northern Territory 0909, Australia
2) and 3)
Sveučilište J.J. Strossmayera u Osijeku, Strojarski fakultet u Slavonskom Brodu, Trg I.B. Mažuranić 2, 35000 Slavonski Brod, **Hrvatska**
J. J. Strossmayer University of Osijek, Mechanical Engineering Faculty in Slavonski Brod, **Croatia**
stefanija.klaric@cdu.edu.au, vpecic@sfsb.hr, mnovoselovic@sfsb.hr

Preliminary Note

Abstract: Due to lower mechanical properties, application of gray iron is primarily related to low production costs. Heat treatment can be used to modify microstructure and mechanical properties of gray iron. In this paper the influence of normalizing parameters (austenitizing temperature and temperature at which samples are removed from furnace) on microstructure and gray iron hardness are investigated.

Prethodno priopćenje

Utjecaj normalizacije na svojstva sivog lijeva

Sažetak: Zbog slabijih mehaničkih svojstava, primjena sivog lijeva prvenstveno je vezana uz niske troškove proizvodnje. Toplinskom obradom može se utjecati na mikrostrukturu, odnosno mehanička svojstva sivog lijeva. U radu je ispitivan utjecaj parametara normalizacije (temperature austenitizacije i temperature ohlađivanja) na mikrostrukturu i tvrdoću sivog lijeva.

Keywords
Gray iron
Normalizing
Hardness,
Microstructure

Ključne riječi
Sivi lijev
Normalizacija
Tvrdoća
Mikrostruktura

1. Introduction

Gray iron is an alloy of iron and carbon with addition of silicon, manganese and phosphorus. With the relatively low production costs and ability to be cast into complex shapes, good machinability, wear resistance, vibration absorption and good behavior under the compression loading, despite lower mechanical properties (lower tensile strength, ductility and fatigue strength), gray iron is widely used in casting production ([1],[2],[3] and [4]). Usual applications of gray iron among other, include machine bases, frames, rolling mills, motor housings, cylinder blocks, decorative parts, parts used in agricultural vehicle etc. ([2],[3] and [4]).

Heat treatment of gray iron influence the matrix microstructure (and properties) by modification of its constituents with almost no effect on graphite formed during solidification ([3] and [5]). The result of the heat treatment is matrix microstructure varying form ferrite-pearlite to tempered martensite [6]. Annealing and stress relieving are usually used heat treatment processes for gray iron, but other processes e.g. hardening and tempering, austempering, martempering and surface hardening are also applied ([4],[5],[6] and [7]).

2. Normalizing of gray iron

Normalizing is consisted of austenitization (the temperature range for gray iron is from 885 to 925 °C [6]) and cooling on calm air in order to achieve uniform and fine-grained structure with pearlite and with complete absence of martensite [5]. Mechanical properties of normalized gray iron castings like hardness and tensile strength are effected by combined carbon content, pearlite spacing (distance between cementitc plates) and graphite morphology, but austenitizing temperature has a marked effect [6].

3. Experimental procedures

In this paper, the influence of austenitizing temperature and the temperature at which the samples are removed from furnace on gray iron hardness and microstructure are investigated.

The chemical composition of selected material is given in table 1.

Symbols/Oznake

A	- Design of experiment factor - Faktor plana pokusa	**Subscripts/Indeksi**	
B	- Design of experiment factor - Faktor plana pokusa	A	- Austenitizing temperature - Temperatura austenitizacije
HB5/750/15	- Brinell hardness - Tvrdoća po Brinellu	f	- Temperature at which samples are removed from furnace - Temperatura pri kojoj se uzorci vade iz peći (ohlađivanja)
	Greek letters/Grčka slova		
ϑ	- Temperature, °C - Temperatura, °C		

Table 1. Chemical composition of gray cast iron samples

Tablica 1. Kemijski sastav uzoraka od sivog lijeva

C	Si	Mn	P	S	Cr	Cu	Ni
3,08	1,916	0,351	0,414	0,090	0,158	0,290	0,117

Samples are conducted to laboratory examinations of hardness and microstructure after the normalizing. Experiment is organised as factorial 3^2 design of experiment in order to statistically determinate the influence of individual factors and their interactions on material hardness.

Table 2 shows plan of experiment with defined heat treatment parameters (factors).

Table 2. Plan of experiment

Tablica 2. Plan provođenja pokusa

Austenitizing temperature, °C/ Temperatura austenitizacije, °C	Temperature at which samples are removed from furnace, °C/ Temperatura pri kojoj se uzorci vade iz peći (ohlađivanja), °C	Sample/ Oznaka uzorka			Analysis type/ Vrsta ispitivanja
880	850	111	112	113	Hardness measurement *HB5/750/15* and metallographic analysis/ Mjerenje tvrdoće *HB5/750/15* i metalografska analiza
	650	121	122	123	
	20	131	132	133	
905	850	211	212	213	
	650	221	222	223	
	20	231	232	233	
930	850	311	312	313	
	650	321	322	323	
	20	331	332	333	

*Normalizing holding time for all samples was 30 min.

After the heat treatment according to plan of experiment given in table 2, all samples were ground and polished using a standard metallographic technique and Brinell hardness measurement (*HB5/750/15*) were performed.

For the analysis of microstructure, etching of the test surfaces with the 2% Nital was used. The microstructures of samples were analyzed using the optical microscopy.

4. Results and discussion

The hardness of the samples before heat treatment was 257 HB. The materials hardness values after the heat treatment are presented in Table 3. The shown hardness values present the average of three measurements. The table is adjusted to 3^2 design of experiment analysis with defined factors (*A* - austenitizing temperature and *B* - temperature at which samples are removed from furnace) and their levels.

Table 3. Hardness *HB5/750/15* of samples at different heat treatment conditions (according to table 2)

Tablica 3. Tvrdoća uzoraka *HB5/750/15* pri različitim uvjetima toplinske obrade (prema tablici 2)

Factor *A* (Austenitizing temperature)/ Faktor *A* (Temperatura austenitizacije)	*A*1 ϑ_A = 880°C			*A*2 ϑ_A = 905°C			*A*3 ϑ_A = 930°C		
Factor *B* (Temperature at which samples are removed from furnace)/ Faktor *B* (Temperatura pri kojoj se uzorci vade iz peći)	*B*1 ϑ_f = 850°C	*B*2 ϑ_f = 650°C	*B*3 ϑ_f = 20°C	*B*1 ϑ_f = 850°C	*B*2 ϑ_f = 650°C	*B*3 ϑ_f = 20°C	*B*1 ϑ_f = 850°C	*B*2 ϑ_f = 650°C	*B*3 ϑ_f = 20°C
Level combination/ Kombinacija nivoa	A1B1	A1B2	A1B3	A2B1	A2B2	A2B3	A3B1	A3B2	A3B3
Repetition/ Ponavljanja	288	167	156	278	169	167	266	163	153
	266	164	156	262	160	154	260	157	146
	285	165	156	280	167	161	272	157	154
Middle value/ Srednja vrijednost	280	165	156	273	165	161	266	159	151

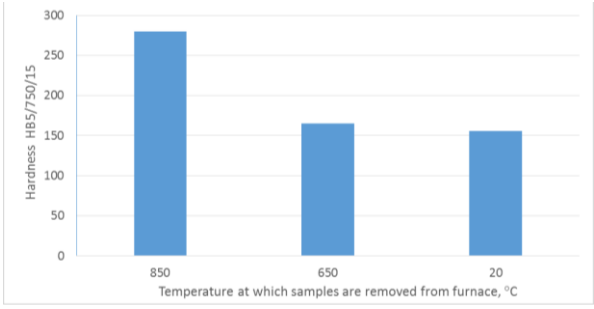

a) Austenitizing temperature ϑ_A = 880°C

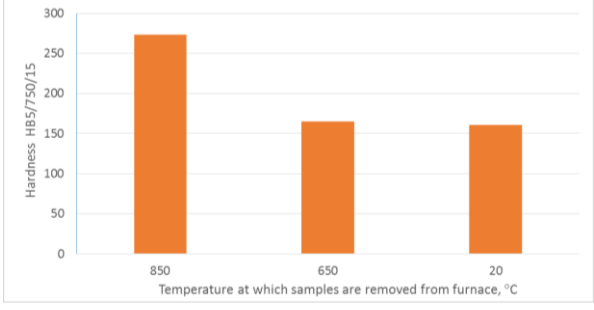

b) Austenitizing temperature ϑ_A = 905°C

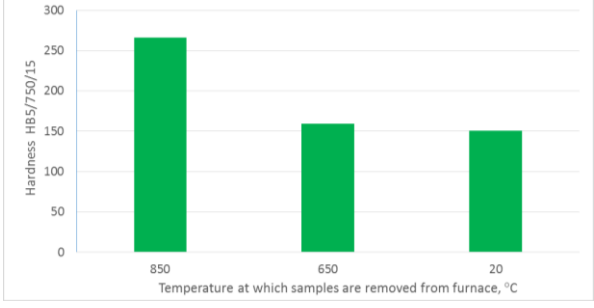

c) Austenitizing temperature ϑ_A = 930°C

Figure 1. Influence of temperature at which samples are removed from furnace: results of hardness measurement of samples after normalizing on temperatures 880°C (a), 905°C (b) and 930°C (c)

Slika 1. Utjecaj temperature vađenja uzoraka iz peći: rezultati mjerenja tvrdoće uzoraka normaliziranih na temperaturama 880°C (a), 905°C (b) i 930°C (c)

The results of hardness measurement are shown in diagrams on figure 1. The influence of temperature at which samples are removed from furnace (temperature at start of air cooling) on hardness values is noticeable on all diagrams 1a, 1b and 1c.

The influence of austenitizing temperature on hardness of samples removed from furnace at 650°C are shown on figure 2. The difference in hardness distribution is visible for sample normalised at 930°C.

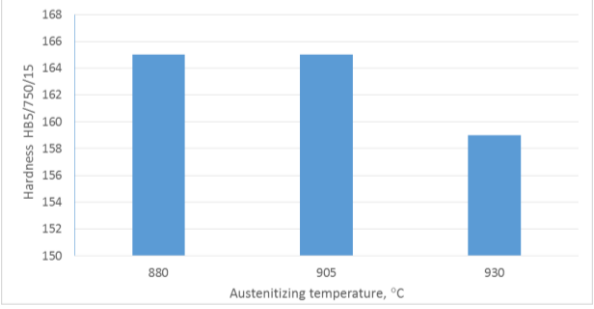

Figure 2. Influence of austenitizing temperature: results of hardness measurement of samples after normalizing on temperatures 880°C, 905°C and 930°C (temperature at which samples are removed from furnace ϑ_f = 650°C)

Slika 2. Utjecaj temperature austenitizacije: rezultati mjerenja tvrdoće uzoraka normaliziranih na temperaturama 880°C, 905°C i 930°C (temperatura pri kojoj su uzorci izvađeni iz peći ϑ_f = 650°C)

Figure 3 shows the microstructure of the samples before heat treatment (a), and after the heat treatment with austenitizing temperature ϑ_A = 880°C and temperature at which samples are removed from furnace ϑ_f = 650°C (b). The normalised pearlitic structure after the heat treatment is visible on figure 3b).

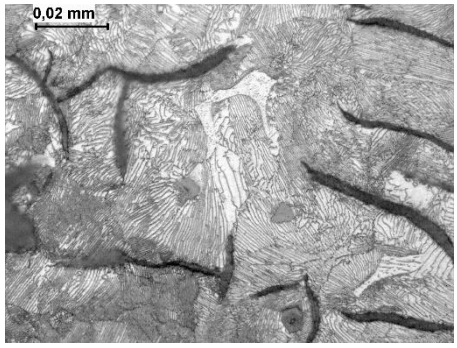

a)

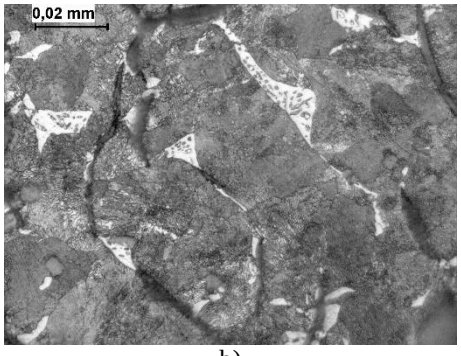

b)

Figure 3. Microstructure of gray iron before heat treatment (a) and normalised (ϑ_A = 880°C and ϑ_f = 650°C) (b)

Slika 3. Mikrostruktura sivog lijeva prije toplinske obrade (a) i nakon normalizacije (ϑ_A = 880°C i ϑ_f = 650°C) (b)

5. Conclusion

Achievement of proper mechanical properties and demand for avoidance of residual stresses in castings requires careful selection and compliance to defined heat treatment parameters. In this paper, two parameters of gray iron normalizing: austenitizing temperature (A) and temperature at which samples are removed from furnace (B) are varied in order to analyze their influence on hardness values. It can be noticed that the temperature at start of air cooling (factor *B*) can have significant influence on hardness; the lowest values of gray iron hardness are achieved after the normalizing by leaving the samples to cool in furnace until room temperature.
For the continuation of the research, the investigation of influence of normalizing time and more detailed influence of temperature at start of air cooling on properties of gray iron is planned.

REFERENCES

[1] Novosel M., Krumes D., (1997), *Željezni materijali*, Strojarski fakultet u Slavonskom Brodu, Slavonski Brod

[2] Seidu S.O., Kutelu B.J., (2013), *Influence of Heat Treatment on the Microstructure and Hardness Property of Inoculated Grey Cast Iron*, International Journal of Engineering and Technology 3, No. 8, p 888-892 UK

[3] Atanda P., Okeowo A., Oluwole O., (2010), *Microstructural Study of Heat Treated Chromium Alloyed Grey Cast Iron*, Journal of Minerals Characterization & Engineering 9, No. 3, p 263-274, USA

[4] Paczkowska M., (2012), *Analysis of gray iron microstructure influence on potential laser heat treatment effects*, Archives of Mechanical Technology and Automation 32, No. 1, p 27-36, Poland

[5] Krumes D., (2000), *Toplinska obradba*, Strojarski fakultet u Slavonskom Brodu, Slavonski Brod

[6] ASM Handbook, (2004), *Vol 4- Heat Treating*, ASM International, Metals Park, OH, USA,

[7] Eperješi Š., Malik J., Vaskova I., Fecko D., (2015), *Increasing of Utility Properties of Grey Cast Iron Castings with Heat Treatment*, Archives of Foundry Engineering 15, No. 2, p 13-16, Poland

ISSN 1847-7917

Preliminary study of severe plastic deformation tool for production of solid state recycled materials

Jure KROLO[1)], ***Branimir LELA***[1)], ***Rafaela VULETA***[1)]

1) Fakultet elektrotehnike, strojarstva i brodogradnje, Sveučilišta u Splitu (Faculty of Electrical Engineering, Mechanical Engineering and Naval Architecture, University of Split) Ruđera Boškovića 32, 21000 Split, **Republic of Croatia**

jkrolo@fesb.hr
blela@fesb.hr
rafaela.vuleta@fesb.hr

Keywords

Solid State Recycling
Severe plastic deformation
Material flow
Extrusion force

Ključne riječi

Recikliranje u čvrstom stanju
Velika plastična deformacija
Tečenja materijala
Sila istiskivanja

Original scientific paper

Abstract: Main aim of this paper is to investigate modified tool for the severe plastic deformation (SPD) processes as well as for solid state recycling (SSR) process. SPD processes are used to produce bulk nanostructured materials (NSM) materials and SSR is recycling process of aluminum or magnesium waste without material remelting. Tool presented in this paper is combination of classic extrusion processes and so called equal channel angular pressing process (ECAP). In order to evaluate tool geometry and forces necessary to push material through complex matrix, model materials lead and plasticine were used to perform a preliminary study.

Izvorno znanstveni članak

Sažetak: Glavni cilj ovog rada je istraživanje modificiranog alata za procese velike plastične deformacija kao i recikliranje u čvrstom stanju. Procesi velike plastične deformacije se koriste za proizvodnju materijala s nanostrukturom dok je recikliranje u hladnom stanju proces recikliranja aluminijskog ili magnezijevog otpada bez pretaljivanja. Alat predstavljen u radu je kombinacija klasičnog procesa istiskivanja i tzv. kutnog kanalnog istiskivanja. S ciljem istraživanja geometrije alata, toka materijala i sile potrebne da se istisne materijal kroz kompleksnu matricu, modelni materijali olovo i plastelin su korišteni za preliminarno istraživanje.

1. Introduction

In the last few decades material scientist and engineers have been attracted by materials with small grain size. It is well known that finer grain size increases strength and fracture toughness of the material and provides potential superplastic deformation at moderate temperatures [1]. There are a few ways to achieve NSM materials such as gas condensation, ball milling with subsequent consolidation and SPD processes. In particular, SPD methods results in overcoming of a number of difficulties connected with residual porosity in compacted samples, impurities from ball milling, processing of large scale billets and practical application of the given materials [2]. There are already some commercial processes like cold rolling and drawing which are capable due to heavy deformations to refine microstructure at low temperature. Main difference of this classical methods and SPD process is in grain boundaries misorientation. Microstructure formed with cold rolling is cellular type having low angle grain boundaries. Requirement to achieve qualitative change in properties of materials can be realized creating structure with prevailing high angle grain boundaries which is possible with SPD processes. Furthermore it is necessary to achieve uniform nanostructure for stable mechanical properties, and last requirement is to create samples without any mechanical damage or cracks [3].

There are various techniques to perform SPD process such as: Severe plastic torsion straining (SPTS), Continuous repetitive corrugation and strengthening, Accumulated roll bonding (ARC), Equal channel angular pressing (ECAP), and others [1]. In this work a new tool for severe plastic deformation was investigate. This tool is combination of classic extrusion process and ECAP, where billet goes directly through ECAP channel. This work is preliminary study to investigate necessary pressure during process as well as created sample shape and material flow. So in that purpose lead and plasticine as model materials were used because recrystallization temperature of lead is below room temperature, so flow stress is reduced.

Furthermore other important application of these tools is for so called solid state recycling (SSR) of aluminum or magnesium chips. During conventional recycling of aluminum chips, 20% is lost during burning or mixing with slag [4, 5]. Other loses depend on the scrap input, the melt treatment, the furnace technology and material efficiency of the forming processes. However yield rate for recycled products by SSR is estimated as high as 95%

Symbols/Oznake

SPD	- Severe plastic deformation - Velika plastična deformacija
NSM	- Nanostructured materials - Nanomaterijali
ECAP	- Equal channel angular pressing - Kutno kanalno istiskivanje
SPS	- Spark plasma sintering - Sinteriranje pomoću plazme
SPTS	- Severe plastic torsion straining - Velika plastična deformacija torzijom
ARC	- Accumulated roll bonding - Akomulirano spajanje valjanjem

Greek letters/Grčka slova

λ	- Extrusion ratio, - Omjer istiskivanja
Φ	- Iner ECAP angle - Unutarnji kut ECAP-a
ψ	- Outer ECAP angle - Vanjski kut ECAP-a
α	- Dead metal zone semiangle - Polukut mrtve zone materijala

and there is 70% reduction of energy consumption, compared to existing melting method [6]. Furthermore overall 70% lower impact on environment is achieved by direct recycling using ECAP (Equal channel angular pressing), or 62% by SPS (Spark Plasma Sintering) in accordance with ReCiPe endpoint Europe H/A LCIA method [7]. On the other hand SSR processes still remains in laboratory investigation phase and that is one of the main problems.

Authors of this work considered that this tool at elevated temperature could fulfil some of the necessary conditions to create recycled samples with good mechanical properties without any residual voids and pores, which are one of the main problems in SSR processes. These conditions are high normal contact stress between chips as well as shear stress, high pressure and high strain [4, 5, 8]. Experiment performed in this work point out that extrusion pressure in modified tool was twice higher than in conventional extrusion process.

Future investigation will be based on using this tool for SSR at elevated temperatures, as well as investigation of influence parameters of the samples processed through this tool at relatively low temperature to achieve NSM.

2. Modified tool design

Main disadvantage for SSR processes as well as NSM production using severe plastic deformation is laboratory scale production. Authors of this work want to investigate possible combination of already existing process and SPD process. In this way industry could easily adapt already existing tools and dies for NSM as well as for SSR materials production. In that purpose modified extrusion container with ECAP die is constructed for rectangular section utilizing direct extrusion process, Fig 1.

There are some crucial differences between above mentioned two processes. Firstly according to various authors high temperature, strain, normal and shear stress are necessary to produce quality SSR recycled samples [4, 5, 8]. So this modified process should be performed at higher temperature, for aluminum that is between 450 °C and 500 °C and for magnesium temperatures are 350 °C to 400 °C [9]. It is expected of ECAP die to create additional resistance for material flow, as well as additional shear stress and strain.

On the other hand production of NSM should be performed at lower temperature and there is contradiction between these two processes. Furthermore flow stress for aluminum at room temperature is high, and aluminum extrusion processes are usually performed at higher temperatures to reduce flow stress, but that is not always necessary. ECAP die is used and that will additionally increase friction condition and pressure

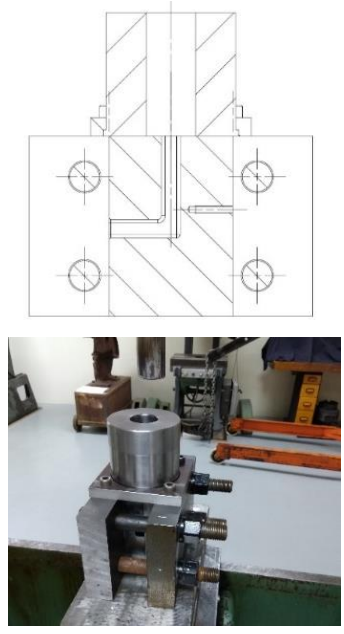

Figure 1. Schematic representation of conventional extrusion process using ECAP die

Slika 1. Shematski prikaz konvencionalnog procesa istiskivanja s ECAP matricom

To investigate this additional pressure in die, in this preliminary study model material lead is used. One of the reasons to use lead is similar extrusion force during conventional process for lead at room temperature and for aluminum at 500 °C. This was proved in experiment which was performed with special rig and die for direct extrusion process, Fig 2.

Extrusion process was performed on a hydraulic press having maximum force of 1 MN and force was measured with HBM load cell C6A 1MN. Obtained diagrams for extrusion force vs time are given in Fig. 3. Maximal extrusion force during convention extrusion process for aluminum at 500 °C was 229 600 N and for lead at room temperature was 217 700 N. Used die was circular shaped with diameter 15 mm, and extrusion container diameter was 40 mm so achieved extrusion ratio was λ = 7,11.

Figure 2. Rig and die for conventional extrusion
Slika 2. Klip i matrica za konvencionalno istiskivanje

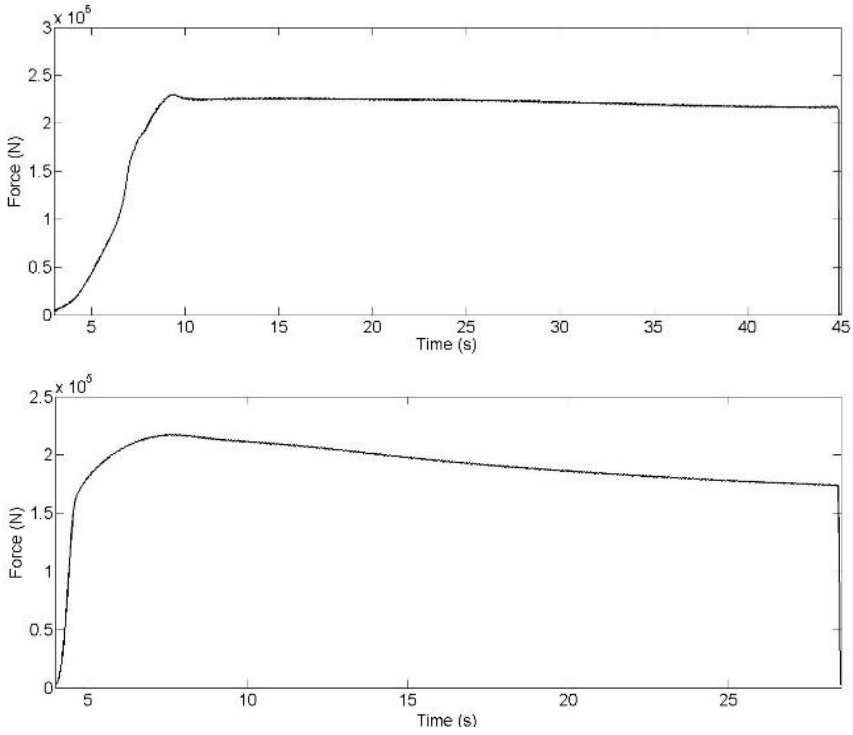

Figure 3. Extrusion force vs time diagram for aluminium at 500 °C (up); extrusion force vs time diagram for lead at 20 °C (down)
Slika 3. Dijagram sila istiskivanja u odnosu na vrijeme za aluminij na 500 °C (gore); dijagram sila istiskivanja u odnosu na vrijeme za olovo na 20 °C (dolje)

3. Process parameters

3.1. Parameters of ECAP process

In this section ECAP process is described. It is one of the most investigated SPD processes. Deformation of billet is achieved through pure shear and main goal is to introduce intense plastic strain into material. During process billet is pressed multiple times through special die with two channels which usually intersects at angle of 90°. Main parameters of ECAP process is tool geometry and two angles Φ and ψ which are showed in Fig. 4.

General relationship to calculate effective strain value e_N of the billet during ECAP for N passes has the following form [2]:

$$e_N = N \left\{ \frac{2\cot\left(\frac{\Phi}{2}+\frac{\psi}{2}\right) + \psi\mathrm{cosec}\left(\frac{\Phi}{2}+\frac{\psi}{2}\right)}{\sqrt{3}} \right\} \quad (1)$$

There is also analytical solution of the extrusion pressure for ECAP die (P_{ecap}) considering Hollomon-type materials and using frictionless condition, where n is strain hardening coefficient and σ_y is flow stress of material [2]:

$$P_{ecap} = \left(\frac{\sigma_y}{n+1}\right)\left[\frac{2\cot\left(\frac{\Phi+\psi}{2}\right)+\psi}{\sqrt{3}}\right]^{n+1} \quad (2)$$

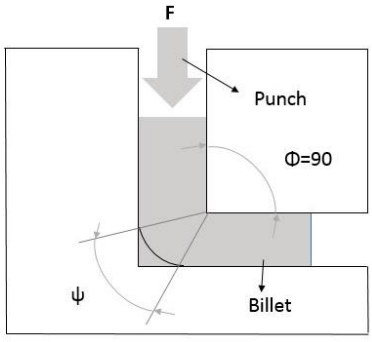

Figure 4. Schematic representation of ECAP process and specific tool geometry
Slika 4. Shematski prikaz ECAP procesa i specifična geometrija alata

3.2. Parameters of conventional extrusion process

Direct conventional extrusion is process where billet is placed in the container and pushed through the die by the ram pressure. There is also relatively simple expression for effective strain in case of direct extrusion [10]:

$$e = 2\ln\sqrt{\lambda} \quad (3)$$

λ - stands for extrusion ratio, and extrusion ratio for single-orifice die is defined by:

$$\lambda = \frac{A_c}{A_e} \quad (4)$$

A_c - cross sectional area of the container bore, A_e - final cross sectional area of the extruded rod.

Furthermore analytic expression for average conventional extrusion pressure, P_{conv} may be written as [10]:

$$P_{conv} = 2\sigma_y\left(1+\frac{cot\alpha}{\sqrt{3}}\right)ln\frac{D_C}{D_E}+\frac{4\sigma Z}{\sqrt{3}D_C} \quad (5)$$

σ_y - flow stress, α - dead metal zone semi angle, Z - extrusion direction path, D_C - container bore, D_E - diameter of extruded rod.

3.3. Parameters of modified tool design

For combined processes effective strain (e_{eff}) according to expression (1) and (3) easily can be writen as:

$$e_{eff} = 2\ln\sqrt{\lambda}+\left\{\frac{2\cot\left(\frac{\Phi}{2}+\frac{\psi}{2}\right)+\psi\mathrm{cosec}\left(\frac{\Phi}{2}+\frac{\psi}{2}\right)}{\sqrt{3}}\right\} \quad (6)$$

For constructed tool angle Φ is 90°, and angle ψ is 12°. And effective strain according to expression (6) for modified tool is e_{eff} = 2,835.

On the other hand to derive expression for effective pressure for combined process very important consideration must be introduced. Derived expression for pressure in ECAP die is only for frictionless condition and for extrusion process friction is taken in consideration. For future research analytic expression could be derived and experimentally confirmed, especially if some lubrication is used in ECAP die.

4. Experimental observation

4.1. Material flow

As was already mentioned for preliminary investigation model materials were used. Process was successfully performed using lead. Fig. 5 shows lead sample at exit of the ECAP die.

Figure 5. Lead sample at modified tool ECAP die exit
Slika 5. Olovni uzorak na izlazu iz ECAP matrice modificiranog alata

Often scientist use physical modelling to investigate material flow in new extrusion die design [11, 12]. So to investigate material flow plasticine in different colours was used. First strip shaped plasticine was arranged in layers to create billet and obtained sample after extrusion is showed at Fig. 6.a. Second sample was obtained using billets with different colours mixed plasticine and sample obtained is showed at Fig 6.b. Material flow is very similar with conventional extrusion process with faster material flow in the middle of the container due to different friction conditions. However at corner of the ECAP die dead zone of material appeared, this observation is in accordance with other investigation [11].

4.2. Maximal extrusion force

Furthermore using lead as model material main aim was to investigate force need to extrude lead through modified tool at room temperature. As was expected extrusion force was much higher than for extrusion process for lead with conventional die. Fig. 7 is graphical representation of extrusion force vs time.

Figure 6. Material flow inside modified extrusion die; a) layer on layer, b) mixed material
Slika 6. Tok materijala unutar modificirane matrice; a) sloj na sloj, b) miješani materijal

Maximal extrusion force during modified process was 419 200 N, and for conventional extrusion of lead maximal extrusion was 217 700 N. Extrusion ratio for modified tool was 5.58. Extrusion force is 92,56 % higher because of ECAP die in modified tool. Same is expected for aluminum at 500 °C. These results are very satisfying for SSR process.

As it was mentioned in introduction higher extrusion force or normal and shear pressure between aluminum or magnesium chips are desirable to achieve better bonding among chips and to obtain recycled samples with better mechanical properties [4, 5, 13].

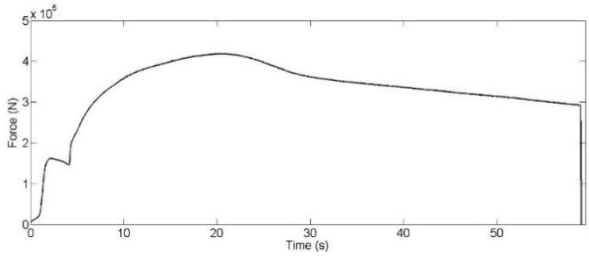

Figure 7. Extrusion force vs time diagram for modified tool
Slika 7. Dijagram sila istiskivanja u odnosu na vrijeme za modificirani alat

Chips bonding can be related with a mathematical model proposed by Copper and Allwood, for aluminum solid bonding [8]:

$$\frac{\sigma_b A_n}{} = \left(\frac{0{,}8A_n}{Y}\sqrt{{\sigma_n}^2 + 3\left(\tau_{app}\right)^2}\right) \text{x } \upsilon \text{ x } (0{,}8\frac{\sigma_n - p_{ex}}{Y}) \text{ x } \sigma_0 \quad (7)$$

σ_b - tensile bond strength; σ_0 - the strength of the cold, bulk aluminum; σ_n - normal contact stress; p_{ex} - the pressure required to micro-extrude the substrate aluminum through the cracks; Y - the aluminum flow stress; τ_{app} - application of a nominal shear stress; A_n - area of contact between clean aluminum surfaces; υ - exposed aluminum without a protective oxide layer.

According to this model higher strain increases the exposed area and oxide crack width, increasing υ and decreasing p_{ex}. Increase in strain rate increases the flow stress of the metal, increasing both Y and p_{ex}. Increase in normal contact stress increases σ_n. Increase in bonding deformation temperature decrease the threshold strain and flow stress of the metal. The reduced threshold strain increases υ, and the reduced flow stress of metal decreases both Y and p_{ex}. A higher shear stress increases τ_{app} and increases the oxide crack width, decreasing p_{ex}. These conclusions are in agreement with assumptions proposed by many others authors who were investigated solid state recycling [4, 5, 14]. Furthermore if extrusion process is performed below 450 °C recycled sample contains internal pores and voids, but above 500 °C microstructure is good [15, 16]. These conclusions can be related with Copper and Allwood model. According to mentioned model not only reduction of material flow stress can be achieved when temperature increases, but also force needed to extrude pure aluminum material between oxide cracks is reduced too. All this contribute to better chips bonding. Main part of the research for SSR recycling is done utilizing conventional extrusion process. For SSR process via extrusion with increasing extrusion ratio, mechanical properties also increase. According to authors this is because oxide layer fracture occurs. Moreover reduction of cracks inside recycled samples is achieved because of increased plastic deformation and pressure [16, 17]. Furthermore extrusion ratio 10:1 was not sufficient to create quality bonding among chips. But with changed material flow using porthole dies, which also cause increased plastic deformation, recycling with extrusion ratio 10:1 was successful, moreover excellent mechanical properties were achieved [13].

According to all mentioned influence parameters, chips recycling using this combination of conventional extrusion process and ECAP die should be investigated in purpose of SSR and moreover better mechanical properties of recycled samples are expected.

On the other hand it is expected for extrusion forces to go much higher if this die is used for aluminum NSM production at room temperature, and possibility to perform such process with this kind of two process combination is questionable with hydraulic press of 1MN. However additional processing of the recycled samples using only ECAP part of the tool can be performed to achieve even better mechanical properties.

5. Conclusion

Combination of conventional extrusion process with severe plastic deformation process was successfully performed using modified tool and model materials to predict maximal extrusion force and material flow. Following conclusions are derived:

- Maximal extrusion force for model material lead in process which combines conventional extrusion and ECAP die was 419 200 N which is 92,56 % higher than in usual extrusion process, 217 700 N.
- Material flow is similar as in conventional extrusion process with faster material flow in middle of the sample. Also dead material zone did appeare at the corner of ECAP die.
- Higher extrusion force is expected to appear for aluminum extrusion at 500 °C and according to various authors this kind of process combination should lead to SSR samples with good mechanical properties in solid state recycling process.

REFERENCES

[1] Vrelinden B.: "Severe plastic deformation of metals", Metalurgija-Journal of Metallurgy, 2003.

[2] Valiec R.Z., Islamgaliev R.K., Alexandrov I.V.: „Bulk nanostructured materials from severe plastic deformation", Progress in Materials Science, Vol 45, pp 103-189, 2000.

[3] Melicher R.: „Numerical simulation of plastic deformation of aluminum workpiece induced by ECAP technology", Applied and Computational Mechanics 3, pp. 319-330, 2009.

[4] Tekkaya A.E., M. Schikorra, D. Becker, D. Biermann, N. Hammer, K. Pantke: „Hot profile extrusion of AA-6060 aluminum chips", Journal of Materials Processing Technology, 209, pp. 3343-3350, 2009.

[5] Gronostajski J., Matuszak A.: „The recycling of metals by plastic deformation: an example of recycling of aluminum and its alloy chips", Journal of Materials Processing Technology, Vol. 92, pp. 35-41, 1999.

[6] Chiba R. Nakamura T., Kuroda M.: „Solid-state recycling of aluminum alloy swarf through cold profile extrusion and cold rolling", Journal of Materials Processing Technology, Vol. 211, pp. 1878-1887, 2011.

[7] Joost R. D., A. Erman Tekkaya, Matthias Haase, T. Welo, K. Vanmeensel, K. Kellens, Wim Dewulf, Dimos Paraskevas: „Environmental assessment of solid state recycling routes for aluminum alloys: Can solid state processes significantly reduce the environmental impact of aluminum recycling?", CIRP Annals - Manufacturing Technology, Vol. 64, pp. 37-40, 2015.

[8] Daniel R. Cooper, Julian M. Allwood.: „The influence of deformation conditions in solid-state aluminum welding processes on the resulting weld strength", Journal of Materials Processing Technology, Vol. 214, pp. 2576-2592, 2014.

[9] Ab Rahim S.N., Lajis M.A., Ariffin S.: „A Review on Recycling Aluminium Chips by Hot Extrusion Process", Procedia CIRP, Vol. 26, pp. 761-766, 2015.

[10] Prapid K. S.: „Aluminum Extrusion Technology", The Materials Information Society, ASM International. Materials Park. Ohio, 2002.

[11] Alexander V. Perig: „2D Upper Bound Analysis of ECAE through 2θ-Dies for a Range of Channel Angles", Materials Research, Vol. 17(5): pp. 1226-1237, 2014.

[12] A .Assempour, S. Razi: „Physical Modeling of Extrusion Process", Journal of Mechanical Engineering Vol. 4, No. 1, April 2003.

[13] Guley V., Khalifa N.B., Tekkaya A.E.: „The Effect of Extrusion Ratio and Material Flow on the Mechanical Properties of Aluminum Profiles Solid State Recycled from 6060 Aluminum Alloy Chips", The 14th International ESAFORM Conference on Material Forming AIP Conf. Proc. 1353, 1609-1614, 2011.

[14] Haase M., Ben Khalifa N., Tekkaya A.E. and Misiolek W.Z.: „Improving mechanical properties of chip-based and equal channel angular pressing (iECAP)", Materials Science and Engineering. A 539, pp. 194-204, 2012.

[15] Lela B., Krolo J., Jozić S.: „Mathematical modeling of solid-state recycling of aluminum chips", International Journal of Advanced Manufacturing Technology, 2016. DOI 10.1007/s00170-016-8569-5

[16] Wiewiora M., Wedrychowicz M., Wzorek L.,: „Mechanical properties of solid state recycled 6060 aluminum alloy chips", Metal, Brno, Czech Republic, 2015.

[17] Mao-Liang Hu, Ze-sheng J., Xiao-yu C.: „Effect of extrusion ratio on microstructure and material properties of AZ91D magnesium alloy recycled from scraps by hot extrusion process", Journal Transactions of Nonferrous Metals Society of China, Vol. 20, pp. 987-991, 2010.

[18] Fogagnolo J.B., Ruiz-Navas E.M., Simon M.A., Martinez M.A.: „Recycling of aluminum alloy and aluminum matrix composite chips by pressing and hot extrusion", Journal of Materials Processing Technology, 143-144, pp. 792-795, 2003.

ISSN 1847-7917

Precision cast turbocharger wheels from TiAl-based alloy

Juraj LAPIN[1)]
1) Institute of Materials and Machine Mechanics, Slovak Academy of Sciences, Dúbravská cesta 9, 845 13 Bratislava, **Slovak Republic**
ummslapi@savba.sk

Keywords
Titanium aluminides, based on TiAl
Melting
Casting
Microstructure
Mechanical properties

Original scientific article
Abstract: Precision cast turbocharger wheels have been prepared by induction melting of TiAl-based alloy with nominal composition Ti-43.5Al-4Nb-1Mo-0.1B (at.%) in oxide crucibles and gravity casting into ceramic moulds under argon atmosphere. Two types of melting crucibles are used: (i) pure Y_2O_3 crucibles and (ii) Al_2O_3 based crucibles with inner face-coat Y_2O_3 layer. The effect of several processing parameters such as metal pouring temperature, type of crucible, mould temperature and holding time at the melt pouring temperature on surface quality, casting defects, contamination by oxygen and volume fraction of Y_2O_3 particles is evaluated. Chemical composition, phase composition and interlamellar spacing are analysed in the as-cast turbocharger wheels. Depending on the processing parameters, the oxygen content is found to vary from 1270 to 3080 wt.ppm and volume fraction of Y_2O_3 particles is measured from 0.4 to 0.8 vol.%. Mechanical properties including Vickers microhardness, tensile properties and creep properties are characterised using specimens extracted from the as-cast turbocharger wheels.

1. Introduction

TiAl-based alloys are of large interests for high-temperature structural applications in aerospace, energy and automotive industries due to their potential to increase thrust-to-weight ratio and efficiency while reducing exhaust and noise pollution [1-6]. Their advantage is mainly seen in low density, excellent mechanical properties and good oxidation and corrosion resistance, which makes them possible replacement for traditional Ni-based superalloys [2-5]. TiAl-based alloys have been already applied as innovative materials for low pressure turbine blades in aircraft engines [6] and they are still assumed as light weight blade material for large stationary gas turbines [7]. The new alloy and technology development in this field has attracted extensive attention to casting of turbocharger wheels, exhaust valves of automotive engines and low pressure turbine blades for aircraft engines. The investment casting process allows mass production of TiAl-based components at a cost-effective way [2, 8, 9].

During precision casting, there is unavoidable contact between the TiAl melt and ceramic mould into which the melt is poured. Although water cooled copper crucibles are currently used for melting, the utilization of ceramic crucibles is considered as a mean of cost reduction of TiAl-based components in the future.

Oxides such as alumina, magnesia, silica, zirconia and yttria, which are more stable than carbides or borides, are employed in production of moulds and crucibles for precision casting of common metallic materials. Considering the specific case of the TiAl precision casting, an appropriate oxide must be selected from the standpoint of both cost and degree of contamination due to the reaction of the melt with the crucible and mould [10, 11]. Although TiAl precision castings are already used for turbine wheels in automotive turbochargers, their production is limited [8, 9]. The reason for this is their high production cost. It can be attributed mainly to the relatively small volume of melted material in water-cooled copper crucibles, the fact that the scrap cannot be used for the raw material and limitation of maximum mould preheating temperature in order to prevent reaction between the mould and the melt. Application of induction melting in ceramic crucibles, utilizing scrap for the raw material and raising the mould preheating temperature can be very effective to reduce the cost of TiAl-based castings.

Development of low cost TiAl-based turbine wheels is conditioned by using low-purity material. Contamination of the alloy can impact negatively the properties of TiAl castings. The maximum oxygen content is often set at around 1000 wt.ppm e.g. maximum oxygen content in low pressure turbine blades for GEnx engines is permitted up to 1200 wt.ppm [2].

Concerning turbine wheels, decrease of toughness due to an increase of oxygen content cannot be real problem as long as the tips of thin blades are able to withstand stresses encountered in handling and grinding during production without cracking. The backside part of the turbine wheel is machined and must have no defects such as exfoliation. Because turbine wheel is usually joint with steel shaft by means of friction welding under high pressure, the root of the wheel must be free of casting defects.

The aim of the present article is to investigate the effect of melting in ceramic crucibles and gravity precision casting into ceramic moulds on contamination, casting defects and properties of TiAl turbocharger wheels. Tensile and creep properties are evaluated using specimens extracted for the as-cast wheels.

Symbols

HV_m	- Vickers microhardness, GPa	γ	- TiAl intermetallic phase
HV_0	- material constant, GPa	β	- Ti-based solid solution with cubic crystal structure
k_{HV}	- material constant	α_2	- Ti_3Al intermetallic phase
λ	- interlamellar spacing, nm		

2. Experimental procedure

2.1. Melting and casting

The as-received ingot of TiAl-based alloy with nominal composition Ti-43.5Al-4Nb-1Mo-0.1B (at.%) and initial oxygen content of 420 wt.ppm were cut to smaller cylindrical pieces with a diameter of 70 mm and length of 50 mm, as seen in Fig. 1a. The melting and casting was carry out in a vacuum induction furnace under argon atmosphere using two types of crucibles: (i) pure Y_2O_3 crucible (Fig. 1b) and (ii) Al_2O_3 based crucible with inner Y_2O_3 surface layer. Before melting and casting, the vacuum chamber of the furnace was evacuated to a pressure of 4 Pa, flushed with argon (purity 99.9995%) three times and then backfilled with argon to a pressure of 5 kPa. The alloy was induction heated to a melt pouring temperature ranging from 1620 to 1680 °C and held constant at this temperature for various time ranging from 30 to 120 s. After stabilization at the temperature, the melt was poured into preheated Al_2O_3 based mould protected by an inner Y_2O_3 layer. The mould was preheated directly in the vacuum chamber to a temperature ranging from 500 to 800 °C using resistance furnace. Figure 2 shows the ceramic mould after removal from the vacuum furnace.

2.2. Mechanical properties testing

Vickers microhardness measurements were performed at an applied load of 0.49 N using fully-automatic microindentation hardness testing system FM-ARS 9000. Average microhardness values were calculated from 15-20 independent measurements performed in each defined position of the casting. Tensile and creep specimens with a gauge length of 25 mm and gauge diameter of 5 mm were lathe machined from the rods with a diameter of 9 mm extracted by spark machining from the root part of the turbocharger wheels. After machining, the specimen surface was polished to a roughness better than 0.3 μm.

Tensile tests were conducted at room temperature on a screw-driven Zwick machine at an initial strain rate of $1x10^{-4}$ s^{-1}. The offset tensile yield strength was measured at 0.2% plastic strain and the ductility was evaluated from the total plastic elongation to fracture. Constant load creep experiments were carried out at a temperature of 750 °C and initial applied load of 300 MPa. The specimen displacement was measured by high-temperature extensometer attached to the ledges of the creep specimen.

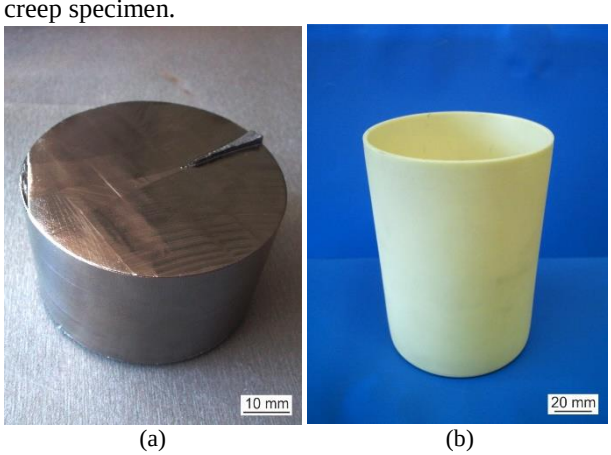

(a) (b)

Figure 1. (a) Ingot of Ti-43.5Al-4Nb-1Mo-0.1B (at.%) alloy before melting and casting, (b) Y_2O_3 crucible.

Figure 2. Al_2O_3 based mould after gravity casting.

2.3. Microstructure evaluation

The as-cast turbocharger wheels were cut longitudinally using wire electrical discharge machining and subjected to metallographic observations. Metallographic preparation of the sample consisted of standard grinding using abrasive papers, polishing on diamond pastes with various grain sizes up to 0.25 μm and etching in a solution of 100 ml H_2O, 6 ml HNO_3 and 3 ml HF. Microstructure evaluation was performed by optical microscopy (OM), backscattered scanning electron microscopy (BSEM), X-ray diffraction (XRD) analysis, energy-dispersive spectroscopy (EDS) and wavelength dispersive spectroscopy (WDS). Oxygen content was

measured with a LECO ONH836 elemental analyser. The analysed samples for oxygen measurement with a weight of about 1 g were cut from the casting by a diamond saw. The melting of the samples was carried out in graphite crucibles under helium. Oxygen content was detected in the form carbon dioxide using infrared detection. Interlamellar spacing was measured on digitalized optical micrographs using a computerized image analyser.

3. Results and discussion

3.1. Effect of melting and casting on quality of castings

Besides selection of appropriate oxide crucible and mould materials, the quality of TiAl-based castings can be significantly affected by two main processing parameters such as melt pouring temperature and the mould preheating temperature [12]. Higher preheating temperature of the mould improves filling and feeding of the mould and reduces cooling rates and temperature gradients during solidification. On the other hand, higher temperatures of the melt and oxide ceramic material of the mould lead to more intensive mould/melt reactions resulting in surface casting defects, increase of oxygen content and formation of ceramic particles [5, 10, 11]. Lower cooling rates lead to a coarse grain structure. Therefore, the present experimental work is focused on finding a balance between these parameters to achieve good surface quality and minimize casting defects and contamination of the castings.

As calculated by Schwaighofer et al. [13] for Ti-43.67Al-4.08Nb-1.02Mo-0.1B (at.%) alloy, the solidus temperature can be estimated to be about 1510 °C and liquids temperature to be about 1610 °C, which represents freezing range of about 100 °C for the studied alloy. Figure 3 shows the casting prepared at a melt pouring temperature of 1620°C, stabilisation time at the pouring temperature of 120 s and mould preheating temperature of 500 °C. The turbocharger wheel has a complex shape consisting of 9 twisted blades with thin leading edge with a thickness of 0.6 mm. The combination of selected casting parameters resulted in some casting defects such as some misruns in the region of thin walled blades and imperfections of the casting surface. After visual inspection of the surface and metallographic analysis of the porosity in the root part of the casting, cylindrical rod with a diameter of 9 mm were extracted by spark machining for mechanical testing from the wheels, as illustrated in Figure 4.

Figure 5 shows turbocharger wheel cast at a pouring temperature of the melt of 1650 °C, stabilization time of 30 s and mould preheating temperature of 800 °C. In this case, the selected combination of the processing parameters resulted in a very good surface quality.

Figure 3. Gravity cast turbocharger wheel after removal from the ceramic mould.

Figure 4. Gravity cast turbocharger wheel with extracted cylindrical sample for mechanical testing.

Figure 5. Gravity cast turbocharger wheel after removal of gating system and sand blast cleaning.

The visual inspection of the casting showed no defects such as misruns of the blades or surface cracks. In addition, metallographic analysis of longitudinal sections of the castings showed no large casting porosities or shrinkage, as shown in Figure 6. Figure 7 shows longitudinal section along the wheel blade. It is clear, that the cast thin blades are of very good quality without surface or large internal porosity, cracks or shape distortion. Also very thin tip parts of the blades with a thickness of 0.6 mm are very well filled with the metal and have a designed shape, as seen in Figure 7.

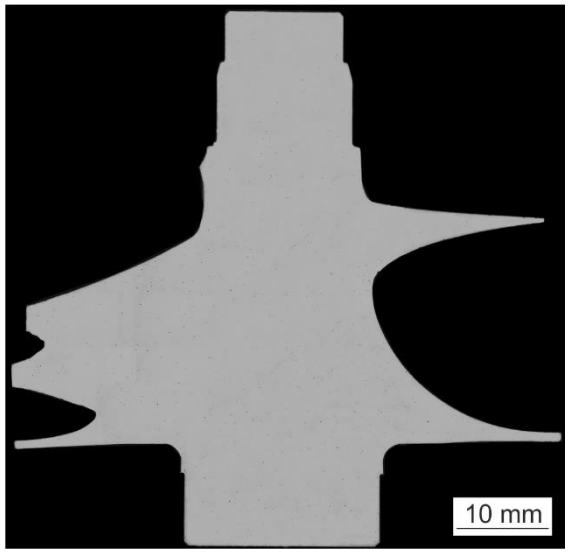

Figure 6. Optical macrograph showing longitudinal section of the turbocharger wheel after removal of gating system.

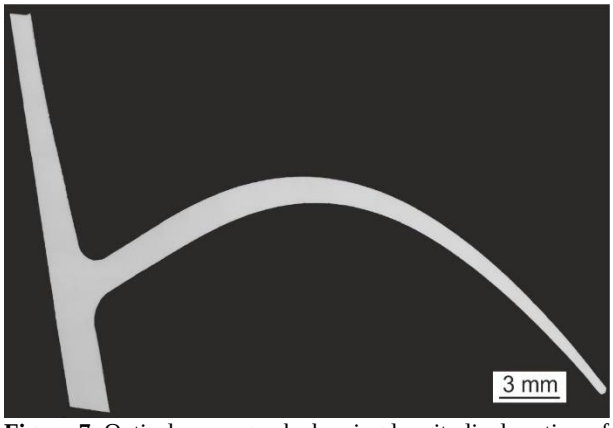

Figure 7. Optical macrograph showing longitudinal section of thin wall turbine wheel blade.

3.2. Microstructure characterization

Figure 8 shows the typical microstructure of the castings. The microstructure consists of lamellar equiaxed grains surrounded by a thick two phase boundary layer. Table 1 summarizes the chemical composition of observed phases measured by EDS and WDS. Chemically, five different regions can be identified in the microstructure. White colour particles 1 are enriched by Y and O and belong the most probably to Y_2O_3 phase. The grain boundaries are decorated by Ti and Mo enriched phase 2, which belongs to the β (Ti-based solid phase solution) phase. The equiaxed grains 3 consist of γ(TiAl) and $\alpha_2(Ti_3Al)$ lamellae. Dark colour phase 4 formed along the grain boundaries belongs to the γ phase. Fine ribbon type particles 5 within the microstructure belongs to borides. The oxygen content in the castings is mainly affected by the type of crucible, melt pouring temperature and stabilisation time at the melt pouring temperature. It is found that Y_2O_3 surface layer significantly reduced reactions between the melt and Al_2O_3 based crucibles. The melting in the Y_2O_3 crucible leads to an oxygen content ranging from 1850 to 3080 wt.ppm, which is significantly higher than that ranging from 1270 to 1540 wt.ppm after melting in the Y_2O_3 coated Al_2O_3 based crucibles.

Figure 9 shows the XRD pattern of the studied alloy after casting. The alloy is composed of $\alpha_2(Ti_3Al)$, γ(TiAl) and β (Ti-based solid solution with cubic crystal structure) phases. Alloying by boron leads to formation of borides in the form TiB and TiB_2 particles. Such phase composition corresponds very well to that reported by Schwaighofer et al. [13] for Ti-43.67Al-4.08Nb-1.02Mo-0.1B (at.%) alloy. However, the XRD pattern indicates also presence of Y_2O_3 phase, which results from thermochemical reaction between the Y_2O_3 surface layer and the melt during melting and casting. The volume fraction of Y_2O_3 particles is measured to vary from 0.4 to 0.8 vol.%. Similar formation of Y_2O_3 particles was observed also by Lapin et al. [11] during directional solidification of Ti-46Al-8Nb (at.%) alloy in pure dense Y2O3 crucibles.

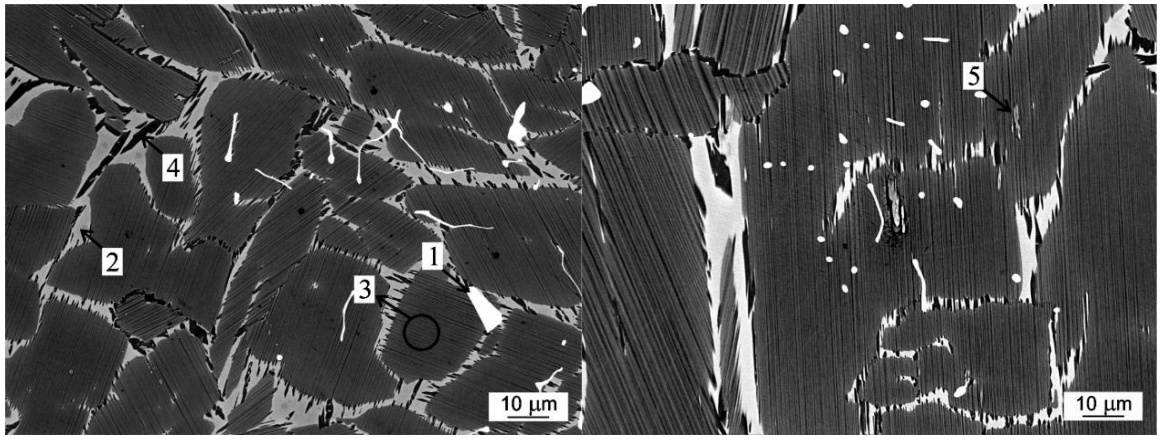

Figure 8. BSEM micrographs showing the typical microstructure of gravity cast turbocharger wheel.

Table 1. Chemical composition of coexisting phases

	Ti (at.%)	Al (at.%)	Nb (at.%)	Mo (at.%)	Y (at.%)	O (at.%)	B (at.%)
1	1.2 ± 0.4	-	-	-	45.2 ±0.6	53.6 ± 0.2	-
2	56.3 ± 0.5	35.8 ± 0.4	5.6 ± 0.4	2.3 ± 0.7	-	-	-
3	52.5 ± 0.1	42.6 ± 0.1	4.1 ± 0.3	0.8 ± 0.1	-	-	-
4	48.7 ± 0.7	47.1 ± 0.2	4.2 ± 0.5	-	-	-	-
5	27.4 ± 0.4	9.6 ± 0.4	3.4 ± 0.2	-	-	-	59.6 ± 0.5

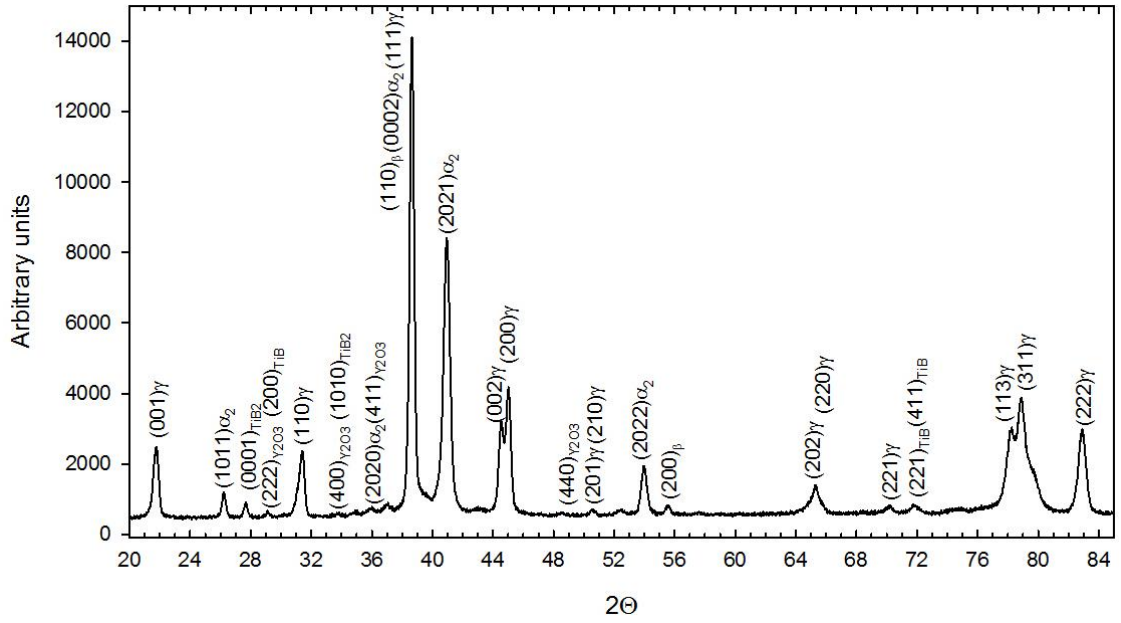

Figure 9. XRD pattern of the turbocharger wheel.

3.3. Mechanical properties

Figure 10 shows variation of the Vickers microhardness measured in the lamellar grains with the position measured from the tip of the blade to the root part of the wheel. The microhardness first decreases with increasing the distance from the tip reaching a minimum value at a distance of 6 mm and then increases towards the central part of the casting. As shown by Lapin [14], the microhardness values HV_m can be well related to interlamellar α_2-α_2 spacing λ according to Hall-Petsch type relationship in the form

$$HV_m = HV_0 + k_{HV}\frac{1}{\sqrt{\lambda}}, \qquad (1)$$

where HV_0 and k_{HV} are the material constants. Figure 11 summarises the dependence of Vickers microhardness HV_m on the reciprocal square root of interlamellar spacing λ. Linear regression analysis of the experimental data yields an equation for Vickers microhardness in the form

$$HV_m = 2.833 + 20.996\frac{1}{\sqrt{\lambda}}. \qquad (2)$$

The correlation coefficient r^2 of this fit is 0.96.

The results of room temperature tensile tests carried out on the specimens extracted from the castings yield an average offset 0.2% yield strength of 620 MPa, ultimate tensile strength of 630 MPa and plastic elongation to fracture of 0.23%. The elongation is reduced when compared to that of 0.8% of the as-received ingot. Creep tests at 750 °C/300 MPa showed that the minimum creep rate measured in the specimens prepared from the castings is $3.52\text{x}10^{-2}$ s^{-1}. This value is significantly lower than that of $1.01\text{x}10^{-7}$ s^{-1} measured in the creep specimens prepared from the as-received ingot. The increase of the creep resistance of the turbocharger wheels can be attributed to the precipitation strengthening of the casting by fine Y_2O_3 particles and to solid solution strengthening by oxygen.

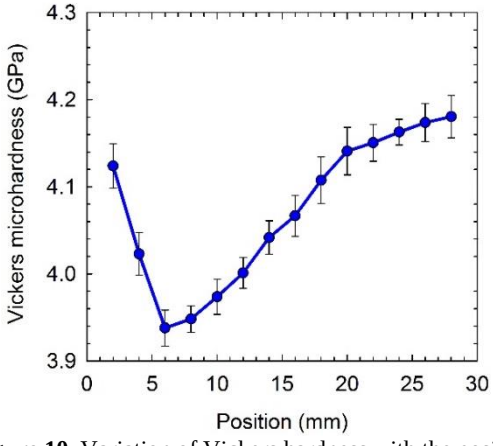

Figure 10. Variation of Vickers hardness with the position on longitudinal section of turbocharger wheel.

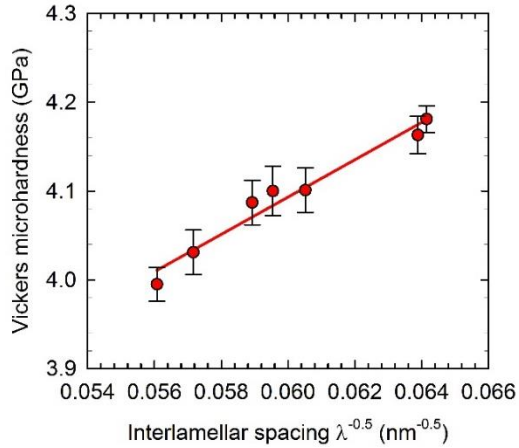

Figure 11. Dependence of Vickers microhardness on the reciprocal square root of inerlamellar spacing.

4. Conclusions

The TiAl turbocharger wheels can be produced by induction melting in Al_2O_3 based crucibles and gravity casting into Al_2O_3 based moulds using appropriate Y_2O_3 face-coat and optimal selection of the processing parameters. The reactions between the melt and Y_2O_3 protective layer lead to an increase of oxygen content and formation of Y_2O_3 particles. Depending on the processing parameters, the oxygen content is found to vary from 1270 to 3080 wt.ppm and volume fraction of Y_2O_3 particles is measured to be from 0.4 to 0.8 vol.%. The castings contain equiaxed grains composed of γ and α_2 lamellae. The grain boundaries are covered by a thick layer composed of the β and γ phases. The precipitation of Y_2O_3 particles and increase of oxygen content improve the creep resistance of the castings.

Acknowledgments

This work was financially supported by the Slovak Research and Development Agency under the contract APVV-15-0660, the Slovak Grant Agency for Science under the contract VEGA 2/0125/16 and the Slovak Academy of Sciences under the contract of MVTS funding of the project GRADECET. The author would like also to acknowledge the technical help of O. Bajana, T. Pelachová and J. Čičman.

REFERENCES

[1] Shouren W., Peiquan G., Liying Y., (2008), *Centrifugal precision cast TiAl turbocharger wheel using ceramic mold*, J. Mater. Process. Technol. 204, p 492-497.

[2] Tetsui T., Kobayashi T., Ueno T., Harada H., (2012), *Consideration of the influence of contamination from oxide crucibles on TiAl cast material, and the possibility of achieving low-*

purity TiAl precision cast turbine wheels, Intermetallics 31, p 274-281.

[3] Harding R.A., Wickins M., Wang H., Djambazov G., Pericleous K.A., (2011), *Development of a turbulence-free casting technique for titanium aluminides*, Intermetallics 19, p 805-813.

[4] Fu P.X., Kang X.H., Ma Y.C., Liu K., Li D.Z., Li, Y.Y., (2008), *Centrifugal casting of TiAl exhaust valves*, Intermetallics 16, p 130-138.

[5] Yang L., Chai L.H., Liang Y.F., Zhang Y.W., Bao C.L., Liu S.B., Lin J.P., (2015) *Numerical simulation and experimental verification of gravity and centrifugal investment casting low pressure turbine blades for high Nb-TiAl alloy*, Intermetallics 66, p 149-155.

[6] Aguilar J., Schievenbusch A., Kättlitz O., (2011), *Investment casting technology for production of TiAl low pressure turbine blades - Process engineering and parameter analysis*, Intermetallics 19, p 757-761.

[7] Lapin J., Nazmy M., (2004), *Microstructure and creep properties of a cast intermetallic Ti–46Al–2W–0.5Si alloy for gas turbine applications*, Mater. Sci. Eng. A 380, p 298–307.

[8] Tetsui T., Ono S., (1999), *Endurance and composition and microstructure effects on endurance of TiAl used in turbocharger*, Intermetallics 7, p 689-97.

[9] Tetsui T., (2007), *Development of a second generation TiAl turbocharger,* Mater. Sci. Forum 361-363, p 379-82.

[10] Lapin J., Ondrúš Ľ., Nazmy M., (2002), *Directional solidification of intermetallic Ti–46Al–2W–0.5Si alloy in alumina moulds*, Intermetallics 10, p 1019–1031.

[11] Lapin J., Gabalcova Z., Pelachova, T., (2011), *Effect of Y_2O_3 crucible on contamination of directionally solidified intermetallic Ti-46Al-8Nb alloy*, Intermetallics 19, p 396-403.

[12] Jovanović M.T., Dimčić B., Bobić I., Zec S., Maksimović V., (2005), *Microstructure and mechanical properties of precision cast TiAl turbocharger wheel*, J. Mater. Process. Techn. 167, p 14–21.

[13] Schwaighofer E., Clemens H., Mayer S., Lindemann J., Klose J., Smarsly W., Güther V., (2014), *Microstructural design and mechanical properties of a cast and heat-treated intermetallic multi-phase γ-TiAl based alloy*, Intermetallics 44, p 128-140.

[14] Lapin J., (2003), *Effect of lamellar structure on microhardness and yield stress of directionally solidified intermetallic Ti-46Al-2W-0.5Si alloy*, J. Mater. Sci Lett. 22, p 747– 749.

ISSN 1847-7917

Production line for coating fuel cell membranes

Antonio Mijić [1)]
1) Fakultet Elektrotehnike, Strojarstva i Brodogradnje, Sveučilišta u Splitu
(Faculty of Electrical Engineering, Mechanical Engineering and Naval Architecture, University of Split)
Ruđera Boškovića 32, 21000 Split,
Republic of Croatia

amijic@fesb.hr

Keywords
Fuel cell
Alkaline anion exchange membrane fuel cell
Festo Didactic production line
Catalyst coated membrane
Decal process

Review article

Abstract: This article presents new type of fuel cell, which was analysed in project work at Institute for sustainable energy and mobility in Esslingen, Germany. New type of fuel cell is called Alkaline anion exchange membrane fuel cell (AAEM FC) and it is a combination of both PEM FC and AFC. It represents significant progress in the research and commercialization of fuel cells because it uses nickel as a catalyst material, and not expensive platinum. Different techniques for making catalyst coated membrane (CCM) were analysed, and one of them was determined for implementation in FESTO Didactic production line. Production process and ingredients needed for preparation of catalyst ink, which was used in coating process were described in detail. Certain variables, force, temperature and speed of the process, which determine the quality of coating process, were examined and the interval of values which meets the criteria was established. Quality of produced CCM was analysed under electron microscope and presence of certain chemical elements in coated layer was investigated. Result of coating analysis gave directions for further work on project, and selection of specific structural elements, which will be incorporated in FESTO Didactic production line.

1. Introduction

As world transition towards use of energy from renewable sources goes forwards, role of hydrogen in world energy management grows. Fuel cells are inevitable factor who have giant role in entire transition process, together with solar and wind energy. Fuel cell is electrochemical energy device that combines hydrogen and oxygen to produce electricity, with water and heat as its by-product. It can generate power almost indefinitely, as long as the needed chemicals are supplied. It environment friendly and doesn't cause air pollution. Fact that the electrolysis is a process which can be done in both directions without big losses, positions stored hydrogen in the centre of the new infrastructure development of renewable energy sources. Surplus of produced electricity from intermittent energy resources (wind and solar) can be, by electrolysis, converted into stored hydrogen. When need, that hydrogen can be again converted into electric energy without significant losses. It can be used for balancing the electricity system and be a fuel for vehicles. Membrane electrode assembly (MEA) is the most important part of fuel cell. It is the core component that helps produce electrochemical reaction needed to separate electrons. It consists of a membrane, catalyst layers and gas diffusion layers (GDL) attached on the outer surface of the catalyst layer. One of the ways of applying the catalyst layer for the MEA fabrication is coating catalyst layer on the surface of polymer electrolyte membrane. The result is catalyst-coated membrane (CCM). Conventional electrodes in fuel cells are coated with a platinum catalyst that splits hydrogen fuel into acide hydrogen ions and electrons. Use of the platinum as a catalyst material reperesents the biggest obstacle for fuel cell vehicles mass production. Platinum is very expensive and it's resources on Earth are limited. The yearly amount of produced platinum is not nearly enough for serious mass production of fuel cell vehicles. New reasearches in 2005 resulted in a new type of fuel cell. It is called Alkaline anion exchange membrane fuel cell (AAEM FC) and it is a combination of PEM FC and AFC. The most significant advantage of AAEMFC is that it uses metal catalyst such as nickel. Use of nickel, as catalyst material, instead of expensive platinum, would highly decrease the price of fuell cell and allow its bigger commercialization.

2. Fuel cell basics

In its simplest form, a single fuel cell consists of two electrodes, anode and cathode, with an electrolyte between them.

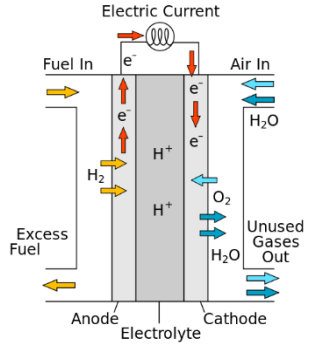

Figure 2.1 Simple scheme of fuel cell [1]

Symbols		**Subscripts**	
T	- Temperature, ºC	*BC*	- Before coating
m	- mass, kg	*AC*	- After coating
F	- Force, N	*AT*	- After transfer
AAEM	- Alkaline anion exchange membrane		
FC	- Fuel cell		
AFC	- Alkaline fuel cell		
PEM FC	- Polymer electron membrane fuel cell		
CCM	- Catalyst coated membrane		
n	- speed, RPM		
RPM	- Rotations per minute		
INEM	- Institute for sustainable energy and mobility at Hochschule Esslingen		

At the anode, hydrogen reacts with the catalyst, creating positively charged ion and a negatively charged electron. The proton then passes through the electrolyte, while the electron travels through a circuit, creating a current. At the cathode, oxygen reacts with the ion and electron, forming water and useful heat.
This single cell generates about 0.4 – 0.9 V, enough to power a single light bulb. When cells are stacked in series the output increases, resulting in fuel cells anywhere from several watts to multiple megawatts.

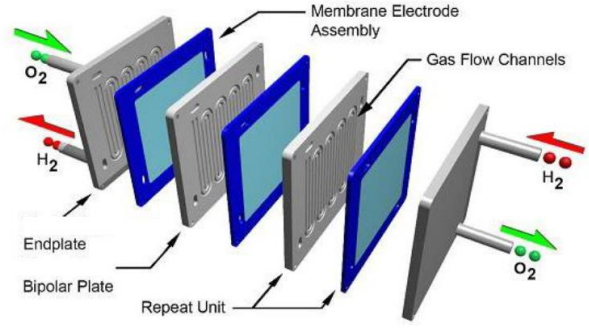

Figure 2.2 Fuel cell stack [2]

Big number of fuel cell types are commercially available today. Each fuel cell has its own unique chemistry, such as different operating temperatures, catalysts, and electrolytes. Fuel cell's operating characteristics help defining its applications, such as power generation, stationary power generationd and power for transportation. Most important part of the fuel cell is MEA (Membrane electrode assmebly). As said, it consists of membrane, catalyst layers and gas diffusion layers.

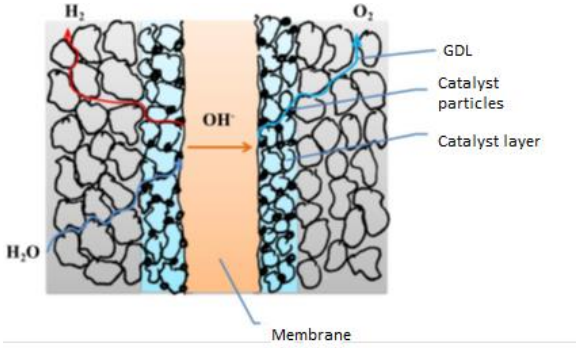

Figure 2.3 Membrane electrode assembly [3]

Catalyst layer is responsible for oxygen reduction, hydrogen oxidation and conduction of electrons. Conventional electrodes in fuel cells are coated with a platinum catalyst that splits hydrogen fuel into acide hydrogen ions and electrons. The main reason for this, is that PEM fuel cell has to use expensive catalyst materials such as platinum. Cheaper metals simply can't withstand the harsh acidic enviroment of the fuel cell. Catalyst layer has to have good chemical stability and electrical conductivity. Platinum is the main reason why fuel cells are so expensive, and because of that fuel cell vehicles price is giant obstacle for fuel cell cars masive production.

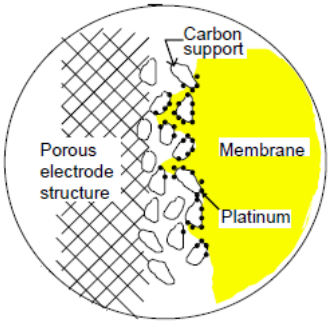

Figure 2.4 Fuel cell stack [4]

On the other hand, platinum resources on Earth are very limited. U.S Gelogical Survey [5] data shows that in 2014 world production of platinum was 161 t and it is less then year before when the production was 183 t. Number of cars produced worldwide in 2014 was around 68.5 millions. Each fuel cell car has around 30-40 grams of platinum [1]. It means that, if each car in world was powered by fuel cell, in 2014 it would need between 2055 and 2740 tonns of platinum only for car industry. It is obviuos that worldwide production of platinum needs to be 10-12 times bigger, just to fullfil the demand for platinum in each fuel cell vehicles, without supplying any other industry in which it is needed.

Within the past few years, reaserches have developed a new type of the fuel cell, which uses new membrane material to operate in alkaline conditions, eliminating the need for an expensive catalyst.

It is called alkaline anion exchange membrane fuel cell (AAEMFC) as combination of PEM FC and AFC. The most significant advantage of AAEMFC is that under alkaline conditions, oxygen reduction reaction kinetics at the cathode are much more facile than in PEM FC, potentially allowing use of non-expensive, non-noble metal catalyst such as silver phthalocyanines for the cathode and nickel for the anode [7].

2.1. Production of CCM

In order to get a highly efficiencient conversion of electrical energy into chemical energy and vice versa, processes inside MEA need to be well adjusted by optimizing the materials and production processes used for MEA preparation. The catalyst coated membrane (CCM) technique uses transfer foils as a substrate. The MEA is prepared by removing the transfer foils after hot pressing and assembling GDL's

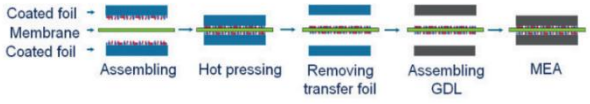

Figure 2.5 The CMM technique [6]

Goal is to have the smallest possible catalyst particles distibuted homogenously on the entire membrane surface. In principle, smaller the particles , better the catalyst surface.

Ideal CCM should have:

- Porous structure
- Small catalyst particles
- Low catalyst loading
- Large catalytic surface
- Direct contact of all catalyst particles both to the membrane as well as to the GDL

Thickness of the catalyst layer should be between 5-20 microns. There are many known processes and techniques for coating the polymer membrane with the catalyst material.

Some of them are calendering, sputter deposition, screen printing, spraying, laser printing, film-drawing and many others. In this work spraying method was used after which came decal method with which catalyst layer was transfered to anion polymer membrane.

2.2. Decal method

Decal method is a method in which a polymer membrane is catalyst coated indirectly. Process starts with spraying the catalyst ink on a Teflon foil or Teflon film. After applying the catalyst, the solvents have to evaporatte, so the Teflon is exposed to a heating process for approximately half an hour at room temperature at which the ink solidifies. After that teflon is pressed on the membrane with supply of heat. After pressing, substrate is removed and result is catalyst coated membrane. Process is good if no ink has been left on the substrate. Temperature in this process should be less than 180 ºC beacuse on higher temperatures teflon substrate could be melted.

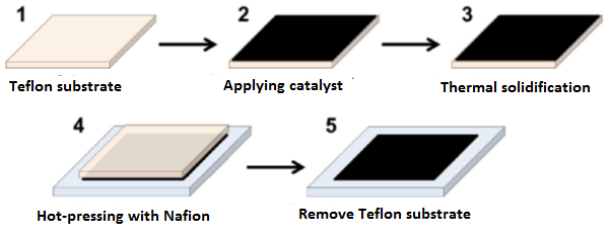

Figure 2.5 Decal method [8]

Because Teflon has a great temperature resistence an low surface energy the ink is transferred particulary well. After the pressing, the Teflon is removed, and result is CCM.

3. Production line

Fuel cell production line at INEM was provided by FESTO Didactic. Production line is an MPS system that consists of four transfer sections which are perpendicular to each other.

The transfer systems (Fig. 3.2) are driven by electric motors. They are square connected to each other and mounted on a roller table. The control of the system is handled by two coupled Siemens S7 1500 PLC units. The system has a great number of sensors and acutataors for usage, and it is managed via Siemens Step-V13 software, which is installed on a laptop at INEM.

Figure 3.1 Fuel cell production line at INEM

Figure 3.2 Transfer system unit [9]

On the production line running driving units can be placed. The driving units are work-piece carriers which are supporting the membrane. implemented in the transfer system. Coating process, in which the catalyst material is applied to the both sides of the membrane, can be divided into maximum four stages of production. With the conlucsions from the previous work and experiments [3] spraying method was chosen as the most suitable one for our production line.

3.1. CCM production through each work station

When the ink is applied directly on the membrane, membrane suffers big deformations because of it's hydrophilic characteristics. During the spraying, membrane swells beacuse of the water content in the ink (Fig. 3.3, left). After that, during the drying process membrane contracts, which leads to the further deformations (Fig. 3.3 , right).

Figure 3.3 Membrane swelling and contracting [3]

Indirect membrane coating is presented as one of the solution against membrane deforming in the coating process. It follows the Decal process principle. Starting with the station 1, two workpiece carriers, one going after another, are horizontally holding the Teflon plate or Teflon film which is then coated on the one side. After coating, they come to the station 2, when they are subjected to drying. On the station 3 they are mounted as a "sandwich", centrally one above the another with the polymer membrane between them, in the way that their coated surface stands on inner side, touching the membrane. The installation has to be done manually, because automation would be to complex. Fixed on the special holder, they come together to the station 4, on which they are slowly pressed by a roller system or regullar surface pressing with application of force and supply of the heat. As a result, a CCM should be formed, without any defomations.

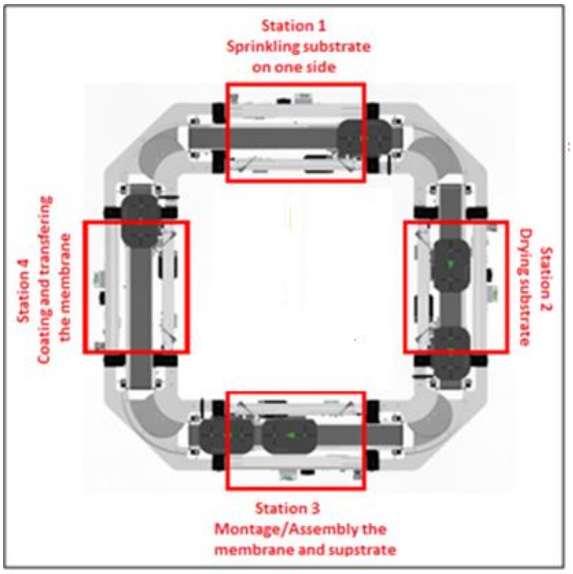

Figure 3.4 Indirect coating process presented on each four stations of production line

3.2. Testing platform

Station 4 requires greatest attention and it is the most complicated station on this production line. After the assembly of the "sandwich" (polymer membrane fixed between two teflon foils sprayed with catalyst ink on one

side), a transfer of the catalyst layer to the polymer membrane is following. It should be done by roller pressing or complete surface pressing of the teflon foils on the polymer membrane with the supply of heat.

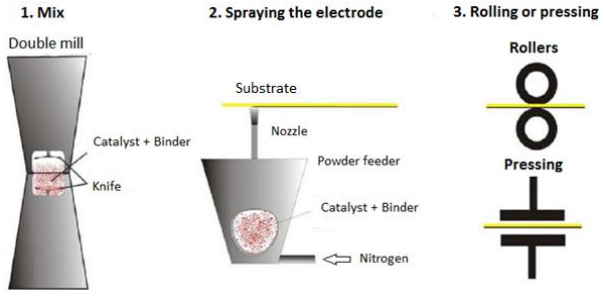

Figure 3.5 Spray and pressing process for creating CCM [3]

Roller pressing is much better solution than normal pressing of the complete surface all-together, because smaller force can be used when the force is applied only in one line, and not on entire surface of the membrane. Forces and temperatures for pressing are variable and they are known only in a certain range. In the following chapter, experiments are about to be made in order to deterimine range of the temperatures and forces which could be used for FESTO Didactic production line. For this purpose, a testing station was first designed in SOLIDWORKS and then built at INEM.

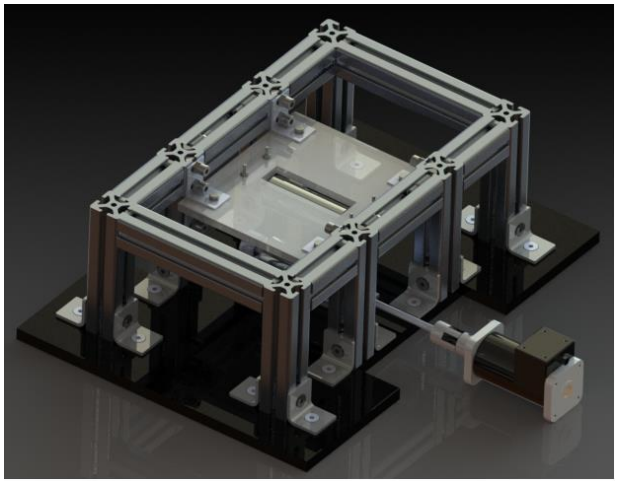

Figure 3.6 Testing platform

The platform is made of aluminium ITEM profiles, and it is fixed on a hard PVC plate. On the inner sides, where sliders come, it is covered with a thin, smooth teflon film. It provides easy sliding up and down for an upper Nylon plate, on which the sliders are fixed. From the down side of the plate, a roller is fixed on the bearings. Opposite of it, down roller is fixed on the down plate, and it can not be moved in any direction. Both rollers need to be parallel to each other and positioned in the same plane. If this condition is not fulfilled, the catalyst ink will not be equaily distributed on the both sides of mebrane. Also, the surface of the rollers have to be polished. Down roller has one shaft longer than other, beacuse that shaft is connected to low RPM electromotor with a spider coupler. Electromotor endures the slow rotation of the roller, which slowly guides the membrane through the transfer process. This platform serves only for the purpose of testing the temperatures, rotating speed and forces in pressing process, and after the results, it should be redesigned in a way that it can be incorporated in the production line as one of the following stations.

4. Production process

4.1. Preparation of catalyst ink

The catalyst ink is composed of following components:

- Carbon powder Vulcan XC-72 (2%)
- Nickel powder (2%)
- Ionomer soultion (20%)
- Water (26.5%)
- 1-Propanol (49.5%)

The percentage in the perentheses represent the weight ratio of the component in the mixture. Carbon powder Vulcan XC.72 (Fig. 4.1) provides excellent conductivity, has good chemical and physical cleanliness and good processability. It is used as a filler, and beacuse of it's spherical surface, it enlarges the catalytically active surface.

Figure 4.1 Vulcan XC-72

Nickel powder is used as a catalyst, but in the following experiments it will be replaced with the Vulcan XC-72 in the same weight ratio. The large number of the conducted experiments will be in this case completed with the placebo ink, in order to save the valuable catalyst material.

Ionomer solution is an important component of the ink. It causes a slight-partial dissolution of the membrane and the inomer particles lead to cross-linking of solids on the membrane, and consequently, to a higher number of the

active sites. If the catalyst ink was made without the ionomer solution the carbon power would have no liability and it would fall off the membrane when touched.

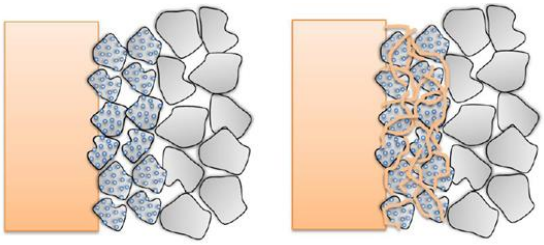

Figure 4.2 Importance of ionomer solution in mixture [3]

The solution (Fig. 5.5) is made of 10% shreded fumion® FAA-3-ionomer anion exchange ionomer film (Fig. 5.6, left) from the firm Fumatech and 90% of the 1-propanol, 99+% (Fig.5 .6, right).

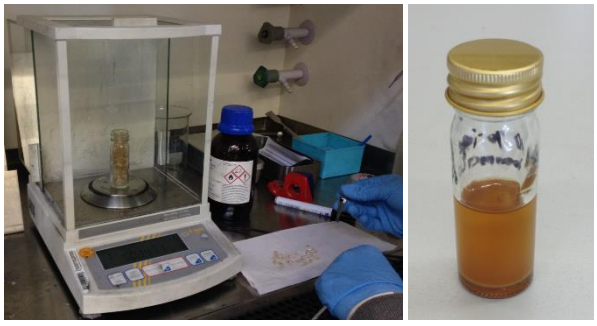

Figure 4.3 Production of ionomer solution at INEM

The film is cut in a tiny pieces and placed in a little container, after which the 1-propanol is added. Two components are mixed together using a disperser in order to form a homogenous dispersion. The resulting mixture can be used in experiments for the next two months. After this time period the soultion becomes too thick and it ruins the viscosity of the ink

Figure 4.4 Left: 1-Poropanol; right: fumion® FAA-3-ionomer film at INEM

4.2. Production of catalyst ink

It was determined that for the following experiments 12 g of ink will be made. The ink is produced adding the components in the following order and weight in little glass container:

- Vulcan XC-72 (4%) → m = 0.48 g
- Water (26.5%) → m = 3.18 g
- Ionomer soultion (20%) → m = 2.4 g
- 1-Propanol (49.5%) → m = 5.94 g

∑ m = 12 g

The weight of each component has to be carefully added in order to get a quality ink.

After adding components, the ink is placed in dispersing device (Fig 5.8) in order to get a homogenous ink. The dispersion of the ink is made on 6000 RPMs for 30 minutes. Total mass of 12 g was chosen because that level of ink inside of the little glass container will not lead to overflow of ink from the container during the dispersion process.

Figure 4.5 Dispersion of the ink at INEM

Total mass of the ink can be produced in bigger number if needed, respecting default weight ratios. Any other change in weight ratios of the components inside the ink will lead to getting too thin or too thick catalyst ink, which will not be able to fit closely on the Teflon foil surface.

Figure 4.6 Catalyst ink made at INEM

4.3. Spraying Teflon substrate and assembly for the transfer process

For Teflon substrate, 3x3m long and 0.1 mm thick role of PTFE virginal "Folie 0.10" was ordered from the firm HighTechflon Technische Gewebe. Two squares, 70x70 mm, had to be cut out for each experiment. Manufacturer guarantees tensile strength higher than 40 N/mm^2 and density 2.18 g/cm^3.

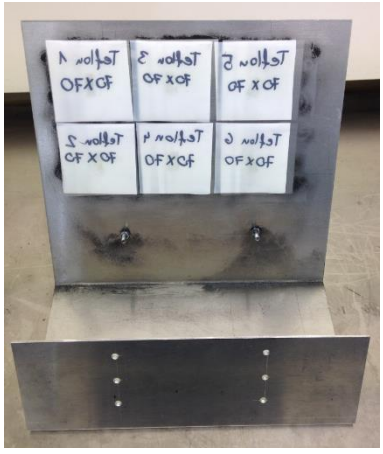

Figure 4.7 Teflon foils ready for spraying

After cutting, each teflon square is weighed and than glued with the tape to the metal plate on which they will be sprayed with prepared catalyst ink. Spraying is carried out at the pressure of 3 bars by spray gun and in the direction shown in Fig.4.8.

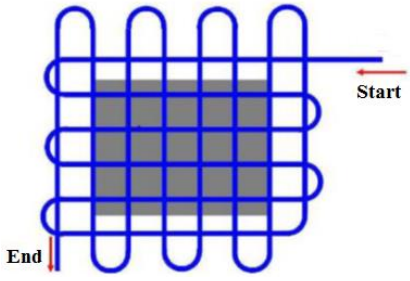

Figure 4.8 Spraying directions

After Teflon foils are sprayed they should be left on a room temperature for at least 30 minutes for ink to dry.

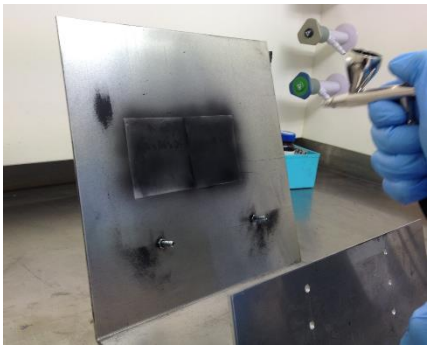

Figure 4.9 Spraying Teflon foils at INEM

After drying, Teflon foils are carefully taken of the plate, and than again weighed on weight scale in order to determine the mass of the ink which was placed on the foil.

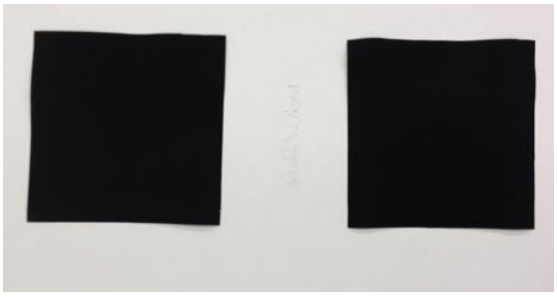

Figure 4.10 Teflon foils covered with layer of catalyst ink

For this experiment an anion-polymer membrane, fumapem® FAA-3 from FuMa-tech is used as an electrolyte. According to the manufacturer, membrane is stable at working temperatures up to 60° C and strong humidification in a pH range between 7-14, thus meets the operating conditions in AEM FC. For each experiment 80x80 mm square was cut from the role. During one of the spraying processes, importance of ionomer solution was demonstrated (Fig 4.11). Difference between needed weight of ionomer solution (2.4 grams) and one that was added to the mixture (2.377 gram) was less than 1%, but the result was very bad. Catalyst ink couldn't stick well enough to the Teflon foil so it was falling off.

Figure 4.11 Catalyst ink without enough ionomer solution

Final step is the assembly of the two Teflon substrates and anion-polymer membrane. Polymer membrane is placed on the table and on its upper side Teflon substrate is glued with thin Teflon tape to the polymer membrane in a way that the coated side is in direct contact with membrane. The same process is repeated on the other side with second Teflon substrate after turning. Result (Fig.5.14) is "sandwich" made of two coated Teflon substrates with polymer membrane in the middle.
Experiments have shown, that the best assembly is when there is tape only on one side, and the other side left free so that air can't be held between foils and membrane.

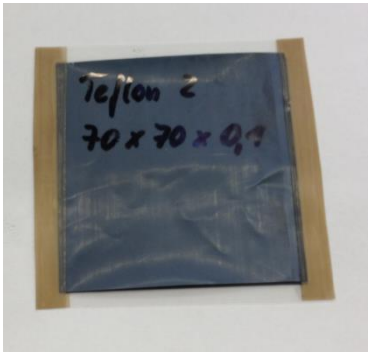

Figure 4.12 Assembly ready for testing

5. Experiments and results

Final goal of following experiments was to determine working presssure (forces), temperature and speed of the process in which the catalyst ink from the Teflon substrate should be transfered to the polymer membrane. Following the results of the previous research, it was easier to determine interval of theese values. Since all of these three factors determine the quality of the transfered process they need to be varied in each experiment in order to find which combination is the best. Speed in this process was easily determined comparing the speeds in similar coating processes with ours. Speed was achieved using low RPM electromotor. In these experiments pressure was achieved by placing weights of different size and weight on the upper sliding platform plate. Required temperature of the rollers was achieved by constant heating with 2 kW powerful hot air dryer. Every few minutes temperature of the rollers were measured with digital thermometar, on each side, until desired temperature was achived. It was also important to meassure distribution of the heat over the complete surface of both rollers in order to have approximately same temperature in each point.

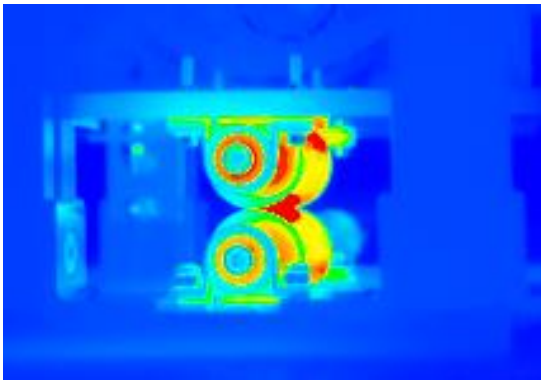

Figure 5.1 Heat distribution on the rollers

5.1. First experiment

For the first experiments, speed and temperature are constant, and the pressure (force) varied. Speed of the process is set to 0.23 m/min, and the temperature is set to 120 ˚C. For each experiment, teflon foils were weight before coating, after coating, and after transfer process, in order to determine the percentage of transfered ink from teflon membrane to polymer membrane. Percentage of the transfered ink is calculated by Formula 5.1

$$Percentage = \frac{m_{AC} - m_{AT}}{m_{AC} - m_{BC}} \qquad (5.1)$$

Table 5.1 Result for various forces

v = 0.23 m/min, T = 120 ºC , F		**275 N**	**250 N**	**225 N**
Substrate 1	m_{BC} [g]	1.1364	1.1288	1.1309
	m_{AC} [g]	1.1631	1.1534	1.1582
	m_{AT} [g]	1.1566	1.1492	1.1552
	Perc.[%]	**24.2%**	**17.3%**	**10.9%**
Substrate 2	m_{BC} [g]	1.1432	1.1376	1.1299
	m_{AC} [g]	1.1713	1.1634	1.1562
	m_{AT} [g]	1.1652	1.1592	1.1540
	Perc. [%]	**21.7%**	**16.2%**	**8.3%**

It is easy to notice that the percentage of transfered ink gets higher with higher force amount . The percentage of transfered ink is always smaller on the down roller, because its temperature is always lower than on the upper roller. This was detected with thermal camera. Fig.5.2 shows polymer membrane and both teflon foils after transfer, for each experiment. First row is result of 275 N force, second is with 225 N, and the last one is made with 250 N. First column from the left shows state of polymer membrane after transfer. Second one shows teflon substrate number two, and the third one shows teflon substrate nuumber one. Results show that the transfer of the ink were not successful. Membrane was not coated and more important, ink was not dispersed equally on both sides. For this reason, second experiment was made with bigger temperature and force, and repeated twice.

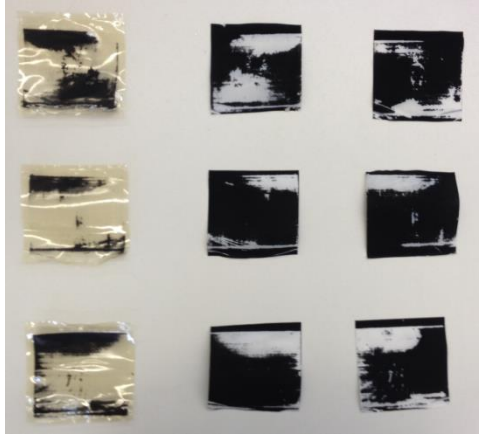

Figure 5.2 Results of the first experiment

5.2. Second experiment

Following the conlusions drawn from first experiment, force and speed were set on constant value for second experiment and temperature varied. First try, with temperature at 100˚C and 300N force, went bad, so it was decided that the temperature should be much higher. Force was set on 300 N of weight, and the speed was left on 0.23 m/min for entire process.

Table 5.2 Result for various temperatures

v = 0.23 m/min, F=300 N, T		150 ºC	160 ºC
Substrate 1	m_{BC} [g]	1.1420	1.1410
	m_{AC} [g]	1.1779	1.1864
	m_{AT} [g]	1.1621	1.1621
	Perc.[%]	**44%**	**53.5%**
Substrate 2	m_{BC} [g]	1.1488	1.1435
	m_{AC} [g]	1.1852	1.1889
	m_{AT} [g]	1.1705	1.1654
	Perc. [%]	**40.3%**	**51.7%**

Teflon substrates and polymer membrane are shown in following order: first row is transfer at 150 ºC, and second one is at 160 ºC. Teflon substrates number two are positioned on left side, polymer membrane is in the centre, an the teflon substrates number one are on the right side.

Figure 5.3 Results of the second experiment

This transfer gave much better results than previous one, and the surface area of the polymer membrane covered with ink was in the best case doubled. In this case also, teflon substrates which were on the down sides had worse percentage of transfered ink, which was result of a few degrees lower temperature than the upper one. Problems with the dispersion of the ink equally on both sides is still present, but in smaller range. It was also noticed, that the start of transfer process was excellent, but with time transfer got worse. One of the problems could be that the temperature was decreasing faster during the process because more energy was given into ink transfer process. Measurments showed that during the process temperature of the rollers deacreases for 15-20 ºC beacuse that energy is given in to the transfer process.

5.3. Third experiment

In third experiment temperature, force and speed values were constant. Idea was to see if transfer results will be approximately the same if we repeat two identical experiments. Important thing was to determine if the problems with non-homogeneous dispersion of the ink on both sides of the membrane were due to low temperature and pressure, or if it was due to unequal, imperfect contact of two rollers with non-ideal smooth surface. Surface of the rollers will never be perfect, but it should be good enough to get a quality ink transfer.

Table 5.3 Result for two experiments with constant variables

v = 0.23 m/min, F=400 N, T= 160 ºC		Experiment 1	Experiment 2
Substrate 1	m_{BC} [g]	1.1578	1.1379
	m_{AC} [g]	1.2033	1.1828
	m_{AT} [g]	1.1685	1.1508
	Perc.[%]	**76.5%**	**71.2%**
Substrate 2	m_{BC} [g]	1.1382	1.1338
	m_{AC} [g]	1.1839	1.1573
	m_{AT} [g]	1.1503	1.1412
	Perc. [%]	**73.5%**	**68.5%**

This experiment gave excellent results. Polymer membrane was coated in a high percentage and ink was homogenously dispersed. If the start of the process was excluded from weighing coating percentage would be much higher. Start of the process is always bad because of hand maniuplation while positioning membrane between the rollers. Transfer actually begins a few milimeters after. It can been seen, that second experiments had worse results, but that was only because the process started later due to imperfections of process being done by hand and not by the machine.

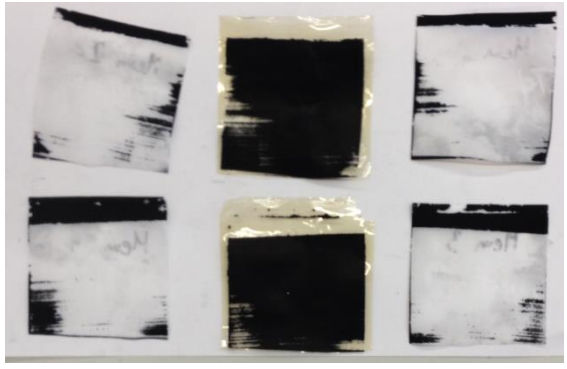

Figure 5.4 Constant force, temperature and speed – results

5.4. Fourth experiment

Fourth experiment shows difference in transfer process when speed is varied. Idea was to determine minimal speed for successful transfer. Force was held on 400 N, and the temperature was 160 ºC. Results for 0.23 m/min speed were already known, so the process was repeated for 0.029 m/min, 0.35 m/min and for 0.7 m/min speed. Goal was to determine inside which speed interval values process gave the best results.

Table 5.4 Result for various speed

T = 160 ºC , F=400 N, v		**0.07 m/min**	**0.035 m/min**	**0.029 m/min**
Substrate 1	m_{BC} [g]	1.1350	1.1066	1.0993
	m_{AC} [g]	1.1715	1.2891	1.1139
	m_{AT} [g]	1.1525	1.1204	1.1021
	Perc.[%]	**52.1%**	**92.4%**	**80.8%**
Substrate 2	m_{BC} [g]	1.1367	1.1119	1.0989
	m_{AC} [g]	1.1719	1.1357	1.1122
	m_{AT} [g]	1.1543	1.1147	1.1018
	Perc. [%]	**50%**	**88.2%**	**78.2%**

Results show that speed interval between 0.035 m/min and 0.029 m/min is ideal for good transfer process. It is important to mention that the results in middle coulmn are made with different approach. Percentage of covered area is much higher, but that is only because transfer process started immediately, and not after few milimeters, as usual. This resulted with deformed polymer membrane at this area, and it shows this was not good approach.

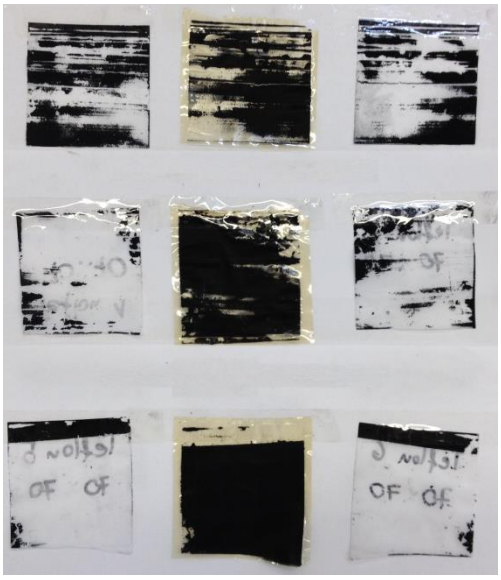

Figure 5.5 Results for constant speed

However, after the start, transfer process was going smoothly and large area of membrane was covered. Teflon substrates and polymer membrane are shown on Fig. 5.18. in following order: first row is transfer at 0.07 m/min, second one is at 0.035 m/min and third one is at 0.029 m/min. Teflon substrates number one are positioned on left side, polymer membrane is in the centre, and the teflon substrates number two are on the right side. For 0.029 m/min process speed percentage of covered are in Table 5.4 doesn't show real image. If start of the process was excluded, pecentage of covered area would be more than 95%.

5.5. Final results

Experiments mentioned above are just a small part of all experiments that were carried out during two months of work, with an intetion to obtain optimum procces condtions. Process is to complex and all parametars are correlated. There is not a single solution, but a certain interval of values within each parameter can be changed without ruining the quality of coated process. Our best results were get by comparing results of all experiments that we made. Conclusion from all of them was that, for good transfer process of catalyst ink form Teflon foils to the Polymer membrane, required parametars have to be inside following intervals:

- Force → between 35- 40 kg
- Temperature → between 150 - 170 ºC
- Speed → between 0.035 - 0.029 m/min

Figure 5.6 Successful catalyst transfer

Fig.5.19. shows the results of successful transfer processes, which were obtained using above specified parameters in recommended intervals. The success percentage of each transfer exceeds 95% and the rest 5%

can be taken as a result of imperfections of the process due to manual manipulation.

5.6. Microscope analysis

After transfer process, coated membrane was subjected to microscopic analysis of surface and cross section. This analysis was also performed on Hochschule Esslingen on electron microsope from the firm Oxford Instruments. Since coated polymer membrane acts like a rubber when it breaks, it should be held in liquid nitrogen for 5 minutes before taped on metal plate. Liquid nitrogen increases stiffnes of the membrane, so when breaking, polymer membrane has a sharp edge, which is then good enough for cross-section analysis and to determine the thickness of coated layer.

Also, in order to get good results on microscope, polymer membrane need to be gold-plated through sputter depostion with 10 nm thick layer of gold, which prevents electrocharging. This layer can be measured, but not seen. Coated membrane surface is shown on following figures.

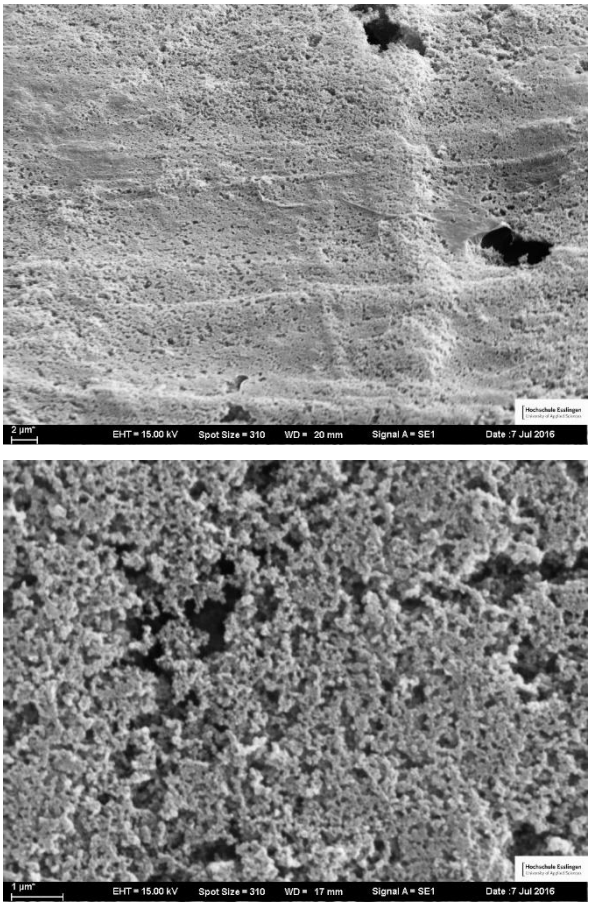

Figure 5.7 Microscope surface analysis in different scales

It is important to mention that only small part of the membrane (2x2 cm), which was completely coated, was cut out of the entire membrane and subjected to analysis. On the first picture it is easy to notice imperfection of the roller surfaces by following coating traces. Also, uncovered areas were not visible when coated, but however, microscopic analysis shows that not all areas are not completely covered.

More important than surface analysis was the analysis of cross-section area, in order to determine the thickness of coated layer. In chapter 3 was mentioned that any layer thickness between 5-20 µm is considered good.

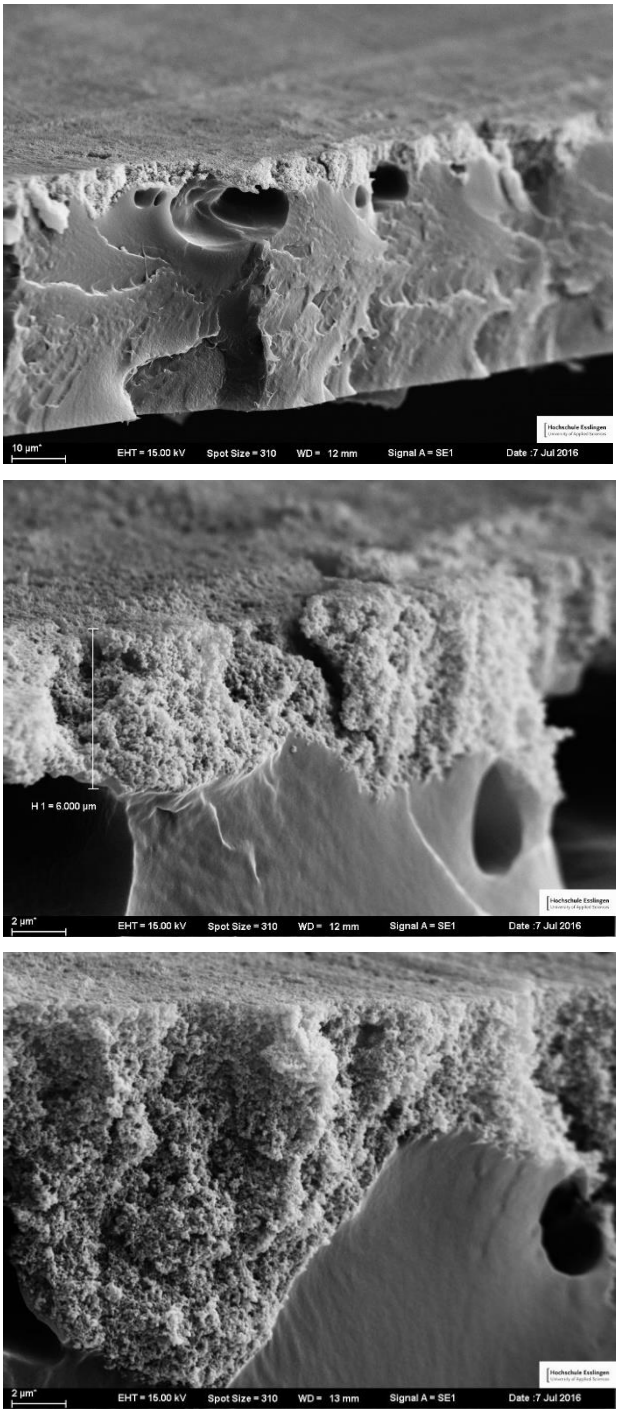

Figure 5.8 Microscope cross-section analysis in different scales

Analysis shows that thickness of coated layer is more than minimum value, which means that transfer was successful. Also, on second picture it can been seen that upper part of the membrane, which has been melted, made a solid connection with the catalyst ink.
Ink structure is excellent, extremely homogenous and without any iregularities. Expected, coated layer thickness is different along entire cross section. On some parts, membrane melted too much, and air-gaps were created. It indicates, that temperature has to be strictly controled on one level through entire roller surface and to avoid temperatures above 170 ºC.
Last thing that was determined with microscope analysis was the presence of certain chemical elements on various points of coated layer.

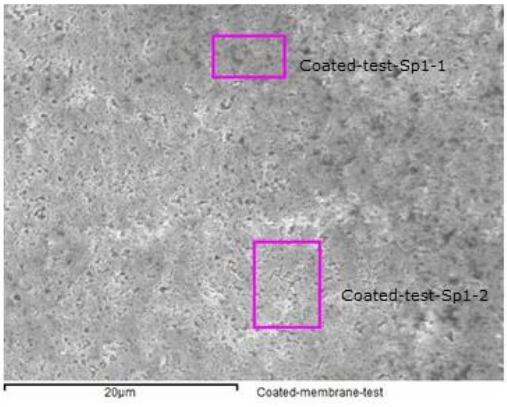

Figure 5.9 Selection of different covered areas for analysis

This analysis indicates process level homogenity, and can also show possible impurities in layer structure, caused mostly by dissolution of fluoride from Teflon foils.

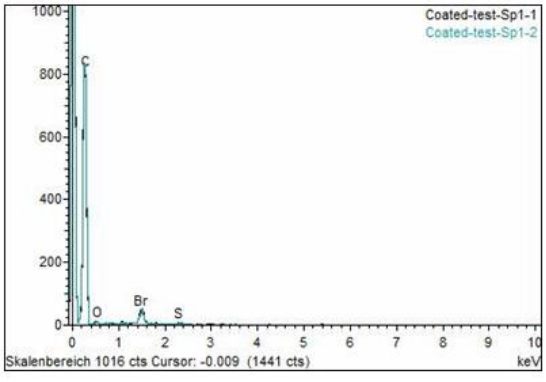

Figure 5.10 Chemical elements presence

Expected, carbon is present in the highest percentage. After carbon comes brom, which is present because polymer membrane usually comes in brominated form. Oxygen and sulfur come in a very low percentage. Process meets all regulations beacuse on both arbitrarily selected areas, shares of the same element are almost identical which indicates that the transfer of ink was good and the coated layer is homogenous. Also, there is no percentage of fluoride present which means that the Teflon foils were not dissolved by increased heat.

6. Conclusion

Main task of this work was to determine ceratin interval of temperature, force and process speed values for coating anion polymer membrane with catalyst layer and producing CCM. Test platform was made only for purpose of these experiments, and after getting results it should be redesigned in a way that it can be implemented in FESTO Didactic production line as Station 4. Design and production of test platform were carried out, trying to get as close as it can be to the ideal values of surface roughness, parallelity and planarity of rollers. However, certain deviations were easily noticed and process was far from ideal. Heating of rollers was the biggest problem, becouse it was carried out by hairdryer until needed temperature, and after that, when source of heat was removed process started. Consequently, temperature of the roller surface was not evenly distributed and during the process it was constantly decreasing. This can be seen on the experiment results, where one side of the membrane, which was in contact with down roller, always had a lower percentage of transfered ink. Also, as the proces was moving forward, covered area of membrane was getting smaller, which was result of temperature decrease. Start of the process was always bad. Top of the membrane had to be always positioned by hand on down roller, and after that upper roler was pressed on them after which came the certain weight. However, all these imperfections gave good results and interval of values in which process gave good quality of covered membrane layer was determined. These values led to the selection of quality process elements which will enable much better transfer process. First of them are electrically heated rollers from the firm AR-WALZEN, which enable constant heating of the rollers and maintain the required temperature throughout the entire process. Also, surface roughness and paralelity of the rollers will be much better and only this change will increase quality of the transfer process greately. It will enable equal ink transfer along entire membrane surface and coated area will be the same on both sides of the membrane.

Figure 6.1 Electrically heated rollers [6]

Because of the better design appearance and simplicity of process control management, force will be achieved by pressing upper roller with push cylinders to the down

roller. By redesign and implementation of existing platform in production line there will be no need for placing additional electromotor which would rotate rollers, but they will be directly connected with drive system of production line.

REFERENCES

[1] Fuel cells basics, http://www.fuelcells.org/uploads/FuelCellTypes.jpg , from Internet, 7.April.2016

[2] Frano Barbir: "*Obnovljivi izvori energije i odrzivi razvoj*", FESB teaching materials, 1.March.2015

[3] Waldemar Schneider: "*Anion Exchange Membrane Electrolysis* ", Master Thesis, 2012

[4] Frano Barbir: " *Fuel cells* ", FESB teaching materials, 29.October.2014

[5] U.S. Geological survey: "*World annual platinum production 2014*", http://minerals.usgs.gov/minerals/pubs/commodity/platinum/mcs-2015-plati.pdf, from Internet, 8.April.2016

[6] AR-WALZEN: "Heizwalzen", http://www.ar-walzen.de/deutsch/heizwalzen.html, from internet, 10.July.2016

[7] Julich: "*Development and Manufacturing of Membrane Electrode Assemblies for Polymer Electrolyte Water Electrolysis and Fuel Cells*, http://www.fz-juelich.de/SharedDocs/Downloads/IEK/IEK-3/Flyer/Flyer_DMFC-Fertigungstechnik_2014%20(E).pdf?__blob=publicationFile, From Internet, 19.May.2016

[8] K.Frohlich: " *Decal Prozecc zur Herstellung katalysatorbeschichteter Membranen fur PEM-Brennstoffzellen* ",Phd Thesis, October.2014

[9] Festo Didactic, http://www.festo-didactic.com/int-en/learning-systems/mps-the-modular-production-system/mps-transfer-system/mps-transfer-system-get-moving-with-mechatronics-and-electronics-training.htm?fbid=aW50LmVuLjU1Ny4xNy4xOC4xMTIzLjY4Mjc, from internet, 10.Juni.2016.

ISSN 1847-7917

Case Study of Croatian manufacturing industry: Industry 4.0 Providers or Users?

Marko MLADINEO[1)]***, Djerdj HORVAT***[2)]***, Ivica VEZA***[1)]

1) University of Split, Faculty of Electrical Engineering, Mechanical Engineering and Naval Architecture
Sveučilište u Splitu, Fakultet elektrotehnike, strojarstva i brodogradnje
R. Boskovica 32, 21000 Split, **Croatia**

2) Fraunhofer Institute for Systems and Innovation Research ISI
Fraunhofer institut za istraživanje sustava i inovacije ISI
Breslauer Strasse 48, 76139 Karlsruhe, **Germany**

mmladine@fesb.hr
djerdj.horvat@isi.fraunhofer.de
iveza@fesb.hr

Keywords
Smart Enterprise
Industry 4.0
Manufacturing System

Ključne riječi
Pametno poduzeće
Industrija 4.0
Proizvodni sustav

Preliminary notes

Abstract: The empirical research within project Innovative Smart Enterprise (INSENT) was made to improve scientific understanding of the current state of Croatian manufacturing industry. It was enterprise-level research on technological and non-technological processes, and organizational innovation of manufacturing enterprises. The aim was to understand how manufacturing enterprise in Croatia acquire new manufacturing technologies, new ICT, new organizational concepts, new products and production-related services, and other demands related to Industry 4.0. The results showed that most of the enterprises of Croatian manufacturing industry are closer to 2nd industrial generation than to 3rd industrial generation, and, therefore, far away from entrance into 4th industrial generation. This paper deals with analysis of possible paths for Croatian enterprises toward Industry 4.0. Research is analyzing the possibility of being Industry 4.0 provider without becoming Industry 4.0 user. It is a specific hypothesis linked to Croatian manufacturing industry, and presented in this paper.

Prethodno priopćenje

Sažetak: U sklopu projekta Inovativno pametno poduzeće (Innovative Smart Enterprise – INSENT) provedeno je empirijsko istraživanje da bi se unaprijedilo znanstveno razumijevanje trenutnog stanja hrvatske prerađivačke industrije. Istraživanje je provedeno na razini poduzeća o tehnološkim i ne-tehnološkim procesima, i organizacijskoj inovativnosti prerađivačkog poduzeća. Cilj je bio razumjeti na koji način prerađivačka poduzeća u Hrvatskoj prisvajaju nove proizvodne tehnologije, novu informacijsko-komunikacijsku tehnologiju, nove organizacijske koncepte, nove proizvode i uz njih vezane usluge, i ostale zahtjeve vezane uz Industriju 4.0. Rezultati su pokazali da je većina poduzeća Hrvatske prerađivačke industrije bliže 2. industrijskoj generaciji, nego 3. industrijskoj generaciji, i samim time daleko od ulaska u 4. industrijsku generaciju. Ovaj članak analizira moguće puteve hrvatskih poduzeća prema Industriji 4.0. Istraživanje analizira mogućnost da se bude dobavljač za Industriju 4.0, a da se isto vrijeme ne bude njen korisnik. To je specifična hipoteza vezana uz hrvatsku prerađivačku industriju i predstavljena je u ovom članku.

1. Introduction

Half of decade of global economic crisis had a significant impact on European economy, especially on European manufacturing industry. The dramatic drop in customer demand has led to reduced working hours, layoffs of workers and idle factories. The situation has been even worse in weaker economies, like Croatian economy [1]. This paper focuses on case study of Croatian manufacturing enterprises, which are cornerstone of Croatian economy.

Croatian economy is still burdened by previous economic system inherited anomalies and some transitional problems. Low productivity is additionally burdened by a great number of employees and obsolete technology. Insufficiently educated and unskilled personnel, particularly in the production and management fields, are decreasing competitiveness necessary for survival in the global market [2]. There is a predominant lack of products and services which are demanded by developed markets. Grey economy is growing, encouraged by infirm justice and unstable tax administering during recent years. However, public property and enterprises privatization, which is a sine qua non prerequisite for sound market basis establishment and prospective growth, has not been successfully implemented. Most public enterprises completely disappeared in the privatization process, and those that managed to survive, have undergone numerous recovery programs or have gone into liquidation. In these conditions, small and medium-sized enterprises development could not have

support by big industrial systems. Therefore, economic development has been mostly turned to the service sector, especially tourism.

There is the lack of a unique and commonly agreed economic strategy at the national level. One of the primary strategic goals is to develop a competitive, diversified, technologically advanced and environmentally sustainable economy that will be oriented to enhance the living standard of the local population. Consequently, such clearly defined goals require a radical change of the existing settings, in which an inadequately competitive economy still prevails.

The main question is how to detect competitive advantages of the manufacturing industry and therefore achieve a higher level of export competitiveness in the regional and the international markets, like the market of the European Union [2]. Croatia's manufacturing industry participates in a large proportion in the gross domestic product, employing a large proportion of the entire workforce, is one of the greatest generators of tax revenues in the country, and is one of the most propulsive export industrial branches of the economy of the Republic of Croatia [1]. Generally speaking, during the transition process there was no industrial development whatsoever, particularly there were no new technologies or new products introduced. Cooperation between economy and science was rather weak, and the accompanying infrastructure required to support technological development and innovations was developing rather sluggishly. Taking all this into consideration, a basic prerequisite for making a turnaround to a successful economic development in Croatia is to restructure its economy.

In order to set things in motion, the following priorities have been defined:

- to strengthen cooperation between research institutions and entrepreneurship that will enable new technologies implementation and technologically innovative products production,
- to restructure organization in traditional manufacturing sectors, agriculture, fishing industry and tourism, in order to achieve bigger competitiveness,
- to support export-oriented, specialized production of products and services with higher added value,
- to encourage regional and inter-regional integration processes (including transnational ones) and to support cluster organizations in order to strengthen overall synergetic impact in the sectors and between them,
- to ensure business, entrepreneurial and managing training,
- to increase employment opportunities.

In near future, the main aims for Croatian enterprise will be flexibility, agility and scalability, in order to survive turbulences caused by erratic customer behavior and market turbulences on a large scale.

Furthermore, every global manufacturer has its unique manufacturing or production system (Toyota, Daimler, Bosch, etc), and some countries are developing their own production platforms, like Germany – Industry 4.0. Model is aligned with their vision, strategy, values and culture. Republic of Croatia hasn't developed its own model or platform of manufacturing enterprise. Therefore, project Innovative Smart Enterprise (INSENT) was launched in 2014 aiming to develop Croatian model of Innovative Smart Enterprise (HR-ISE model) by acquiring state-of-the-art organizational principles, like Lean Management, and organizational-technical platforms, like Industry 4.0.

In this paper, part of INSENT project about position of Croatian manufacturing enterprises regarding Industry 4.0, is presented and some hypotheses are discussed.

2. Analysis of the current state of Croatian manufacturing enterprises

2.1. Project Innovative Smart Enterprise

Croatian Science Foundation (CSF) is financing the project Innovative Smart Enterprise (INSENT) according to the priority to strengthen cooperation between research institutions and entrepreneurship.

Manufacturing enterprises are in the main focus of this project. Vision of Innovative Smart Enterprise for with long term sustainability can be summarized into following features [2]: Lean, Flexible, Agile, Efficient, Responsive, Information enabled, Predictive, and Safe.

The main objective of this project is to develop Croatian model of Innovative Smart Enterprise (HR-ISE model). The aim is to develop model for regional fit, i.e. to harmonize Innovative Smart Enterprise model with specific regional way of thinking, manufacturing and organizational tradition and specific education. Its results should help Croatian enterprises to bridge the gap between their competencies and EU enterprises' competencies and capabilities. Following objectives are crucial to achieve main objective of this project:

- Objective 1: Profound research to describe the current state of the Croatian manufacturing enterprise. It represents answer to the question: "Where is Croatian manufacturing industry?"
- Objective 2: A synthesis of analysis of Croatian manufacturing enterprises through development of Croatian model of Innovative Smart Enterprise (HR-ISE model). It represents answer to the question: "Where Croatian manufacturing industry wants to be?"
- Objective 3: Establishment of special learning environment a laboratory: Learning Factory, i.e. simulation of a real factory through specialized equipment. Learning Factory represents a place in which transfer of developed HR-ISE model to the economy subjects could be achieved. It represents

answer to the question: "How can Croatian manufacturing industry get there?"

Results of this project could be of high value for competitiveness of Croatian industry. The development of Croatian model of Innovative Smart Enterprise (HR-ISE model) and its transfer to economy could have significant impact on recovery of Croatian industry. HR-ISE model could help improve competencies and capabilities of Croatian enterprises to make them more competitive on EU market.

2.2. Methodology and results

In order to obtain a maturity level of Croatian industrial enterprises, a specialized methodology has been established. It consisted of a profound literature review, questionnaires and visits with interviews. The literature review was a foundation for the design of questionnaires for Web and for visits (Figure 1).

The Web questionnaire has been sent to more than 1980 industrial enterprises. Database "Biznet.hr" of Croatian Chamber of Economy was used. The sample of 8% of total, representing 161 enterprises, has been gathered. Taking into account the enterprise size and geographical coverage and industrial sectors coverage, the sample can be considered as a representative one.

Besides the basic questions about the enterprise itself, a set of nine questions was given, that represent the most important aspects of manufacturing as follows: Product Development, Technology, Work Orders Management System, Production Traceability Monitoring, Materials Inventory Management, Stocks of Finished Products Management, Quality Assurance, Product Lifecycle Management, and Application of Toyota Production System and Green and Lean Production Concept.

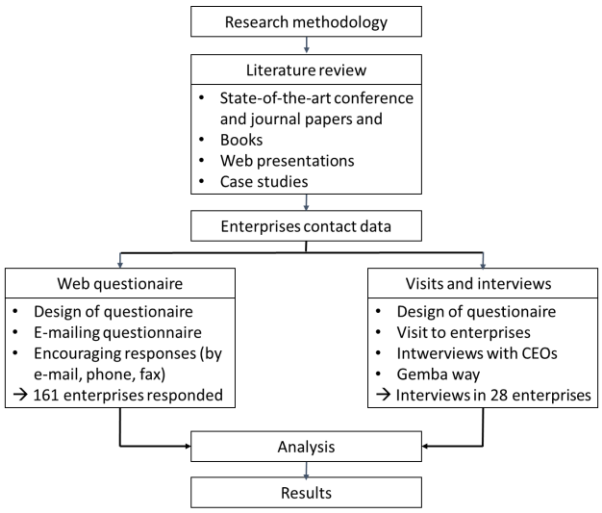

Figure 1. Methodology for obtaining maturity level of Croatian industrial enterprises [3]

Slika 1. Metodologija za određivanje razine industrijske zrelosti hrvatske prerađivačke industrije [3]

Each answer was converted to a score from 1 to 4 representing one of the four historical industrial generations [4]. Depending on the selected answer(s), an overall score for each question was calculated as an average value of all selected answers and their scores.

In Figure 2 it is shown that the average score of the industrial maturity level for the Croatian manufacturing industry is 2.15 which represents the 2nd industrial generation, i.e. the middle of the 20th century [2].

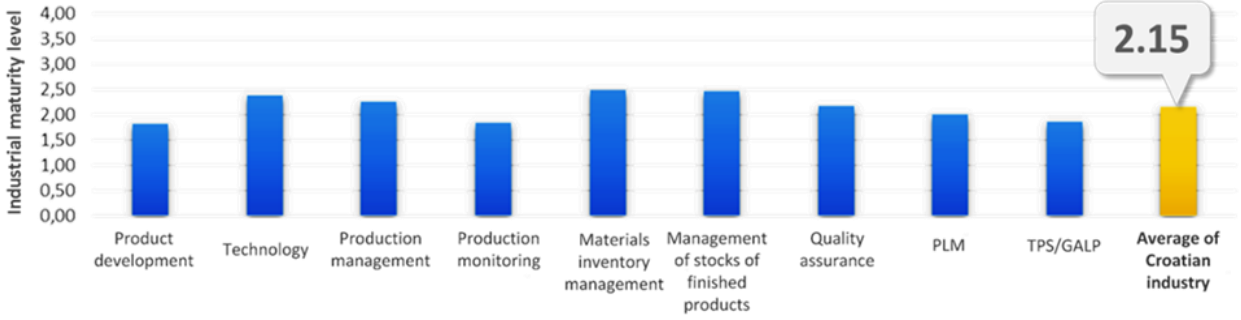

Figure 2. Level of industrial maturity for specific segment of production and average of entire Croatian industry [2]

Slika 2. Razina industrijske zrelosti za pojedine segmente proizvodnje kao i prosjek za cjelokupnu hrvatsku industriju [2]

The second step was to select the best enterprises and make interviews with their CEOs and technical directors. More than 50 interviews were made in 28 enterprises. The basic elements of the enterprise's technique, organization and personnel were analyzed. Analysis has showed that Personnel has been identified as more important issue than Technique and Organization. Furthermore, Lifelong learning and innovation are seen

as most important issues in the development of human resources, i.e. personnel.

Furthermore, Industry 4.0, as a new type of industrial platform, is based on Smart Factory model. And the main features of Smart Factory can be summarized into the following:

- Smart personalized product – requires flexibility and high level of ICT integration into manufacturing;
- Product and service provider – ability to offer extended products: product and service integrated into single, or to be manufacturing service provider;
- High level of collaboration – requires high level of ICT integration to support collaborative product development, and collaborative manufacturing.

Therefore, a special synthesis of analysis of Croatian manufacturing industry has been made in order to understand the plans of strategic positioning regarding Industry 4.0. This synthesis and its hypotheses are presented in rest of the paper.

3. Positioning of Croatian manufacturing enterprises regarding Industry 4.0

In this research, a synthesis of analysis of Croatian manufacturing industry regarding Industry 4.0 is given. Generally, some hypothesis regarding current position of Croatian manufacturing enterprises in contrast to Industry 4.0 are set. Main question is: can enterprise survive on the market without taking strategic directions toward Industry 4.0 till year 2020? Especially, if an enterprise is OEM, and not a manufacturer of a final product. Because, it is very likely that OEMs will be affected by manufacturers of a final product to integrate elements of Industry 4.0 into their parts.

Taking into account skepticism against Industry 4.0 that exists, not just among people from industry, but also in scientific community (22% of operations management academics characterized Industry 4.0 as "just a 'buzzword'" on EurOMA 2016 conference debate about Industry 4.0 [5]), in this research set of enterprises is hypothetically divided into two sets: Industry 4.0 users and Industry 4.0 providers. Regarding this division, six hypotheses have been set based on questionnaire among 160 enterprises and interviews with 30 CEOs of manufacturing enterprises. These hypotheses are presented in Figure 3, and they arose as conclusions from interviews and questionnaire. It means that these hypotheses were actually set by the enterprises themselves, when they strategic plans were interpreted regarding adoption of Industry 4.0.

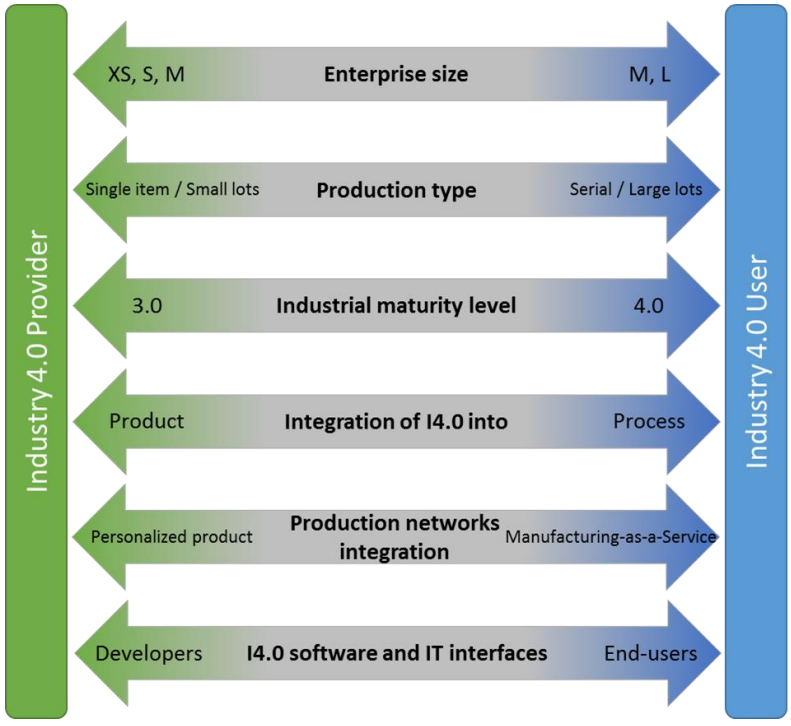

Figure 3. Hypothesis on existence of Industry 4.0 (I4.0) providers and users

Slika 3. Hipoteza o postojanju pružatelja i korisnika Industrije 4.0 (I4.0)

From Figure 3, it is clear that most of the large enterprises and some of the medium-sized enterprises will probably adopt Industry 4.0 as their new industrial platform. On the other hand, most of the micro and small-sized enterprises and some of the medium-sized enterprises will probably reject Industry 4.0 as their own platform, but they will be developing and designing Industry-4.0-ready machines and tools based on single item / small lot production. Therefore, these two groups are called Industry 4.0 providers and Industry 4.0 users.

I4.0 providers are focused on integration of I4.0 into products, i.e. if the product is a milling machine, it will be equipped with sensors for collecting data important to I4.0 CPS, it will have plug & play interface for modular integration into production system, etc. Additionally, I4.0 provider needs to be able to develop proper I4.0 software and interfaces. Furthermore, it cannot offer Manufacturing-as-a-Service due to low integration of ICT into production system, but it can offer personalized product.

However, some facts about hypothesis on existence of I4.0 providers and users must be highlighted. First of all, it is a hypothesis set only for Croatian manufacturing industry, at the moment. Secondly, hypothesis should be proved using further empirical research and analysis. But, without proving hypothesis, the whole idea of being I4.0 provider is doubtful. Therefore, in rest of the paper this idea is discussed and some suggestions for the further research are given.

4. Discussion on I4.0 providers

The reason why Croatian manufacturing enterprises are skeptical to move toward Industry 4.0 is in the fact that most of them still belong to 2nd industrial generation (Figure 4). And the reason why they are on Industry 2.15 level in average is, first of all, historical – almost 50 years of real-socialism's mass production. Secondly, transition toward market-oriented production was unsuccessful in most cases, because technological transition from 2nd industrial generation to 3rd industrial generation was also demanded by the market, i.e. transition from mass production toward mass customization. Since this transition, according to McKinsey [6], requires replacement of 80-90% technology (Figure 4), significant investments in new technology must be made. These two reasons explain why most of the enterprises remained in 2nd industrial generation.

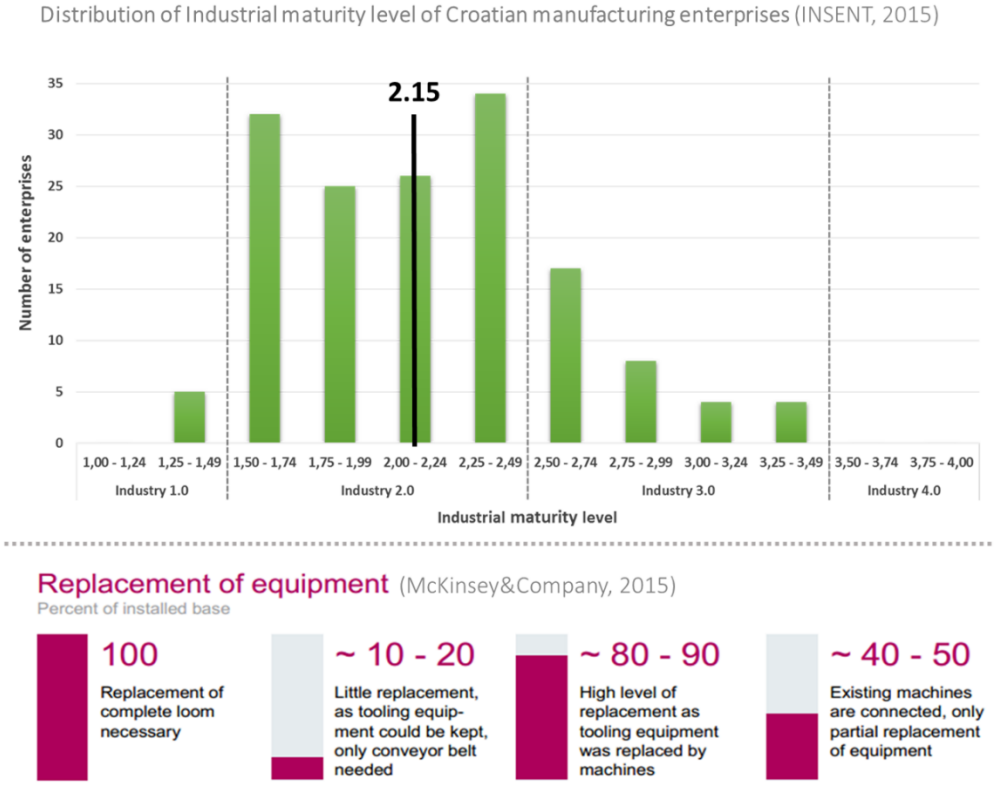

Figure 4. Distribution of Industrial maturity level of Croatian manufacturing enterprises [2], together with replacement of equipment percent needed to jump from one industrial generation to the next one [6]

Slika 4. Distribucija razine industrijske zrelosti hrvatskih proizvodnih poduzeća [2], zajedno s postotkom zamjene opreme potrebnim za skočiti iz jedne industrijske generacije u sljedeću [6]

Fact that average Croatian manufacturing enterprise is on level I2.15, makes I4.0 as a target difficult to reach. Therefore, most of the enterprises are planning to move toward I3.0, or remain in it, if they already reached it. It explains how this hypothesis, of being I4.0 provider, was born. But it is very doubtful whether will be possible to remain in I3.0, especially for OEMs which dominate in Croatian manufacturing industry. It is very likely that OEMs will be affected by manufacturers of a final product to integrate elements of Industry 4.0 into their parts – for example to have an RFID tag with all manufacturing data on the product, or to create all kinds of simulation regarding product's performances, or, perhaps, to give real-time information regarding quantity of production, etc. If an enterprise integrates these elements, it will actually move toward I4.0, although it is not its strategic plan.

Therefore, it can be concluded that vision of many enterprises, especially micro and small-sized enterprises, to remain in 3rd industrial generation doesn't have long-term sustainability. Sooner or later they will integrate some elements of I4.0 (digitalization of a product and manufacturing system, traceability of manufacturing, extended data about product, etc.), and thus become an I4.0 user and they will not be any more just an I4.0 provider. The existence of I4.0 providers is probably possible only in short-time period, but this hypothesis should be supported with some further empirical research.

5. Conclusion

In this paper hypothesis about being Industry 4.0 provider, without being Industry 4.0 user at the same time, is presented and discussed. Hypothesis is a result of analysis of Croatian manufacturing industry, and hypothesis is actually an idea of manufacturing enterprises themselves. A schematic representation of this hypothesis is presented. Most of the micro and small-sized enterprises and some of the medium-sized enterprises are influenced with this kind of thinking, i.e. with the idea of rejecting Industry 4.0 as their new industrial platform. I4.0 providers are more focused on integrating I4.0 principles into products, but not into their production process, and they are producing single item products or small lots, not the large lots. They are also developers of I4.0 software and IT interfaces, but they themselves have low level of ICT integration into production, therefore they cannot be part of modern production networks. However, in the discussion it is concluded that the existence of I4.0 providers is probably possible only in short-time period, but this hypothesis should be supported with some further empirical research. For a long-time period all enterprises will eventually implement at least some of the Industry 4.0 elements, thud become I4.0 users and providers at the same time. That's why it is important for Croatian manufacturing industry to continue with this research, in order to make an influence on the enterprises to make correct strategic positioning regarding Industry 4.0.

Acknowledgements

This work has been fully supported by the Croatian Science Foundation under the project 1353 Innovative Smart Enterprise (INSENT).

REFERENCES

[1] Bezic M, Cerovic Lj., Galovic T., (2011), *Changes in the competitive advantages of Croatia's manufacturing industry*, Zbornik radova Ekonomskog fakulteta Rijeka, Vol. 29, No. 2, p 465-487, Croatia

[2] Veza I., Mladineo M., Peko I., (2015), *Analysis of the current state of Croatian manufacturing industry with regard to industry 4.0*, Proceedings of International Conference CIM 2015, p 249-254, Croatia

[3] Mladineo M., Veza I., Gjeldum N., (2016), *Lifelong Learning in Learning Factory*, 23th EurOMA Conference – EurOMA 2016, Trondheim, Norway

[4] Kagermann H, Wahlster W., Helbig J., (2013), *Recommendations for implementing the strategic initiative INDUSTRIE 4.0*, Heilmeyer und Sernau, Berlin, Germany

[5] Lillebrygfjeld Halse L., (2016), *Report on EurOMA special session on Industry 4.0*, http://panorama.himolde.no/2016/06/23/industry-4-0-pandoras-box-or-a-fuzzy-concept, Accessed: 01-07-2016

[6] McKinsey&Company, (2015), *Industry 4.0 – How to navigate digitization of the manufacturing sector*, Digital McKinsey, New York, USA

ISSN 1847-7917

Rapid Prototyping of Mechanical Measurement Level Device

Ivan PEKO [1)]***, Ivan ŠPAR*** [1)]***, Andrej BAŠIĆ*** [1)]

1) University of Split, Faculty of Electrical Engineering, Mechanical Engineering and Naval Architecture, Department for Production Engineering
Sveučilište u Splitu, Fakultet elektrotehnike, strojarstva i brodogradnje, Zavod za proizvodno strojarstvo
R. Boskovica 32, 21 000 Split, **Croatia**

ipeko@fesb.hr
ivan.spar@gmail.com
andrej@fesb.hr

Keywords

Measurement device
Rapid Prototyping
Fused Deposition Modeling

Ključne riječi

Mjerni uređaj
Brza izrada prototipova
Taložno očvršćivanje

Professional paper

Abstract: The term Rapid Prototyping means creating a physical prototype or the basic model from which would later emerge newer models and consequently the final product. Rapid prototyping models are widely used in many different industrial applications, particularly in the area of product development. Existing rapid prototyping processes provide the capability to produce a tangible solid part rapidly, directly from three dimensional CAD (Computer Aided Design) data, from a range of materials. In this paper will be shown a rapid prototyping of innovative mechanical measurement level device using the Fused Deposition Modeling (FDM) process. This device was designed by a local innovator who ordered this prototyping and protected the innovation officially by State Intellectual Property Office.

Stručni rad

Sažetak: Termin brza izrada prototipova podrazumijeva kreiranje fizičkog prototipa ili osnovnog modela iz kojeg će kasnije proizići noviji modeli i naposljetku konačan proizvod. Modeli izrađeni postupcima brze izrade prototipova se koriste u različitim industrijskim primjenama, posebno u području razvoja proizvoda. Postojeći procesi brze izrade prototipova omogućuju proizvodnju opipljivih krutih dijelova proizvoda izravno iz trodimenzionalnih CAD (Računalom podržani dizajn) podataka iz različitih vrsta materijala. U ovom radu će biti prikazana brza izrada prototipa inovativnog mehaničkog mjernog uređaja ''libele'' postupkom taložnog očvršćivanja (FDM). Ovaj uređaj je dizajniran od strane lokalnog inovatora koji je naručio izradu prototipa i službeno zaštitio svoj patent preko Državnog zavoda za intelektualno vlasništvo.

1. Introduction

Rapid prototyping technologies are frequently used in the beginning of the product development lifecycle to create prototypes or parts used to test and verify designs before full blown production begins. Rapid prototyping services are used in nearly every industry and can be used to prototype every single product that exists on the market today. Physical prototypes are created by these technologies directly from digital data without detailed planning of technological process and production. Hereby, all production process is significantly simplified. Machines used for this application produce objects by applying material in layers. Each applied layer is a thin cross section of a model generated in some software for 3D design.

There is a high number of different rapid prototyping technologies on the market today. These technologies differ according to the type of material, dimensional accuracy of produced parts, sourface roughness, mechanical properties, speed of process, costs.

In this paper a process of creating a physical prototype of innovative mechanical measurement level device (Figure 9) using the Fused Deposition Modeling process on 3D Systems CubePro Duo machine will be described.

Standard spirit measurement level device (Figure 1) enables obtaining only a fact that something is or is not enough accurate. This new mechanical measurement level device differs from standard spirit level devices by possibilty to precisely read a correct deviations from desired accuracy.

Figure 1. Standard spirit measurement level device

Slika 1. Standardna mjerna libela

2. Rapid prototyping

Rapid prototyping includes conceptual modeling and functional prototyping. Conceptual modeling refers to the process of producing a model that spatially shows the basic concept of some idea or innovation. In most cases these workpieces cannot be loaded by force.
They are used to illustrate the physical appearance of the future product and its dimensions and proportions.
Also, they are often used to verify the accuracy of CAD documents and drafts, and to stimulate discussion within the group of experts, which can result in design modifications. Often these models are produced in a variety of colors for the evaluation of the concept and to highlight some specific parts of the model. This is also a way to encourage discussion.
Functional prototypes are made to perform an inspection and control of individual functions of future products over them and to make it easier to decide about the start of production. They are often used to test ergonomics and suitability of the future products for handling.
Also, neither of these workpieces can not be treated and used in practice as finished products [1].
Prototype of innovative mechanical measurement level device is a good example of functional prototype that can be used only to check whether main functions of imagined product work or not, but it will not be able to use this prototype in practice, make measurements and expect accurate data after that.

3. Steps in rapid prototyping process

Rapid prototyping process involves a number of steps that move from virtual CAD description to the physical part. Most of Rapid prototyping processes involve the following steps (Figure 3):

1) **Computer Aided Design:** All prototyped parts must start from a software model that fully describes the external geometry. This can involve the use of almost any professional CAD solid modeling software, but the output must be a 3D solid or surface representation. Reverse engineering equipment can also be used to create this representation.

2) **Conversion to STL (STereoLitography) format:** Nearly every machine for rapid prototyping accepts the STL file format, which has become de facto standard, and nearly every CAD system can output such a file format. This file describes the external closed surfaces of the original CAD model and forms the basis for calculation of the slices.

3) **Transfer to machine and STL file manipulation:** The STL file describing the part must be transferred to the Rapid prototyping machine. There may be some general manipulation of the file in order to put it into the correct size, position, and orientation for building.

4) **Machine setup:** The machine must be properly set up prior to the build process. Such settings would relate to the build parameters like the material constraints, energy source, layer thickness, timings, etc.

5) **Build:** Building the part is mainly an automated process and the machine can largely carry on without supervision.

6) **Removal:** Once the Rapid prototyping machine has completed the build, the parts must be removed. This may require interaction with the machine, which may have safety interlocks to ensure, for example it must be ensured that the operating temperatures are sufficiently low or that there are actively moving parts.

7) **Postprocessing:** Once removed from the machine, parts may require an amount of additional cleaning up before they are ready to use. Parts may be weak at this stage or they may have supporting features that must be removed. This often requires time and careful, experienced manual manipulation. However, they may also require additional treatment before they are acceptable for use. For example, they may require priming and painting to give an acceptable surface texture and finish. Treatments may be laborious and lengthy if the finishing requirements are very demanding. They may also be required to be assembled together with other mechanical or electronic components to form a final model or product [2].

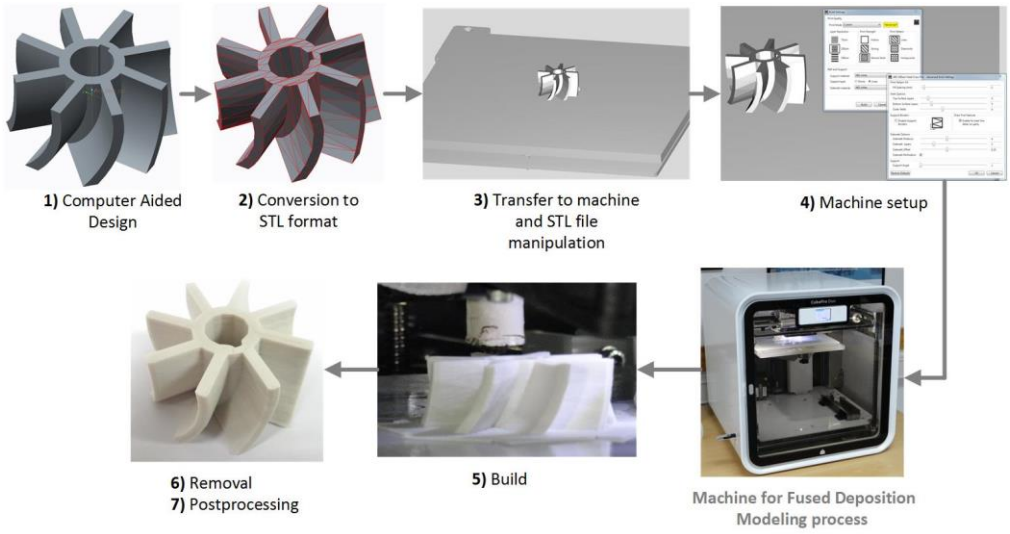

Figure 2. Steps in rapid prototyping process

Slika 2. Koraci u procesu brze izrade prototipova

4. Fused Deposition Modeling process

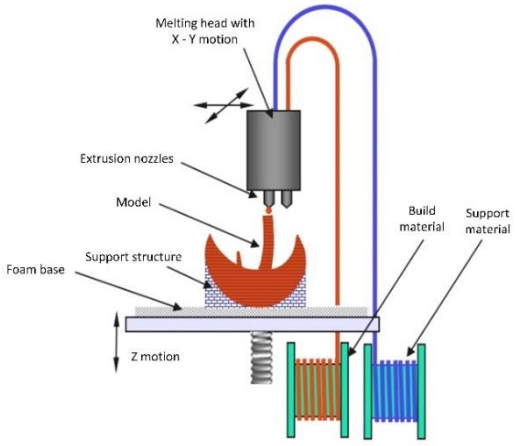

Figure 3. Fused Deposition Modeling process [3]

Slika 3. Postupak taložnog očvršćivanja [3]

A Fused Deposition Modeling process [4] (Figure 3) takes up more than 50% of today's rapid prototyping market. In this process the polymer material passes through the nozzle in the form of a wire. That material comes out of the nozzle in a molten state. Also, it quickly solidifies at room temperature and because of that it is necessary to maintain the temperature of the molten material just above the solidification temperature. After making the first layer, the build platform moves down with the thickness of the new layer (z axis) and after that new layer applies. Extrusion head moves in x-y plane. If some complex geometric models should be created by this process, then a supporting structure is required. In that case it is good to use a double extrusion head. A build material is located in the first nozzle and a support material in the other. Once the model is built supporting structure can be very easily removed by melting in water or fracturing. Also models can be further processed by turning, milling, grinding or by some other processes. Materials that can be used in this process are: ABS, PLA, PC, PP, PE-HD, PE-LD, etc., [1].

5. Creating a mechanical measurement level device prototype

After obtaining a CAD model of innovative assembled mechanical measurement level device (Figure 4 and 5) from innovator, next step is to estimate which parts can and which cannot be produced on available rapid prototyping machine CubePro Duo by Fused Deposition Modeling process.

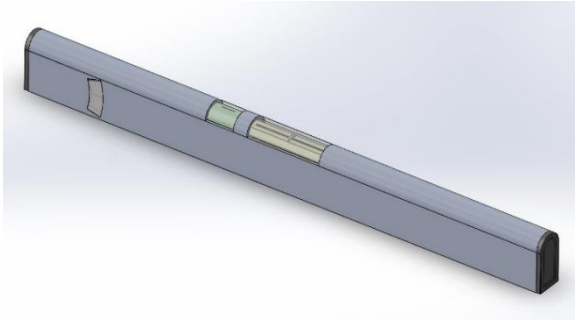

Figure 4. CAD model of assembled mechanical measurement level device

Slika 4. CAD model inovativnog mehaničkog mjernog uređaja ''libele''

Some parts of designed product are very small, thin and should be produced very precisely. For example, the shafts between all crank joints are supposed to have very small deviations from nominal value and the clearance between parts shouldn't be notable. Also, the thickness of central prismatic cover of linear nonius shall be less than 0.5 mm. It is understandable that this is not achievable by this prototyping process and on this machine.

Also, the measurement machine's prototype will work properly only if there would be lead weights on some places in structure. Regarding the housing of measurement device, it was imagined that it needs to be produced from aluminum in combination with few transparent plastic parts that shall be placed on gapes. Because of these requirements, these parts were purchased as semiproducts and after prototyping process has finished they were assembled together with other parts.

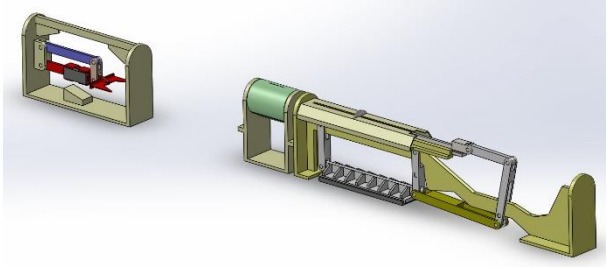

Figure 5. Internal mechanism of innovative mechanical measurement device

Slika 5. Unutarnji mehanizam inovativnog mehaničkog mjernog uređaja ''libele''

Next problem that appears during a process of prototyping is the complexity of geometrical structure of some parts of imagined product. Because the geometrical structure of some parts is too complex, a supporting structure should be built during Fused Deposition Modeling process. Once the process has finished, this structure must be removed and that can damage the surface texture of created part badly. Because of this, the complex structures were cut into simpler parts which were later glued together to form an original designed shape.

Orientation of STL models in printing chamber (Figure 6) and process parameters (Table 1), like layer resolution, print strength, print pattern, fill spacing, top and bottom surface layers, etc. must be defined to get a surface roughness and dimensional accuracy as best as possible. The orientation mostly depends on the individual part's shape.

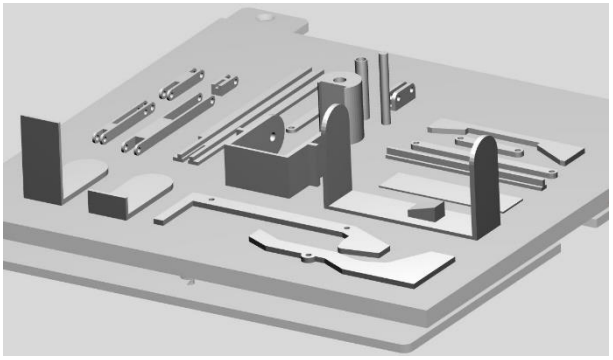

Figure 6. Parts orientation in printing chamber

Slika 6. Orijentacija dijelova u komori za tiskanje

Table 1. Parameters of Fused Deposition Modeling process

Tablica 1. Parametri procesa taložnog očvršćivanja

Parameters of Fused Deposition Modeling Process:	
Machine:	CubePro Duo
Print Quality:	
Print Mode:	Standard
Layer Resolution:	200 µm
Print Strength:	Strong
Print Pattern:	Cross
Sidewalk and Support:	
Support Material:	None
Support Type:	Points
Sidewalk Material:	ABS white
Print Pattern Fill:	
Fill Spacing (mm):	4
Shell Options:	
Top Surface Layers:	3
Bottom Surface Layers:	2
Outer Walls:	2
Support Borders:	Enabled
Draw Line Features:	Enabled
Sidewalk Options:	
Sidewalk Distance (mm)	4
Sidewalk Layers:	2
Sidewalk Offset (mm):	0,25
Sidewalk Perforation:	Enabled
Support:	
Support Angle:	35

After a prototyping process has finished, the parts (Figure 7) must be cleaned and honed by special rasps and fine sandpaper. After that, all parts can be assembled together as it is shown in Figure 8.

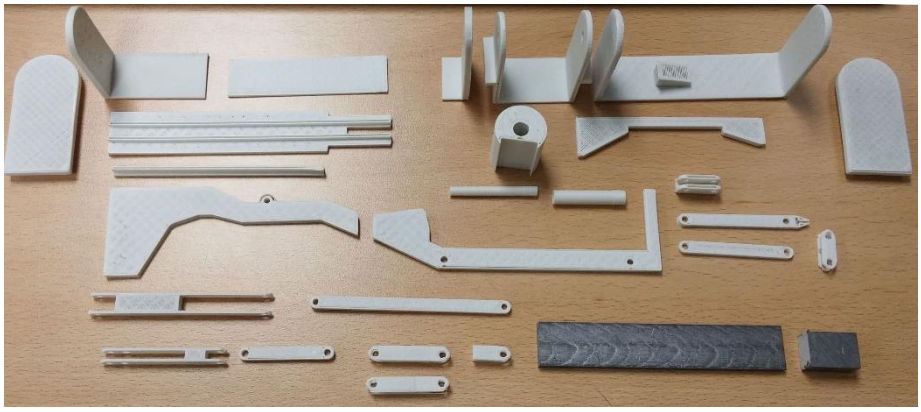

Figure 7. Internal parts of prototype obtained by Fused Deposition Modeling process (plus some lead parts)

Slika 7. Unutarnji dijelovi prototipa dobiveni postupkom taložnog očvršćivanja (plus neki olovni dijelovi)

Figure 8. Assembled internal segment of mechanical measurement level device's prototype

Slika 8. Sklopljeni unutarnji dio prototipa mehaničkog mjernog uređaja "libele"

Figure 9. Created mechanical measurement level device's prototype

Slika 9. Izrađeni prototip mehaničkog mjernog uređaja "libele"

6. Advantages and disadvantages of Fused Deposition Modeling process

Advantages of Fused Deposition Modeling process in producing mechanical measurement level device:

- horts time from an idea to product’s prototype;
- Less energy consumption compared with traditional technological processes;
- Lower price of producing such a prototype compared with standard processes like metal cutting, turning, milling, etc.;
- Low maintenance costs of used rapid prototyping machine;
- Simpler handling with used machine for Fused Deposition Modeling process CubePro Duo in comparison with traditional machines like lathes, milling machines, drilling machines, etc.;
- Possibility to produce more prototypes in one cycle;

- Less waste of material;
- High dimensional stability of parts produced by this technology and on this machine;
- Produced parts can be easiliy subsequently processed and finished;

Disadvantages of Fused Deposition Modeling process in producing mechanical measurement level device:

- It is necessary postprocessing of produced parts, operations like grinding, coating, etc.:
- A support structure is necessary in producing some parts of device with more complex geometry;
- Temperature fluctuations during Fused Deposition Modeling process can lead to delamination of produced parts of mechanical measurement level device;
- Lower dimensional accuracy of produced parts in comparison with those produced by traditional technological processes especially the little ones and those which should have low dimensional tolerances like little shafts;
- Lines between applied layers are visible and because of that obtained surface roughness of produced parts is higher;
- Higher surface roughness complicates movements between moveable parts in final assembly structure and extends a postprocessing time;
- Mechanical properties of parts depend on their position on machine's workplate.

7. Conclusion

Rapid prototyping is a technique for direct conversion of 3D CAD data into physical prototype using a number of processes. These processes have been used in automotive, consumer products, casting and toy industries. Rapid prototyping parts are mainly used for visual inspection, ergonomic and functional evaluation. This new technology has gained importance to speed up product development process in recent years. This is especially true since the manufacturing process is being outsourced to nations with cheaper labor and 70% of the product cost is committed at the design stage. Research has shown that the total cost for new products can be reduced by as much as 30-60%, and lead times can be reduced by 50-60% using the rapid prototyping technology [5]. Rapid prototyping has a strong impact on productivity, which means getting a product from concept to prototype in reality in as fast and as an inexpensive method as possible. Moreover, rapid prototyping computerizes the fabrication of prototypes from 3D CAD designs. A physical prototype provides more information about a product compared with the information that can be obtained from the design drawing.

In this paper a rapid prototyping process of one innovatively designed product was described thoroughly. This prototype consists of parts that were produced mostly by Fused Deposition Modeling process. However, a few parts were produced conventionally. Although this mechanical measurement level device prototype could be produced with higher quality by some other rapid prototyping processes, aim of this paper was to show how can this one relatively cheap, widespread and simple rapid prototyping process be used to make prototype like this one regardless of its complexity, number, size and shape of parts. This product's created prototype can be used further in the following activities: better customization of product according to market's requirements and customer's demands, product's design simplification, planning of production process, designing of tools and fixtures, calculations of costs, organizing of resources, etc. It is obviously that all these benefits of rapid prototyping processes help today's companies to be more competitive and to win the global marketplace.

8. Acknowledgement

This work has been fully supported by Croatian Science Foundation under the project Innovative Smart Enterprise – INSENT (1353).

REFERENCES

[1] Gebhardt, A., (2011), *Understanding Additive Manufacturing, Rapid Prototyping, Rapid Tooling, Rapid Manufacturing*, Hanser

[2] Gibson, I., Rosen, D.W., Stucker, B., (2010), *Additive Manufacturing Technologies, Rapid Prototyping to Direct Digital Manufacturing*, Springer

[3] Bual Singh, G., Kumar, P., (2014), *Methods to Improve Surface Finish of Parts Produced by Fused Deposition Modeling*, Manufacturing Science and Technology 2(3), 51-55.

[4] Novakova Marcincinova, L., Novak Marcincin, J., (2012), *Applications of rapid prototyping fused deposition modeling materials*, Annals of DAAM for 2012 and Proceedings of the 23rd International DAAM Symposium, Volume 23, No. 1, DAAM International, Vienna, Austria

[5] Kamrani Ali, K., Nasr Abouel, E., (2010), *Engineering Design and Rapid Prototyping*, Chapter 12, Rapid Prototyping, 339-354.

ISSN 1847-7917

SANS and PIXE characterization of Polymer Cement Concretes

***Massimo ROGANTE*[1)], *Vladimir HAVRÁNEK*[2)], *Pavol MIKULA*[2)], *Vasyl RYUKHTIN*[2)]**

1) Rogante Engineering Office, I-62012 Civitanova Marche, **Italy**

2) Nuclear Physics Institute ASCR v.v.i., 25068 Řež near Prague, **Czech Republic**

main@roganteengineering.it

Keywords

Cements
Polymer cement concretes
SANS
PIXE
Porosity
Industrial Applications

Original scientific paper

Abstract: Study of polymer cement concrete (PCC) is performed to make novel components for diverse categories of constructing materials. PCCs possess good functional properties (e.g., hardness and stability of mechanical modules, ageing and cracks' formation resistance) and they can be adopted for different purposes.

This paper concerns the characterization at the nano-scale level of Portland cement with added γAl_2O_3 and redispersible dry polymer (RDP), carried out by Small Angle Neutron Scattering (SANS). The reported results are related in particular to the size distribution of nanosized pores which can help to comprehend the structural basis for the physico-chemical properties and thus to improve quality and durability of the considered materials. A complementary Proton Elastic X-ray Emission (PIXE) investigation has been also carried out, with the aim of a non-destructive orientative assessment of the elemental composition of the considered samples.

1. Introduction

Analyses of cements are usually performed to get information on characteristics connected with fatigue behaviour, computational mechanics and structure, and they involve investigations, theoretical studies and simulation-based tests. Differential thermal analysis, infrared spectroscopy, optical and electronic microscopy and X-ray diffraction are the main techniques generally adopted. Modal-based simulations and stress analyses allow forecasting the cement's performance subsequently to ageing, contributing to the safety enhancement of buildings. Porosity is a main parameter, influencing mechanical and heat-insulation properties, and it is usually assessed by acoustic methods, gas and liquid porosimetry (such as mercury intrusion porosimetry) and gravimetric techniques. The acoustic-electric approach allows determining the relation between porosity and the characteristics of electric and acoustic responses to pulsed mechanical excitation [1]. Other important parameters are the balance between crystalline and gel phases of formed hydrated compounds, the hydration degree of binder, morphology and sizes of crystal hydrates.

The results obtained by adopting neutron techniques in materials characterization have often proved their strong support for better understanding of material's characteristics and behaviour [2-4]. These techniques are a crucial tool also in case of the cements, to increase lifetime and performances and to prevent degradation related to ageing. SANS, in particular, provides key data to complement the analytical and crystallographic information, which are crucial to comprehend the structural basis for the chemical and physical properties of materials.

In this work, specimens of Polymer Cement Concretes (PCC) [5], produced by the Department of Building Materials of the Ural Federal University (DBM-URFU), made of Portland cement with added γAl_2O_3 and RDP with different additives ratios, are considered for a SANS investigation complementary to that already carried out [6-8].

Symbols/Oznake

λ	- neutron beam wavelength, Å - ...		**Greek letters/Grčka slova**
Q	- scattering vector, $Å^{-1}$ - ...	γ	- γ phase of Al_2O_3 -
r	- radius (size), nm - ...	λ	- neutron beam wavelength, Å - ...
$S(Q)$	- scattering cross section, cm^{-1} - ...	ρ	- scattering length density, $Å^{-2}$ - ...

These RDP alter the structure of concrete, once the binding agent and water create the cement stone, which joins particles together to make a monolith. This work is a part of a complete study of innovative cements and related materials that the Rogante Engineering Office has designed by adopting advanced methodologies, including e.g. laser interferometry [9]. It is focused in particular on the size distribution of nanosized pores, useful to understand the structural basis for the physico-chemical properties and consequently to advance quality and durability. Previous SANS and X-ray analyses of cements are reported in [6], and confirm that SANS allows characterizing the pore-structure and verifying the pore-size distribution in cement pastes, studying the fine-pore porosity without any drying or pre-treatment of specimens.

The present SANS investigation has been performed to complete the knowledge of the effects due to the different additives on nanostructure and of the particularities of the interfaces structure inside the cement stone.

2. Materials and Methods

2.1. Polymer cement concretes

PCCs are cement-based composites with the supplement of diverse high-molecular weight compounds in dry powdered or in aqueous dispersions form. By adding polymers it is possible to change the PCC's structure to a needed direction and to produce a composite material possessing improved elasticity, abrasive resistance, chemical resistance and tensile strength, as well as reduced porosity and water absorption. Such characteristics are due to articulated joint of hydrates containing more flexible particles, nets and films of strong elastic organic polymers having adhesiveness. By increasing the polymer/cement ratio, a decrease of the elasticity modulus is produced [10-15]. The active components of these PCC are the organic matter and the mineral binding agent. The latter, by adding water, forms the cement stone that joints together particles of aggregate, to produce a monolith. The RDP, through the removal of water from the concrete, create a thin layer on the surface of pores, cement and aggregate nodules. Such layer possesses a good adhesive behaviour, consequently the added RDP retards the hardening process of cement stone [6].

The chemical composition of the specimens investigated in this work involves:

– ordinary Portland cement

RDP - copolymer of vinyl acetate in powdered form (vinyl acetate and vinyl versatate, with a 5°C vitrification temperature, a 100 % content of solid substance and a 80 μm particle size; the vitrification temperature is a mayor parameter amongst the characteristics stating the viscoelastic behaviour of a polymer, and it need to be known if a polymer cement is to be used efficaciously or the viability is to be estimated)

– γAl_2O_3, produced by thermal hydrolysis [6, 16].

Also in the present work, as in the past SANS investigation, two methods of RDP mixing have been considered, i.e. polymer dispersion by joint grinding and dry blending.

Table 1 contains the list of the samples with the respective additives and the type of the mixing procedure.

Table 1. Composition and features of the studied PCC samples

sample	RDP (wt. %, type)	γAl_2O_3 (wt. %)	mix.
CEM00	0	0	dry
CEM01	1.5 (RDP-22)	1.5	dry
CEM02	1.5 (RDP-22)	1.5	wet
CEM03	0	0	dry
CEM04	0	max	dry
CEM05	0	max	dry
CEM06	2.5 (RDP-22)	0	dry
CEM07	2.5 (RDP-23)	0	dry
CEM08	2.5 (RDP-22)	max	dry
CEM09	2.5 (RDP-22)	max	wet
CEM10	2.5 (RDP-23)	max	dry
CEM11	2.5 (RDP-23)	max	wet
max = maximum amount of nanostructured Al_2O_3 = 2.5 %			

The CEM00 and CEM03 control samples were altered by adding mineral substance (γAl_2O_3-powder, CEM04, CEM05) or polymers RDP-22, RDP-23 (CEM06, CEM07), or both additives γAl_2O_3 + RDP-22 or γAl_2O_3 + RDP-23, (CEM01, CEM08, CEM10 by dry mixing; CEM02, CEM09, CEM11 by wet mixing). Concerning dry blending, RDP powder and γAl_2O_3 were added to cement and mixed for 2-3 minutes. For the wet blending, joint grinding copolymer and γAl_2O_3 were mixed in tempering water by using a planetary mill. The latter method enhances bending and compression strength by 10-15%, due to a more uniform distribution of the RDP particles and aluminium oxide in the cement composition. Table 2 reports the characteristics of the RDP additives [6].

Table 2. Characteristics of the RDP additives [6]

RDP	vitrification temperature (°C)	composition	content of solid substance %	particles size (μm)
22	5	vinyl acetate + vinyl versatate	100	80
23	6	vinyl acetate + vinyl versatate	100	90

Micrographs have been carried out of samples CEM00 and CEM09. In the case of samples CEM00 and CEM03, the presence of gel phase and crystalline phases

(hydroaluminate and hydrosilicate calcium) is detected. Specimens without additions contain the maximal amount of gel phase. In the case of sample CEM09, the gel phase results nearly absent, but crystallites of identical size compose the cement stone.

2.2. SANS and PIXE techniques

SANS allows characterising materials at the nano- and micro-levels in a non-destructive way: it provides statistical information averaged over a macroscopic volume, giving possibility to investigate the nanoscopic features of materials and processes, obtaining information related to the whole investigated volume. Parameters as diameter, concentration, volume fraction and area of interface can be monitored by measuring the scattering of the neutrons from the samples in angles smaller than 5 degrees. Knowledge of nano- and microstructural factors obtained by SANS (e.g., voids, and inhomogeneities) can play a decisive role in the debugging of material selection and design requirements. This technique makes possible investigations on fine-pore porosity, measuring also the pore size distribution. The structural features of nanoscale inhomogeneities are reflected by key parameters involved in the mathematical functions modelling the scattering intensity curves. The structure of cement and concrete materials generally shows a fractal character, and the fractal dimensions are linked with the mechanical characteristics (in particular, the mechanical strength). By studying the variation of the fractal dimension through the addition of diverse components to the base material, it is possible to comprehend how such addition effects the internal surface variations, which is related to the mechanical properties of the PCC [6]. The theoretical base of the SANS technique can be found in various references [2, 4, 17]. The measurements have been carried out using the high resolution double bent crystal instrument MAUD at the CANAM infrastructure of the NPI ASCR Řež [18, 19]. This setup is operating with a monochromatic neutron beam having a wavelength λ=2.01 Å. Figure 1 shows some of the investigated samples installed at the SANS sample changing table.

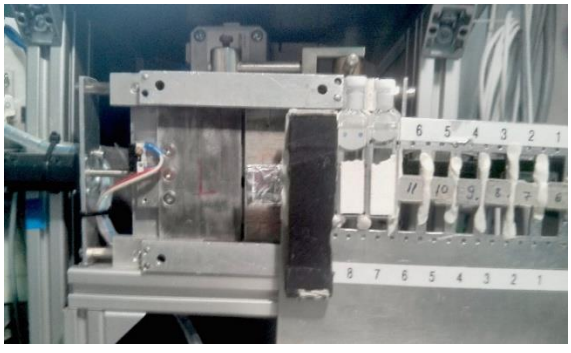

Figure 1. Samples installed at the SANS sample changing table

PIXE spectroscopy is a powerful elemental analysis technique adopted to assess the elemental composition of a material or object. The method was proposed in 1970 by S. Johansson et al. [20]. For a detailed treatment of the theoretical bases, see [21-22]. Some of the considered PCC samples have been analysed by Proton Elastic X-ray Emission (PIXE) at the Tandetron Laboratory of NPI. For the measurements, proton beam with 2.6MeV energy was used. Cross section of proton beam was of 2x2 mm^2. Quite low current (0.6 nA) was selected in order to minimise high intensity Fe K X-rays.

3. Results and discussion

Figure 2 reports the scattering curves covering a Q-range from 0.0003 Å^{-1} to 0.01 Å^{-1}, corresponding to a size range from about 30 nm to 2 μm in real space.

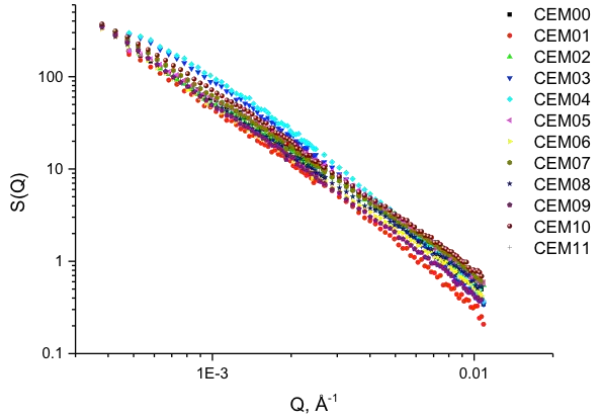

Figure 2. Scattering curves

Log-log scale graphical representation shows that scattering in close to be proportional to power law with exponent of about -2. Such dependence might say about a very rough surface fractal structure of pores, which also can be reconstructed by combination of spherical particles. We used spline distributions for fitting these data, by using the SASfit software [23, 24]. The resulted e distributions weighted by volume fraction are shown in Figure 3.

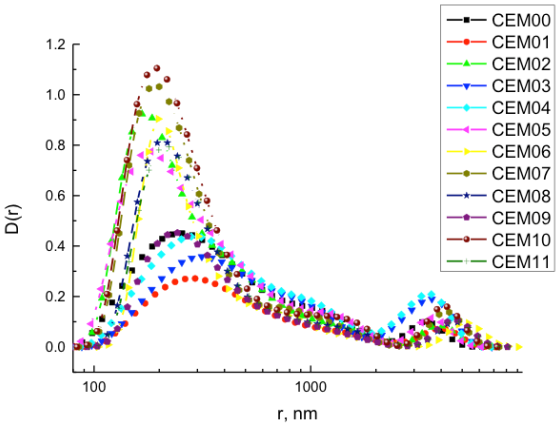

Figure 3. Model size distributions fitted to SANS data

Ten splines equidistantly distributed at log scale were used for this fitting. The mean values of radia of the spheres are about 160-260 nm (see Figure 4). Volume fractions calculated as integral over whole size range of volume weighted size distributions are shown in Figure 5.

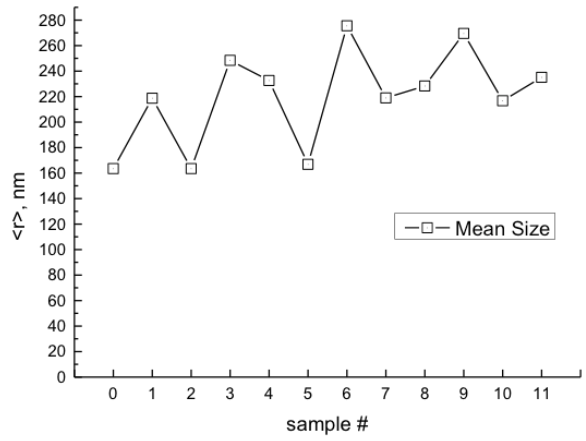

Figure 4. Fitted mean sizes of the pores

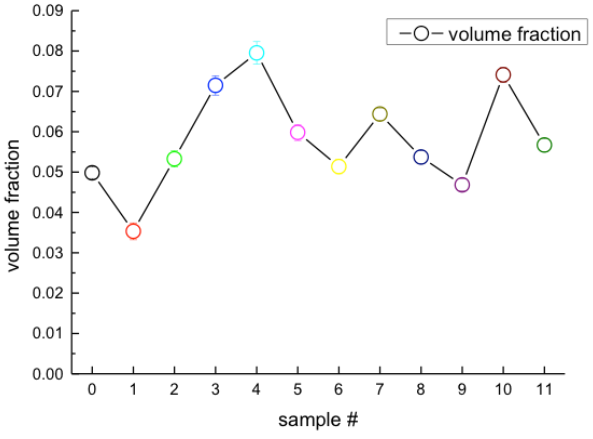

Figure 5. Total volume fractions of the pores as fitted by the model

The scattering length density of the material was calculated analytically by assumption that the main phase is formed by 70 mass% of calcium oxide, 25 mass% of silicon dioxide and 5 mass% of aluminium oxide.
By analysing the size distributions and volume fractions data, it is possible to say that the higher values of porosity volume fraction for samples CEM03, CEM04 and CEM11 are due to large pores (r≈3 μm). Despite such size is practically slightly out of the resolution of the used instrumentation, since the smooth model we expect that such porosity can be found in these samples. Same of the investigated samples show a rather low nanoporosity (r≈200 nm) i.e. samples CEM01 and CEM09. A high amount of nanoporosity was detected in samples CEM02, CEM06, CEM07, CEM08 CEM10 and CEM011.
The concrete samples were further measured at ion microbeam facility at Tandetron 4130MC with 2.0MeV proton beam focused down to 1.5μm beam spot and proton current of 40pA. Some samples were scanned over 1×1 mm^2 and 100×100 μm^2 areas, in order to investigate the homogeneity of mixure and determine the mean concentration of matrix elements. Both PIXE spectra and those obtained by Rutherford backscattering spectrometry (RBS) were collected. No absorption X-ray filter in front of PIXE detector was used, in order to see elements down to Na. The obtained X-ray spectra were evaluated by using the PIXE-INP software [25]. The results are summarized in Table 3.

Table 3. Mean concentration of elements in mass % over the 1×1mm^2 scan a-from RBS spectra

Element	CEM01	CEM05	CEM09
Na	2.54	1.78	1.02
Mg	1.95	2.07	1.92
Al	2.69	3.62	3.20
Si	7.53	8.70	8.06
S	1.11	1.22	1.250
K	0.83	0.61	0.48
Ca	26.2	26.0	25.5
Ti	0.055	0.069	0.068
Cr	0.045	0.060	0.041
Mn	0.020	0.022	0.023
Fe	1.50	1.54	1.58
Cu	0.015	0.022	0.023
Zn	0.104	0.110	0.112
Sr	0.048	<0.05	0.031
C [a]	8.1	8.0	7.8
O [a]	48.5	48.6	48.4
Sum	101.2	102.5	99.5
a - from RBS spectra			

Since the PIXE analysis is carried out by micro-beam and it is related to the surface of the sample, these results are orientative: for more precise data, especially considering the grain size of the considered cement, higher statistics are needed, i.e. several PIXE analyses per sample.
Figures 6 to 9 show, e.g., some elemental colour maps (black –lowest concentration, red –highest concentration) related to the CEM01, CEM05 and CEM09 investigated samples.

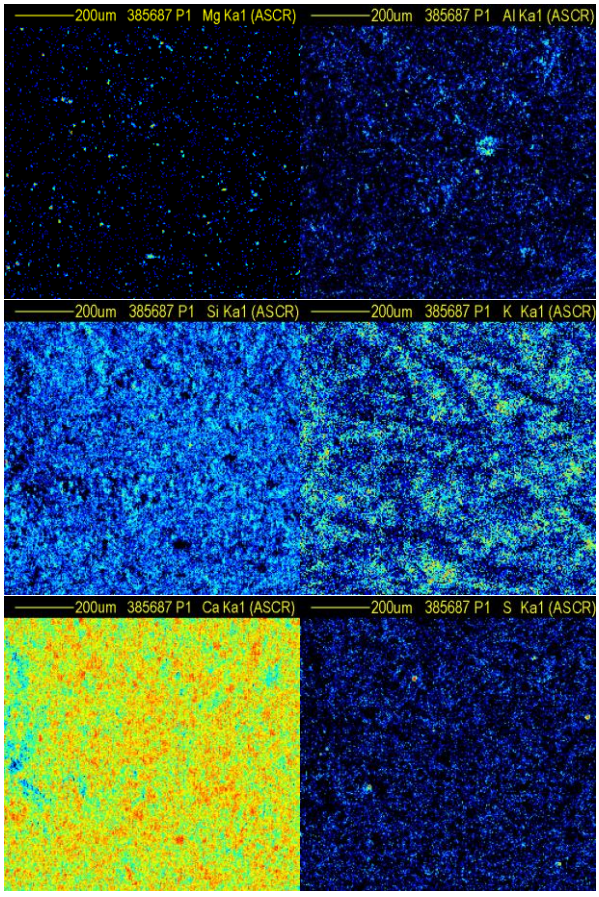

Figure 6. Elemental maps (Mg, Al, Si, K, Ca, S) of the sample CEM01 (scan 1×1mm^2)

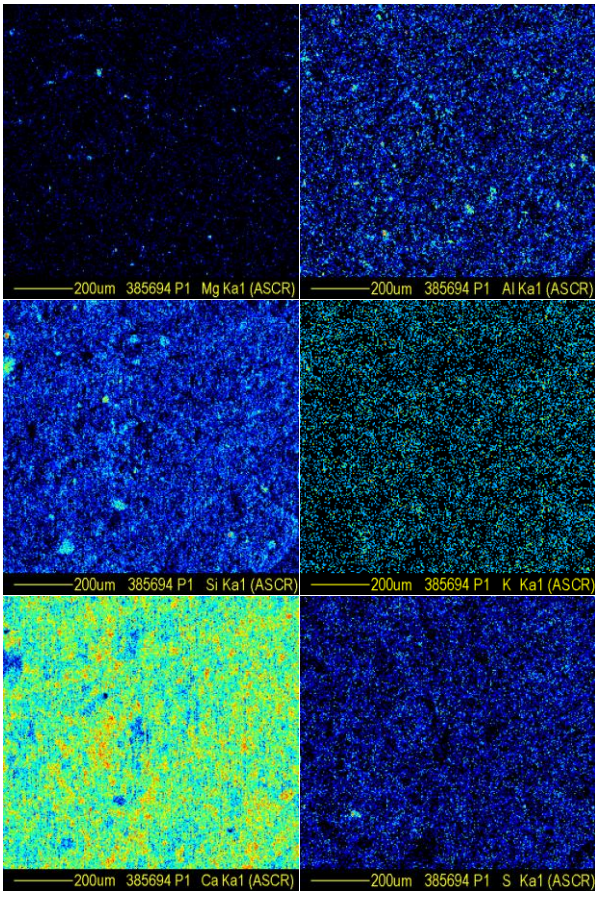

Figure 7. Elemental maps (Mg, Al, Si, K, Ca, S) of the sample CEM09 (scan 1×1mm^2)

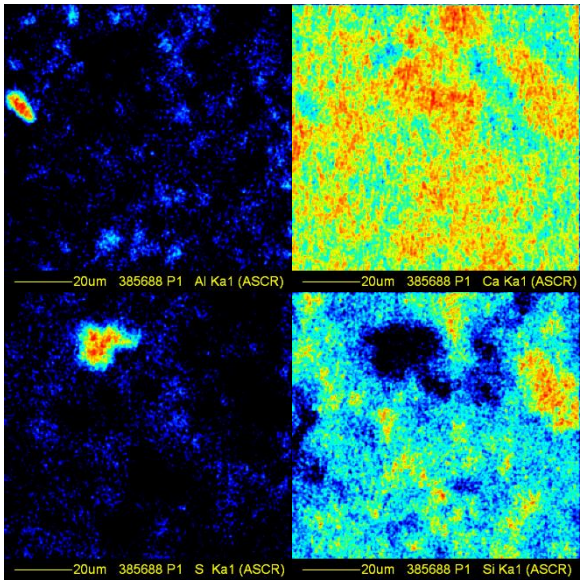

Figure 8. Elemental maps (Al, Ca, S, Si) of the sample CEM01 (scan 100×100μm^2)

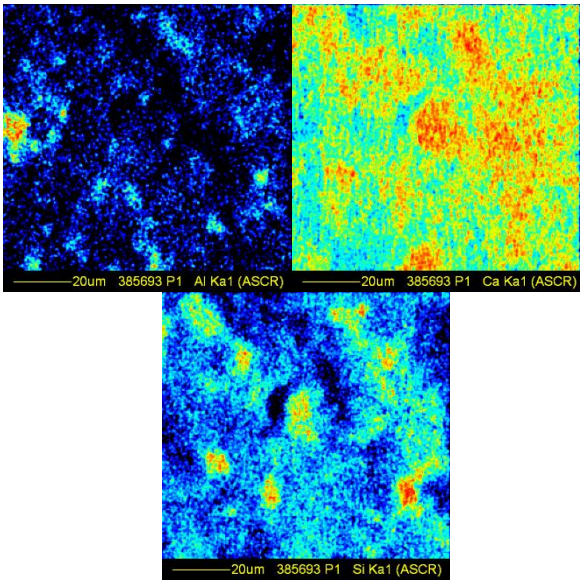

Figure 9. Elemental maps (Al, Ca, Si) of the sample CEM05 (scan 100×100μm^2)

4. Conclusions

A complementary SANS characterization of different PCC samples made of Portland cement with added γAl_2O_3 and RDP has been carried out, mainly related to the study of porosity. A very rough surface fractal structure of the pores has been detected, and the mean sizes as well as the total volume fractions of the pores have been evaluated.

PIXE, as multielemental non-destructive detection technique efficient of measuring elements' concentrations with a sensitivity down to the ppm scale, has been successfully adopted to investigate the homogeneity of mixure and determine the mean concentration of matrix elements of the considered PCC samples. Both PIXE and RBS spectra were collected, and the data from these microprobe experiments give an additional contribution to the nano-structural information obtained from SANS analyses.

The achieved information can be useful for the building sector and can help optimizing PCCs, their manufacture for diverse applications and the quality of the final product.

Acknowledgements

Financial support from EU's NMI3-II (FP7) grant number 283883 and from MŠMT project No. LM2015056 (CANAM) are acknowledged.

REFERENCES

[1] Fursa T. V., Surzhikov A. P., Osipov K. Yu., (2007), *Development of an acoustoelectric method for determining the porosity of dielectric materials*, Defektoskopiya 43 No. 2, p 27-34 Russian Federation

[2] Rogante M., (2008), *Applicazioni Industriali delle Tecniche Neutroniche*, Proc. 1st Italian Workshop for Industry "Industrial Applications of Neutron Techniques", Civitanova Marche, Italy

[3] Rogante M., Rosta, L., (2005), *Nanoscale characterisation by SANS and residual stresses determination by neutron diffraction related to materials and components of technological interest*, Proc. SPIE 5824, p 294-305 U.S.A.

[4] Rogante M., (1999), *Caratterizzazione, mediante scattering neutronico, di materiali e componenti per l'impiantistica nucleare ed industriale*, PhD thesis, University of Bologna, Italy

[5] Rogante M., Domanskaya I. K., Gerasimova E. S., (2016), *Resistenza meccanica ed elasticità dei calcestruzzi polimerici*, Il Nuovo Cantiere, Vol. 1, p 66-68 Italy

[6] Rogante M., Domanskaya I. K., Gerasimova E. S., Len A., Rosta L., Székely N. K., Vladimirova E., (2015), *Nanoscale investigation of Polymer Cement Concretes by Small Angle Neutron Scattering*, Sci. Eng. Comp. Mat. ISSN (Online) 2191-0359, ISSN (Print) 0792-1233, DOI: 10.1515/secm-2015-0013 Germany

[7] Rogante M., Domanskaya I. K., Gerasimova E. S., Vladimirova, E., (2013), *Feasibility Study for a Neutron-Based Investigation of Polymer Cement Concretes*, Univ. J. Appl. Sci. 1 No. 1, p 11-17 U.S.A.

[8] Rogante M., Selezneva A., *Cements for nuclear industry: a feasibility study of neutron-based investigations*, MTMS2011, Split, Croatia

[9] Rogante M., Capelli G., Domanskaya I. K., *Laser interferometry investigation of polymer cement concrete samples for vibration measurements*, MTMS2013, Split, Croatia

[10] Puterman M., Malorny W., (1998), *Some doubts and ideas on the microstructure formation of PCC*, *ICPIC 1998*, Bologna, Italy

[11] Domanskaya I. K., Kapustin F., Mokhort E., Oleynik V., (2003), The main approaches of component selection for fine polymercement products and coatings *15th Int. Conf. on Building Materials "Ibausil"*, Weimar, Germany

[12] Dimmig A., (2004), *Chemical and Physical Effects on the Microstructure of PCC*, *IX.ICPIC*, BAM, Berlin, Germany

[13] Wang R., Wang P. M., Li X. G., (2005), *Physical and mechanical properties of styrene-butadiene rubber emulsion modified cement mortars*, Cem. Concr. Res., 35 No. 5, p 900-906 United Kingdom

[14] Bhikshma V., Rao K. J., Balaji B., (2010), *An experimental study on behavior of polymer cement concrete*, As. J. Civ. Eng. (Building and Housing) 11 No. 5, p 563-573 IRAN

[15] Kruglitsky N. N., Boyko G. P., (1981), *Physico-Chemical Mechanics of cement polymer compositions*, Naukova Dumka, Kiev

[16] Vasiliev V., Bazhenov A., Vladimirova E., Kozhevnikov V., Nosov A., Mohort E., Chistyakova T., (2010), *Patent RU 2384522 C1: Method of obtaining oxide nanoparticles of metal*, Institute of solid state chemistry, Ural branch of the Russian Academy of Sciences, Byull. № 8.

[17] Williams C., May R. P., Guinier A., (1994), *Small-Angle Scattering of X-rays and Neutrons*, Characterisation of Materials, Materials Science and Technology, Vol. 2B, VCH Verlagsgesellschaft, Weinheim, Germany

[18] http://neutron.ujf.cas.cz/en/instruments/lvr15/5-hk8a

[19] Mikula P., Lukaš P., Eichhorn F., (1988), *A new version of a medium-resolution double-crystal diffractometer for the study of small-angle neutron*

scattering (SANS), J. Appl. Cryst. 21, p 33-37 United Kingdom

[20] Johansson T. B., Akselsson R., Johansson, S. A. E., (1970), *X-ray analysis: elemental trace analysis at the 10^{-12} g level*, Nucl. Instr. & Methods 84, p 141-143 United Kingdom

[21] Maenhaut W., Malmqvist K. G., (2002), *Particle-Induced X-ray Emission Analysis*, Handbook of X-Ray Spectrometry, Second Edition, M. Dekker, New York, U.S.A.

[22] Mandò P.A., Przybyłowicz W. J., (2009), *Particle-Induced X-Ray Emission (PIXE)*, Encyclopedia of Analytical Chemistry, John Wiley & Sons, Ltd, Hoboken, New Jersey, U.S.A.

[23] Šaroun J., (2000), *Evaluation of double-crystal SANS data influenced by multiple scattering*, J. Appl. Cryst. 33, p 824-828 United Kingdom

[24] http://neutron.ujf.cas.cz/SAS/

[25] Havránek V., Hnatowicz V., Kvítek J., Obrusník I., (1994), *PIXE-INP computer code for PIXE analyses of thin and thick samples*, Nucl. Instr. & Meth. B 85 No. 1-4, p 637-641 United Kingdom

ISSN 1847-7917

Numerical modelling of case hardening of steel

Božo SMOLJAN, Dario ILJKIĆ, Lovro ŠTIC, Loreta POMENIĆ, Sunčana SMOKVINA HANZA

1) Department of Materials Science and Engineering, University of Rijeka - Faculty of Engineering
Zavod za materijale, Sveučilište u Rijeci - Tehnički fakultet
Vukovarska 58, 51000 Rijeka, **Croatia**

smoljan@riteh.hr
darioi@riteh.hr
lstic@riteh.hr
lpomenic@riteh.hr
suncana@riteh.hr

Keywords

Mathematical modelling
Mechanical properties
Case hardening

Ključne riječi

Matematičko modeliranje
Mehanička svojstva
Cementiranje

Original scientific paper

Abstract: The mathematical model and computer simulation for the prediction of mechanical properties of case hardened steel was developed. The computer simulation of case hardening of steel is consisted of simulation of diffusion of carbon, simulation of heat transfer, and simulation of microstructure composition and mechanical properties. The hardness of case hardened steel has been predicted by conversion of calculated time of cooling from 800 °C to 500 °C to the hardness. After that, distribution of relevant mechanical properties of case hardened steel was found out. Because of wide range of applicability and ease of use of finite volume method (FVM), integrated computer program for simulation of diffusion of carbon, transient temperature field, microstructure transformation and mechanical properties during case hardening of steel was created by FVM numerical method. The established numerical model was applied in computer simulation of case hardened steel.

Izvorni znanstveni rad

Sažetak: Razvijen je matematički model i računalna simulacija predviđanja mehaničkih svojstava cementiranih čelika. Računalna se simulacija postupka cementiranja čelika sastoji od simulacije difuzije ugljika, simulacije razmjene topline, kao i simulacije mikrostrukturnog sastava i mehaničkih svojstava nakon kaljenja čelika. Tvrdoća cementiranog čelika predviđena je konverzijom izračunatih vremena ohlađivanja od 800 do 500 °C u tvrdoću. Nakon toga je predviđena i raspodjela relevantnih mehaničkih svojstava cementiranog čelika. Metoda konačnih volumena (MKV) je zbog vrlo široke primjene i lakoće uporabe pogodna za primjenu u razvoju integriranog računalnog programa za simulaciju difuzije ugljika, promjenjivog temperaturnog polja, mikrostrukturnih pretvorbi i mehaničkih svojstava tijekom cementiranja čelika. Uspostavljeni numerički model primijenjen je u računalnoj simulaciji cementiranja čelika.

1. Introduction

The mathematical modelling of case hardening is consisted of mathematical modelling of carburizing, quenching and tempering.

Since results of mathematical modelling of carburizing depend on numerous different parameters, such as: chemical composition of steel, carburizing atmosphere, temperature and time of carburizing, the industrial carburizing application show that the carbon concentration profiles and case depths often differ from those of the predicted ones.

The mass mobility of carbon is complex function of the carburizing media composition, carbon potential, temperature and surface carbon content on one side, and the coefficient of carbon diffusion in austenite, which is strongly influenced by the carburizing temperature and carbon concentration in steel on another side [1, 2].

The computer simulation of quenching includes prediction of hardness distribution in quenched steel specimens. It consists of computer simulations of specimen cooling, specimen hardening and respectively of prediction of mechanical properties. For the simulation of specimen cooling which is thermodynamical problem, it is necessary to establish the appropriate algorithm which describes cooling process, and to accept appropriate input data [3].

One of the most common methods of computer prediction of quenching results is based on the chemical composition of steel and on the specimen dimensions [4]. Moreover, prediction of mechanical properties usually is based on semiempirical methods derived from kinetic equations of microstructure transformation [5, 6].

Hardness distribution can be also estimated based on time of cooling from 800 to 500 °C, $t_{8/5}$, which could be relevant for microstructure transformation. It can be accepted that if the cooling time $t_{8/5}$ is equal in two different specimens, the hardness of these two specimens could be equal to each other. To accept the assumption that the equal cooling time $t_{8/5}$ of several samples indicates their equal hardness, the history of quenching of these samples must be the same or similar. By involving the cooling time $t_{8/5}$ in the mathematical model of steel hardening, the Jominy test results could be involved in the model [7-9].

Symbols/Oznake

a	- material constant - konstanta materijala	K	- factor - faktor
A	- material constant - konstanta materijala	K_{Ic}	- fracture toughness, $MPam^{1/2}$ - lomna žilavost
A_1	- equilibrium temperature of eutectoid transformation, °C - ravnotežna temperatura eutektoidne transformacije	M_f	- temperature of finish of martensitic transformation, °C - temperature završetka martenzitne pretvorbe
A_3	- equilibrium temperature at which transformation of austenite to ferrite begins, °C - ravnotežna temperatura na kojoj počinje transformacija austenita u ferit	M_s	- temperature of start of martensitic transformation, °C - temperature početka martenzitne pretvorbe
B	- material constant - konstanta materijala	n	- strain-hardening exponent - eksponent deformacijskog očvršćivanja
B_s	- temperature of start of bainitic transformation, °C - temperatura početka bainitne transformacije	n_1	- material constant - konstanta materijala
c	- specific heat capacity, $Jkg^{-1}K^{-1}$ - specifični toplinski kapacitet	N	- total number of control volumes - ukupni broj kontrolnih volumena
C	- carbon concentration, wt.% - koncentracija ugljika	r	- radius, m - polumjer
C_p	- carbon potential, wt.% - potencijal ugljika	R	- radius, m - polumjer
C_s	- surface carbon concentration, wt.% - koncentracija ugljika na površini	R_e	- yield strength, MPa - granica razvlačenja
D	- diffusion coefficient, m^2s^{-1} - koeficijent difuzije	R_m	- ultimate tensile strength, MPa - vlačna čvrstoća
E	- modulus of elasticity, MPa - modul elastičnosti	S	- ratio between the actual hardness and hardness of martensite in Rockwell C hardness - stupanj zakaljenosti
HV	- hardness HV - tvrdoća HV	t	- time, s - vrijeme
$HRC_{quenched}$	- as-quenched hardness HRC - tvrdoća HRC nakon kaljena	$t_{8/5}$	- time of cooling from 800 to 500 °C, s - vrijeme ohlađivanja od 800 do 500 °C
$HRC_{tempered}$	- hardness HRC after quenching and tempering - tvrdoća HRC nakon kaljenja i popuštanja	t_{M50}	- $t_{8/5}$ for characteristic points in Jominy specimen with 50 % of martensite in microstructure, s - $t_{8/5}$ za karakterističnu točku u Jominyjevom uzorku s 50 % martenzita u mikrostrukturi

Symbols/Oznake

HRC_{min}	- material constant - konstanta materijala	t_{M95}	- $t_{8/5}$ for characteristic points in Jominy specimen with 95 % of martensite in microstructure, s - $t_{8/5}$ za karakterističnu točku u Jominyjevom uzorku s 95 % martenzita u mikrostrukturi
t_{P100}	- $t_{8/5}$ for characteristic points in Jominy specimen with 100 % of pearlite in microstructure, s - $t_{8/5}$ za karakterističnu točku u Jominyjevom uzorku s 100 % perlita u mikrostrukturi	ϑ	- temperature, °C - temperatura
t_{P50}	- $t_{8/5}$ for characteristic points in Jominy specimen with 50 % of pearlite in microstructure, s - $t_{8/5}$ za karakterističnu točku u Jominyjevom uzorku s 50 % perlita u mikrostrukturi	ρ	- density, kgm^{-3} - gustoća
T	- temperature, K - temperatura		**Subscripts/Indeksi**
T_{tr}	- reference value of tempering temperature, °C - referentna vrijednost temperature popuštanja	a	- austenitization - austenitizacija
Z	- reduction of area, % - kontrakcija	f	- quenchant - medij za kaljenje
	Greek letters/Grčka slova	M	- martensite - martenzit
α	- heat transfer coefficient, $Wm^{-2}K^{-1}$ - koeficijent prijelaza topline	M	- number of time steps during the cooling from 800 to 500 °C - broj koraka ohlađivanja od 800 do 500 °C
ε_f	- true fracture strain - stvarna deformacija u trenutku loma	P	- pearlite - perlit
λ	- coefficient of heat conductivity, $Wm^{-1}K^{-1}$ - koeficijent toplinske vodljivosti	s	- surface - površina
β	- mass transfer coefficient, ms^{-1} - koeficijent prijelaza mase		

2. Mathematical modelling of heat transfer and carbon diffusion

The temperature field change in an isotropic rigid body with coefficient of heat conductivity, λ/$Wm^{-1}K^{-1}$, density, ρ/kgm^{-3} and specific heat capacity, c/$Jkg^{-1}K^{-1}$, without heat sources can be described by Fourier's law of heat conduction:

$$\frac{\delta(c\rho T)}{\delta t} = div(\lambda\, gradT) \tag{1}$$

Characteristic boundary condition is:

$$-\lambda \left.\frac{\delta T}{\delta n}\right|_s = \alpha\left(T_s - T_f\right) \tag{2}$$

where T_s/K is surface temperature, T_f/K is quenchant temperature, α/$Wm^{-2}K^{-1}$ is heat transfer coefficient. Transient temperature field in an isotropic rigid body can be defined by 2-D finite volume formulation [10, 11].

Discretization system has N linear algebraic equations with N unknown temperatures of control volumes, where N is total number of control volumes. Time of cooling from T_a to specific temperature in particular point is determined as sum of time steps, and in this way, the diagram of cooling curve in every grid-point of a specimen is possible to found out.

$$t_M = \sum_{m=1}^{M} \Delta t_m \quad (3)$$

Physical properties included in Eqs 1 and 2 should be defined [11, 12]. Variable ρ for steel is equal ~ 7800 kgm^{-3}. Accepted values of specific heat capacity, c are shown in Table 1 [13]. Coefficient of heat conductivity, λ was estimated according to variables ρ and c, as function of microstructure composition [12].

Heat transfer coefficients of quenchants were estimated simultaneously with estimation of heat conductivity coefficients [12, 14]. Calibrated values of heat transfer coefficient, α for water are presented in Table 2.

Table 1. Specific heat capacity of different microstructural compositions of steel

Tablica 1. Specifični toplinski kapacitet pojedinih mikrostrukturnih sastojaka čelika

	Temperature/ Temperatura, ϑ/°C	Ferrite + Pearlite (Bainite)/ Ferit + perlit (bainit)	Martensite/ Martenzit	Austenite/ Austenit
Specific heat capacity/Specifični toplinski kapacitet, c/Jkg^{-1}K^{-1}	0	378	376	415
	300	446	445	440
	600	509	507	467
	800	570	-	490

Table 2. Calibrated values of heat transfer coefficient for water

Tablica 2. Kalibrirane vrijednosti koeficijenta prijelaza topline za vodu

Temperature/Temperatura, ϑ/°C	20	116	316	703	1000
Heat transfer coefficient/Koeficijent prijelaza topline, α/Wm^{-2}K^{-1}	1636	1722	14523	1417	1250

The diffusion process can be described by the same type of equations as were applied in heat transfer modelling. The mathematical formulation of the diffusion problem during carburization is based on the following set of equations [1, 15]. The differential carbon content balance can be described by Fick's second law:

$$\frac{\delta C}{\delta t} = div(D\, grad C) \quad (4)$$

where C is the carbon concentration in the steel, D/m^{2}s^{-1} is the diffusion coefficient of carbon in the steel.

As the first approximation, the diffusion coefficient can be assumed to be independent of position in the sample. The diffusion equation is to be solved focus to following boundary conditions:

$$-D\frac{\delta C}{\delta n}\bigg|_s = \beta\left(C_s - C_p\right) \quad (5)$$

where C_p is carbon potential of surrounding atmosphere, C_s is surface carbon concentration, The quantity β/ms^{-1} is the mass transfer coefficient giving the rate of transfer of carbon atoms from the atmosphere into the surface of the steel. The mass transfer coefficient determines the thickness of the boundary gas layer (D/β) at the gas-solid interface and defines the maximum flux of carbon atoms reaching the steel surface and available for further carbon diffusion towards the bulk of the steel [16]. The mass transfer coefficient is very sensitive to the changes in the atmosphere composition and carburizing potential.

The surface carbon concentration C_s varies with time t. Several models have been proposed to model the evolution of surface carbon content with carburizing time; most of them have some limitations and do not always yield accurate results [17]. It is reasonable assume carbon diffusivity to be either constant at fixed temperature or vary with carbon concentration only [18, 19].

There is no doubt, that the diffusion process in carburizing can be defined by 2-D finite volume formulation in similar way as was applied in the numerical formulation of heat transfer.

3. Mathematical modelling of hardness and microstructure composition

The hardness at different workpiece points is estimated by the conversion of the cooling time $t_{8/5}$ to the hardness. This conversion is provided by the relation between the cooling time $t_{8/5}$ and distance from the quenched end of the Jominy specimen [7, 10]. A new method of prediction of as-quenched hardness has been developed. In this method, equivalent cooling time $t_{8/5e}$ was used instead of cooling time $t_{8/5}$. Equivalent cooling time $t_{8/5e}$ is function of cooling time, $t_{8/5}$ and history of cooling [20].

Contents of ferrite, pearlite, bainite, martensite and austenite at some temperature can be estimated using the diagram in the Fig. 1.

Characteristic cooling times in Fig. 1 are depend on

cooling times t_{M95}, t_{M50}, t_{P100}, t_{P50} which are cooling time from 800 to 500 °C for characteristic points in Jominy specimen with 95 % of martensite, 50 % of martensite, 100 % of pearlite and 50 % of pearlite in microstructure, respectively [21].

Characteristic temperatures in diagram shown in Fig. 1 are depend on temperatures M_s, M_f, B_s, A_1, A_3. M_s is temperature of start of martensitic transformation, M_f is temperature of finish of martensitic transformation, B_s is temperature of start of bainitic transformation, A_1 is equilibrium temperature of eutectoid transformation, A_3 is equilibrium temperature at which transformation of austenite to ferrite begins. Between critical temperatures A_3, B_s, M_s and M_f of austenite decomposition and hardenability properties, regression relations are exist [21].

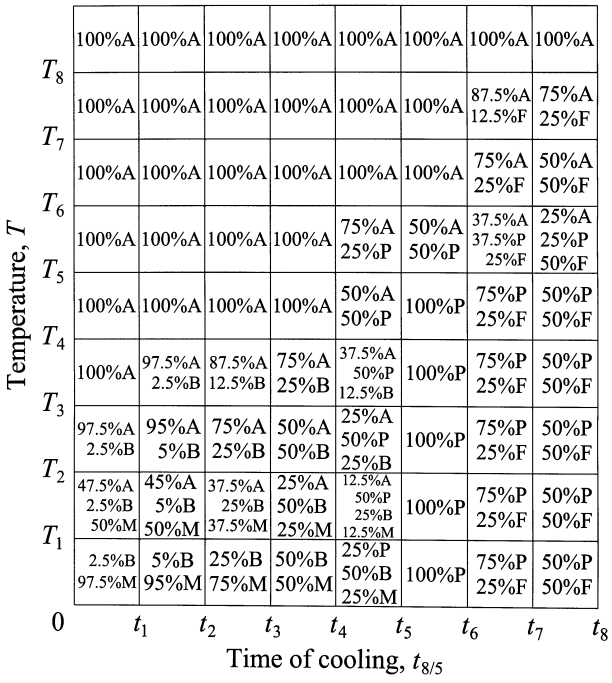

Figure 1. Contents of ferrite, pearlite, bainite, martensite and austenite at some temperature

Slika 1. Udjeli ferita, perlita, bainita, martenzita i austenita na određenoj temperaturi

Relations for prediction of hardness of quenched and tempered steel was established by regression analysis [22]. The reference hardness, or hardness of quenched and tempered steel after one hour of tempering can be estimated based on as-quenched hardness, $HRC_{quenched}$, by [23, 24]:

$$HRC_{tempered} = \frac{HRC_{quenched} - HRC_{min}}{K} + HRC_{min} \quad (6)$$

where HRC_{min} is the material constant with known physical meaning. K is the factor or ratio between normed, relative, or a reference as-quenched and tempered hardness. Factor K can be expressed by:

$$K = \exp\left[AB\left(\frac{T_{tr}}{a} \right)^{n_1} \right] \quad (7)$$

where T_{tr}/K is the reference value of tempering temperature, while A, B, a and n_1 are the material constants, that are established by regression analysis of hardness of quenched and tempered steel.

Mechanical properties of quenched steel or quenched and tempered steel directly depends on degree of quenched steel hardening [21]. One most tested relation in material science is relation between hardness and ultimate tensile stress. Relation between hardness HV and ultimate tensile stress, R_m/MPa is equal to:

$$R_m = 3.3\text{HV} \quad (8)$$

By experimental work it was found out that relation given by Eq 8 is valid for tensile strength range between 400-2500 MPa [25].

Relation between hardness HV and yield strength, R_e/MPa is equal to [26]:

$$R_e = R_{p0,2} = (0.8 + 0.1S)R_m + 170S - 200 \quad (9)$$

Coefficient S which is ratio between the actual hardness and hardness of martensite in Rockwell C hardness, should be taken in account since as-quenched and quenched and tempered steel properties depends on degree of quenched steel hardening [21].

Fracture toughness, K_{Ic}/MPam$^{1/2}$, can be estimated from the mechanical properties obtained by tensile test. The Hahn-Rosenfield correlation can be successfully used for that purpose [27]:

$$K_{Ic} = \sqrt{\frac{\varepsilon_f n^2 E R_e}{60}} \quad (10)$$

where ε_f is the true fracture strain, n is the strain-hardening exponent, E/MPa is the modulus of elasticity.

True fracture strain can be expressed by percent reduction of area, Z/%:

$$\varepsilon_f = \ln\left(1 - \frac{Z}{100} \right)^{-1} \quad (11)$$

Percent reduction of area, Z/% can be estimated from the tensile strength by [26]:

$$Z = 96 - (0.062 - 0.029S)R_m \quad (12)$$

The strain-hardening exponent can be defined by:

$$\frac{R_m}{R_e} - \left(\frac{n}{0.002e} \right)^n \approx 0 \quad (13)$$

4. Application

The established relations were applied in computer simulation of blank/case hardening of steel specimen made of steel EN 20CrMo. Computer simulation was done using the computer software BS-QUENCHING [10]. Numerical calculation of the carbon distribution and cooling time $t_{8/5}$ was based on finite volume method [10].

The chemical composition of investigated steel specimen is: 0.20 % C, 0.25 % Si, 0.55 % Mn, 0.95 % Cr, 0.20 % Mo. Jominy test results of the investigated steel are shown in Table 3. The geometry of the steel specimen is shown in Fig. 2. Steel specimen was pack carburized at 950 °C for 8 h/air in DURFERRIT KG 30. After carburizing specimen was quenched from 850 °C for 45 min/water. Simulation was done for quenching in water with H value equal to 1. After quenching specimen was tempered at 200 °C for 60 min/air.

Carbon content, hardness, tensile strength, yield strength, percent reduction of area and fracture toughness profile in location A (Fig. 2) of the case hardened steel specimen are shown in Figs. 3-8.

The distribution of hardness of the blank hardened steel specimen is shown in Fig. 9. The distribution of hardness of the case hardened steel specimen is shown in Fig. 10 [28].

Table 3. Jominy test results of steel EN 20CrMo

Tablica 3. Rezultati Jominyjevog pokusa čelika EN 20CrMo

Jominy distance/Jominyjeva udaljenost/mm	1.5	3	5	7	11	15	20	80
Hardness HRC/ Tvrdoća HRC	44	40	32	28	23	21	20	19

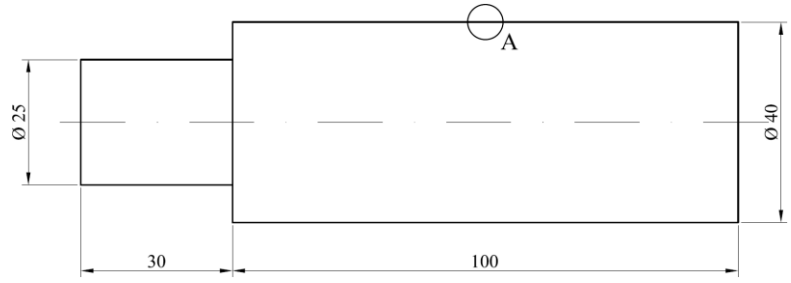

Figure 2. Geometry of the specimen

Slika 2. Geometrija čeličnog uzorka

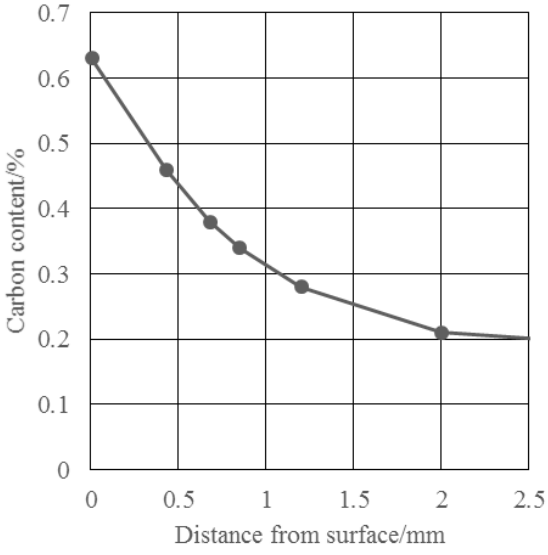

Figure 3. Profile of carbon content of the case hardened steel specimen in location A (Fig. 2)

Slika 3. Profil sadržaja ugljika cementiranog čeličnog uzorka u lokaciji A (Sl. 2)

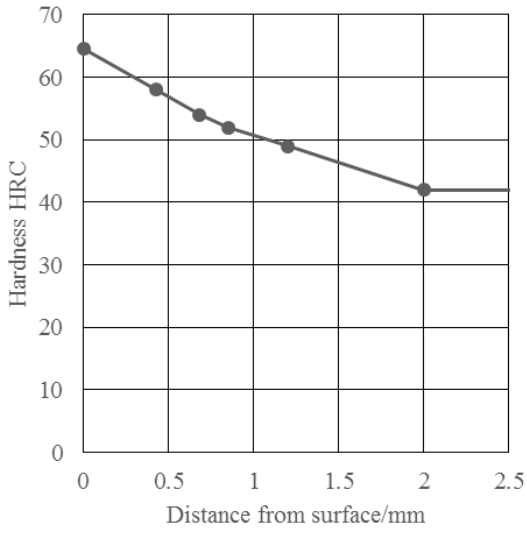

Figure 4. Profile of hardness of the case hardened steel specimen in location A (Fig. 2)

Slika 4. Profil tvrdoće cementiranog čeličnog uzorka u lokaciji A (Sl. 2)

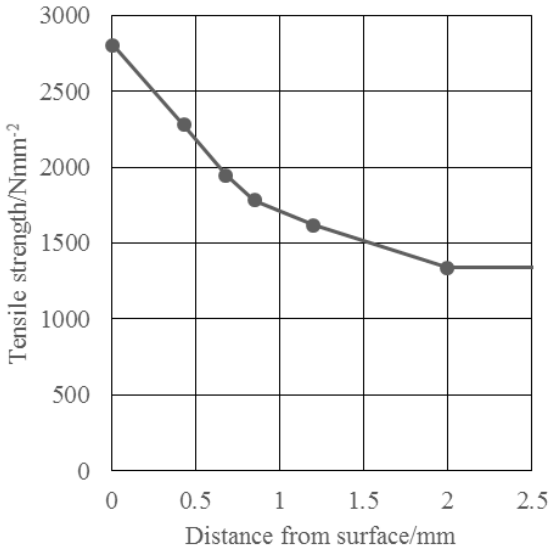

Figure 5. Profile of tensile strength of the case hardened steel specimen in location A (Fig. 2)

Slika 5. Profil vlačne čvrstoće cementiranog čeličnog uzorka u lokaciji A (Sl. 2)

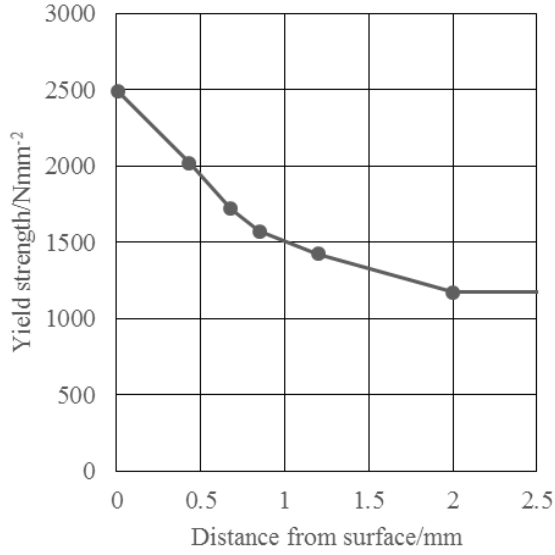

Figure 6. Profile of yield strength of the case hardened steel specimen in location A (Fig. 2)

Slika 6. Profil granice razvlačenja cementiranog čeličnog uzorka u lokaciji A (Sl. 2)

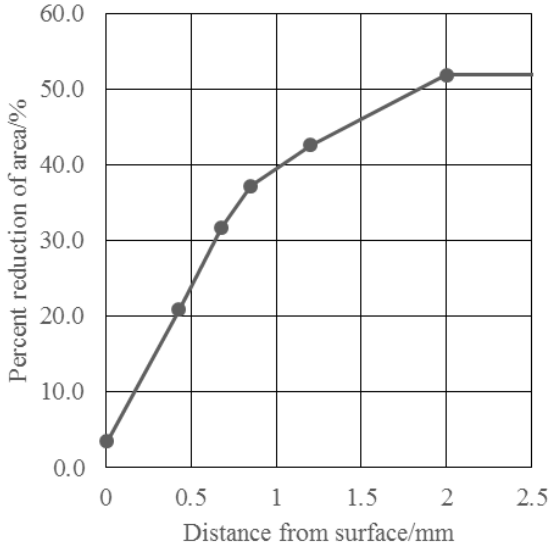

Figure 7. Profile of percent reduction of area of the case hardened steel specimen in location A (Fig. 2)

Slika 7. Profil kontrakcije cementiranog čeličnog uzorka u lokaciji A (Sl. 2)

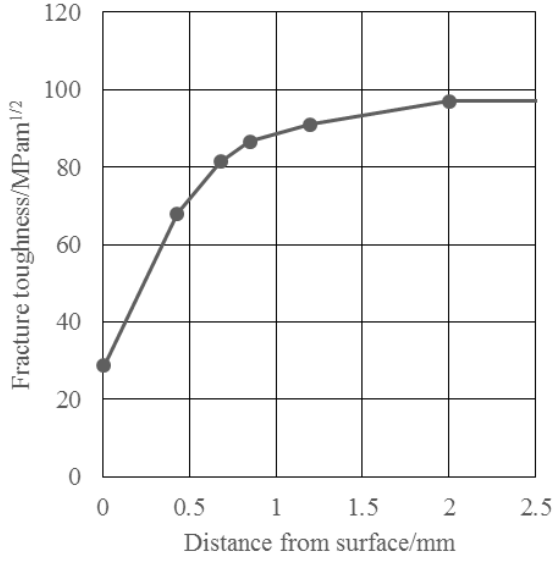

Figure 8. Profile of fracture toughness of the case hardened steel specimen in location A (Fig. 2)

Slika 8. Profil lomne žilavosti cementiranog čeličnog uzorka u lokaciji A (Sl. 2)

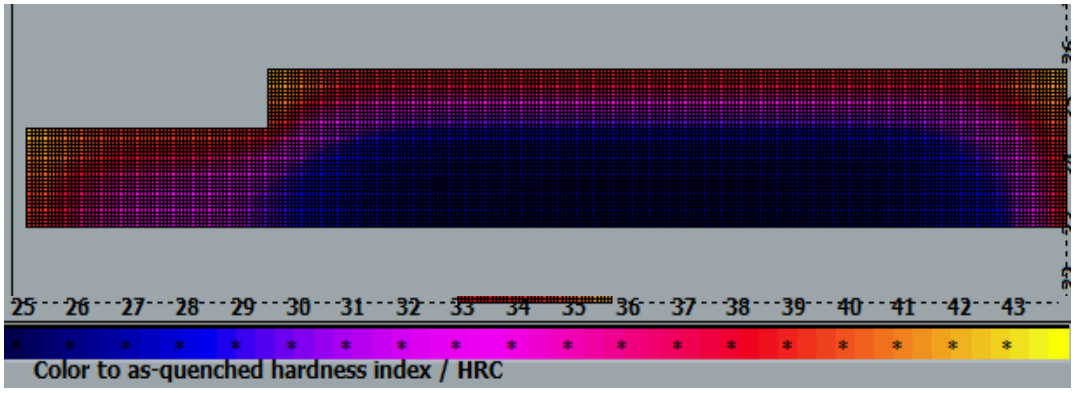

Figure 9. Distribution of hardness of blank hardened steel specimen [28]

Slika 9. Raspodjela tvrdoće slijepo kaljenog čeličnog uzorka [28]

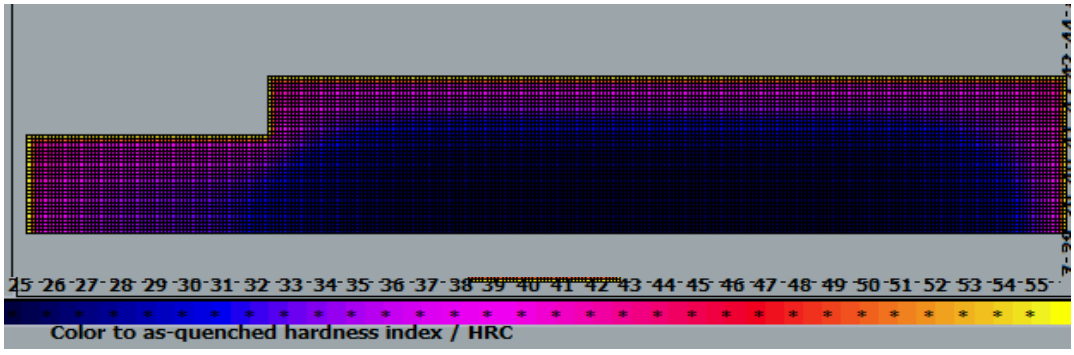

Figure 10. Distribution of hardness of case hardened steel specimen [28]

Slika 10. Raspodjela tvrdoće cementiranog čeličnog uzorka [28]

5. Conclusions

Mathematical model for estimation of case hardening of steel was developed. Developed mathematical model is consisted of mathematical model of steel carburizing, mathematical model of quenching and of mathematical model of tempering of steel.

In the root of mathematical modelling of case hardening are development of mathematical model of heat transfer and diffusion of carbon. Modelling of heat transfer and diffusion of carbon are based on the finite volume method and it is applicable to steel specimen with complex geometry. Prediction of hardness is based on Jominy test results and on effect of carbon content on Jominy test results. Hardness in specimen points was calculated by the conversion of calculated time of cooling from 800 to 500 °C to hardness.

By proposed model, it is possible to predict both, the carbon content in surface layer of carburized steel specimen and to predict the mechanical distribution of mechanical properties in case hardened steel specimen.

The possibilities of application of developed model in computer simulation of case hardening was applied in case hardening of steel specimen made of steel EN 20CrMo. Developed mathematical model can be successfully applied in simulation of case hardening of steel. For more serious application in industry practice, further experimental research have to be done.

Acknowledgements

This work has been supported in part by Croatian Science Foundation under the project 5371.
This work has been supported in part by University of Rijeka, Support No 13.09.1.1.02.

REFERENCES

[1] Goldstein J. I., Moren A. E., (1978), *Diffusion modeling of the carburization process*, Metallurgical and Materials Transactions A 9 No. 11, p 1515-1525

[2] Totten G. E., Howes M. A. H., (1997), *Steel Heat Treatment Handbook*, New York, NY: Marcell Dekker, Inc.

[3] Smoljan B., (2000), *Mathematical modeling of steel quenching*, AMME'2000, Gliwice-Sopot-Gdansk, Poland

[4] Dobrzański L. A., Trzaska J., (2004), *Application of neural networks to forecasting the CCT diagram*, Journal of Materials Processing Technology 157–158 No. 1, p 107-113

[5] Serajzadeh S., (2004), *A mathematical model for prediction of austenite phase transformation*, Materials Letters 58 No. 10, p 1597-1601

[6] Reti T., Horvath L., Felde I., (1997), *A comparative study of methods used for the prediction of nonisothermal austenite decomposition*, Journal of Materials Engineering and Performance 6 No. 4, p 433-442

[7] Rose A., Wever F., (1954), *Atlas zur Wärmebehandlung der Stähle I*, Verlag Stahleisen M. B. H., Düsseldorf

[8] Mayner P., et al., (1978), *Hardenability Concepts with Application to Steels*, Metal. Soc. of AIME, New York

[9] Smoljan B., (1999), *The calibration of the heat conductivity coefficient in mathematical model of steel quenching*, MicroCAD`99, Miskolc, Hungary

[10] Smoljan B., (1998), *Numerical simulation of as-quenched hardness in a steel specimen of complex form*, Communications in Numerical Methods in Engineering 14 No. 3, p 277-285

[11] Patankar S., (1980), *Numerical Heat Transfer and Fluid Flow*, McGraw Hill Book Company, New York

[12] Smoljan B., Iljkić D., Novak H., (2013), *Estimation of coefficient of heat conductivity and heat transfer coefficient in the numerical model of the steel quenching*, MCHT&SE2013, Dubrovnik-Cavtat, Croatia

[13] Bhadeshia H. K. D. H., (2002), *Material Factors, in: Residual Stress and Deformation of Steel*, ASM International, Materials Park, Ohio

[14] Smoljan B., (1995), *The calibration of the mathematical model of steel quenching*, 5th World Seminar on Heat Treatment and Surface Engineering, Isfahan, Iran

[15] Crank J., (1979), *The Mathematics of Diffusion*, 2nd. ed., Clarendon, Oxford

[16] Stolar P., Prenosil B., (1984), *Kinetics of transfer of carbon from carburizing and carbonitriding atmospheres*, Metallic Materials (English translation of Kovove Materialy) 22 No. 5, p 348-353

[17] Yan M., Liu Z., Zu G., (1992), *The mathematical model of surface carbon concentration growth during gas carburization*, Materials Science Progress (in Chinese) 6 No. 3, p 223-225

[18] Callister W. D., (1997), *Materials Science and Engineering: An Introduction*, 4th ed., John Wiley & Sons, Inc.

[19] Gamsjäger E., Svoboda J., Fischer F. D., (2005), *Austenite to ferrite phase transformation in low-alloyed steels*, Computational Materials Science 32, p 360-369

[20] Smoljan B., Iljkić D., Štic L., (2016), *Mathematical modeling and computer simulation of non-monotonic quenching*, 23rd IFHTSE Congress, Savannah, Georgia

[21] Smoljan B., (2006), *Prediction of mechanical properties and microstructure distribution of quenched and tempered steel shaft*, Journal of Materials Processing Technology 175 No. 1, p 393-397

[22] Iljkić D., (2010), *A contribution to the development of the mechanical properties prediction of quenched and tempered steel and cast steel*, Doctoral Thesis, Department of Materials Science and Engineering, Faculty of Engineering in Rijeka, (in Croatian)

[23] Smoljan B., Iljkić D., Totten G. E., (2015), *Mathematical modeling and simulation of hardness of quenched and tempered steel*, Metallurgical and Materials Transactions B 46, p 2666-2673

[24] Reti T., Felde I., Guerrero M., Sarmiento S., (2009), *Using generalized time-temperature parameters for predicting the hardness change occurring during tempering*, International Conference on New Challenges in Heat Treatment and Surface Engineering (Conference in honour of Prof. Božidar Liščić), Dubrovnik-Cavtat, Croatia

[25] Pavlina E. J., Van Tyne C. J., (2008), *Correlation of yield strength and tensile strength with hardness for steels*, Journal of Materials Engineering and Performance 17 No. 6, p 888-893

[26] Just E., (1976), *Verguten-werkstoffbeeinflussung durch harten und anlassen*, VDI-Berichte 256, p 125-140

[27] Smoljan B., Butković M., (1998), *Simulation of mechanical properties of hardened steel*, MicroCAD'98, Miskolc, Hungary

[28] Smoljan B., Iljkić D., Štic L., Rubeša D., (2016), *Numerical modelling of steel carburizing*, MCHT&SE2016, Portorož, Slovenia

ISSN 1847-7917

Analysis of Variance for Aluminium Alloy Surface Roughness Data

Katica ŠIMUNOVIĆ, Ilija SVALINA, Tomislav ŠARIĆ, Sara HAVRLIŠAN, Roberto LUJIĆ, Goran ŠIMUNOVIĆ

University of Osijek, Mechanical Engineering Faculty in Slavonski Brod, Trg I. Brlic-Mazuranic 2, 35000 Slavonski Brod, **Croatia**
Sveučilište u Osijeku, Strojarski fakultet u Slavonskom Brodu, Trg I. Brlić-Mažuranić 2, 35000 Slavonski Brod, **Hrvatska**

katica.simunovic@sfsb.hr
ilija.svalina@sfsb.hr
tomislav.saric@sfsb.hr
sara.havrlisan@sfsb.h
roberto.lujic@sfsb.hr
goran.simunovic@sfsb.hr

Keywords

Aluminium alloy
Analysis of variance
Factorial design
Surface roughness

Ključne riječi

Aluminijska legura
Analiza varijance
Faktorski plan pokusa
Površinska hrapavost

Original scientific paper

Abstract: With the main aim of studying the effects of three input variables, namely depth of cut *a*, feed rate *f* and spindle speed *n* as well as their interactions on the output response (the arithmetic average of the roughness profile *Ra*) of face-milled aluminium alloy, the analysis of variance for experimental data was performed. The experimental results were obtained from a full factorial design with three factors at four levels with two replicates ($4^3 \times 2$). This experimental design was previously used for the generation of the fuzzy inference system to predict and control the surface roughness using the adaptive neuro-fuzzy inference system (ANFIS). In the present study, the obtained experimental data were statistically analysed. The results indicate that the depth of cut and feed rate are statistically significant. A linear two-factor interaction between the feed rate and the depth of cut is also significant, i.e., varying the feed rate does not have the same effect on the surface roughness at different levels of the depth of cut and vice versa.

Analiza varijance podataka površinske hrapavosti aluminijske legure

Izvorni znanstveni rad

Sažetak: Cilj ovoga rada je, primjenom analize varijance eksperimentalnih podataka, istražiti utjecaj tri ulazne varijable (dubina rezanja *a*, posmak po zubu *f* i učestalost vrtnje *n*) te njihove interakcije, na izlaznu varijablu (srednje aritmetičko odstupanje profila *Ra*) čeono glodane aluminijske legure. Eksperimentalni podaci su dobiveni faktorskim planom pokusa s tri faktora na četiri razine uz dva ponavljanja svake kombinacije faktora. Podaci iz provedenog plana pokusa su prethodno bili temelj za generiranje sustava neizrazitog zaključivanja za predviđanje i kontrolu hrapavosti površine pomoću metode prilagodljivog neuro-neizrazitog sustava zaključivanja. U ovom su radu podaci statistički analizirani. Analizom varijance dobivenih eksperimentalnih podataka utvrđeno je da su faktori dubina rezanja i posmak po zubu značajni kao i linearna interakcija tih faktora, tj. promjena razina posmaka za različite razine dubine rezanja ima različit utjecaj na površinsku hrapavost i obrnuto.

1. Introduction

The design of experiment (DOE) methodology has often been applied in surface roughness investigations. Full factorial design, also applied in the current work, is used by the authors [1-7] in order to investigate the effects of the factors or to obtain regression models and/or to optimize the processing of different aluminium alloys. Milling by varying the helical angle, axial and radial depth of cut is performed in [1] with the main aim to study the following responses: surface roughness, cutting force and material removal rate. The process of abrasive water jet cutting is applied by the authors [2] to investigate the influence of jet pressure, abrasive mixing rate, cutting feed and plate thickness on surface finish, maximum width of cut and percentage proportion of striation free area. The authors [3] also deal with the abrasive water jet cutting of Al alloy to study the effect of material thickness, feed rate and abrasive flow rate on the surface roughness. The ball burnishing process [4] as well as electrical discharge machining by using magnetic abrasive finishing [5] of Al alloys are investigated to study the effects of processing parameters on surface hardness [4] and surface roughness together with recast layer thickness [5]. Turning of zinc-aluminium alloy reinforced with SiC [6] and aluminium alloy reinforced with SiC [7] is applied to vary the common parameters as cutting speed, depth of cut and feed rate. Finally, from the above described recently published papers the conclusion can be made that the statistical analysis of data has been widely applying to draw valuable conclusions.

Symbols/Oznake

a	- depth of cut, mm - dubina rezanja, mm	*n*	- spindle speed, min^{-1} - učestalost vrtnje, min^{-1}
f	- feed rate, mm/tooth - posmak, mm/zubu		

2. Experimental procedure

The examined material is aluminium alloy Al6060 T66 (in accordance with the European norms EN AW-6060 [AlMgSi]) whose nominal chemical composition is shown in Table 1. Mechanical and physical properties (at 20 °C), according to EN755-2 are presented in Table 2. The experiment is conducted on the CNC vertical milling machine, type TM-2P of manufacturer HAAS with the technical data presented in Table 3.

Table 1. Chemical composition of Al6060 according to EN573-3

Tablica 1. Kemijski sastav aluminijske legure Al6060 prema EN573-3

Chemical Element/ Kemijski element	Si	Fe	Cu	Mn	Mg	Cr	Zn	Ti
wt. (%)/ Težinski udio (%)	0.3-0.6	0.1-0.3	max 0.1	max 0.1	0.35-0.6	max 0.1	max 0.1	max 0.1

Table 2. Mechanical and physical properties of Al6060 (at 20 °C) according to EN755-2

Tablica 2. Mehanička i fizikalna svojstva aluminijske legure Al6060 (pri 20 °C) prema EN755-2

Yield tensile strength, MPa/ Vlačna čvrstoća, MPa	150
Ultimate tensile strength, MPa/ Granica razvlačenja, MPa	195
Elongation at break, %/ Istezanje, %	8
Hardness, Brinell/ Tvrdoća Brinell	65
Modulus of elasticity, GPa/ Modul elastičnosti, GPa	70
Density, kg/m^3/ Gustoća, kg/m^3	2700
Melting point, °C/ Talište, °C	585-650
Thermal conductivity, W/mK/ Toplinska vodljivost, W/mK	200-220
Coefficient of thermal expansion, 10^{-6}/K/ Koeficijent toplinskog širenja, 10^{-6}/K	23.4

Table 3. Technical data of vertical CNC machine

Tablica 3. Tehničke značajke vertikalne CNC glodalice

Slideway longitudinal, X axis, mm/ X os, mm	1016
Slideway cross, Y axis, mm/ Y os, mm	406
Slideway vertical, Z-axis, mm/ Z os, mm	406
Maximal power, kW/ Maksimalna snaga, kW	5.6
Maximal spindle speed, min^{-1} Maksimalna učestalost vrtnje, min^{-1}	6000
Pallete size, mmxmm/ Veličina radnog stola, mmxmm	1466x267

The characteristics of tool used are as follows:
- diameter of 40 mm
- tool holder WALTER type F 4042.B.040.Z04.15 (Figure 1)
- four cutting inserts type ADMT160608R-F56 WKP35S (Figure 2).

Figure 1. Tool WALTER type F4042.B.040.Z04.15

Slika 1. Alat WALTER tip F4042.B.040.Z04.15

Figure 2. Cutting inserts type ADMT160608R-F56 WKP35S

Slika 2. Pločice tip ADMT160608R-F56 WKP35S

The specimens were cut on the band saw with cooling/lubricating. The raw material used was flat bar

(thickness of 10 mm and width of 100 mm). After the cutting on saw machine, the side ragged edges were machined by face milling tool because they were used as the technological bases. The dimensions of specimens were 100×54×10 mm. Figure 3 presents all 128 specimens.

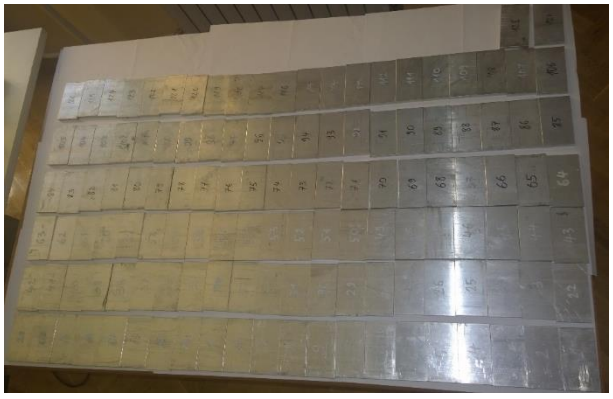

Figure 3. The examined material specimens

Slika 3. Uzorci istraživanog materijala

For the surface roughness measurement (the arithmetic average of the roughness profile *Ra* was measured according to ISO 4288), portable Surtronic S128 roughness tester (Figure 4) manufactured by Taylor & Hobson was used.

Figure 4. Surtronic S128 roughness tester

Slika 4. Prijenosni uređaj za mjerenje hrapavosti Surtronic S128

2.1. Statistically designed experiment

Since the experimental design was the basis for generating the integrated fuzzy inference system to predict and control the surface roughness using the adaptive neuro-fuzzy inference system (ANFIS) as well as to optimize the machining parameters by genetic algorithm [8] the experimental objective was to obtain as much experimental data as possible to provide the needed input/output data for the training and validation phase for the surface roughness prediction and control parts of the above mentioned integrated system. Both parts of system needed the three input variables. For generating fuzzy inference system the three membership functions per each input were used which means that the base of fuzzy rules consisted of 27 different rules [9]. Each of the 27 rules has an output connected to the output function defined by three different inference parameters. From the foregoing it can be concluded that in the training phase 81 parameters will be needed that determines the minimum 81 sets of input/output experimental data for the training phase. In addition to the training phase, input/output experimental data were also needed for validation phase (it was necessary to provide 10 % of the input/output experimental data). As the fuzzy inference system had three inputs the chosen experimental design must have three factors. Taking into consideration the number of system inputs the same as the number of input/output experimental data a full factorial design 4^3 is selected. The design is replicated twice, i.e., each factor combination is repeated twice. Each of 128 observations is run in random order, i.e., the experiment is performed in random order which means that the runs and allocation of the experimental material were both randomly determined. In this way, the observations (or errors) are independently distributed random variables [10] and some impact of undesirable factors is reduced to a minimum [10]. There were two repeated measurements on each sample and the maximum *Ra* is used as the output response for the statistical analysis.

The levels and ranges for the three numeric (quantitative) factors – spindle speed, feed rate and the depth of cut are shown in Table 4.

Table 4. Held-constant factors and levels of design factors

Tablica 4. Nepromjenjivi faktori te razine faktora plana pokusa

Name/Naziv	Factor/ Faktor	Units/ Jedinice mjere	Level 1/ Razina 1	Level 2/ Razina 2	Level 3/ Razina 3	Level 4/ Razina 4
Spindle speed, *n*/ Učestalost vrtnje, *n*	A	min^{-1}	1000	2000	3000	4000
Feed, *f* / Posmak, *f*	B	mm/tooth	0.025	0.1	0.175	0.25
Depth of cut, *a*/ Dubina rezanja, *a*	C	mm	0.5	1	1.5	2
Held-constant factors/ Faktori koji se nisu mijenjali u pokusu	Tool, tool stepover between neighbour paths, number of passes, total length of paths, Maxol company cooling/lubricating fluid produced by Forol					

3. Conducting the experiment

Prior to running the main experiment, some trial runs were performed to check the milling machine, measurement device, operators and to choose the levels and ranges of the factors. For the pilot experiment, the minimum *Ra* was 0.4 μm and therefore it was decided to use the cooling/lubricating fluid in the main experiment to get better quality of surface, i.e. lower values of *Ra*.

Table 5 shows the results of measured roughness for conducted experiment. The last column represents the maximum *Ra* of two repeated measurements. For 128 observations some descriptive statistics parameters are as follows: mean *Ra* 0.708 μm, minimum *Ra* 0.261 μm, maximum *Ra* 1.63 μm and standard deviation of *Ra* 0.253 μm.

Table 5. Experimental design and results for the arithmetic average of the roughness profile *Ra*

Tablica 5. Plan pokusa i rezultati za srednje aritmetičko odstupanje profila *Ra*

Run/ Broj pokusa	Standard Order/ Broj uzorka	Factor 1 C: Spindle speed (min^{-1})/ Faktor 1 C: Učestalost vrtnje (min^{-1})	Factor 2 B: Feed rate (mm/tooth)/ Faktor 2 B: Posmak (mm/zubu)	Factor 3 A: Depth of cut (mm)/ Faktor 3 A: Dubina rezanja (mm)	Arithmetic average of the roughness profile *Ra* (μm)/ Srednje aritmetičko odstupanje profila *Ra* (μm)
31	1	1000	0.025	0.5	0.325
71	2	1000	0.025	0.5	0.301
59	3	2000	0.025	0.5	0.381
116	4	2000	0.025	0.5	0.504
10	5	3000	0.025	0.5	0.357
82	6	3000	0.025	0.5	0.389
39	7	4000	0.025	0.5	0.339
81	8	4000	0.025	0.5	0.453
24	9	1000	0.1	0.5	0.877
120	10	1000	0.1	0.5	0.768
5	11	2000	0.1	0.5	0.619
118	12	2000	0.1	0.5	0.641
47	13	3000	0.1	0.5	0.855
77	14	3000	0.1	0.5	0.936
30	15	4000	0.1	0.5	0.806
69	16	4000	0.1	0.5	0.76
63	17	1000	0.175	0.5	0.84
113	18	1000	0.175	0.5	0.412
36	19	2000	0.175	0.5	0.638
85	20	2000	0.175	0.5	0.999
46	21	3000	0.175	0.5	0.605
75	22	3000	0.175	0.5	0.635
41	23	4000	0.175	0.5	0.666
117	24	4000	0.175	0.5	0.509
17	25	1000	0.25	0.5	0.912
66	26	1000	0.25	0.5	1.06
45	27	2000	0.25	0.5	0.695
94	28	2000	0.25	0.5	0.616
35	29	3000	0.25	0.5	0.851
121	30	3000	0.25	0.5	0.945
34	31	4000	0.25	0.5	0.962
76	32	4000	0.25	0.5	0.719
27	33	1000	0.025	1	0.356
92	34	1000	0.025	1	0.453
1	35	2000	0.025	1	0.421
109	36	2000	0.025	1	0.371
8	37	3000	0.025	1	0.348
123	38	3000	0.025	1	0.312
37	39	4000	0.025	1	0.403
79	40	4000	0.025	1	0.357
22	41	1000	0.1	1	0.657

Table 5 continued. Experimental design and results for the arithmetic average of the roughness profile *Ra*

Tablica 5 nastavak. Plan pokusa i rezultati za srednje aritmetičko odstupanje profila *Ra*

Run/ Broj pokusa	Standard Order/ Broj uzorka	Factor 1 C: Spindle speed (min^{-1})/ Faktor 1 C: Učestalost vrtnje (min^{-1})	Factor 2 B: Feed rate (mm/tooth)/ Faktor 2 B: Posmak (mm/zub)	Factor 3 A: Depth of cut (mm)/ Faktor 3 A: Dubina rezanja (mm)	Arithmetic average of the roughness profile *Ra* (μm)/ Srednje aritmetičko odstupanje profila *Ra* (μm)
122	42	1000	0.1	1	0.515
20	43	2000	0.1	1	0.512
111	44	2000	0.1	1	0.84
4	45	3000	0.1	1	0.688
70	46	3000	0.1	1	0.697
28	47	4000	0.1	1	0.65
80	48	4000	0.1	1	0.555
14	49	1000	0.175	1	0.967
115	50	1000	0.175	1	0.714
32	51	2000	0.175	1	0.709
95	52	2000	0.175	1	1
49	53	3000	0.175	1	0.957
114	54	3000	0.175	1	1.01
26	55	4000	0.175	1	0.752
84	56	4000	0.175	1	0.641
44	57	1000	0.25	1	0.828
90	58	1000	0.25	1	0.528
9	59	2000	0.25	1	0.923
105	60	2000	0.25	1	0.589
3	61	3000	0.25	1	0.735
83	62	3000	0.25	1	0.894
52	63	4000	0.25	1	0.734
106	64	4000	0.25	1	0.922
21	65	1000	0.025	1.5	0.347
67	66	1000	0.025	1.5	0.525
56	67	2000	0.025	1.5	0.342
127	68	2000	0.025	1.5	0.362
55	69	3000	0.025	1.5	0.261
125	70	3000	0.025	1.5	0.378
7	71	4000	0.025	1.5	0.393
128	72	4000	0.025	1.5	0.377
53	73	1000	0.1	1.5	0.573
93	74	1000	0.1	1.5	0.835
40	75	2000	0.1	1.5	0.658
107	76	2000	0.1	1.5	0.982
13	77	3000	0.1	1.5	0.636
98	78	3000	0.1	1.5	0.681
60	79	4000	0.1	1.5	0.66
104	80	4000	0.1	1.5	0.934
18	81	1000	0.175	1.5	0.897
96	82	1000	0.175	1.5	1.06
54	83	2000	0.175	1.5	0.74
97	84	2000	0.175	1.5	0.638
25	85	3000	0.175	1.5	0.809
102	86	3000	0.175	1.5	0.592
29	87	4000	0.175	1.5	0.759
89	88	4000	0.175	1.5	0.478
50	89	1000	0.25	1.5	1.63

Table 5 continued. Experimental design and results for the arithmetic average of the roughness profile *Ra*

Tablica 5 nastavak. Plan pokusa i rezultati za srednje aritmetičko odstupanje profila *Ra*

Run/ Broj pokusa	Standard Order/ Broj uzorka	Factor 1 C: Spindle speed (min^{-1})/ Faktor 1 C: Učestalost vrtnje (min^{-1})	Factor 2 B: Feed rate (mm/tooth)/ Faktor 2 B: Posmak (mm/zub)	Factor 3 A: Depth of cut (mm)/ Faktor 3 A: Dubina rezanja (mm)	Arithmetic average of the roughness profile *Ra* (μm)/ Srednje aritmetičko odstupanje profila *Ra* (μm)
108	90	1000	0.25	1.5	0.87
61	91	2000	0.25	1.5	1.25
87	92	2000	0.25	1.5	0.883
51	93	3000	0.25	1.5	1.21
112	94	3000	0.25	1.5	0.924
23	95	4000	0.25	1.5	0.831
126	96	4000	0.25	1.5	0.881
48	97	1000	0.025	2	0.364
110	98	1000	0.025	2	0.428
64	99	2000	0.025	2	0.365
103	100	2000	0.025	2	0.355
12	101	3000	0.025	2	0.318
74	102	3000	0.025	2	0.567
15	103	4000	0.025	2	0.38
91	104	4000	0.025	2	0.561
43	105	1000	0.1	2	0.82
72	106	1000	0.1	2	0.84
16	107	2000	0.1	2	0.811
88	108	2000	0.1	2	0.735
2	109	3000	0.1	2	0.621
78	110	3000	0.1	2	0.808
33	111	4000	0.1	2	0.813
101	112	4000	0.1	2	0.591
57	113	1000	0.175	2	0.902
124	114	1000	0.175	2	0.997
62	115	2000	0.175	2	0.917
99	116	2000	0.175	2	0.953
38	117	3000	0.175	2	1
100	118	3000	0.175	2	0.831
11	119	4000	0.175	2	0.848
68	120	4000	0.175	2	0.884
19	121	1000	0.25	2	1.21
119	122	1000	0.25	2	1.26
58	123	2000	0.25	2	0.984
73	124	2000	0.25	2	0.928
42	125	3000	0.25	2	1.08
65	126	3000	0.25	2	0.873
6	127	4000	0.25	2	1.03
86	128	4000	0.25	2	0.8

4. Statistical analysis of the data

Statistical analysis of the measured response – roughness *Ra*, as well as the generation of run order is performed by the licensed software Design Expert (version DX8, 8.0.7.1, Stat-Ease, Inc. Minneapolis, 2010). Since in this paper the basic experimental results were processed from the statistical point of view, included in this section of the paper are the graphical presentations of arithmetic average of the roughness profile *Ra* versus design factors (Figures 5, 6 and 7) as well as the analysis of variance of the experimental data to investigate the individual effects of each factor (the main effects) and to determine whether the factors interact.

From the figures 5, 6 and 7 it is visible that for the spindle speed of 1000 min^{-1}, feed of 0.25 mm/tooth and depth of

cut of 1.5 mm, the outlier exists, i.e. the value *Ra* of 1.63 μm is higher than other values.

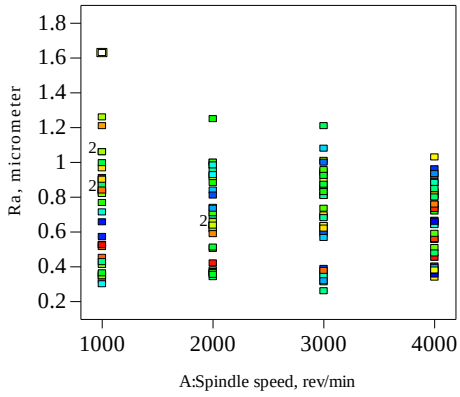

Figure 5. Surface roughness versus spindle speed

Slika 5. Površinska hrapavost – učestalost vrtnje

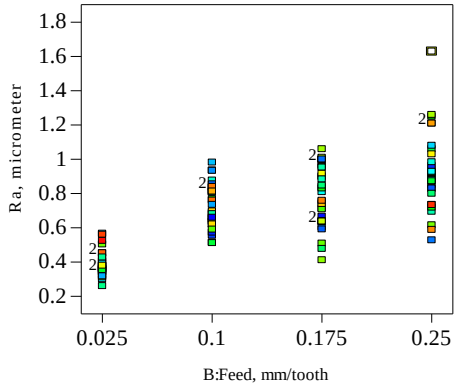

Figure 6. Surface roughness versus feed rate

Slika 6. Površinska hrapavost – posmak

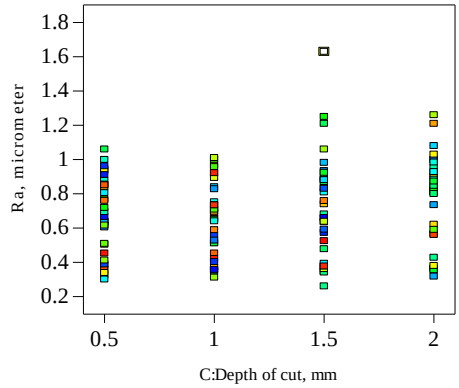

Figure 7. Surface roughness versus dept of cut

Slika 7. Površinska hrapavost – dubina rezanja

The analysis of variance for the surface roughness data is summarized in Table 6. It can be seen that the depth of cut and feed rate are statistically significant. A two-factor interaction is also significant. For these factors and two-factor interaction BC, *p* values for the *F* ratio (80.85; 4.89 and 3.00) are lower than the probability of type I error 0.05. From the experimental results, the empirical models can be derived. The simulation of different empirical models is presented in Table 7. The coefficient of determination R^2 is the highest for the model with all the factors including the two- and three-factor interactions. According to the information on possible statistical models, it can be concluded that it is not effective to derive models with a good coefficient of determination since the models could have so many terms to obtain a good R^2.

Table 6. ANOVA for surface roughness data

Tablica 6. Analiza varijance za eksperimentalne podatke

Source/ Izvor varijacije	Sum of squares/ Suma kvadrata odstupanja	Degrees of freedom/ Broj stupnjeva slobode	Mean square/ Srednje kvadratno odstupanje	*F* ratio/ Vrijednost *F* varijable	*p* value/ Vjerojatnost *F* varijable
A - Spindle speed, min^{-1}/ A - Učestalost vrtnje, min^{-1}	0.11	3	0.037	1.79	0.1570
B - Feed rate, mm/tooth/ B - Posmak, mm/zubu	5.02	3	1.675	80.85	< 0.0001
C - Depth of cut, mm/ C - Dubina rezanja, mm	0.30	3	0.101	4.89	0.0040
Two-factor interaction AB/ Interakcija dva faktora AB	0.18	9	0.020	0.99	0.4593
Two-factor interaction AC/ Interakcija dva faktora AC	0.16	9	0.017	0.84	0.5865
Two-factor interaction BC/ Interakcija dva faktora BC	0.56	9	0.062	3.00	0.0047
Three-factor interaction ABC/ Interakcija tri faktora ABC	0.49	27	0.018	0.87	0.6505
Error/ Pogreška	1.33	64	0.0207		
Total/ Ukupno	8.15	127			

Table 7. Information on possible statistical models

Tablica 7. Podaci o mogućim statističkim modelima

Included factors/interactions in model/ Uključeni faktori/interakcije u model	Coefficient of determination R^2/ Koeficijent determinacije R^2	Number of terms in the model/ Broj članova u modelu
A, B, C, AB, AC, BC, ABC	0.8373	64
A, B, C, AB, AC, BC	0.7778	37
B, C, BC	0.7224	16

5. Conclusion

In this paper, a statistically designed experiment is performed to investigate the face milling process of aluminium alloy. The response variable is the arithmetic average of the roughness profile *Ra*. Four spindle speeds, four feeds and four depths of cut are chosen, and two replications of each factor combination of a 4^3 factorial design are run.

By the analysis of variance of the experimental surface roughness data it is determined that the variables feed rate and the depth of cut are most influential on the surface roughness *Ra*. The same is valid for the interaction between these two variables, i. e. there is the difference in response on the levels of depth of cut at different levels of feed rate. It means that the effect of one factor depends on the level of another factor. Some effective empirical models could not be derived as many terms should be included which is proven by Table 7.

Finally, a conclusion can be made that the factorial designs are very efficient when a large number of data is needed (artificial intelligence methods) since all possible combinations of the levels of the factors are included thus allowing finding also the interactions between the factors.

REFERENCES

[1] Pan, Y. Z., Zhao, J., Fu, X. L., Ai, X., (2009), *Optimization of Surface Roughness Based on Multi-linear Regression Model and Genetic Algorithm*, International Conference on Manufacturing Science and Engineering ICMSE 2009, Zhuhai, China

[2] Iqbal, A., Dar, N. U., Hussain, G., (2011), *Optimization of Abrasive Water Jet Cutting of Ductile Materials*, Journal of Wuhan University of Technology-Materials Science Edition 26, No. 1, p 88-92

[3] Jankovic, P., Radovanovic, M., Baralic, J., Nedic, B., (2013), *Prediction Model of Surface Roughness in Abrasive Water Jet Cutting of Aluminium Alloy*, Journal of the Balkan Tribological Association 19, No. 4, p 585-595

[4] Sagbas, A., Kahraman, F., (2009), *Determination of Optimal Ball Burnishing Parameters for Surface Hardness*, Materiali in tehnologije 43, No. 5, p 271-274

[5] Amineh, S. K., Tehrani, A. F., Mohammadi, A., (2013), *Improving the surface quality in wire electrical discharge machined specimens by removing the recast layer using magnetic abrasive finishing method*, International Journal of Advanced Manufacturing Technology 66, No. 9-12, p 1793-1803

[6] Marigoudar, R. N., Sadashivappa, K., (2012), *Study of Cutting Force and Surface Roughness in Machining of ZA43 SiC Particulate MMC*, Advanced Composites Letters 21, No. 3, p 76-83

[7] Gaitonde, V. N., Karnik, S. R., Davim, J. Paulo, (2009), *Some Studies in Metal Matrix Composites Machining using Response Surface Methodology*, Journal of Reinforced Plastics and Composites 28, No. 20, p 2445-2457

[8] Svalina, I.; (2014), *Integrirani neuro-neizraziti sustav za predviđanje i kontrolu hrapavosti površine (An integrated neuro-fuzzy system for prediction and control of surface roughness)*, PhD thesis, Strojarski fakultet u Slavonskom Brodu, p 120

[9] Jang, J.-S. R., (1993), *ANFIS: Adaptive-Network-Based Fuzzy Inference System*, IEE Transactions on System, Man, and Cybernetics 23, No 3, p 665-685

[10] Montgomery D. C., (2009), *Design and Analysis of Experiment*, John Wiley and Sons Inc, Hoboken

ISSN 1847-7917

Effect of annealing in argon and hydrogen on tensile deformation behavior of ferritic-pearlitic steel

Michaela ŠTAMBORSKÁ[1)], Juraj LAPIN[1)], Oto BAJANA[1)]
1) Institute of Materials & Machine Mechanics Slovak Academy of Sciences, Dúbravská cesta 9, 845 13 Bratislava, **Slovakia**
ummsmsta@savba.sk

Keywords
Digital image correlation
Numerical simulation
Argon atmosphere
Hydrogenation

Original scientific paper
Abstract: The effect of annealing in flowing argon and hydrogen on room temperature tensile deformation behavior of ferritic-pearlitic steel was studied. The annealing of cylindrical tensile specimens was carried out at a temperature of 550 °C for 8 hours in flowing argon or hydrogen. After the annealing the specimens were rapidly cooled to 400 °C in argon and then cooled into water. Room temperature tensile deformation behavior of the specimens annealed in argon and hydrogen was studied by the digital image correlation (DIC) method. The tensile tests were carried out at an initial strain rate of 1×10^{-3} s^{-1} up to fracture. Elongation and contraction were measured on the surface of the tensile specimens with random speckle pattern using stereo CCD camera system. DIC elongation data were related to the data measured by an extensometer touching the specimens. The data from the DIC method were used for calculations of true stress-true strain tensile curves. Numerical simulations of strain fields within the gauge region of the specimens using finite element method were validated by the experimental data from the DIC method.

1. Introduction

Low carbon structural steels are widely applied in many engineering applications due to their low-cost, good plasticity, viscosity, and sufficiently high level of mechanical properties. It has been found in a majority of control-rolled steel plates, bars or pipes that the microstructure is composed of alternating layers of banded ferrite and pearlite (F/P) structure [1, 2]. Ferrite-pearlite microstructures are also found in the intermediary state of the hot-rolled strips required for the production of the newest high strength steels such as dual phase (DP) and transformation induced plasticity (TRIP) steels [3]. It has also been found that at room temperature the main diffusive path for hydrogen in a F/P structure was along the ferrite grain boundaries or interfaces between ferrite and pearlite, and pearlite colonies acted as effective barriers to hydrogen diffusivity [2, 4]. Classical tensile tests can provide only limited information about deformation behavior of these materials. Tensile specimens of metallic materials experience elastic deformation, plastic yielding, necking instability, and neck growth eventually leading to fracture due to a decrease in the load bearing capability. In order to understand tensile deformation behavior related to intrinsic and extrinsic properties of materials, not only experiments using precise machines and sensors but also deep interpretation of the deformation curves, specimen geometries, and specific testing conditions are important. Contactless sensing digital image correlation (DIC) optical method for tracking and image registration technique allows accurate 2D and 3D measurements of gauge section of specimens during tensile testing and can provide new information about tensile deformation behavior of materials [5, 6]. The additional data obtained during testing can be used to understand more deeply whole tensile deformation process including calculations of local elongation, local contraction and redistribution of strain fields on the surface of the specimen. Hence, application of the DIC method for tensile testing of classical ferritic-pearlitic steels is of great interest to extend the existing knowledge about the deformation behavior of this widely used group of materials.

The aim of this article is to study the effect of annealing in argon and hydrogen on tensile deformation behavior of low-carbon ferrite-pearlite steel. DIC method is applied for tracking, image registration and 2D measurements of changes in gauge section of specimens during tensile testing at room temperature. The achieved experimental results are supported by numerical calculations of the strain fields on the surface of tensile specimens using experimental data from DIC measurements as well as redistribution of strains within the gauge section using finite element analysis (FEA).

Symbols			
			Greek letters
YS	- yield strength, MPa	ε_t	- true strain
UTS	- ultimate tensile strength, MPa	σ_t	- true stress, MPa
A	- elongation	ε_{xx}	- strain fields in x direction
Z	- contraction	ε_{yy}	- strain fields in y direction
OM	- optical microscopy	γ_{xy}	- shear strain
		Θ	- work hardening rate, MPa

2. Experimental procedure

The studied ferritic-pearlitic steel was received in the form of cylindrical bars with a diameter of 10 mm. Chemical composition of these bars was determined by glow discharge surface analyzer LECO GDS 750A.

Tensile specimens with threaded heads, gauge diameter of 5 mm and gauge length of 30 mm were prepared by lathe machining. The gauge section of the specimens was polished to a roughness better than 0.3 μm. The annealing of the specimens was carried out at a temperature of 550 °C for 8 hours in flowing argon or hydrogen. After annealing the specimens were rapidly cooled to 400 °C in argon and then cooled into water. Hydrogen content was measured by LECO ONH836 analyzer using small samples with a weight of 1 g, which were cut from cylindrical samples with a diameter of 5 mm and length of 30 mm annealed with the tensile specimens in argon or hydrogen.

Room temperature tensile tests were carried out at an initial strain rate of 1×10^{-3} s^{-1} using Zwick/Roell Z100 tensile machine. Elongation of the specimens was measured by extensometer MAYTEC touching the surface of the gauge section of the specimen. The deformation was also measured by a 3D digital image correlation (DIC) method using two high-speed CCD cameras MCR-2048-53 2/3".

Microstructure examination of the tensile specimens before testing was performed by optical microscopy (OM) using Olympus GX51 optical microscope. Samples for OM were prepared by grinding on water resistance abrasive papers with grit size ranging from 320 to 2400 and polishing on diamond pastes with various grains size ranging from 7 to 1 μm. The polished samples were etched in a solution consisting of 90 ml of 96% ethanol and 10 ml HNO_3.

3. Results and discussion

3.1. Chemical composition and microstructure

Table 1 summarizes the results of GDS measurements of the chemical composition of the as-received ferritic-pearlitic steel. The measured chemical composition of the studied material fulfils all requirements for the medium carbon steel according to the Slovak technical standards STN 411550 (DIN 17100 St 55). The studied steel produced as a trial batch the Slovak producer, is usually used for the production of seamless tubes.

Figures 1a) and 1b) shows the typical grain microstructure on transverse sections of the tensile specimens annealed in argon and hydrogen before deformation, respectively. Similar grain morphology was also observed on longitudinal sections of the tensile specimens indicating negligible anisotropy of the bars before tensile testing. The microstructure of the both types of the tensile specimens consists of slightly elongated ferritic grains and pearlitic colonies before tensile testing (Figure 1).

The measurements of hydrogen content in the specimens annealed in argon and hydrogen vary from 0.16 to 0.62 wt.ppm and from 1.19 to 2.82 wt.ppm, respectively. These values indicate that the studied steel is not prone to an intensive hydrogenation at the studied annealing temperature. As shown by Chan and Charles [4], the ferrite/pearlite and pearlite/pearlite interfaces are effective hydrogen trapping sites. However, the ferrite/cementite interfaces within the pearlite colonies have only little effect on the hydrogen occlusivity. Although the ferrite/cementite lamella interface has little effect on the hydrogen occlusivity, the lamellae interfere with the hydrogen diffusion path across the pearlite colonies.

Table 1: Chemical composition of original state of material obtained by LECO GDS 750A

Weight %										
C	**Mn**	**Si**	**P**	**S**	**Cr**	**Ni**	**Cu**	**Co**	**Zr**	**Al**
0.33	0.85	0.26	0.021	0.016	0.089	0.039	0.053	0.018	0.024	0.013

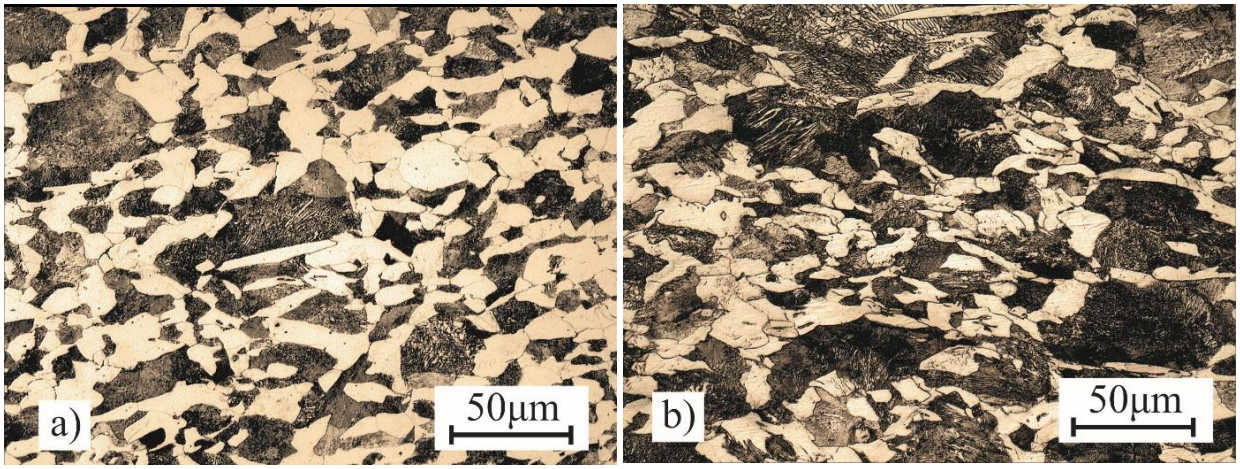

Figure 1. OM microstructure of the tensile specimens annealed in a) argon and b) hydrogen before testing

3.2. Tensile deformation behavior

Figure 2 shows the typical tensile engineering stress-strain curve of the specimens annealed in argon and hydrogen tested to the fracture. The elongation was measured by extensometer MAYTEC touching from one side the gauge section of the specimen. The stress-strain curves of the specimen annealed in hydrogen do not exhibit clear yielding point. The offset yield strength is determined as the stress corresponding to 0.2% plastic deformation. As we can see the values of yield strength and ultimate tensile strength for the specimen annealed in hydrogen are higher by about 6% than those for the specimen annealed in argon. Table 2 summarizes average values of offset 0.2% yield strength (YS), ultimate tensile strength (UTS), elongation (A), reduction of area (Z) and maximum values of local strain (ε_{max}) calculated from 5 tensile specimens tested for each type of annealing. As seen in this table, elongation of the tensile specimens is evaluated from the tensile curves, measured by the DIC method using Mercury RT software and manually measured on specimens after tensile testing. For the measurements of contraction, direct manual measurements on the specimens and the DIC measurements are applied. The direct manual measurements of elongation and contraction on the specimens allow to achieve only discrete values after tensile testing to the fracture. On the other hand, the DIC method equipped with video extensometer of Mercury RT software provides large elongation and contraction data set allowing mapping whole tensile deformation process. In addition, the Mercury RT software enables to calculate strain fields and maximum value of local strain (ε_{max}) from the experimentally measured displacement fields during the entire tensile tests.

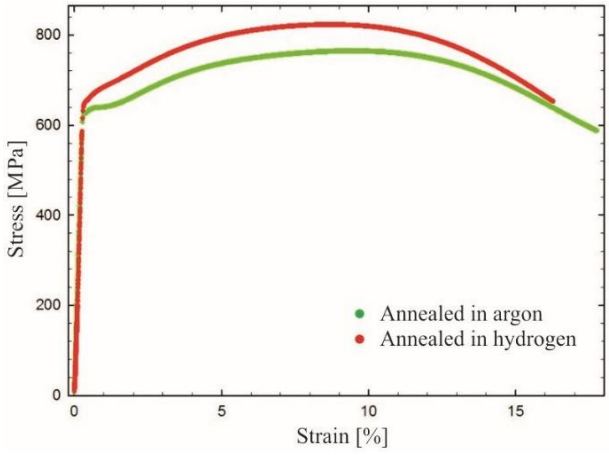

Figure 2. Room temperature tensile stress-strain curve

Table 2. Room temperature tensile properties

Averaged values of specimens	Tensile curves			Measurements on specimens		DIC measurements	
	YS [MPa]	UTS [MPa]	*A* [%]	*Z* [%]	*A* [%]	*A* [%]	ε_{max} [%]
Annealed in hydrogen	662±4	823±5	16±1	44±2	16±1	16±1	43±1
Annealed in argon	630±7	764±6	17±1	50±3	17±1	18±1	48±2

Figure 3 shows the typical pictures of the tensile specimen taken by the CCD cameras. The random black color speckles pattern is very well visible on the gauge surface before and after tensile testing [7]. The green line indicated along the gauge section of the specimen is drawn by video extensometer with 5 dividers of Mercury RT software before tensile testing (Fig. 3a) followed the elongation of the specimen during whole deformation process (Fig. 3b). The specimen shows non-uniform deformation with well-developed necked region before fracture, as seen in Fig. 3b.

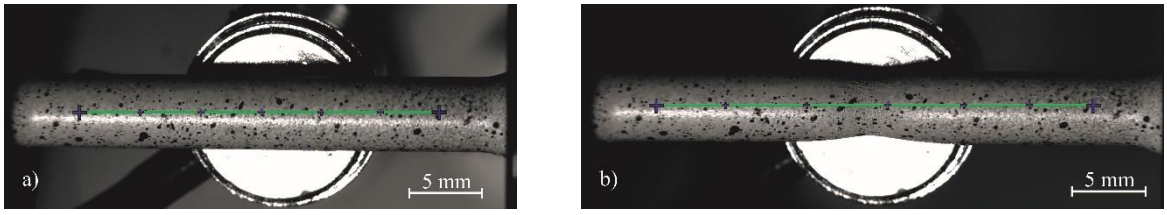

Figure 3. Pictures of tensile specimen taken by the CCD cameras: (a) before deformation, (b) after deformation

Figures 4a) and 4b) show the 2D visualization of ε_x, ε_y and γ_{xy} strain fields measured by the DIC method on the surface of the tensile specimens annealed in argon and hydrogen and tested to fracture, respectively. Both figures clearly indicate highly non-uniform deformation and achieving maximum local strains in x direction up to 50.6% and 43.8 %, in y direction up to -25.3% and -22.4 % and shear strains in xy direction in the range from 18.2% to -18.2% and 12.1% to -12.1% for the specimens annealed in argon and hydrogen, respectively. As can be seen, the values measured by DIC method for the specimens annealed in hydrogen are lower by about 15%.

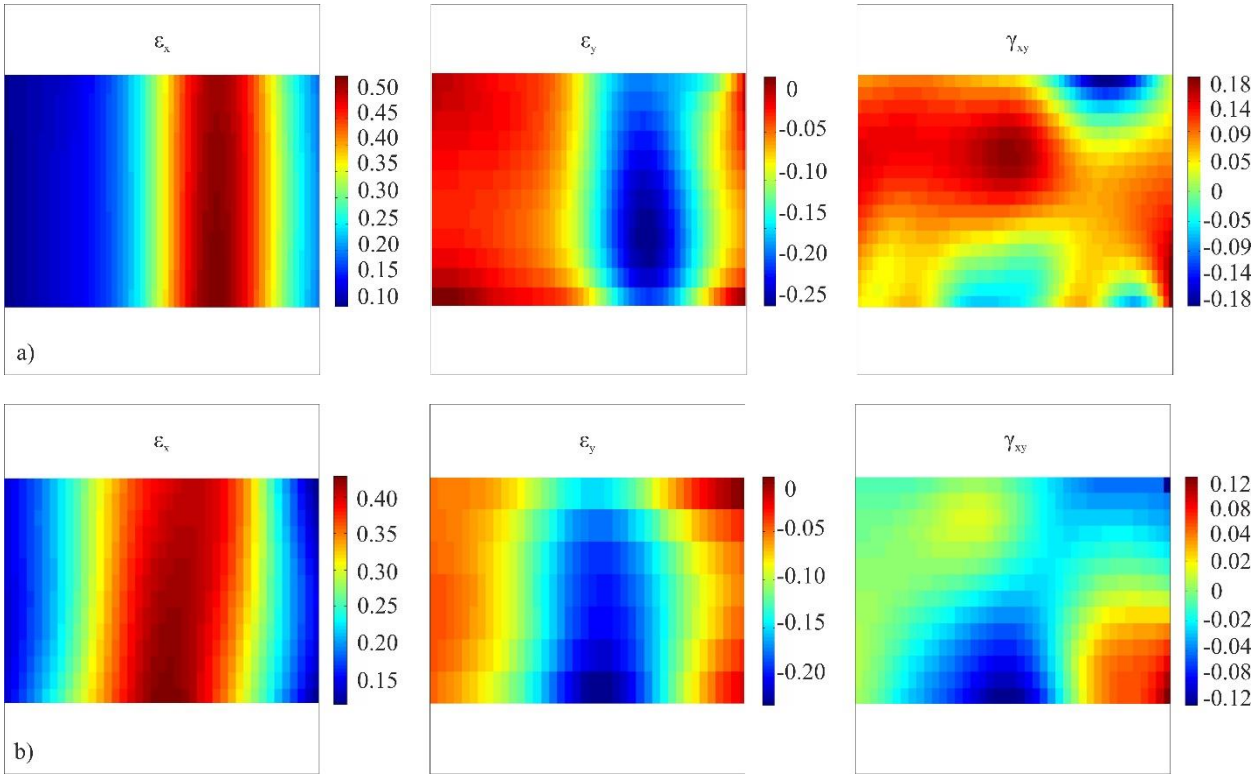

Figure 4. Calculated strain fields ε_x, ε_y and γ_{xy} by the DIC method for the specimens annealed in: a) argon and b) hydrogen

Figures 5a) and 5b) show the 2D visualization of ε_x, ε_y and γ_{xy} strain fields calculated by the FEA method indicating the local deformation along the gauge section of the specimens annealed in argon and hydrogen, which were tested to fracture, respectively. Both figures clearly indicate highly non-uniform deformation with extensive necking and achieving maximum local strains in x direction up to 51.4% and 45.8 %, in y direction up to -30.1% and -23.2 % and shear strains in xy direction in the range from 20.1% to -20.1% and 14.2% to -14.2% in the

necked region for the specimens annealed in argon and hydrogen, respectively. Very good agreement between strain fields calculated by the experimental DIC method and those resulting from the FEA calculations indicates the appropriateness of the input data experimentally determined for the studied steel in the frame of this work.

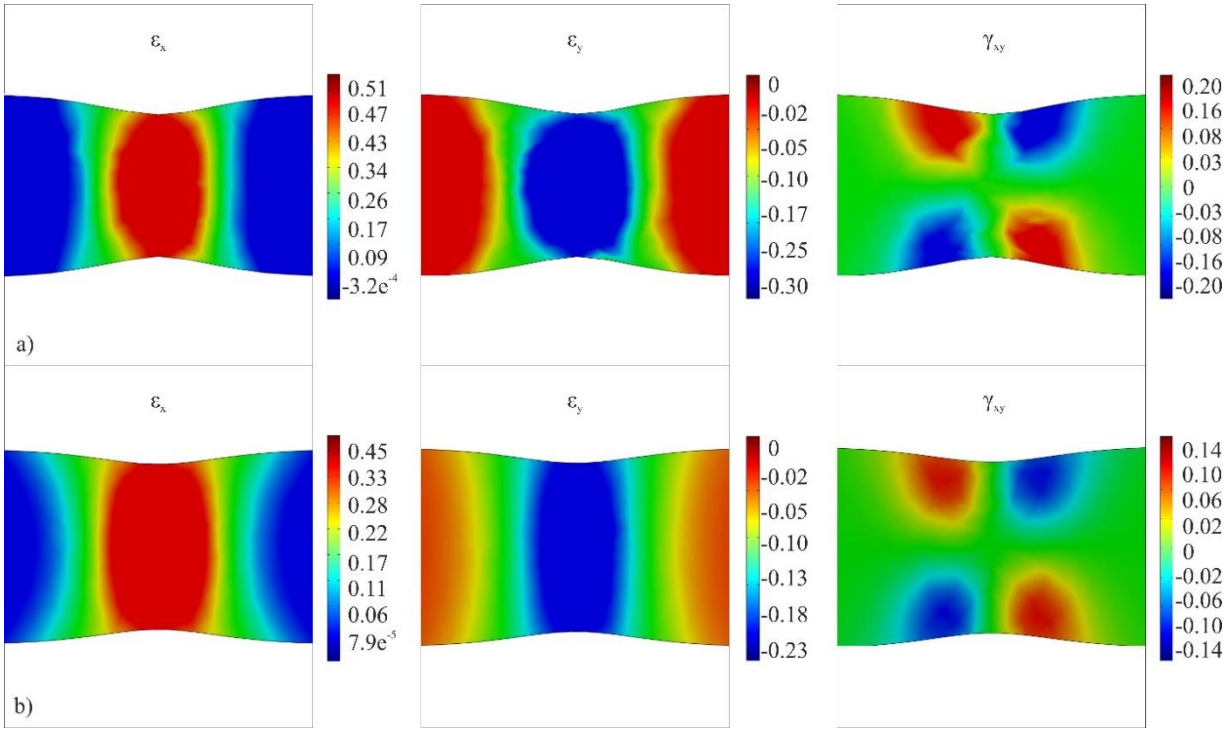

Figure 5. Calculated strain fields ε_x, ε_y and γ_{xy} by the FEA method for the specimens annealed in: a) argon and b) hydrogen

3.3. Work hardening behavior

Measurements of elongation and contraction by the DIC method during entire tensile deformation enable to calculate true stresses and true strains along the gauge section of the tensile specimens annealed in argon and hydrogen. Figure 6 shows the true stress-true strain curves calculated assuming an engineering, uniform, non-uniform and local deformation of the gauge section of the specimens. For the engineering curve the stresses and strains are obtained from the tensile machine. For the uniform deformation (blue curve in Figure 6), the true stresses σ_t are calculated assuming uniform contraction along the entire gauge section as a function of the elongation. The average true strains ε_t are calculated from the engineering strains ε according to relationship $\varepsilon_t = \ln(1+\varepsilon)$. For the non-uniform deformation, the true stresses are calculated assuming the experimentally measured contractions (maximum values) by the DIC method and assuming the calculated average true strains ε_t. For the local deformation, the true stresses are calculated assuming measured contractions (maximum values) by the DIC method and local true strains calculated from the average local engineering strains measured for the necked region. The diagrams clearly indicate that the values of elongation of the specimens annealed in hydrogen are less by about 10% but the values of the yield strength and ultimate tensile strength reach higher values than those of the specimens annealed in argon.

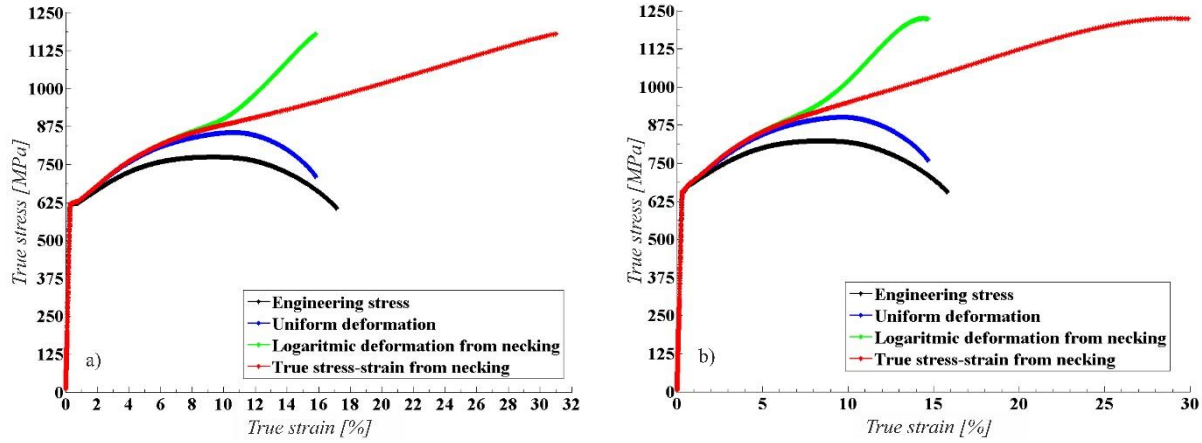

Figure 6. Example of true stress–true strain curves calculated assuming an engineering, uniform, non-uniform and local deformation of the tensile specimens annealed in: a) argon and b) hydrogen

Figure 7 shows the evolution of the work hardening rate Θ with the true strain. It is clear from this figures that the evolution of the work hardening rate with the true strain is different for the uniform, non-uniform and local deformation of the specimens annealed in argon and hydrogen up to the true strains of about 3%. For true strains higher than 3%, the work hardening rate continuously decreases with increasing true strain up to the tensile fracture for the uniform and local deformation (Figures 7a) and 7c)). For the non-uniform deformation (Figure 7b)), the work hardening rate slightly decreases with increasing ε_t after achieving true strain of about 8% starts rapidly increases before tensile fracture. For the local deformation (Figure 7c)), the work hardening rate decreases to a minimum value of about 1200 MPa at ε_t of about 10% and then slightly increases with increasing true strain up to tensile fracture. It should be noted that three stages of the work hardening were also reported by Zuo et al. [8] for medium carbon low-alloy steels when analysed in the terms of deformation.

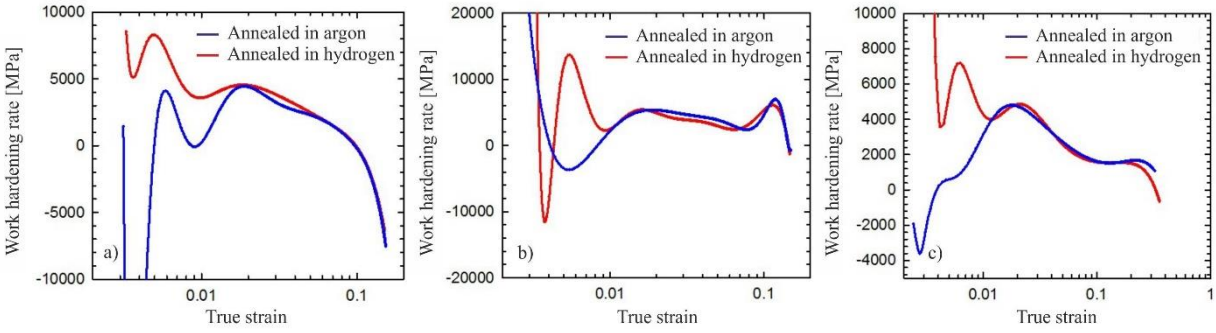

Figure 7. Dependence work hardening rate on true strain calculated the tensile specimens annealed in argon and hydrogen assuming: a) uniform, b) non-uniform and c) local deformation

4. Conclusions

The present study yield following conclusions:

1. The microstructure of the studied low-carbon ferrite-pearlite steel consists of slightly elongated ferritic grains and pearlite colonies.
2. The annealing of tensile specimens in hydrogen increases room temperature offset 0.2% yield strength and ultimate tensile strength but tensile elongation and contraction are decreased when compared to those of the specimens annealed in argon.
3. The strain fields determined by the experimental 2D DIC method on the surface of the tensile specimens correspond very well to the 2D calculations of the strain fields performed by FEA using the input data for the studied steel measured in the frame of this work.
4. The evolution of work hardening rate with strain calculated assuming uniform, non-uniform and local deformation of the tensile specimens annealed in argon is significantly different for that of the specimens annealed in hydrogen up to the true strains of about 3%.

Acknowledgements

This work was financially supported by the Slovak Research and Development Agency under the contract

APVV-15-0660, the Slovak Grant Agency for Science under the contract VEGA 2/0125/16, Slovak Research and Development Agency under the contract APVV-0434-10 and the contract MVTS founding of the project INCAST.

REFERENCES

[1] Lavender J.D., Jones F.W., (1949), J. Iron Steel Inst. 9, p. 14.

[2] Tau L., Chan S.L.I., (1996), *Effects of ferrite/pearlite alignment on the hydrogen permeation in a AISI 4130 steel*. Materials Letters 29, p. 143-147.

[3] Gladshtein L. I., Larionova, N. P., Belyaev, B. F., (2012), *Effect of Ferrite-Pearlite microstructure on Structural Steel Properties*, Metallurgist 56, No. 7-8, p. 579-590.

[4] Chan S. L. I., Charles J. A., (1986), *Effect of carbon content on hydrogen occlusivity and embrittlement of ferrite pearlite steels*. Materials Science Technology 2, p. 956–962.

[5] Štamborská M., Lapin J., Bajana O., Losertová M., (2015), *Application of DIC method for assessment of tensile deformation of medium carbon steel*. International conference "Mechanical Technologies and Structural Materials". Split, 24-25.09. p. 161-166 ISSN 1847-7917.

[6] Štamborská M., Lapin J., Bajana O., Losertová M., (2015), *Tensile deformation behavior of ferritic-pearlitic steel studied by digital image correlation method*, Kovove Mater. 53, no. 6, p. 399-407. DOI: 10.4149/km_2015_6_399.

[7] Schrötter M., Hagara M., Kalina M., (2014), *The analysis of different stochastic patterns during loading in plastic area using DIC method*, Applied Mechanics and Materials 611, pp. 490-495.

[8] Zuoa X., Chen Y., Wang M., (2012), *Study on Microstructures and Work Hardening Behavior of Ferrite-Martensite Dual-Phase Steels with High-Content Martensite*, Materials Research 15, No. 6, pp. 915-921.

ISSN 1847-7917

Computer analysis of injection molding process
Računalna analiza procesa injekcijskog prešanja

Branimir TADIĆ[1)]***, Mladen PERINIĆ***[1)]***, Zoran JURKOVIĆ***[1)]

1) Sveučilište u Rijeci, Tehnički fakultet/ University of Rijeka, Faculty of Engineering, Vukovarska 58, 51000 Rijeka, Hrvatska/Croatia

E-mail:btadic@riteh.hr, mladen.perinic@riteh.hr, zoran.jurkovic@riteh.hr

Keywords

Injection moulding
Mould for injection moulding
Simulation of melt flow
Computer amalysis
Polymer process

Ključne riječi

Injekcijsko prešanje
Kalup za injekcijsko prešanje
Simulacija toka taljevine
Računalna analiza
Prerada polimera

Professional paper

Abstract: Modern production of molded parts by injection molding demands quick launching of products on the market with high demands in terms of quality and dimensional accuracy of the molded product. A mold for injection molding is the central part of the system for injection molding which depends on the dimensional accuracy of the final product. In addition, there are also parameters of the process of molding who have an affect on the end product, such as: molding temperature, pressure, cycle time, cooling, pressure rate, etc... By using modern tools for design and simulation of melt flow a simulation model can obtained, and by the results of the analysis a final decision on the construction of the injection mold can be made. In this study, the goal was to combine the simulation models with experimentally derived models to the end user to provide valuable information which will predict the deviation of computer simulations from real models following the dimension, shape and properties of the molded parts. Obtaining optimal results of the process parameters (pressure, time and the speed of pressing) can ensure an efficient designing of the mold which will result in positive techno-economic indicators.

Stručni članak

Sažetak: Suvremena proizvodnja otpresaka injekcijskim prešanjem zahtijeva brzo lansiranje proizvoda na tržište s visokim zahtjevima u pogledu kvalitete i dimenzijske točnosti prešanih proizvoda. Kalup za injekcijsko prešanje predstavlja centralni dio sustava za injekcijsko prešanje o kojem ovisi dimenzijska točnost konačnog proizvoda. Osim kalupa za injekcijsko prešanje na dimenzijsku točnost krajnjeg proizvoda utječu parametri procesa prešanja kao što su: temperatura prešanja, pritisak, vrijeme ciklusa, hlađenje, brzina prešanja itd… Korištenjem suvremenih alata za konstruiranje i simulaciju toka taljevine moguće je dobiti simulacijski model, te prema rezultatima analize donijeti konačnu odluku o konstrukciji kalupa za injekcijsko prešanje. U ovom radu cilj je bio povezati simulacijske modele s eksperimentalno dobivenim modelima koji će krajnjem korisniku osigurati vrijedne podatke na temelju kojih će moći predviđati odstupanja računalne simulacije od realnog modela prateći dimenziju, oblik i svojstva otpreska. Dobiveni optimalni rezultati parametara procesa (tlak, vremena i brzine prešanja) konstruktoru kalupa za injekcijsko prešanje osiguravaju učinkovitije konstruiranje kalupa što će rezultirati pozitivnim tehno-ekonomskim pokazateljima.

1. Uvod

Postupak injekcijskog prešanja predstavlja jedan od najraširenijih cikličkih postupaka preradbe polimera. Postupak omogućuje izradu dijelova u velikim količinama, složene geometrije bez potrebe za završnom i dodatnom obradom. Ovim postupkom moguće je prerađivati različite vrste polimera kao što su: plastomeri, duromeri i elastomeri. Zbog svoje jednostavnosti i pouzdanosti u današnjoj industriji najraširenij je postupak injekcijskog prešanja plastomera. Ovu vrstu polimera predstavlja sintetski ili modificirani prirodni polimerni materijal koji je izgrađen od linearnih ili granatih makromolekula koje mogu imati kristalnu, kristalastu ili amorfnu građu. Dovođenjem topline dolazi do pucanja veza između makromolekula koje uzrokuju promjenu agregatnog stanja polimera te se mogu oblikovati u željene oblike. Daljnjim hlađenjem dolazi do skrućivanja te zauzimaju definiran oblik. Vrlo važno svojstvo ovih materijala predstavlja mogućnost ponavljanja procesa zagrijavanja i hlađenja bez velikih posljedica na strukturu, što omogućuje proces reciklaže, te rezultira velikom primjenom plastomera u svim granama industrije.

Kada se kaže da je postupak injekcijskog prešanja ciklički, podrazumijeva se da se postupkom u jednom ciklusu (vremenu) od tvari ili materijala stvara tvorevina - obradak. Proces injekcijskog prešanja moguće je podijeliti u dvije faze; punjenje i hlađenje. U fazi punjenja polimerna taljevina ubrizgava se u kalupnu šupljinu pri čemu se taljevina širi kalupom u različitim smjerovima sve dok se u potpunosti ispuni kalupna

šupljina. Da bi se omogućilo ubrizgavanje u kalupnu šupljinu polimerna tvar treba imati potrebnu temperaturu koju prati odgovarajuća smična viskoznost. Ubrizgana polimerna tvar naknadnim hlađenjem i djelovanjem naknadnog tlaka – druga faza procesa, zauzima oblik i geometriju kalupne šupljine te se nakon određenog vremena hlađenja izbacuje iz kalupa te se postupak ponavlja. Pri interakciji taljevine i kalupne šupljine može doći do različitih proizvodnih oštećenja koja mogu u konačnici rezultirati iznimno velikim troškovima. Neka od čestih proizvodnih oštećenja koja se javljaju pri procesu injekcijskog prešanja mogu biti: sakupljanje, usahline, toplinska naprezanja, toplinska deformacija i ostale pogreške koje mogu utjecati na konačna svojstva i dimenzijsku točnost proizvoda. Proizvodna oštećenja često nisu isključivo uzrokovana samo jednim uzrokom nego nizom više različitih uzroka koji mogu biti vanjski, unutarnji ili kombinacija unutarnjih i vanjskih uzroka. Vanjskim uzrocima možemo smatrati uzroke koji nisu vezani uz ubrizgavalicu, kao što su: operater, materijal, okolina itd. Pod unutarnje uzroke možemo smatrati uzroke koji su vezani uz ubrizgavalicu kao što su: kalup, parametri procesa, karakteristika stroja itd. Slika 1 prikazuje podjelu uzroka proizvodnih oštećenja prilikom procesa injekcijskog prešanja.

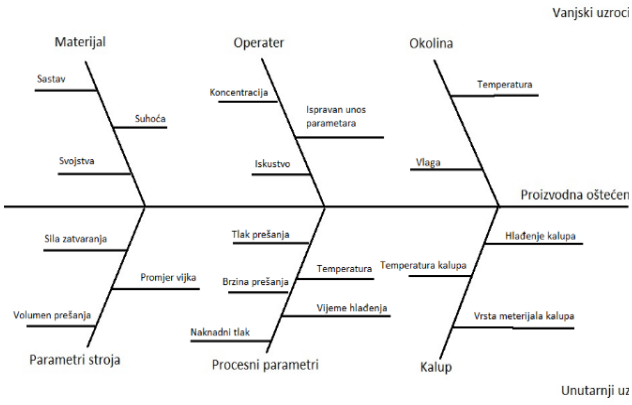

Slika 1. Prikaz parametara koji utječu na process injekcijskog prešanja

Jedan od najvažnijih dijelova sustava za injekcijsko prešanje je kalup koji svojom geometrijom određuje konačan oblik proizvoda. Osim određivanja geometrije, tj. očvršćivanja kalup ima druge funkcije, kao što su temperiranje i izbacivanje gotovih obradaka. Prilikom konstruiranja kalupne šupljine vrlo je važno ispuniti sve uvjete te predvidjeti moguća proizvodna oštećenja koja se mogu javiti tokom procesa prešanja. S ciljem smanjenja rizika javljanja proizvodnih oštećenja na obradcima koristit ćemo programski alat *SolidWorks plastics 2014* koji pomoću računalne simulacije temeljene na metodi konačnih elemenata omogućuje uvid u proces injekcijskog prešanja. Na temelju ulaznih parametara ovaj programski alat predviđa proizvodna oštećenja uslijed netočne geometrije obratka, kalupa ili odabira netočnih parametara. Ovakav pristup problemu omogućuje optimizaciju konstrukcije alata za injekcijsko prešanje te smanjenje troškova u ranim fazama razvoja projekta. Slika 2 prikazuje utjecaj troškova promjene u ovisnosti o razvojnoj fazi projekta.

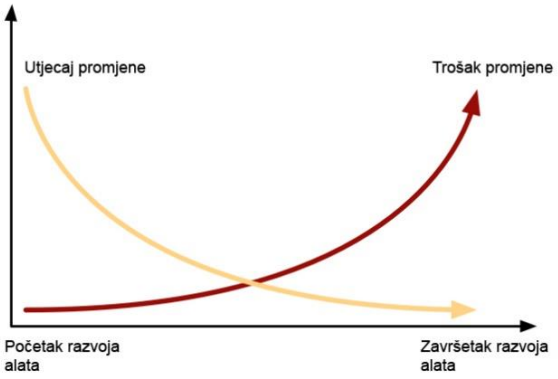

Slika 2. Utjecaj troškova promjene u ovisnosti o razvojnoj fazi

U ovom radu koristit će se programski alat *SolidWorks plastics 2014* te dobivene rezultate uspoređivat će se s realnim modelom. Realni model predstavljat će obradak sa slike 2 koji je dobiven postupkom injekcijskog prešanja na ubrizgavalici tipa Arburg T 450. Međusobnom usporedbom odabranih rezultata nastojat će se evaluirati oba modela te dobiti međusobna poveznica simulacijskog modela i pokusa. Pokus će se sastojati od namjernog prekidanja procesa prešanja te vađenja otpresaka iz kalupne šupljine. Cilj pokusa je dobivanje informacije o smjeru i načinu napredovanja taljevine kroz kalupnu šupljinu te kasnija usporedba s rezultatima dobivenim simulacijom.

2. Primjena metode konačnih elemenata pri simulaciji injekcijskog prešanja

Metoda konačnih elemenata je metoda koja se temelji na fizičkoj diskretizaciji kontinuuma. Razmatrani kontinuum s beskonačno stupnjeva slobode gibanja zamjenjuje se s diskretnim modelom međusobno povezanih elemenata s ograničenim brojem stupnjeva slobode. Može se reći, područje kontinuuma dijeli se na konačan broj podpodručja koja se nazivaju konačni elementi, pa se razmatrani kontinuum prikazuje kao mreža konačnih elemenata. Konačni elementi međusobno su povezani u točkama na konturi elementa koji se nazivaju čvorovi. Stanje u svakom elementu, kao što je npr. polje pomaka, deformacije, naprezanja, temperature te ostalih veličina, opisuje se pomoću interpolacijskih funkcija. Te funkcije moraju zadovoljavati odgovarajuće uvjete da bi se diskretizirani model što više približio ponašanju kontinuiranog sustava. Uz pravilnu formulaciju konačnih elemenata, približavanje točnom rješenju raste s povećanjem broja

elemenata. Prilikom izvođenja algebarskih jednadžbi polazi se od definicije jednadžbi koje opisuju stanje u elementu ili se rabi varijacijska formulacija. Nakon izvođenja jednadžbi za konačni element, gdje su nepoznanice neovisne varijable u čvorovima, odgovarajućim postupcima izvode se globalne jednadžbe za diskretizirani model.

Pomoću izračunatih čvornih veličina moguće je, primjenom poznatih teorijskih relacija, odrediti sve veličine potrebne za analizu opisanoga kontinuiranog sustava.

Razvoj računala omogućio je uvođenje metode konačnih elemenata u svakodnevnu inženjersku praksu te izbjegavanje mukotrpnoga ručnog računanja. Osim skraćivanja vremena potrebnog za izradu proračuna, primjenom metode konačnih elemenata moguće je u vrlo kratkom roku napraviti i veliki broj eksperimenata, što omogućuje dodatnu uštedu vremena, ali i izradu bolje optimiranih konstrukcija. Osnovno što korisnik mora znati o konačnim elementima jest da je to skup elemenata povezanih u prostoru određenim brojem točaka, koji mogu opisati razne oblike. U određenim točkama zadani su uvjeti pomaka, slika, viskoznog naprezanja. Vrlo je važno da korisnik zna odabrati pogodan element i navodi računalo da odabrane elemente spoji u suvislu simulaciju. Važno je moći prepoznati koje detalje je potrebno uključiti u simulaciju, a koje je moguće sa sigurnošću zanemariti (kao npr. rupe i sl.) Dizajn elemenata utječe na tijek proračuna na posredan način, preko svog utjecaja na trošak analize i na točnost rezultata. S obzirom da svi elementi nemaju jednaka svojstva, njihov utjecaj na točnost rezultata je različit. Isto tako isti elementi nemaju jednaku točnost za različite probleme. Pri izradi simulacije programski paket *SolidWorks plastics* omogućuje odabir više tipova konačnih elemenata. Nakon odabira tipa konačnog elementa provodi se proces *meshiranja* te mreža elemenata predstavlja novi sustav koji ima mogućnost daljnje analize.

2.1. Shell konačni elementi

Ovaj tip konačnih elemenata predstavlja trokutne elemente koji su prikladni za analizu tankostjenih 3D modela. Trokutni elementi su 2D tipa elementi, te ovisno o njihovoj veličini i broju čvorova možemo razlikovati linearne trokutne elemente i parabolične trokutne elemente. Za simulacije niže kvalitete možemo koristiti linearne trokutne elemente koji imaju tri čvora, a za kvalitetnije simulacije koristit ćemo parabolične trokutne elemente koji imaju šest čvorova. U ovom radu zbog kvalitete rezultata simulacije koristit će se parabolični trokutni elementi. Slika 3. prikazuje linearne i parabolične trokutne elemente.

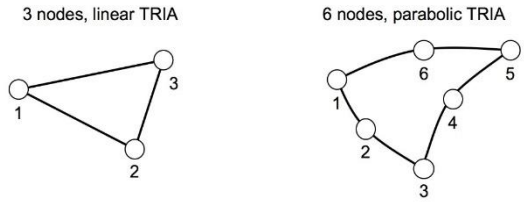

Slika 3. Prikaz forme konačnih elemenata

2.2. Metoda vizualne usporedbe

Cilj ove metode je povezivanje rezultata simulacije i pokusa. S obzirom da se kroz rad želi dobiti veza simulacije i pokusa za napredovanje taljevine kroz kalupnu šupljinu uz pomoć digitalne fotografije rezultati pokusa bit će digitalizirani te će se usporediti sa rezultatima računalne simulacije. Ova metoda temelji se na digitalizaciji fotografije i prepoznavanju kontura na digitalnoj fotografiji. Metodom spajanja kontura računalni program koristi matematičke algoritme i referentne točke za izvršavanje preklapanja digitalizirane fotografije i rezultata simulacije. Nakon izvršenog procesa preklapanja računalni program prepoznaje razlike nastale uslijed preklapanja dvije slike te definira ih odstupanjem. Ova metoda omogućuje vizualnu usporedbu rezultata računalne simulacije i rezultata pokusa te daje kvalitativni prikaz odstupanja. Računalni program je razvijan samostalno na Tehničkom fakultetu u Rijeci te zasada nije razvijena mogućnost očitavanja kvantitativnih rezultata. Vrlo važan preduvjet za ispravan prikaz rezultata je umjeravanje modela kojeg se želi digitalizirati, a za umjeravanje je korišten marker definiranih dimenzija koji se inače koristi pri metodama 3D skeniranja.

3. Usporedba simulacijskog modela i pokusa

Dobiveni rezultati korištenjem navedenih metoda mogu se međusobno usporediti te na temelju usporedbe moguće je donijeti procjenu odstupanja simulacijskog modela i pokusa.

3.1 Definiranje parametara pokusa

Za početak usporedbe potrebno je definirati ulazne parametre te definirane parametre koristiti u svim slučajevima. Ulazne parametre predstavljaju parametri injekcijskog prešanja ubrizgavalice koji su prikazani u tablici1.

Tablica 1. Parametri procesa

Rb.	Vrijeme ubrizgavanja [s]	Temp Taljevine [°C]	Temp kalupa [°C]	Tlak prešanja [bar]	Vr. Naknadnog tlaka [s]	Vr. Hlađenja [s]
001	1.80	220	35	1000	3	33
002	2.47	220	35	1000	3	33
003	3.13	220	35	1000	3	33
004	4	220	35	1000	3	33

Podaci u tablici predstavljaju ključne podatke za postupak injekcijskog prešanja. Ovi parametri svojim vrijednostima direktno utječu na otpresak te se definiraju na upravljačkoj jedinici stroja za ubrizgavanje. Iz tablice je vidljivo da će tijek procesa biti definiran vremenom ubrizgavanja te na taj način omogućit će se praćenje napredovanja taljevine kroz kalupnu šupljinu. Zbog preciznosti konačnih rezultata ostali parametri u procesu ostat će nepromijenjeni. Tip polimernog materijala je propilen (PP) trgovačkog naziva Borealis GB205U čija svojstva su definirana u specifikaciji. Za potrebe ovog rada korišten je stroj Engel Victory 450 koji ima nazivnu silu zatvaranja 4500 KN. Navedeni stroj koristi se za injekcijsko prešanje koljenastih cijevi za odvodnju promjera 110 mm. U kalupnoj šupljini nalazi se četiri otpreska, kroz jezgre odvodi se jedan dio topline nastale prešnajem. Slika 4 prikazuje montiran alat na stroj i dio koji nastaje u alatu prilikom prešanja.

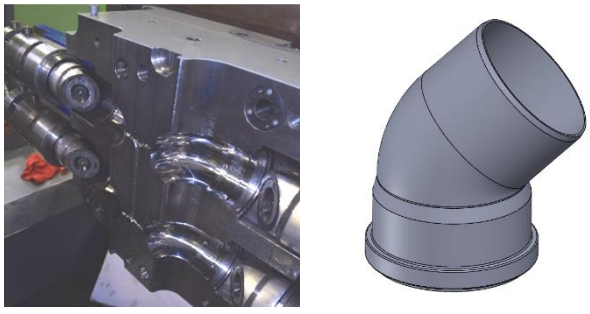

Slika 4. Prikaz alata za prešanje i konačnog proizvoda

3.2 Definiranje parametara simulacije

Za postavljanje parametara simulacijskog modela koristit će se podatci iz tablice 1, s ciljem da pokus i simulacijski model budu što sličniji. Jedina promjena u odnosu na pokus bit će pojednostavljivanje alata, te će se simulacija izvesti samo za jedan obradak kako bi se uštedjeli resursi i vrijeme potrebno za simulaciju. Slika 5. prikazuje simulacijski model u programskom alatu *SolidWorks Plastics 2014*.

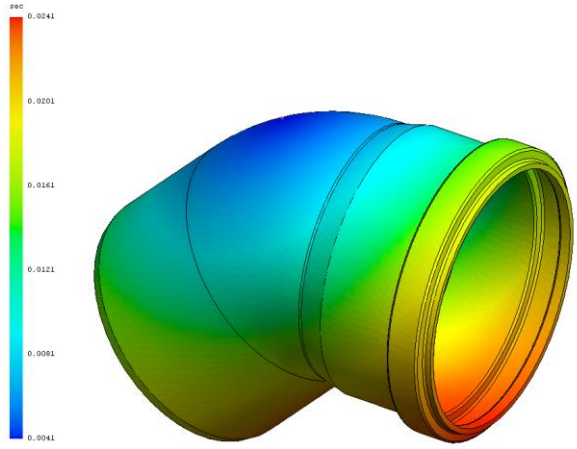

Slika 5. Konačni rezultat simulacije

3.3 Usporedba rezultata simulacijskog modela i pokusa

Koristeći metodu vizualne usporedbe uspoređeni su rezultati simulacijskog modela i pokusa. Slika 6 prikazuje smjer napredovanja taljevine u prvih 1.80 s.

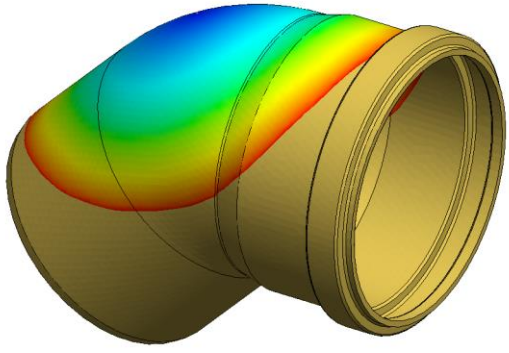

Slika 6. 3D prikaz simulacije u vremenu 1.80 s

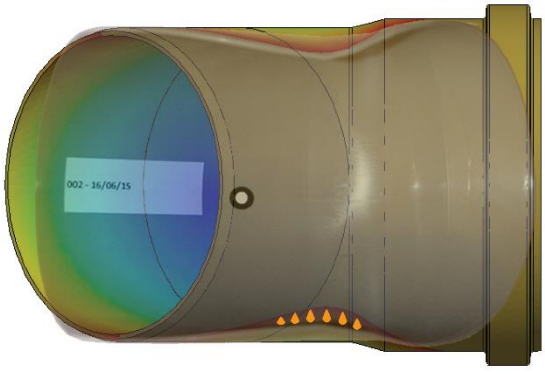

Slika 7. Usporedba rezultata ispitivanja i simulacijskog modela

Iz slike 7 može se vidjeti međusobna zavisnost kretanja taljevine između rezultata pokusa na stroju i računalne simulacije. Linija napredovanja taljevine u kalupnoj šupljini prati simulacijski model te prema rezultatima možemo zaključiti da je simulacija ispravna. Pri usporedbi rezultata moguće su greške koje su rezultat matematičkog algoritma, no uz te greške rezultat je prihvatljiv.
Za vrijeme od 2.47 s, slika 8 prikazuje nastavak napredovanja taljevine kroz kalupnu šuplinu.

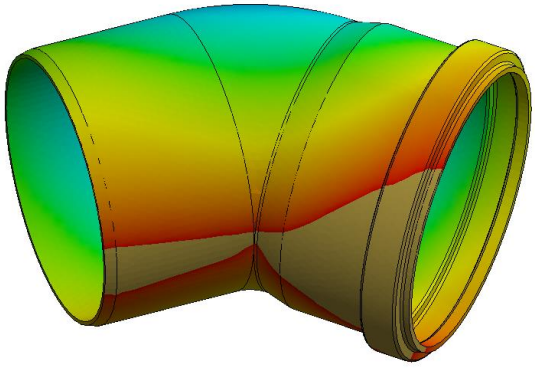

Slika 8. 3D prikaz simulacije u vremenu 2.47 s

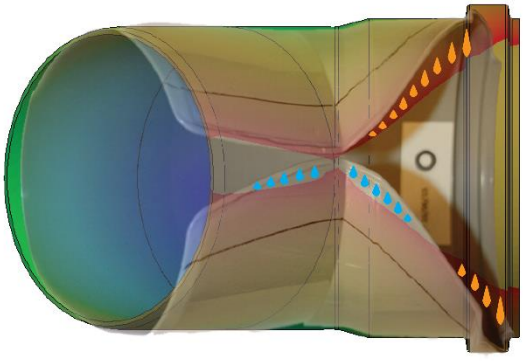

Slika 9. Usporedba rezultata ispitivanja i simulacijskog modela

Daljnjom analizom može se uočiti odstupanje između simulacijskog modela i pokusa te uračunavajući greške koje se mogu pojaviti pri uspoređivanju rezultata može se zaključiti da su rezultati u skladu s očekivanim te da simulacija u maloj mjeri odstupa od realnog modela kojeg predstavlja pokus.
Za vrijeme od 3.13 s, slika 10 prikazuje napredovanje taljevine kroz kalupnu šupljinu te je taljevina ispunila veći dio kalupa.

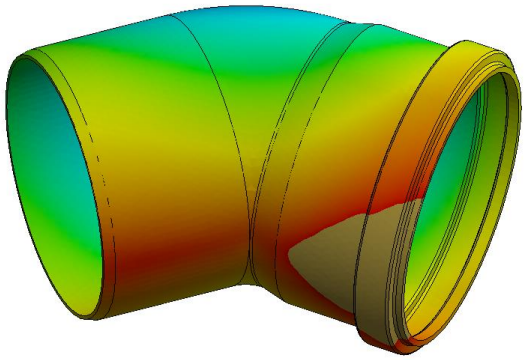

Slika 10. 3D prikaz simulacije u vremenu 3.13 s

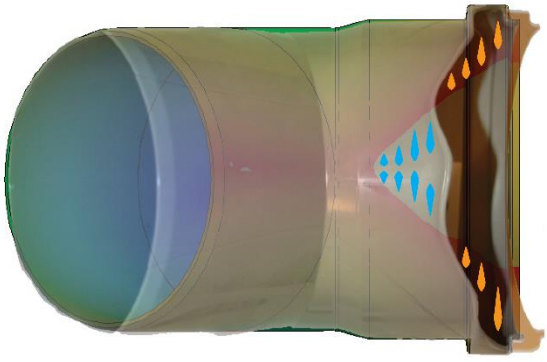

Slika 11. Usporedba rezultata ispitivanja i simulacijskog modela

Iz rezultata poklapanja (slika 11) moguće je uočiti da se rezultati simulacijskog modela i pokusa međusobno ne poklapaju te da dolazi do greške.
Za vrijeme od 4 sekunde, rezultati nisu prikazivani iz razloga što se u tom vremenu kalupna šupljina potpuno ispunila te nema potrebe za ispitivanjem te faze procesa.
Temeljem analize možemo zaključiti da su rezultati bili najvjerodostojniji u prvih 1.80 s te je preklapanje rezultata iznosilo 90%. Za vrijeme od 2.47 s, iz priloženog može se uočiti da dolazi do opadanja točnog rezultata te međusobno preklapanje iznosilo je 80%. Najveća razlika u preklapanju rezultata odgovara vremenu od 3.13 s te odstupanje u preklapanju iznosi 60%. Ovakvi rezultati ukazuju da računalna simulacija ne može s potpunom točnosti dati informacije o smjeru taljevine, ali mogu biti od velike koristi. Opisati realni problem te simulirati ga zahtijeva veliku količinu resursa te rezultati dobiveni pojednostavljenim modelima mogu biti dovoljno točni da se izbjegnu mogućnosti za javljanje proizvodnih grešaka kod procesa injekcijskog prešanja.

4. Zaključak

Razvojem današnjih računala povećani su procesorski resursi te su procesori u mogućnosti obavljati nizove složenih matematičkih operacija u vrlo kratkom vremenu. Proširenjem ove karakteristike računala otvorio

se niz mogućnosti. Jedna od mogućnosti je upotreba metode konačnih elemenata u brojnim granama industrije. Računalna simulacija često može predstavljati zamku za krajnjeg korisnika s obzirom da zahtijeva poman odabir niza parametara i rubnih uvjeta koji mogu utjecati na konačan rezultat simulacije. Kroz ovaj rad željelo se pronaći poveznicu između simulacijskog modela i realnog model (pokusa) kako bi se pojasnio način širenja taljevine kroz kalupnu šuplinu. Pri izradi simulacijskog modela težilo se odabiru istih parametara kao u pokusu kako bi odstupanja bila što manja. Prikazani rezultati nastali kroz pokus vrlo dobro prate rezultate simulacijskog modela te u određenim područijima dolazi do odstupanja, no s obzirom na pojednostavljenja koja su bila uvedena u simulacijski model u konačnici ne čine veliku razliku. Programski alati kao što su *SolidWorks Plastics*, iznimno su važno pomagalo pri početnim fazama konstruiranja kako bi se minimalizirale moguće graške i tako izbjegli veliki troškovi izmjene konstrukcije alata.

REFERENCE

[1] Čatić, I.: *Uvod u proizvodnju polimernih tvorevina*, Društvo plastičara i gumaraca, Zagreb, 1990.
[2] *Prospektni materijal tvrtke Engel*, 2008
[3] Pie, R. G. W: *Injection mould design* George Godwin, London, 1978.
[4] M. Stanek, D. Manas, M. Manas and O. Suba: Optimization of Injection Molding Process, INTERNATIONAL JOURNAL OF MATHEMATICS AND COMPUTERS IN SIMULATION